Università degli Studi di Genova

Doctorate School in

Civil, Chemical and

Environmental Engineering

Doctorate in Structures, Materials and Geotechnics

XXXI CYCLE

Characteristics, weather scenario and statistics of thunderstorm outflows based on measured data

Shi Zhang

Tutor: **Prof. Giovanni Solari**

Prof. Qingshan Yang

To my grandfather, Yushan Zhang!

Abstract

Wind is the most destructive natural phenomenon: 70% of damage and death caused by nature in the world comes from wind. And extreme winds such as typhoons, tornadoes and thunderstorms are crucial for structural damage. Inside, during a thunderstorm, the transient downdraft that impinges on the ground produces radial outflows that can produce strong transient wind, which is the main cause of the collapse of tall structures such as transmission tower, besides one of the threat to human life and property security, for instance, the accident of transmission line towers in Ontario, Canada in August 2006 and "Oriental star" sinking in China in June, 2015 and so on. The study of thunderstorm outflows and their loading and response of structures already become a key topic in modern wind engineering. Despite this, the understanding, the representation and the modeling of thunderstorm outflows are still full of uncertainties and problems to be clarified. This happens because the complexity of the thunderstorm outflows makes it difficult to establish physically realistic and simple engineering schemes, their short duration and small size means few data are available, and a large gap exists between wind engineering and atmospheric science. It follows that the wind loading of structures is still evaluated by the Davenport's model for extra-tropical cyclones without any concern for the real nature and the properties of the meteorological event that causes the loading. This is nonsense because extra-tropical cyclones and thunderstorm outflows are different phenomena that need separate assessments.

To overcome these limits, this PhD thesis carries out a deep research mainly on the characteristics of thunderstorm outflow according to wind field measurement and meteorological data based on a thunderstorm catalogue created extracted from a mixed climate, which mainly contains the proposal of more reasonable directional decomposed approach of thunderstorm outflow signal, the properties of thunderstorm related to wind loading on structures, the comprehensive analysis of field measurements and weather scenarios related to thunderstorms, the extreme wind speed distribution in a mixed wind climate and the preliminary study of the crucial question if thunderstorms in different areas have similar properties. The major contents and achievements are summarized as follows:

Firstly, measurements for up to 6 years related to 14 high-sampling rate anemometers of the monitoring network in the Northern Mediterranean ports are analyzed. Three intense phenomena, namely extra-tropical cyclones, thunderstorm outflow, and intermediate events are separated successfully by a semi-automatic procedure. The results lead to a wide dataset of 277 wind velocity records characterized by strong transient properties and labeled by thunderstorm outflow, which are catalogued into three families, named 10 minutes, 1 hour and 10 hours, according to the different time-scale of the gust front passage, and fundamental for the subsequent study.

Analyses are then executed to extract the parameters of major interest for evaluating the wind loading effects of structures. And a novel directional decomposition strategy is formulated here, which makes it possible to analyse quantitatively the directional

shift of thunderstorm outflows, makes the study of thunderstorm outflows and synoptic winds fully coherent and is strategic to perform directional analyses of the dynamic behaviour of structures in terms of alongwind and crosswind response. Then this strategy is applied to thunderstorm records comparing with the classical decomposition approach and furnishing a comprehensive statistical characterization.

While the general analysis in wind engineering has a shortcoming that it misses the knowledge of the weather scenarios that occur during events classified as thunderstorms, without recognizing their actual meteorological nature. In order to take the first step towards filling this gap, a typical thunderstorm downburst and three events, each one representative of the corresponding class of duration, detected by our network are investigated from the meteorological point of view to represent a first step and a pilot attempt in this direction. The results obtained bring new insights into a thunderstorm's onset and detection in the Mediterranean, its evolution at the local scale, and possible connections to specific synoptic-scale weather conditions.

Design wind speeds based on the statistical analysis of conventional extreme mean wind speed data in a mixed wind climate may prove to be imprecise and unsafe due to the occurrence of intense, small and rapid extreme wind events such as thunderstorm outflows. Considering the continuous records registered in two Port areas of the monitoring network, a preliminary but representative analysis of the extreme wind speed distribution is carried out in this mixed wind climate area frequently struck by thunderstorms. Results show that wind speeds with high return period are always related to thunderstorm outflows. It proves that gathering the ensemble of all extreme values into a single set and the analyses of the local wind climate ignoring thunderstorms may lead to underestimating the extreme wind speed.

At the end of the research, this analysis procedure is applied to the 5-year data from the 9 anemometers installed at different heights on Beijing 325m high meteorological tower to study the characteristics of thunderstorms in the Beijing urban area, to compare these with northern Mediterranean ones and to understand if thunder-storms in different areas have similar properties. In addition, the property of the mean wind speed profile and coherent function of thunderstorms are described, which provides a reference for the simulation of thunderstorm signal.

Hope this thesis could make some contributions to step further research on thunderstorm-resistant design for building structures.

Keyword: extreme wind speed; measured data; mixed climate; thunderstorm outflow; wind property; weather scenarios; wind speed decomposition.

Acknowledgements

My most special gratitude to my advisors, Prof. Giovanni Solari, from the University of Genoa, Italy and Prof. Qingshan Yang, from Beijing Jiaotong University, China, first of all for making my visits to Genoa possible three times, and during the whole period, for all their help, advice, time, support, patience, insight and encouragement throughout this research, without whom this PhD research would not have been possible. It has been an honor to be their Ph.D. student and I benefit a lot from the joy and enthusiasm they have for the scientific research.

I am indebted to the professors helped me in University of Genoa, particularly, Prof. Massimiliano Bulando, Prof. Maria Pia Repetto, who gave me a lot of expert guidance, and post doctors, Dr. Marco Tizzi, Dr. Patrizia De Gaetano, Dr. Marina Pizzo, who kindly assisted me on various Matlab routines. I felt very honored to work with them. I also would like to thank the administrative staff in the department, who gave me the help in the past several years.

I would like to express my sincere gratitude to Dr. Djordje Romanić and Prof. Horia Hangan for their help on the thesis research. I thank all my colleagues in Beijing Jiaotong University, in particular, Prof. Bo Li, Prof. Yuji Tian, Prof. Jian Zhang, Dr Danyu Li, who provided me their strong support and valuable discussion. Besides, I thank all my colleagues in University of Chongqing, Dr. Min Liu, Dr Liuliu Peng, Prof Bowen Yan, Prof. Yi Hui and Prof Guoqing Huang who provided me their strong support and valuable discussion.

I would also like to express a very special thank to Prof. Yikou Tamura, who is so kind and invites me and my boyfriend to many dinners. Thanks to Prof. Ahsan Kareem, Prof Xinzhong Chen and Prof. Theodore Stathopoulos who gave me many suggestions during the research with patient.

I would also like to thank my Chinese friends in Genoa: Anda Liu, Chunzheng Wu, Lina Zhou, Mengjiao Wang, Mengying Yan, Renyong Tu, Tao Li, Tianwen Qi, Yao Wang, Yinuo Yin, Tianyi Yang, Xue Bai. Thank all of you for bringing a lot of fun and help for me. I would also like to thank my Italian friends in Genoa: Daniela Camilletti, Eluina, Luca, Mateo Solari, Simone. Thanks to the friends Ileana and Valentin Bucuresti from Romani for a lot of memory. I know more about the world from them.

I would also like to thank my Chinese friends in Beijing: Liang Yin, Mingyue Wang, Yan Tian, Yuan Xue, Jijie Zhang, Zixi Wei, Teng Wang, Jingxue Wang, Tian Li, Rong Gao, Wenshan Shan, Chen Li, Kunpeng Guo, Fan Bai. And I would also like to thank my Chinese friends in Chongqing: Ms. Zhishan Mo, Zihe Liu, Hao Zhan, Liang Xu, Pan Yu, Hua Xie, Kangkang Liu, Feixin Chen, Yifan Xu, Bowen Jiang, Xingwei Du and so on. Because of them, I love and miss the period in Chongqing.

There are also other friends who encouraged and backed up me on several occasions and I sincerely thank Tianshu Wang, Liping Guo, Lin Shi, Meng Bai, Lin Zhu and many others I cannot list their names one by one here - with whom I shared wonderful times and I shall always treasure those moments.

I would also like to thank to my ex-boyfriend while already husband now, Mr. Xiaoda

Xu for his support and love. And thanks to my parents in law, Yanping Peng and Xinsheng Xu for giving me the perfect husband and thoughtful care.

Last but not least, I should owe my gratitude to my family. Words cannot express how grateful I am to my parents, Yingwu Zhang and Lijuan Shi, and my little sister, Yi Zhang, for their love and encouragement during my study career. Their long-standing love, support and patience, have always been the greatest motivation throughout my entire life. This dissertation is dedicated to them with my endless love and gratitude.

This research is financed by the National Natural Science Foundation of China (51720105005) and “111 Project” of China (B18062, B13002). The data used for this research were recorded by the monitoring network set up as part of the European Projects “Winds and Ports” (grant No. B87E09000000007) and “Wind, Ports and Sea” (grant No. B82F13000100005), funded by the European Territorial Cooperation Objective, Cross-border program Italy-France Maritime 2007–2013, and the ultrasonic anemometers mounted at the Beijing 325 m high meteorological tower. It is also funded by European Research Council (ERC) under the European Union's Horizon 2020 research and innovation program (grant agreement No. 741273) for the project THUNDERR - Detection, simulation, modelling and loading of thunderstorm outflows to design wind safer and cost-efficient structures – through an Advanced Grant 2016. The thesis has been carried out in the framework of the “111 Project” and “ERC” Project.

Finally, I want to thank myself. Thank you for not following the crowd and making the right choice at every fork in the road.

Shi Zhang
June, 2019

Contents

List of Tables

List of Figures

List of Acronyms

ABL	Atmospheric Boundary Layer
AdG	An Advanced Grant
AGL	Above Ground Level
ASL	Above Sea Level
CAPE	Convective Available Potential Energy
CDF	Cumulative Distribution Function
CFD	Computational Fluid Dynamics
D	Extra-tropical Depression
ERC	European Research Council
EV	Extreme Value
IN/F	Intermediate Event/ Gust Front
GE	Genoa
GEV	General Extreme Value
GFS	Global Forecast System
LaMMA	Laboratorio di Monitoraggio e Modellistica Ambientale
LES	Large Eddy Simulation
LFKJ	Airport of Ajaccio, Corsica
LI	Livorno
LIML	Milan Linate Airport
LIRE	Pratica di Mare Air Force base, Rome
LIX	Lifted Index
MSG	Meteosat Second Generation
NCEP	National Center for Environmental Prediction
NOAA	National Oceanic and Atmospheric Administration
NTE	Number of Thunderstorm Outflow Event
NTR	Number of Thunderstorm Outflow Record
NTO	Overall number of the records detected during thunderstorm events
NWP	numerical weather prediction
PDF	Probability Density Function
POT	Peak-over-threshold

PSD	Power Spectral Density
RANS	Reynolds Averaged Navier–Stokes
RH	Relative Humidity
SEVIRI	Spinning Enhanced Visible & Infrared Imager
SP	La Spezia
SRH	The Storm-Relative Helicity
SV	Savona
SWEAT	Severe Weather Threat Index
T	Thunderstorm Outflow
TEMP	Temperature
THUNDERR	Detection, Simulation, Modelling, and Loading of Thunderstorm Outflows to Design Wind-safer and Cost-efficient Structures
UTC	Universal Time Coordinated
WI	the Wind Index (WINDEX)
WinDyn	the Wind Engineering and Structural Dynamics
WindEEE	The Wind Engineering Energy and Environment Dome at Western University
WP	‘Wind and Ports’ Project
WPS	‘Wind, Ports and Sea’ Project

List of Notation

a_K	Scale factor for type I distribution
$\boldsymbol{C}$	Storm's translation velocity
f	Probability density function
F	Cumulative distribution function
G	Gust factor
h	Height of anemometer above ground level
H_M	Height of the melting level above ground
I	Turbulence intensity
$\boldsymbol{k}$	Unit vector in the vertical direction
K	One kind of the storm phenomenon (D, T or IN)
L_u	Integral length scale of the longitudinal reduced turbulence components
L_v	Integral length scale of the lateral reduced turbulence components
L_U	Integral length scale of the horizontal resultant reduced turbulence components
m	Mean value
N_K	Average number of independent extreme peak wind speed values in one year for the K phenomenon
Q_L	Mixing ratio in the first 1 km above the surface
Q_M	Mixing ratio at the melting level
R	Return period
S	Power spectral density
t	Time
T	Time period
u	Longitudinal component of the wind velocity

$\bar{u}$	Longitudinal mean average velocity
u'	Longitudinal turbulent fluctuation
$\hat{u}$	1-s horizontal resultant peak wind velocity
$\tilde{u}'$	Reduced longitudinal turbulence component
u_K	Mode factor for type I distribution
U	Horizontal resultant wind speed
$\overline{U}$	Mean horizontal resultant wind speed
U'	Horizontal resultant turbulent fluctuation
$\widehat{U}$	1-s horizontal resultant peak wind velocity
$\widetilde{U}'$	Reduced horizontal resultant turbulence component
$\overline{U}_{max}$	Maximum value of the moving average wind speed
U_{m1}	Maximum mean wind velocity averaged over 1-min
U_{m10}	Mean wind velocity in 10 min
U_{m60}	Mean wind velocity in 1 h
v	Lateral components of the wind velocity
v'	Lateral turbulent fluctuation
$\bar{v}$	Lateral mean average velocity
$\tilde{v}'$	Reduced lateral turbulence component
$\boldsymbol{V}$	Environmental wind vector
V_X	Measured wind speed directed from West to East
V_Y	Measured wind speed directed from South to North
V_Z	Vertical and positive upwards
$\bar{V}_{\mathrm{X}}$ and $\bar{V}_{\mathrm{Y}}$	Mean values of V_{X} and V_{Y} over the time interval ΔT
V'_{X} and V'_{Y}	Residual turbulent fluctuations of V_{X} and V_{Y} with respect to $\bar{V}_{\mathrm{X}}$ and $\bar{V}_{\mathrm{Y}}$.
$\boldsymbol{V}$	Environmental wind vector
z	Height above ground
z_0	Surface roughness length
	Greek letters
α	Clockwise directional angle, computed from *Y* (North)
$\bar{\alpha}$	Moving average wind direction
β	Anti-clockwise directional angle, computed from *X* (East)
γ	Skewness
κ	Kurtosis
σ	standard deviation

τ	Time period
γ	Non-dimensional function of t that describes the slow variation of moving average velocity
μ	Non-dimensional function of t that describes the slow variation of turbulent intensity
Γ	Temperature lapse rate from the surface to the melting point
ρ	Cross-correlation coefficient

1 Introduction

1.1 Background and significance

A primary aim of politics, science, and technology is to pursue the safety and cost-efficiency of built-up environments exposed to natural hazards by forecasting catastrophic events, assessing their precursors, and evaluating and managing the risks they cause. Wind is the most destructive natural phenomenon, over 70 % of the damage and deaths caused by nature are due to the wind (Tamura and Cao, 2012; Ulbrich et al., 2013), so the evaluation of its actions is crucial to guarantee the safety and limit the cost of structures, infrastructure and territory management, thus representing a cornerstone in the field of civil engineering and atmospheric sciences and a societal need.

A climatological condition in which wind phenomena of different natures coexist, for example, extra-tropical and tropical cyclones, monsoons, tornadoes, downslope winds, and thunderstorms, is referred to as a mixed wind climate (Gomes and Vickery, 1977/1978). Extra-tropical cyclones are the most typical events that strike the mid-latitude areas. Tropical cyclones, monsoons, tornadoes, and downslope winds are key features of the wind climate of specific zones. Thunderstorms occur almost everywhere. At any given time approximately 2,000 thunderstorms are occurring on Earth (Choi and Hidayat, 2002a) and more than 50,000 thunderstorms occur each day throughout the world, hence, over 18 million occur annually (Ahrens, 2009). The European wind climate and that of many countries at the mid-latitudes is dominated by extra-tropical cyclones (Deroche et al., 2014) (**Figure 1.1 (a)**) and thunderstorms (Letchford et al., 2002) (**Figure 1.1 (b)**).

(a) (b)

Figure 1.1 Synoptic extra-tropical cyclone (a, © 2018 EUMETSAT) and mesoscale thunderstorm downburst (b, photo by Mike Hollingshead, www.extremeinstability.com, last access: 20 July 2018).

The polar front theory (Bjerknes and Solberg, 1922) explains and describes the

genesis and life cycle of extratropical cyclones. These are synoptic phenomena that develop in a few days on a few thousand kilometres (**Figure 1.1(a)**). The surface velocity field in extra-tropical cyclones is characterized by a mean wind profile in equilibrium with an atmospheric boundary layer whose depth is of the order of magnitude of 1–3 km. Here, within time intervals between 10 min and 1 h, turbulent fluctuations are stationary and Gaussian. Davenport (1961) identified the most intense wind events with the extra-tropical cyclones and introduced a model, based on this hypothesis, to determine the wind loading of structures. After over half century from the Davenport's model definition, it is still a foundation of wind engineering (Simiu and Scanlan, 1996; Holmes, 2015).

The modern study of thunderstorms started when Byers and Braham (1949) proved that these events are mesoscale phenomena that develop over a few kilometres (**Figure 1.1(b)**). They consist of convective cells that evolve in about 30 min through three stages in which an updraft of warm air is followed by a downdraft of cold air. Fujita (1985) showed that the transient downdraft that impinges on the ground produces radial outflows (**Figure 1.2**) that, even though in most cases do not produce really damaging winds, can be as high as about 75 m/s (Fujita, 1990). The whole of these air movements is called downburst and is referred to as a macroburst or a microburst depending on whether the downdraft diameter is greater or smaller than 4 km, respectively. Radial outflows exhibit non-stationary and non-Gaussian wind speed properties, and a vertical "nose profile" that increases up to about 50–100 m height, then decreases above, as shown in **Figure 1.3**. These studies gave rise to an extraordinary fervour of research in atmospheric science (Goff, 1976; Wakimoto, 1982; Hjelmfelt, 1988).

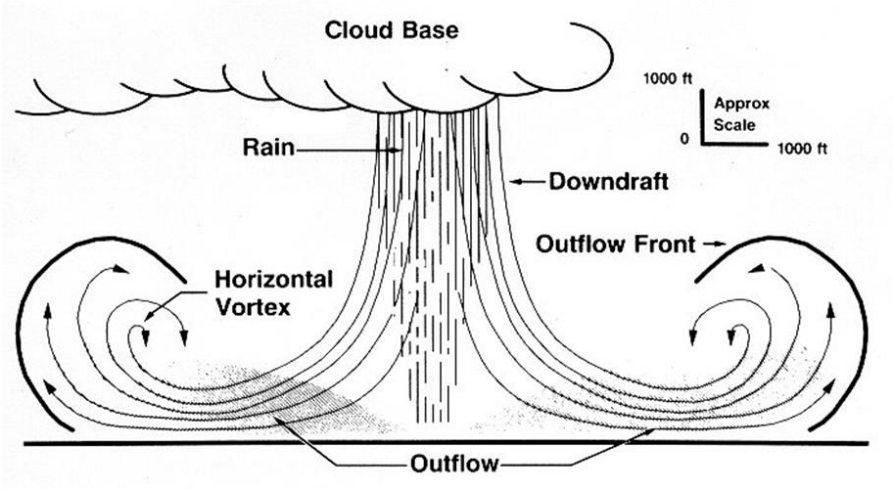

Figure 1.2 Downburst (Fujita, 1981, 1985, 1990).

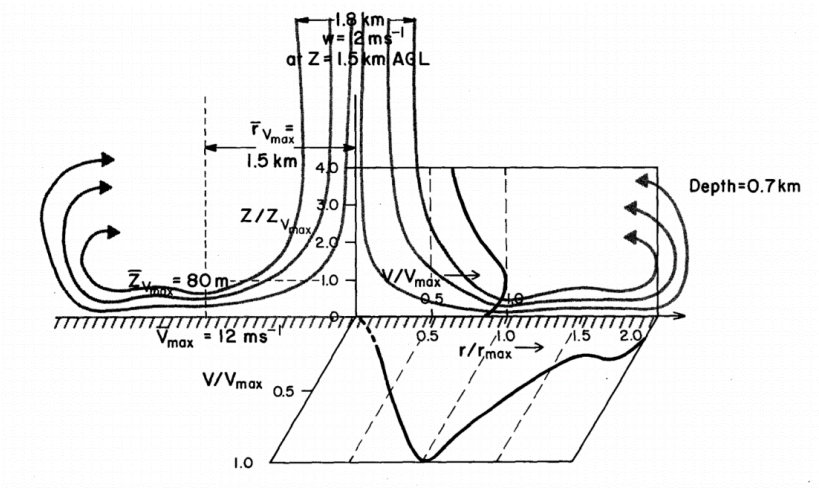

Figure 1.3 Scheme of a thunderstorm downburst and nose velocity profile in the radial outflow (adapted from Hjelmfelt, 1988).

In the same period, wind engineering realized that many catastrophic wind events (**Figure 1.4**) that strike the mid-latitudes areas are often due to thunderstorm outflows (Letchford et al., 2002). Hence, an extensive research arose, dual to the one that took place in atmospheric science, along four main directions (Solari, 2014): (1) wind statistics in mixed climates (Gomes and Vickery, 1977/1978; Kasperski, 2002); (2) monitoring and data analysis (Choi and Hidayat, 2002a; Holmes et al., 2008; Lombardo et al., 2014; Gunter and Schroeder, 2015; Yu et al., 2016); (3) modelling and simulation via wind tunnel tests (Letchford et al., 2002; Mason et al., 2005, 2010; Xu and Hangan, 2008; McConville et al., 2009), computational fluid dynamics (Selvam and Holmes, 1992; Kim and Hangan, 2007; Vermeire et al., 2011a; Zhang et al., 2013; Aboshosha et al., 2015; Karmakar et al., 2017) and analytical methods (Oseguera and Bowles, 1988; Vicroy, 1992; Holmes and Oliver, 2000; Li et al., 2012; Abd-Elaal et al., 2014; Chen and Letchford, 2004a); (4) wind actions on ideal systems (Choi and Hidayat, 2002b; Chen and Letchford, 2004b; Chen, 2008; Kwon and Kareem, 2009; Le and Caracoglia, 2015) and real structures (Darwish et al., 2010; Aboshosha and El Damatty, 2015; Elawady et al., 2017).

However, despite this huge amount of research, this matter is still dominated by large uncertainties; furthermore, there is not yet a shared model of thunderstorm outflows and their actions on structures like that developed by Davenport (1961) for extra-tropical cyclones. This happens because the complexity of the thunderstorm downbursts makes it difficult to establish physically realistic and simple engineering schemes, their short duration and small size means few data are available, and a large gap exists between wind engineering and atmospheric science. It follows that the wind loading of structures is still evaluated by the Davenport's model without any concern for the real nature and the properties of the meteorological event that causes the loading. This is nonsense because extra-tropical cyclones and thunderstorm outflows are different phenomena that need separate assessments (Solari, 2014). Moreover, in mixed climate environment, the latter are often more violent than the

former. Therefore, if the influencing factors of thunderstorms are ignored, it is likely to lead to the unsafety of building due to the underestimation of the design wind speed, or result in the excessive cost because of the blind raise of the design wind speed.

(a) (b) (c)

Figure 1.4 Damages caused by the thunderstorm downburst that occurred in the Port of Genoa (Italy) on 31 August 1994.

The research on thunderstorm outflows carried out by the Wind Engineering and Structural Dynamics (WinDyn) Research Group (www.windyn.org, last access: 29 August 2018) at the University of Genoa takes cue from two European Projects, i.e. "Wind and Ports" (WP) (2009–2012) (Solari et al., 2012) and "Wind, Ports and Sea" (WPS) (2013–2015) (Repetto et al., 2018), financed by the European Cross-border Cooperation Program "Italy–France Maritime 2007–2013". They handled the problem of the safe management and risk assessment of North Tyrrhenian seaport areas with respect to strong wind conditions through a joint cooperation between the Windyn group – the unique scientific partner in these projects – and the port authorities of Genoa, Savona – Vado Ligure, La Spezia, Livorno (Italy) and Bastia – L'Île-Rousse (France). In this framework, a wide in situ wind monitoring network has been created that is generating an unprecedented amount of high quality wind measurements, which will be illustrated details in **Chapter 2**. In addition to their institutional role of supporting the activities of port authorities, they represent an unlimited source of information for carrying out scientific research in several different fields.

The analysis of these data shows the presence of recordings due to wind phenomena of a different nature, namely extra-tropical cyclones, thunderstorms outflows, and intermediate events (Kasperski, 2002; Zhang et al., 2018a). Thus, in order to focus on the study of intense thunderstorm outflows, a semi-automatic procedure was implemented to recognize and extract these phenomena (De Gaetano et al., 2014). This approach is consistent with previous procedures developed and calibrated in order to process a huge amount of data, based on a few synthetic elements, derived from the sole anemometric recordings (Riera and Nanni, 1989; Twisdale and Vickery, 1992; Choi and Tanurdjaja, 2002; Kasperski, 2002; Duraño na et al., 2007; Lombardo et al., 2009), without carrying out systematic and prohibitive meteorological surveys of the weather scenarios out of which they took place. According to this criterion, a small set of records labelled as thunderstorms has been gathered and subjected to probabilistic signal analyses aiming at evaluating their main properties relevant to the wind loading of structures (Solari et al., 2015a). These properties have formed the

base on which two novel methods have been proposed to determine the structural response to thunderstorm outflows (Solari et al., 2015b, 2017; Solari, 2016).

Despite its inherent advantages and merits, there are still some aspects worth discussing, improving and opening:

(1) The past analysis is based on a small number of thunderstorm outflows for preliminary understanding this phenomenon and foundation of the further research;

(2) The separation and classification procedure should be improved as the data increases;

(3) As increase with the number of thunderstorm outflows detected, gathering all the records with different duration together may be not appropriate for learning exactly their properties.

(4) Almost all the existing analysis about the thunderstorm signals are related to the horizontal resultant velocity and ignore the direction or give it a qualitative definition, namely the classical decomposed method, while direction surely is a crucial factor.

(5) It misses the knowledge of the weather scenarios that occur during events classified as thunderstorms, without recognizing their actual meteorological nature.

(6) The design wind speed in a mixed climate region where thunderstorm is often more intense than cyclonic ones may result in considerably imprecise and especially unsafe without the consideration of this intense phenomenon.

(7) There have been no comparative analysis about thunderstorm properties learning if they are similar in the different areas of the world.

In order to take the first step towards refining, deepening and extending the current research, the PhD thesis, thanks to the more and more data and advancement of the technology as time goes on and the support of the European “THUNDERR” project and Chinese “111” project, aims to improve the separation approach, to detect an extensive number of thunderstorm records with high resolution, to classify them and create a catalogue considering the duration of the gust front passage for discussing the characteristics of thunderstorm outflow in more detail, to formulate a novel signal decomposition method making it possible to analyse quantitatively the directional shift of thunderstorm outflows and fully coherent with synoptic winds, to study their main characteristics related to wind loads on structures accordingly, which is strategic to carry out directional analyses of the dynamic behaviour of structures in terms of alongwind and crosswind response and to accurately simulate thunderstorms, to learn their meteorological properties according to several cases in the catalogue for building a foundation for improving the qualitative judgment method which can be widely used in a large number of thunderstorm outflows and creating a bridge between atmospheric physics and wind engineering, to exploit the method to understand the extreme wind speed distribution in a mix wind climate based on the limited number of the available years of wind measurements, and to apply the similar analysis to the data from Beijing urban area and complete a preliminary comparison providing a preliminary answer to the crucial question if thunderstorms in different areas have similar properties. The results obtained from this research can contribute to formulate a novel, interdisciplinary and unitary model of thunderstorm outflows, with the dual

prospect of being itself a challenging scientific result and, at the same time, of being a robust basis to carry out engineering analyses with a ground-breaking impact on construction and society.

1.2 Evolution of thunderstorm

Thunderstorm is a type of storm characterized by the presence of lightning and thunder and sometimes producing gusty surface winds with heavy rain and hail as shown in **Figure 1.5** (Fujita, 1985; Letchford et al., 2002).

(a) (b)

Figure 1.5 Pictures of thunderstorm (a) http://tech.ifeng.com/a/20180417/44956723_0.shtml; (b) http://www.thunderr.eu/.

The storm itself may be a single cumulonimbus cloud, or several thunderstorms may form into a cluster. In some cases, a line of thunderstorms will form that may extend for hundreds of kilometers (Ahrens, 2009). They are convective storms that form with rising air. So the birth of a thunderstorm typically involves warm, moist air rising in a conditionally unstable environment. The rising air may be a parcel of air ranging in size from a large balloon to a city block. Or an entire layer, or slab of air, may be lifted. As long as the rising air is warmer (less dense) than the air surrounding it, there is an upward-directed buoyant force acting on it. The warmer the parcel is compared to its surroundings, the greater the buoyant force and the stronger the convection. The trigger (or"forcing mechanism") needed to start air moving upward may be:

(1) random, turbulent eddies that lift small bubbles of air;
(2) unequal heating at the surface;
(3) the effect of terrain (such as small hills) or the lifting of air along shallow boundaries of converging surface winds;
(4) large-scale uplift along mountain barriers and rising terrain;
(5) diverging upper-level winds, coupled with converging surface winds and rising air;
(6) warm air rising along a frontal zone.

All thunderstorms, regardless of type, go through three stages: the developing stage or cumulus stage, the mature stage, and the dissipation stage (Mogil, 2007; Battan, 1961). The average thunderstorm has a 24 km diameter. Depending on the conditions present in the atmosphere, each of these three stages take an average of 30 minutes.

Developing stage/Cumulus stage: The first stage of a thunderstorm is known as the cumulus stage or developing stage as shown in **Figure 1.6 (a)**. During this stage, a parcel of warm, humid air are lifted upwards into the atmosphere due to the trigger. The moisture carried upward cools into liquid water droplets and ice crystals due to lower temperatures at high altitude, which appear as cumulus nimbus clouds. As the water vapor condenses into liquid, latent heat is released, which warms the air, causing it to become less dense than the surrounding, drier air. The air tends to rise in an updraft through the process of convection. This process creates a low-pressure zone within and beneath the forming thunderstorm. As the cloud builds above the freezing level, the cloud particles grow larger and become heavier.

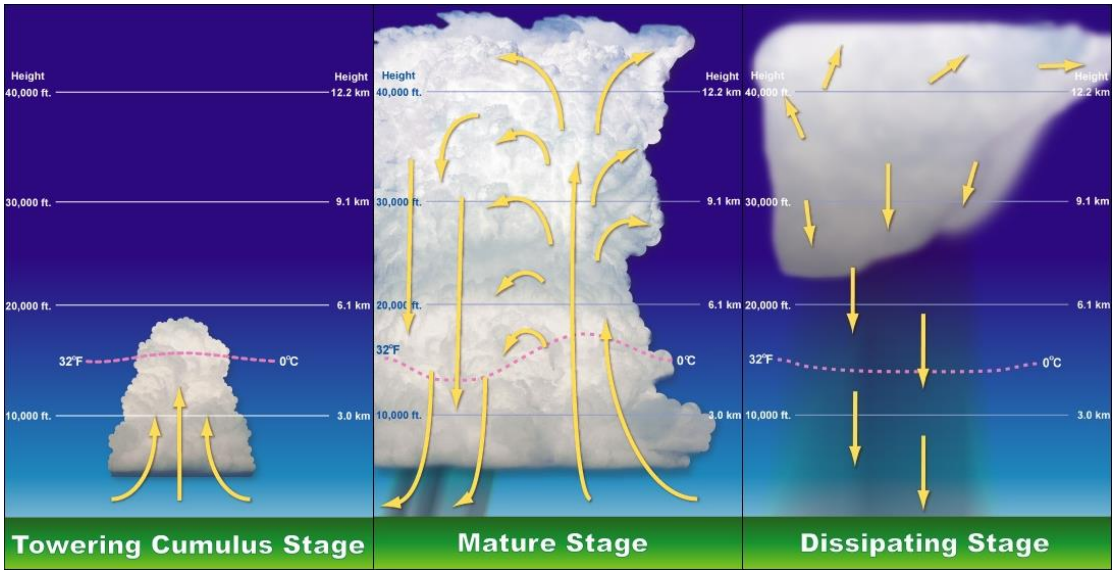

(a) (b) (c)

Figure 1.6 Stages of an isolated cell (wikipedia).

Eventually, the rising air is no longer able to keep these water and ice particles suspended, as and they begin to fall through the updraft. While this is happening, drier air from around the cloud is being drawn into it in a process called entrainment, which evaporates some of the raindrops, chilling the air. The air, colder and heavier than its surrounding, begins to descend as a downdraft, which may be enhanced as falling precipitation of raindrops and ice particles drags some of the air along it (Ahrens, 2009).

Mature stage: The appearance of the downdraft marks the beginning of the mature stage (**Figure 1.6 (b)**), at which the storm is usually most intense. The downdraft and updraft within the mature thunderstorm now constitute the cell. In some storms, there are several cells, each of which may last for less than 30 minutes.

The top of the cloud, having reached a stable region of the atmosphere (which may be as high as the stratosphere), begins to take on the familiar anvil shape, as upper-level winds spread the cloud's ice crystals horizontally as shown in **Figure 1.6 (b)**. The cloud itself may extend upward to an altitude of over 12 km and be several kilometers

in diameter near its base. Updrafts and downdrafts are strongest in the middle of the cloud, creating severe turbulence lightning and thunder are also present in the mature stage. Heavy rain (and occasionally small hail) often falls from the cloud. And, at the surface, there is often a downrush of cooler air with the onset of precipitation.

Where the cold downdraft reaches the surface, the air spreads out horizontally in all directions. The surface boundary that separates the advancing cooler air from the surrounding warmer air is called a *gust front* as shown in **Figure 1.7**. Along the gust front, winds rapidly change both direction and speed. Look at **Figure 1.6 (b)** and notice that the gust front forces warm, humid air up into the storm, which enhances the cloud's updraft. In the region of the downdraft, rainfall may or may not reach the surface, depending on the relative humidity beneath the storm. In the dry air of the Desert Southwest, for example, a mature thunderstorm may look ominous and contain all of the ingredients of any other storm, except that the raindrops evaporate before reaching the ground. However, intense downdrafts from the storm may reach the surface, producing strong, gusty winds and a gust front.

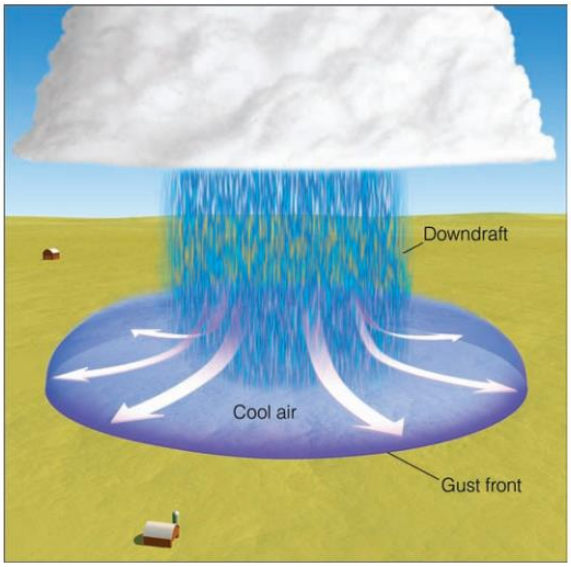

Figure 1.7 When a thunderstorm's downdraft reaches the ground, the air spreads out, forming a gust front.

Dissipation stage: In the dissipation stage (**Figure 1.6**), the thunderstorm is dominated by the downdraft (Letchford et al., 2002). If severe weather occurs, it usually takes place near the transition from the mature to dissipating stages, or about the time when the maximum fallout of precipitation occurs. During this stage, the downdraft tends to cut off the supply of warm humid air required to form cloud droplets (Ahrens, 2009). In the case of isolated cells, the precipitation falls through the updraft rather than being deposited away from the updraft, and the associated hydrometeor loading reduces updraft buoyancy (Duraña, 2015). The updraft then weakens and the downdraft tends to dominate the cell. The downdraft will push down out of the thunderstorm, hit the ground and spread out creating an outflow boundary.

This phenomenon is known as a *downburst*, and when the stationary downburst is combined with the translational movement of the thunderstorm cell, it will present an inclined jet as shown in **Figure 1.8**, a potential hazardous condition for aircraft to fly through, as a substantial change in wind speed and direction occurs, resulting in a decrease of airspeed and the subsequent reduction in lift for the aircraft. The cool air carried to the ground by the downdraft cuts off the inflow of relatively warm, moist air, the updraft disappears and the thunderstorm will dissipate.

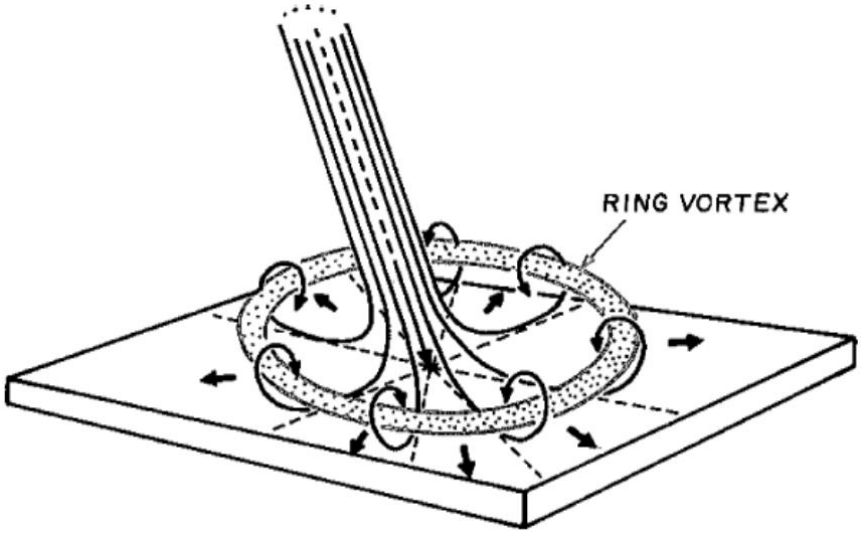

Figure 1.8 Downburst model (Fujita, 1985).

The length scale of the area affected by high winds is characterised, they are sometimes referred to as microbursts or macrobursts. Weisman (2003), for example, defines a downburst as an event that presents diverging outflows with wind speeds greater than 25m/s. They can also be classified as wet or dry depending on whether downburst events are accompanied by precipitation or not, respectively. It has been observed that dry downbursts are typically produced in high-based cumulonimbus or altocumulus clouds (Wakimoto, 1985), whereas wet downbursts are usually associated with well-developed thunderstorms (Atkins and Wakimoto, 1991; Straka and Anderson, 1993). Dry downbursts occur when the ambient temperature lapse rate below the cloud base is close to dry adiabatic or even superadiabatic in the surface boundary layer (Wakimoto, 1985). While descending below the cloud base, the downdraft temperature first increases following the moist-adiabatic lapse rate until all raindrops evaporate, after which the temperature follows the dry-adiabatic lapse rate. In contrast to this dry microburst sounding model, the subcloud dry-adiabatic layer is shallower and the lower-atmospheric levels are moister when wet downbursts occur (Proctor, 1989).

There are four main types of thunderstorms: single-cell, multi-cell, squall line (also called multi-cell line) and supercell. Which type forms depends on the instability and relative wind conditions at different layers of the atmosphere ("wind shear").

Single-cell Thunderstorm This term technically applies to a single thunderstorm with

one main updraft as shown in **Figure 1.9 (a)**. Also known as air-mass thunderstorms, these are the typical summer thunderstorms in many temperate locales. They also occur in the cool unstable air that often follows the passage of a cold front from the sea during winter. Within a cluster of thunderstorms, the term "cell" refers to each separate principal updraft. Thunderstorm cells occasionally form in isolation, as the occurrence of one thunderstorm can develop an outflow boundary that sets up new thunderstorm development. Such storms are rarely severe and are a result of local atmospheric instability; hence the term "air mass thunderstorm". When such storms have a brief period of severe weather associated with them, it is known as a pulse severe storm. Pulse severe storms are poorly organized and occur randomly in time and space, making them difficult to forecast. Single-cell thunderstorms normally form in environments of low vertical wind shear and last only 20 – 30 minutes.

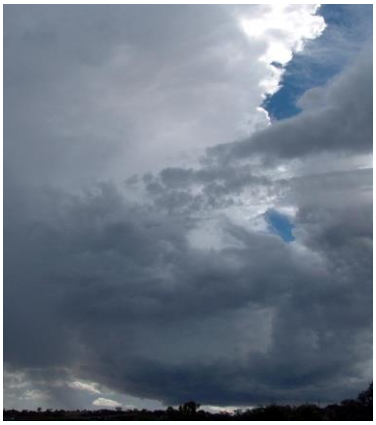

(a)

(b)

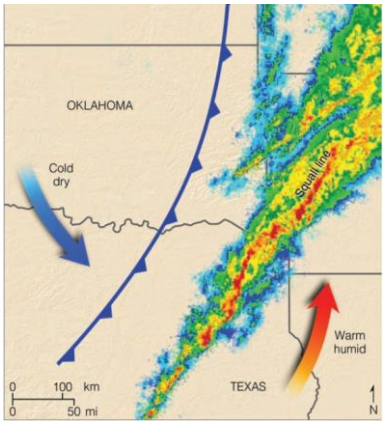

(c)

(d)

Figure 1.9 (a) A single-cell thunderstorm over Wagga Wagga (https://en.wikipedia.org/wiki/Thunderstorm) (b) Multi-cell thunderstorm (c) Squall line (d) Supercell thunderstorm (Ahrens, 2009).

Multi-cell Thunderstorm This is the most common type of thunderstorm development. Multi-cell thunderstorms contain a number of cells, each in a different stage of development. Such storms tend to form in a region of moderate-to-strong vertical wind speed shear. For example, as shown in **Figure 1.9 (b),** this multi-cell storm complex is composed of a series of cells in successive stages of growth. The

thunderstorm in the middle is in its mature stage, with a well-defined anvil. Heavy rain is falling from its base. To the right of this cell, a thunderstorm is in its cumulus stage. To the left, a well-developed cumulus congestus cloud is about ready to become a mature thunderstorm. With new cells constantly forming, the multi-cell storm complex can exist for hours. Long-lasting multi-cell storms can become intense and produce severe weather for brief periods. Hazards with the multi-cell cluster include moderate-sized hail, flash flooding, and weak tornadoes.

Squall-Line Thunderstorm Multi-cell thunderstorms may form as a line of thunderstorms, called a squall line. The line of storms may form directly along a cold front and extend for hundreds of kilometers, or the storms may form in the warm air 100 to 300 km out ahead of the cold front. These prefrontal squall-line thunderstorms of the middle latitudes represent the largest and most severe type of squall line, with huge thunderstorms causing severe weather over much of its length (Ahrens, 2009). They generally contains heavy precipitation, hail, frequent lightning, strong straight line winds, and possibly tornadoes and waterspouts. As shown in **Figure 1.9 (c),** Doppler radar display superimposed on a map shows a prefrontal squall line extending from Texas into Oklahoma and Arkansas during February 2011. Some of the thunderstorms embedded within the squall line (dark red and orange color) produced high winds, heavy rain, and large hail.

Supercell thunderstorm In a region where there is strong vertical wind shear (speed and/or directional shear), a thunderstorm may form in such a way that the outflow of cold air from the downdraft never undercuts the updraft. In such a storm, the wind shear may be so strong as to create horizontal spin, which, when tilted into the updraft, causes it to rotate. An intense, long-lasting thunderstorm with a single violently rotating updraft is called a supercell. Storms of this type are capable of generating an updraft that may lead to damaging surface winds and the formation of strong tornadoes. As presented in **Figure 1.9 (d)**, a tornado descends from beneath a low-precipitation supercell thunderstorm in eastern Colorado on June 10, 2010. The internal structure of a supercell is organized in such a way that the storm may maintain itself as a single entity for hours.

Thunderstorms can form and develop in any geographic location, even in polar and desert regions. It is estimated that more than 50,000 thunderstorms occur each day throughout the world. Hence, over 18 million occur annually. Until now, the only place where thunderstorms have never occurred is in the Atacama Desert in northern Chile, South America, where the weather is too dry and rain clouds are difficult to form. And they can occur most frequently within the mid-latitude, where warm, moist air from tropical latitudes collides with cooler air from polar latitudes.

Thunderstorms, and the severe weather phenomena that occur along with them, pose great hazards (Choi, 2000; Orwig and Schroeder, 2007; Kwon and Kareem, 2009; Solari et al., 2015a). Damage resulting from them is mainly inflicted by downburst winds, large hailstones, and flash flooding caused by heavy precipitation. Stronger thunderstorm cells are capable of producing tornadoes and waterspouts as illustrated before. Many structural damage and life-threatening disasters induced by

thunderstorms have been recorded around the world (Zhang et al., 2019b).

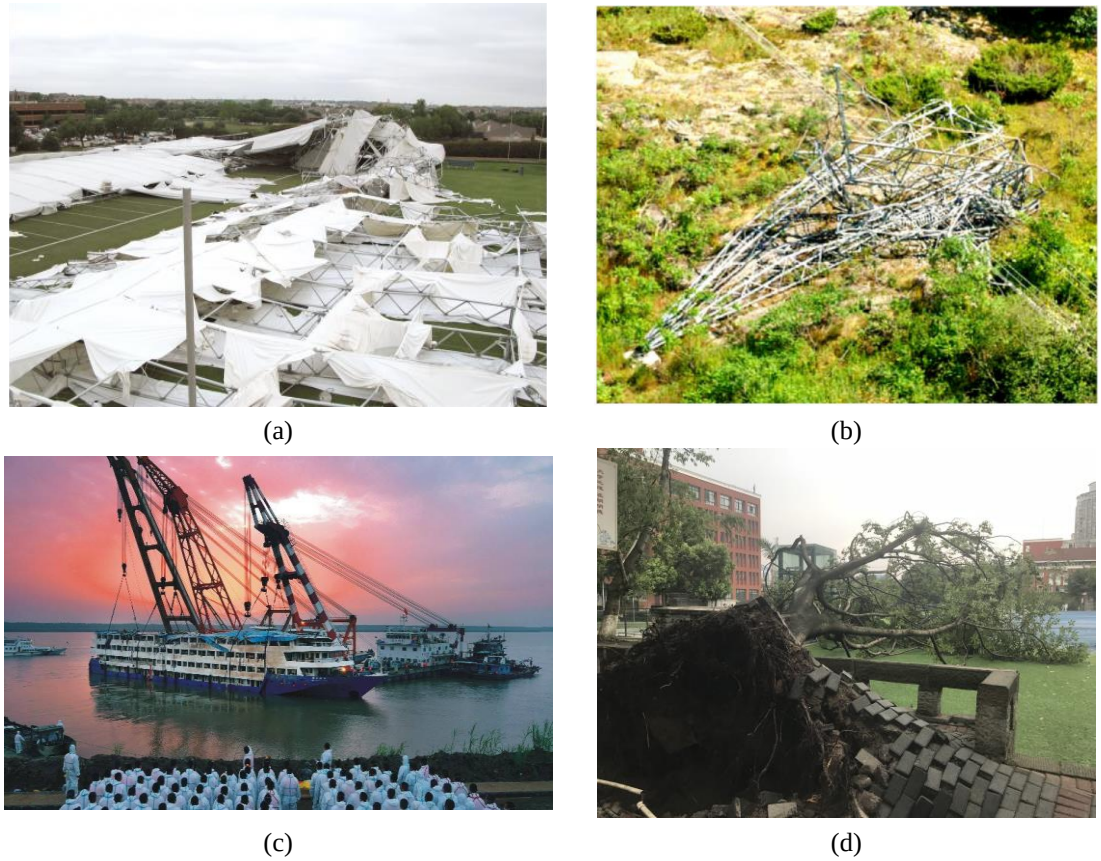

(a) (b)

(c) (d)

Figure 1.10 The hazards due to thunderstorm. (a) Electric power pylon The Dallas Cowboys practice facility http://www.sgh.com/projects/dallas-cowboys-training-facility#solution; (b) Guyed tower failure in Ontario (Elawady, 2017); (c) http://jianli.gov.cn/item/7222.aspx, By Peng Zhang; (d) Falling tree in University of Chongqing, By Yukio Tamura.

In the central areas of the United States, thunderstorms dominated the wind climate at return periods of about 50 years or larger (Twisdale and Vickery, 1992). On 2 May 2009, the Dallas Cowboys Training Facility, located in in Texas, America, collapsed during high winds by thunderstorm downburst (Trautner et al., 2013), which fell on approximately seventy people, trapping some under the rubble as shown in **Figure 1.10 (a)**. Letchford and Ghosalkar (2004) also found the domination of thunderstorms in wind climate in West Texas. Different design guidelines (CIGRÉ, 2012; AS/NZS 7000, 2010) have highlighted the fact that thunderstorm downburst and tornado events are the main cause of transmission line failures in various countries, for example Canada (McCarthy and Melsness, 1996), China (Zhang, 2006), Australia (Australian Wind Alliance, 2016) and so on. As shown in **Figure 1.10 (b)**, two 500kV single circuit guyed towers collapsed during a severe thunderstorm in August 2006, and belonged to Hydro One, Ontario, Canada. Holmes (2015) stated that thunderstorms dominated the climate at return periods of 100 years and greater in Melbourne. There are more than one hundred thunderstorms days in one year recorded in Singapore often producing significant strong and gusty surface winds (Choi and Tanurdjaja,

2002). Kasperski (2002) illustrated that the wind climate in Germany was mainly governed by frontal depressions and thunderstorms. Gomes and Vickery (1977) showed thunderstorms dominated the wind climate of Australia when hurricanes were excluded. Hawes and Dempsey (1993) carried out a survey of the destruction reason of 94 power pylons in Australia, which was found that more than 90 percent of the damage was due to downburst or tornadoes caused by thunderstorm. It is also the main disastrous weather in Beijing, China. In July 22, 1997, 27 houses were destroyed and dozens of trees up to 40cm in diameter were blown up by a thunderstorm downburst (Liu, 2001). At about 2132 BT, June 1, 2015, 'Oriental Star' cruise from Nanjing for Chongqing (**Figure 1.10 (c)**) suffers severe stormy weather, which is confirmed to be a sudden downburst of squall line weather, when sailing in the Yangtze River near Jianli County, resulting in 442 people killed (Duan et al., 2017). There was one tree uprooted during a transient thunderstorm in Chonqing University on August 6, 2018 as shown in **Figure 1.10 (d)**.

They are in fact the dominant wind type for structural design in many parts of the world (Holmes et al., 2005), especially in mid-latitudes, as in some regions of North America (Vega and Letchford, 2009), South America (Durañona, 2011; Natalini et al., 2012; Riera, 2013), South Africa (Kruger et al., 2010), Australia or New Zealand (AS/NZS 7000, 2010). While the methods currently used to determine the wind actions on structures are still mostly based on the synoptic extratropical cyclone model introduced by Davenport (1961); this model assumes neutral atmospheric conditions, statistical stationarity features and wind velocity profiles in equilibrium with the atmospheric boundary layer (ABL). Thunderstorm outflows are transient phenomena at the mesoscale (Fujita, 1985 and 1990) that occur in convective conditions with ''nose'' velocity profiles (Goff, 1976) (**Figure 1.11 (a)**) totally different from those that are typical of the ABL (**Figure 1.11 (b)**). Therefore, the study of thunderstorm outflows and their loading of structures is a key topic of modern wind engineering (Letchford et al., 2002; Solari, 2014), and the fundamental step is to detect accurate data of thunderstorm to learn their property and propose appropriate methods to define the design wind speed in mixed climate that thunderstorm outflows play a key role based on limited measured data.

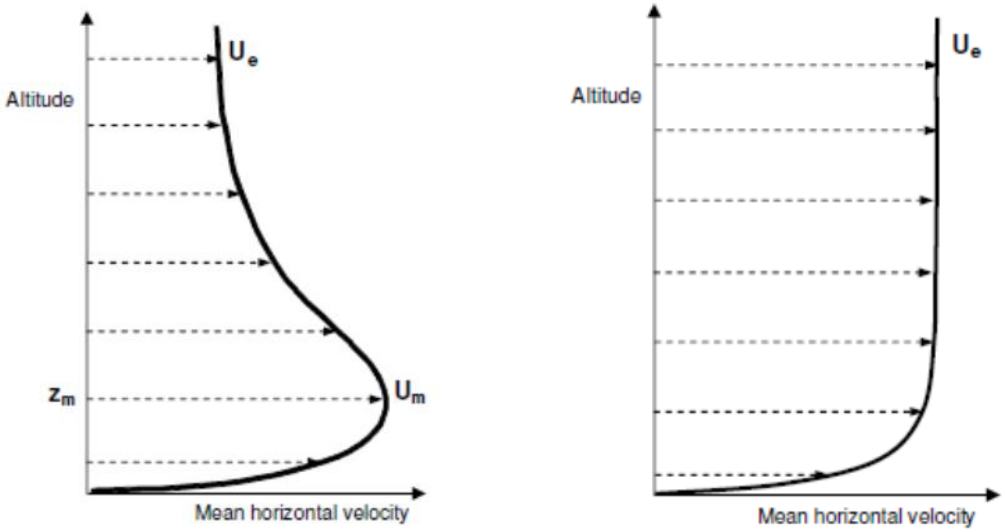

(a) (b)

Figure 1.11 Expected wind speed profiles for (a) a downdraft outflow (from Lin, 2010) and (b) a flow of ABL type.

1.3 Literature review

Scholars from all over the world have adopted various methods to carry out the relevant research on thunderstorms these years, which mainly includes field measurement, theoretical analysis model, experimental simulation and numerical simulation. Three aspects of the state of the art about thunderstorm are summarized here relevant the research of this PhD thesis: 1) wind statistics and climate; 2) thunderstorm wind characteristics and 3) extreme wind speed analysis.

1.3.1 Wind statistics and separation

In mixed wind climates, the separation and classification of intense wind events into homogeneous families is a crucial aspect to determine sound distributions of the extreme wind velocity, to learn the characteristics of some kind of wind storm and to carry out homogenous analyses of the wind-excited response of structures.

With reference to statistical analysis, the research on wind statistics and climate separation began in 1967 when Thom (1967) first proposed to deal with the mixed populations of extra-tropical and tropical cyclones by means of two combined distributions, then showed that one third of the yearly peak wind velocities in U.S. occur during thunderstorms (Thom, 1968a). Gomes and Vickery (1976) carried out a study of the extreme wind velocities in Australia, in which they separated thunderstorm from non-thunderstorm winds, determined the distributions of these two phenomena and derived a mixed distribution. Also Riera et al. (1977) first represented thunderstorms and cyclones by different distributions, then they combined such distributions into a unique mixed distribution. Gomes and Vickery (1977/1978)

extended the above formulations to mixed climates including several phenomena of different nature, namely extra-tropical pressure systems, thunderstorms, hurricanes and tornadoes; in addition to increasing the accuracy, they noted that the separate analysis of different phenomena enables the use of statistical models especially suited to each phenomenon; this paper is a milestone of this topic. Twisdale and Vickery (1992), Choi (1999), Choi and Hidayat (2002a) and Lombardo et al. (2009) separated thunderstorm from nonthunderstorm winds, determined the distributions of the maximum wind velocity of each phenomenon, and combined them into a mixed distribution. Choi and Tanurdjaja (2002) performed the same operation by separating large scale phenomena, identified with monsoons, from small scale phenomena, including squall lines and thunderstorms. The role of the thunderstorm size in evaluating its occurrence probability at a site was examined by Oliver et al. (2000) and Li (2000). Kasperski (2002) first introduced the idea that in temperate climates at mid latitudes, thunderstorms cannot be separated clearly from frontal depressions, since a third class of phenomena exist, called gust fronts, with intermediate properties; therefore he applied mixed statistics to these three families of events; he also proposed a criterion to subdivide the data belonging to different phenomena, whose application is strongly conditioned by the effectively available measures. Cook et al. (2003) extended the theory of Gomes and Vickery (1977/1978) in a wider and more general analytical and operative framework Lombardo et al. (2009) investigated the separation between thunderstorm and non-thunderstorm winds, implementing an automated method for U.S.A..

The methods for the separation and classification of intense wind events may be subdivided into two families mainly associated with the meteorological and wind engineering sectors.

The first family of methods is aimed at examining specific phenomena of relevant interest through detailed inspections and reconstructions of the meteorological conditions that occurred in such events. For this reason, it relies on the surface measurement of the main meteorological parameters, radar and satellite images, soundings, and any other suitable data to clarify the atmospheric conditions. Charba (1974) studied an intense gust front that occurred in Oklahoma on 31st May 1969 by anemometers, thermometers, barometers and hygrometers mounted above or around a 444 m high transmission tower; he also used radar images. Goff (1976) carried out the analysis of the outflows of 20 thunderstorms that occurred in Oklahoma between 1971 and 1973; he used the meteorological instruments put on a 461 m high tower and the radar images acquired by the National Severe Storm Laboratory. Wakimoto (1982) examined the life cycle of thunderstorms in the framework of the Project NIMROD; the data is provided by 3 doppler radars and 27 surface stations collecting temperature, pressure and wind velocity; radiosondes were also launched in serial ascents. Sherman (1987) provided a detailed description of a downburst that struck Bald Hills in Queensland on 5th November 1977; for this, he used the wind velocity records acquired at 4 levels of a transmission tower, surface measurements of temperature, pressure and humidity, images provided by the meteorological radar in the airport of

Brisbane, 13.5 km far from the tower. Hjelmfelt (1988) examined the morphology of the downbursts acquired for the 1982 JAWS (Joint Airport Weather Studies) project, adopting doppler radar images, surface measurements of the wind velocity and soundings. Fujita (1990) described the results of the experiments carried out for the projects NIMROD, JAWS and MIST, respectively in 1978, 1982 and 1986; he used between 27 and 81 surface anemometers and 5 doppler radars. Gast and Schroeder (2003) studied the wind records caused by a super-cell that produced a rear-flank downdraft that passed over 7 monitored towers in Lubbock, Texas, on 4th June 2002; this phenomenon was also examined through doppler radars data and meteorological soundings. A detailed analysis of the same phenomenon was carried out by Holmes et al. (2008). Gunter and Schroeder (2015) recently started a research project aimed at furnishing a detailed description of thunderstorms based on surface meteorological measurements and images produced by couples of mobile doppler radars with high space and time resolution.

The second family of methods consists in the systematic separation and classification of the measurements belonging to large wind datasets, with the aim of developing statistical analyses of the extreme wind velocities and their effects on structures. In the light of the huge amount of the examined data, this family of methods rejects the prohibitive idea of providing a detailed meteorological representation of all the wind phenomena that take place. Therefore, synthetic information is adopted, based on the available data, to make the separation and classification process as automatic as possible. Gomes and Vickery (1976) identified the peak values of the thunderstorm winds with the daily peak values of the wind velocity during thunderstorm days. Riera and Nanni (1989) separated thunderstorm from synoptic wind events depending on the duration of the intense event, the occurrence of thunder and lightning, rainfalls and abrupt temperature drops. Twisdale and Vickery (1992) assumed that the maximum daily velocity has thunderstorm origins during thunderstorm days. Holmes (1999) noted that this assumption is often wrong. Choi (1999) and Choi and Hidayat (2002a) distinguished wind phenomena into thunderstorm and non-thunderstorm winds by defining thunderstorms as those events that occur with thunders and rainfalls; they noted also that the gust factor of thunderstorms is always much greater than the gust factor of nonthunderstorm winds. Choi and Tanurdjaja (2002) separated wind phenomena into large- and small-scale events through visual examinations of long wind velocity records. Kasperski (2002) subdivided the data belonging to frontal depressions, thunderstorms and intermediate events, or gust fronts, based on three parameters: the mean wind velocity, the peak wind velocity and the gust factor. Cook et al. (2003) classified as thunderstorm events the daily maximum wind velocities that occurred in the course of days tagged as “thunderstorms seen or thunderstorms heard”. Duraõna et al. (2007) defined as non-synoptic those events that satisfy the following four criteria: the peak velocity is greater than 15 m/s; the ratio between the peak and the mean wind velocity is greater than 1.5; the velocity increases in less than 3 min; the velocity diminishes in less than 10 min. Lombardo et al. (2009) developed an automated procedure, applied to the US datasets acquired through the ASOS network,

in order to separate thunderstorms from non-thunderstorm events; after observing that the manual separation of the data is prohibitive, they formulated a method framed into the following steps: (1) the peak wind velocities are extracted from each dataset; (2) the beginning and the end of each thunderstorm are registered; (3) the peak wind velocities that occur between the beginning and the end of a thunderstorm are associated to thunderstorms, all the other peaks being associated to non-thunderstorm events; (4) two datasets including independent thunderstorm and non-thunderstorm events are created, by defining as independent thunderstorm events those separated by at least 4 h, as independent non-thunderstorm events those separated by at least 4 days. Rowcroft (2011) extracted thunderstorm events from measurements carried out on monitored Australian towers for over 20 years; first, he selected the peak wind velocities greater than 40 m/s; then, he defined as thunderstorms those events that satisfy the following four conditions: (1) they last between 5 and 30 min; (2) the temperature has a drop of -1.5 ℃ or more; (3) there is an increase in wind speed at more than one height of the towers; (4) the wind speed differential is greater than 10 m/s.

Considering the wind-excited response of structures, the separation of the analyses related to different phenomena is mainly associated with their stationary or non-stationary an Gaussian or non-Gaussian properties. Choi and Hidayat (2002b) first discussed the different behaviour of single-degree-of-freedom (SDOF) systems subjected to non-stationary thunderstorms and stationary synoptic winds. Analogous studies were carried out later by Chen and Letchford (2004b) and Chay and Albermani (2005). Kwon and Kareem (2009, 2013) proposed a method through which the dynamic response and the equivalent static force due to non-stationary thunderstorm winds are evaluated as a correction of the corresponding quantities due to stationary synoptic phenomena. Solari et al. (2014) determined the dynamic response of SDOF systems to different families of wind events, focusing on the main differences among the behaviour of structures. Yeo (2011) and Lombardo (2012) separated thunderstorm from non-thunderstorm winds in order to carry out a dataset assisted design of structures in mixed climates. Besides, despite the existence of the above definition and the classification method, due to the local characteristics and randomness of thunderstorm, the methods are not applicable to the measured data of other areas.

For the analysis of measurement from the northern Mediterranean ports of this PhD thesis, at the beginning of the study, the second family of methods is adopted mainly. First the semi-automatic process proposed by De Gaetano et al. (2014) is improved, which is a suitable mix of quantitative controls and qualitative judgments to separate and classify the different local extreme wind events according to their stationary or non-stationary and Gaussian or non-Gaussian properties for the analysis of thunderstorm characteristics related to the wind load of structures and the extreme wind velocity distribution in mixed climate. In the later stage of the study, several typical thunderstorm events extracted by the semi-automatic method are analyzed by combining the technology of the first family, i.e. meteorological survey data, in an

attempt to make a preliminary attempt of interdisciplinary research and learn the weather scenario of thunderstorm.

1.3.2 Thunderstorm wind characteristics

The literature on this matter has followed two complementary pathways. On the one hand, a research line has been developed, of meteorological imprint, which studies the causes, the morphology and the life cycle of thunderstorms also with reference to their classification and other relevant weather scenario (Goff 1976, Fujita 1981, Fujita and Wakimoto 1981, Wakimoto 1982, Wilson et al. 1984, Sherman 1987, Hjelmfelt 1988). On the other hand, in a typical engineering spirit, there has been a proliferation of literatures in accordance with schemes aimed at learning their characteristics interested in evaluating thunderstorm actions on structures (Choi 2000, Choi and Hidayat 2002a, Choi 2004, Gast and Shroeder 2003, Chen and Letchford 2005a, 2005b, 2006, Orwig and Schroeder 2007, Holmes et al. 2008, Durañona et al. 2007, Kasperski 2009, Rowcroft 2011, Gunter and Schroeder 2015, Lombardo et al. 2014).
And the study of thunderstorm wind characteristics has followed four main lines associated with empirical analysis (Oseguera and Bowles, 1988; Vicroy, 1992; Wood et al., 2001), measurements (Choi and Hidayat, 2002a; Chen and Letchford, 2005a and 2006; Orwig and Schroeder, 2007; Holmes et al., 2008; Lombardo et al., 2014; Gunter and Schroeder, 2015; Solari et al., 2015a; Yu et al., 2016), experiments (Hangan et al., 2003; Mason et al., 2005; Chay et al., 2006; Kim and Hangan, 2007; Sengupta et al., 2008; Xu and Hangan, 2008; Aboshosha et al., 2015)and simulations (Chay et al., 2006; Kim and Hangan, 2007; Sengupta et al., 2008). Herein, the literature review about the thunderstorm wind characteristics is along these four lines as following.

1.3.2.1 Empirical models

At the beginning of the systematic study about the thunderstorm, due to the limited number of measured data and the immaturity of the technology of numerical simulation and experimental simulation, the characteristics of the thunderstorm can only be theoretically analyzed according to the empirical model to facilitate the application of these loads during structural analysis and for industrial aviation (Li, 2015).
The formulation of the analytical models has get leverage from measurements, experiments and simulations. At least initially, these models applied basic fluid dynamic laws to stationary flows, in order to obtain simplified analytical expressions, independent of time, of the vertical and radial components of the wind velocity. This led to the development of the impinging wall jet and of the vortex ring models. The first originated from the theory formulated by Glauert (1956). He analyzed theoretically the flow due to a jet spreading out over a plane surface and obtained a similarity solution in laminar flow, while for turbulent flow, an eddy viscosity was introduced, and complete similarity was not attainable, but that confident predictions

could nevertheless be made about the nature of the velocity distribution and the rate of growth of the wall jet. Then this theory was developed by Oseguera and Bowles (1988), who firstly proposed a simple downburst model representing an axisymmetric stagnation point flow, based on velocity profiles from the Terminal Area Simulation System (TASS) model developed by Proctor (1987a, b) and satisfies the mass continuity equation in cylindrical coordinates. Then the radial shape function was improved by Vicroy (1991, 1992). According to the results obtained from the experimental data of wind tunnel, Woos et al. (2001) developed the previous empirical model for the vertical distribution of horizontal wind speed and the dimensionless model is as following:

$$U_z/U_{max} = 1.55(z/\delta)^{1/6}[1 - erf(0.70z/\delta)] \tag{1.2}$$

in which, U_z is the mean velocity at height z above flat ground, U_{max} is the maximum mean wind speed, δ is the height where the velocity is equal to half its maximum value, which can be seen that the mean velocity profile stabilizes beyond approximately 1.5D (D is the jet diameter) and erf is the error function. The comparison of several empirical wind profile models for thunderstorm downburst is shown in **Figure 1.12**. Besides, some researcher (Oseguera and Bowles, 1988; Vicroy, 1991, 1992; Holmes and Oliver, 2000) also proposed several radial horizontal distribution functions of horizontal wind speed. For example, Holmes and Oliver (2000) developed the impinging wall jet model by providing a simplified expression of the radial component of the wind velocity as a function of the distance from the jet axis and of the time; they also expressed the horizontal velocity as the vector summation of the stationary radial velocity and the moving or background velocity of the downburst. Then, Li et al. (2012) upgraded the earlier models of Oseguera and Bowles (1988) and Vicroy (1991) by studying the change in steady state thunderstorm downburst at the different coordinates. They added the nonlinear effects of boundary layer growth to depict the variations in the horizontal and vertical coordinates of maximum horizontal wind speed.

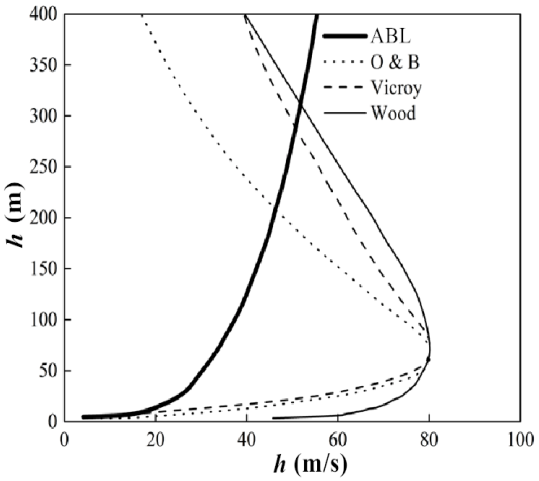

Figure 1.12 Comparison of empirical wind profile models for thunderstorm downburst (Li, 2015).

According to the meteorological data, Tang (2011) simulated the downburst as a 3D circular eddy current field, applied the classical fluid mechanics theory and considered the linear heat source model, and proposed a wind speed calculation method for the downburst wind field for engineering application. Abd-Elaal et al. (2013) developed a new pair of shaping functions incorporating the nonlinear effects of boundary layer growth and did not ignore the continuity equation that confirms the relationship between the vertical and horizontal speed. Abd-elaal et al. (2014) established a pair of intensity decay functions using estimated ages for thunderstorm downburst events from several recorded field events combined with numerical simulation, which can depict the changes in the temporal profile of wind speeds with space.

The turning point in the analytical modeling of thunderstorms is represented by a paper in which Choi and Hidayat (2002b) expressed the instantaneous wind velocity as the sum of its time-varying mean part, averaged on a suitable moving period, plus a zero mean fluctuation dealt with as a stationary random process. This approach was developed by Chen and Letchford (2004a, 2005a, b, 2006), who expressed the time-varying mean part of the wind velocity as the product of a function depending on space, provided by the previous time-independent analytical models, and a function slowly varying with time. The fluctuation, dealt with as non-stationary, is given by the product of its time-varying standard deviation by a random stationary Gaussian process with zero mean and unit standard deviation; Chen and Letchford (2005a, 2006) discussed the vertical and horizontal coherences of the fluctuations. New developments are reported by Chay et al. (2006, 2008) and by Ponte and Riera (2007). Huang and Chen (2009) represented the fluctuations by wavelet transforms and evolutionary spectra. Ponte and Riera (2010) merged these models into a Monte Carlo algorithm aimed at providing the distribution of the maximum velocity in mixed climates. De Gaetano and Solari (2013) studied the role of the wind velocity decomposition and of the moving average period.

Although the theoretical or empirical models are simple and practical to describe the wind field of thunderstorm downburst, it is difficult to present the realistic and real properties due to their complexity.

1.3.2.2 Field measurement

The study of the phenomenology of thunderstorms and of the related wind fields has received great impulse from the evolution of detection and measurement systems - mainly anemometers installed on antenna masts, radar doppler and aircrafts instrumented for meteorological surveys – and from the first monitoring campaigns – above all those carried out for the projects NIMROD (Northern Illinois Meteorological Research on Downbursts, 1978), JAWS (Joint Airport Weather Studies 1982) and MIST (Microburst and Severe Thunderstorms 1986) (Fujita 1990). Based on the field measurement, the researchers are mainly carried our from the

meteorology and wind engineering.

In view of the weather scenario of thunderstorms, some field measurement studies have been carried out at home and abroad, and some valuable information have been obtained in some countries and widely spread. Whittingham (1964) recognized the importance of thunderstorms in the Australian extreme wind climate in the early 1960s and Gomes and Vickery (1976) specifically analyzed Sydney thunderstorms for extreme wind speeds in 1975. In Charba (1974) was the first to present a comprehensive study of the vertical structure of the lowest 500 m of a severe thunderstorm gust front. Goff (1976) determined four life-cycle stages from 20 outflows sampled by a multi-level 461 m tower in central Oklahoma, U.S.A. Wakimoto (1982) investigated and defined four life cycle of thunderstorm gust fronts as viewed with Doppler Radar and Rawinsonde data. Based on the JAWS Project in Colorado, Wakimoto (1985) shew that microburst parent clouds frequently develop in environments exhibiting a deep larger than 3 km, dry atmospheric boundary layer (ABL). In such environments common to the western United States, even weakly precipitating cumulus clouds may generate intense downdrafts and associated damaging winds (Hjelmfelt, 1988; Srivastava, 1985). Srivastava (1987) determined that increasingly higher (ice-phase) precipitation mixing ratio was required to produce strong downdrafts as static stability is increased from dry adiabatic values of -9.6 ℃/km to -6.6℃/km. Sherman (1987) described the passage of a weak thunderstorm downburst over an instrumented tower in Australia. On Sep. 8, 1994, a severe thunderstorm passed over the north of Tokyo, which was analyzed by Takayama et al. (1997) by using data from a damage survey, surface meteorological stations, upper air soundings, satellite images and a conventional radar. Choi, (1999; 2004) investigated the thunderstorm measurement in Singapore. Geerts (2001) estimated the regional climatology of strong wind gusts associated with thunderstorms and the ability to estimate gust strength from ambient conditions was tested based on the measurement in New South Wales, Australia. It could be found that most events took place between midafternoon and late evening and during the warmer months of the year, which was broadly consistent with the occurrence of severe thunderstorms in general. Järvi et al. (2007) estimated the micrometeorological observations of a microburst occurred on the afternoon of 3 July 2004 in Hyytiälä (Juupajoki, Finland). At the time of the event, a squall line associated with a cold front was crossing Hyytiälä with a reflectivity maximum in the middle of the squall line. Rowcroft (2011) clarified the vertical wind shear profiles in downburst events detected from sixteen Austrailian sites. As shown in **Figure 1.13 (a)**, Pistotnik et al., 2011 described the development of a severe local downburst in Austria by using remote sensing data and objective analysis fields, as well as its damage analysis by presenting photographs and maps created during the site survey.

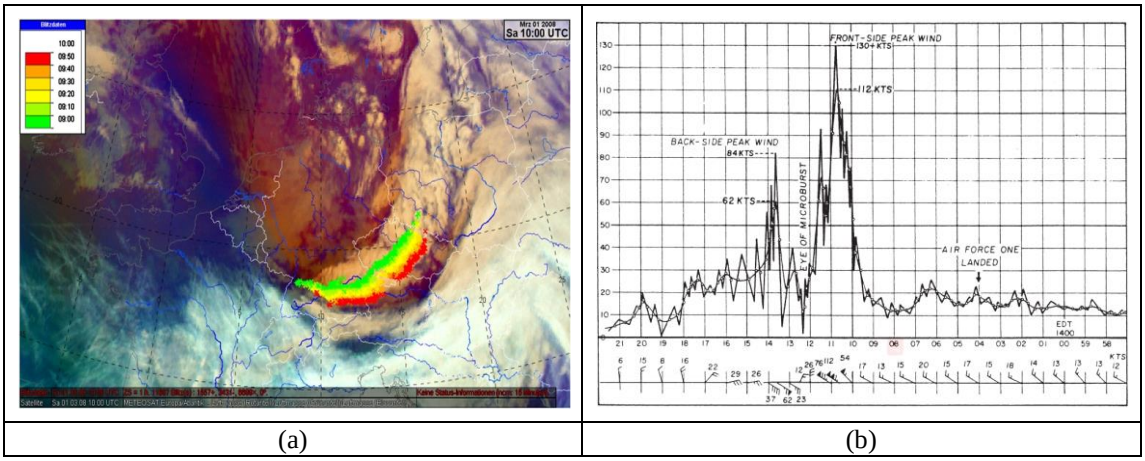

(a) (b)

Figure 1.13 (a) MSG RGB "air mass product" image plus detected lightning flashes within the last hour; (b) Time history of downburst at Andrews AFB downburst, August 1, 1983 (Fujita, 1985).

The literature is rich in contributions that illustrate measurements of thunderstorm outflows whose analysis is carried out in order to extract their parameters of major interest for evaluating the wind loading of structures. Choi (2000, 2002b and 2004) describe the results of a monitoring program in Singapore, which gave particular prominence remark to the definition and values of the gust factor. Holmes and Holmes and Oliver (2000) introduced an empirical model of downbursts by assuming the downburst wind speed is the vector summation of the ''environmental'' wind speed, or translation speed, and the radial wind generated by an impinging jet based on the the Andrews AFB downburst record as shown in **Figure 1.13 (b)**. Choi and Hidayat (2002b) expressed the instantaneous wind velocity as the sum of its time-varying mean part, averaged on a suitable moving period, plus a zero mean fluctuation dealt with as a stationary random process. This approach was developed by Chen and Letchford (2004a, 2005a,b, 2006), who expressed the time-varying mean part of the wind velocity as the product of a function depending on space, provided by the previous time-independent analytical models, and a function slowly varying with time. The fluctuation, dealt with as non-stationary, is given by the product of its time-varying standard deviation by a random stationary Gaussian process with zero mean and unit standard deviation; Chen and Letchford (2005a, 2006) discussed the vertical and horizontal coherences of the fluctuations. New developments are reported by Chay et al. (2006, 2008) and by Ponte and Riera (2007). Duraõna et al. (2007) analyzes the time evolution of the vertical profile of the mean wind velocity and the turbulence properties of transient events registered in the north north-European coastal areas. Orwig and Schroeder (2007) investigates the space-time properties of the rear-flank downdraft of a super-cell and of a derecho detected in a thunderstorm outflow experiment conducted in 2002 in Lubbock, Texas. Inspecting the same rear-flank downdraft, Holmes et al. (2008) discussed the general characteristics of the rear-flank downdraft that was recorded near Lubbock, Texas on 4 June 2002 and developed the decomposition of its velocity in a moving average mean and a residual turbulent component whose characteristics are examined in detail. Similar evaluations

are reported in Järvi (2007) with reference to a downburst occurred in 2004 at the SMEAR II Station in Finland. Huang and Chen (2009) represented the fluctuations by wavelet transforms and evolutionary spectra. Ponte and Riera (2010) merged these models into a Monte Carlo algorithm aimed at providing the distribution of the maximum velocity in mixed climates. Lombardo et al. (2014) investigates some thunderstorms that occurred in Lubbock based on the full-scale thunderstorm wind data collected at Texas Tech University and field campaigns from 2003 to 2010 in order to elucidate their properties relevant to wind engineering. De Gaetano and Solari (2013) studied the role of the wind velocity decomposition and of the moving average period. Gunter and Schroeder (2015) depicts high-resolution field measurements of thunderstorm outflows carried out at Texas Tech University by means of surface instruments and mobile Doppler radars. Besides, almost all the existing analysis about the thunderstorm signals are related to the horizontal resultant velocity and ignore the direction (Choi, 2004; Lombardo et al., 2014) or give it a qualitative definition (Zhang et al., 2018a), namely the classical decomposed method (Chen and Letchford, 2004a; Holmes et al., 2008; Solari et al., 2015a). While it is incoherent with the traditional analysis of synoptic wind speeds.

As we all know, field measurement is the most direct and reliable method to learn the phenomena (Solari, 2014). Despite these and many other analyses, the understanding, the representation and the modeling of thunderstorm outflows are still full of uncertainties and problems to be clarified (Gunter and Schroeder, 2015) due to the complexity of these atmospheric phenomena, the limited available data and a gap between the meteorology and wind engineering. And it can be found that most thunderstorm-related studies are based on or validated against the monument data obtained above the continental parts of the United States, the Asia–Pacific region, and a few continental parts of Europe, while the learning about the characteristics of thunderstorm in the Mediterranean is very preliminary (Solari et al., 2015a) and none has used meteorological data in the Mediterranean as of yet.

1.3.2.3 Experimental methods

Experimental methods can be framed, in turn, into three main families. The first family, pioneered by Lundgren et al. (1992), Alahyari and Longmire (1995) and Yao and Lundgren (1996), involves the release of a liquid mass into a body of less dense liquid; this allows to simulate the effects of buoyancy and to produce the classical ring vortex, favoring the study of the morphology and physics of thunderstorms. However, it is limited to small geometric and velocity scales, not suitable to determine wind loading on structures.

The second family involves the use of wind tunnels, where a jet is impinged on a flat surface to create a wall radial outflow as shown in **Figure 1.12**. The first impinging wall jet tests were carried out by Bakke (1957) to investigate experimentally the wall jet theory formulated by Glauert (1956). Advances of this technique are reported Poreh et al. (1967), Snedeker (1971), Launder and Rodi (1981), Didden and Ho (1985), Landreth and Adrian (1990), Letchford and Illidge (1999) and Wood et al.

(2001). Chay and Letchford (2002) first studied the downburst by means of a classical stationary wall jet simulation, then realized an equipment to reproduce the effects of a moving downburst (Letchford and Chay 2002). Mason et al. (2005) developed the method of the pulsed wall jet. Xu and Hangan (2008) discussed the scaling criteria between model experiments and full-scale conditions; this topic is also the focus of the studies presented by McConville et al. (2009) and Sterling et al. (2011).

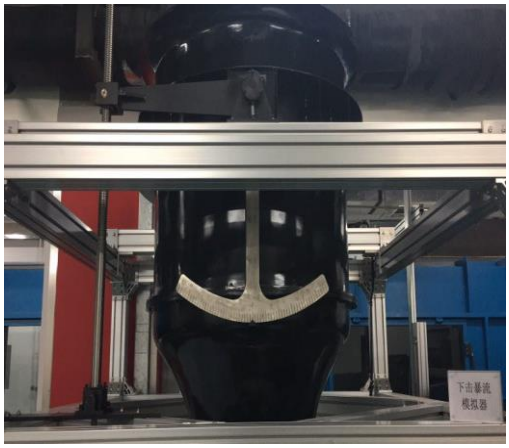

Figure 1.14 Downburst simulator in Beijing Jiaotong University.

The third family involves the techniques that modify the traditional axial flow of a wind tunnel in order to simulate the outflow of a downburst. This family includes the stationary and non-stationary slot jet technique (Lin and Savory 2006, Lin et al. 2007), the method of the pivoted plate suddenly introduced in the oncoming flow (Butler and Kareem 2007), the generation of gust fronts by a multiple fan wind tunnel with individually controlled fans (Cao et al. 2002, Butler and Kareem 2007), and the use of shutter mechanisms (Matsumoto et al. 2007).

1.3.2.4 Numerical methods

The numerical methods may be also classified into three main groups. The first group includes the full-cloud models that simulate the whole region, the life cycle and the complex microphysical processes involved by thunderstorms. The first full-cloud models, appeared in 2-D version in the 60's (Orville 1965, Liu and Orville 1969, Wisner 1972) and in 3-D version in the 70's (Steiner 1973, Miller and Pearce 1974, Pastushkov 1975), were conditioned by the computational limits and by the scarcity of observed data. This situation improved in the mid 80's, thanks to the evolution of the computing power and to the first experimental campaigns.

Among many others, the 3-D model named Terminal Area Simulation System (TASS) (Proctor 1987a, b) and the studies carried out by Hjelmfelt et al. (1989), Knupp (1989) and Straka and Anderson (1993) deserve special mention. Nicholls et al. (1993) simulated first the actions induced by a downburst on a building by a multi-scale LES 3-D model.

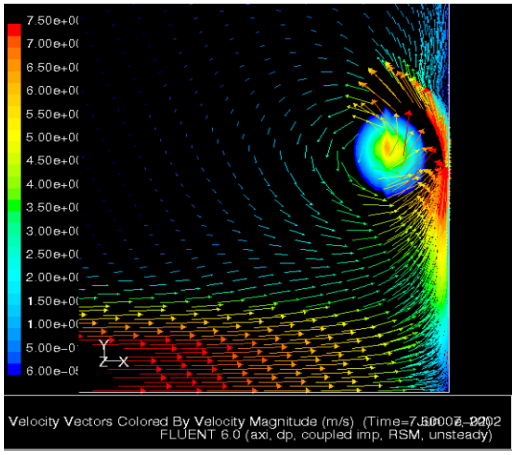

Figure 1.15 Unsteady simulation of downburst (Hangan)

The second group includes the sub-cloud models; they waive to simulate the whole thunderstorm to focus on the near-ground flow dynamics, i.e., on the domain of major interest for engineering applications. With such aim, the sub-cloud models are driven by a sort of thermal forcing, imposed under the cloud at an elevated region of the domain, which simulates the cooling processes of microphysical nature. This method, introduced by Mitchell and Hovermale (1977), was developed later by Srivastava (1985), Droegemeier and Wilhelmson (1987), Proctor (1988, 1989), Anderson et al. (1992), Straka and Anderson (1993), Orf et al. (1997), Orf and Anderson (1999), Lin et al. (2007), Mason et al. (2009, 2010), Vermeire et al. (2011b). Orf et al. (2012) pointed out that future computational advances will allow to use full-cloud models also for wind engineering applications.

The third group includes the CFD models that simulate the impinging wall jet experiments as shown in **Figure 1.15**. For this reason they have analogous properties to the sub-cloud models: they waive to simulate the whole thunderstorm to focus on the near-ground flow field; diversely from the sub-cloud models, however, the forcing source is not thermal but mechanical. This technique, introduced in a pioneering paper of Selvam and Holmes (1992), was developed later by Wood et al. (2001), Chay et al. (2006), Kim and Hangan (2007), Sengupta and Sarkar (2008), Vermeire et al. (2011a).

1.3.3 Extreme wind speed analysis

Defining the design wind speed is a key step in evaluating the wind loading of structures and their safety with regard to the wind (Solari et al., 2015a). And of course safety consideration must be balanced with the additional cost of overdesigning, for which the accurate evaluation of the extreme wind speed is a dominant factor. In the meanwhile, it is one of the most debated and controversial issues in scientific and technical literature on modern wind engineering (Zhang et al., 2018b).

The 50-year return period wind speed is typically for the design application in many

codes of countries (GB50009-2012, 2012; CNR-DT 207/2008, 2008). And in most cases, the available wind data series have lengths between 10 and 20 years. A theoretical distribution is usually fitted to the extreme wind speed values in order to calculate the maximum wind speed which is exceeded, on average, once every *T* years, namely the return period. And several factors will effect strongly on the results. First of all, the quality of the wind data series and of its associated metadata is essential to obtain reliable results (Wieringa, 1996; Aguilar et al., 2003). Besides, the average period of the wind speed values applying to carry out the extreme wind value analysis should be clearly specified (Holmes and Ginger, 2012). And of course, the methods to fit the extreme wind speed distribution is also the dominant.

Following the original assessment provided by Davenport (1968), the wind loading models and codes of countries in mid-latitude areas traditionally adopt design wind speeds related to the synoptic extra-tropical cyclones that develop over a few thousand kilometers on a horizontal plane, with a duration of a few days. This facilitates the acquisition of several pieces of data, providing a complete picture of these events and justifying the development of refined extreme wind speed statistical analyses (Gomes and Vickery, 1977; Cook, 1982; Lagomarsino et al., 1992; Simiu and Heckert, 1996; Holmes and Moriarty, 1999; Cook and Harris, 2004; Harris, 2009, 2014; Torrielli et al., 2013, 2014).

Modern wind engineering design requires the probabilistic characterization of extreme values (EV), usually, the annual maximum wind speed distribution (Torrielli et al., 2013). EV analysis is still a controversial matter, where the difference in opinions obstructs agreement on clear guidelines for practical applications. This subject became a discussion topic with the publication of the pioneering paper by Fisher and Tippett (1928) on asymptotic analysis, followed by contributions from Von Mises (1936) and Cramér (1946). Gumbel (1958) demonstrated the existence of three main asymptotic distributions, referred to as the type I (Gumbel), II (Fréchet) and III (reversed Weibull) extreme distributions, which encourages widely its applications. The three distributions may be expressed by means of a unique model known as generalized extreme distribution, known as GEV (Jenkinson, 1955):

$$\begin{aligned} F_{\hat{v}}(v) &= exp\left\{-[1-\beta\alpha(v-\eta)]^{1/\beta}\right\} \ (\beta \neq 0) \\ F_{\hat{v}}(v) &= exp\{-exp[\alpha(v-\eta)]\} \ (\beta = 0) \end{aligned} \tag{1.2}$$

In this case, the mean value and variance of $\hat{v}$ are given by:

$$\begin{aligned} \mu_{\hat{v}} &= \eta + [1-\Gamma(1+\beta)]/\alpha\beta \ (\beta > -1) \\ \sigma_{\hat{v}}^2 &= (1/\alpha\beta)^2[\Gamma(1+2\beta) - \Gamma^2(1+\beta)] \ (\beta > -1/2) \end{aligned} \tag{1.3}$$

in which, β is the shape factor determining the type of extreme value distribution and is the , η is the mode or location parameter of the extreme value distribution.

Jenkinson demonstrated that: for β tending to 0, the generalized extreme distribution

tends to the distribution of the type I; for $\beta < 0$, the generalized extreme distribution tends to the distribution of the type II, provided that $v > (\eta + 1/\alpha\beta)$; for $\beta > 0$, the generalized extreme distribution tends to the distribution of the type III, provided that $v < (\eta + 1/\alpha\beta)$. Type III distribution is bounded at the upper end, while Types I and II are unbounded at the upper end, with Type II having a thicker tail than Type I.

Unfortunately, no guidelines were provided on which asymptote to select in practical applications. The lack of such guidelines has led to a heated ongoing debate, which has nevertheless produced the development of alternative techniques addressing the same issue of EVs (Torrielli et al., 2013).

The principal drawback to the classical GEV method is that only one maximum value is selected per sample or epoch. As the extreme data series needs to be independent and identically distributed according to Fisher and Tippett, 1928, and extreme wind data may exhibit seasonal variability, they are usually constructed only from yearly maxima. This approach has the shortcoming that only a limited number of information is used and extremes lower than yearly maxima are often neglected. Poor datasets are strongly impacted by sampling errors, leaving space for serious doubts on the description of the annual maximum speed distribution and resulting predictions for design values. In order to improve the accuracy of knowledge about this distribution, alternative techniques have been developed, such as process or level-crossing analysis (Gomes and Vickery, 1977), which describes the distribution of extreme values by analyzing the population of data.

In parallel, several other methods have been proposed were developed to over the shortcoming of limited extremes, which considered more than one single value per year. The peak over threshold (POT) method (Weiss, 1971) analyzes all values exceeding a predefined threshold, which is probably the oldest, although it has come to be applied widely only over the last two decades (Simiu and Heckert, 1996; Holmes and Moriarty, 1999; Holmes, 2003).

The r-Los method selects the r largest order statistics in T = 1 year (Weissman, 1978). The method of Independent Storms (MIS) (Cook, 1982) increases the number of the data available for the regression of the extreme distribution considering the highest value of each independent storm; the collection of independent events is based on the assumption of suitable thresholds to identify the storm and given breaks for the event separation, according to the climatic features and to the typology of data available.

However, as observed by Palutikof et al. (1999), techniques such as POT, r-LOS and MIS require subjective decisions to be taken during the calculation; in particular, the minimum separation time between extremes, the size of r and the left-censor speed value all strongly influence the estimate of the parameters of the distribution.

More recently, the type I penultimate distribution (Cook and Harris 2004, 2008), deriving from classical asymptotic analysis, overcomes this limitation by taking into account the actual finite values for the annual rate of independent events. This approach assumes the following easy and elegant shape when the extremes are drawn from a tail-equivalent Weibull parent distribution.

Although the different extreme value distributions have been used with varying

degree of success, the statistical evidence in favor of any particular probability distribution still appears to be inconclusive. In spite of the progress achieved these years, the selection of laws for the distribution of extreme winds and the suitability of methods of parameter estimation still constitute subjects of debate.

According to Palutikof et al., 1999, extreme gust and mean wind speed data for temperate latitudes have been traditionally fitted to a Type I distribution. The usual current choice is regarded by Palutikof et al., 1999 to be between the Type I (Gumbel) and Type III (Weibull) distributions, while some authors also find that in some situations, a Type II distribution presents a better fit (Beck and Correa, 2012). When the choice is between a Type I and a Type III distribution, as the first is unbounded at the upper end, and the last is bounded from above, the Type I distribution is often chosen by those that argue that there is no natural upper bound for wind speed. There are mainly two reasons for the section of the former. First is that the assumption of a Type I distribution has the added attraction, so the solution is simpler. And another reason is than as the Type III will normally give lower extreme wind speeds for a given return period, therefore, selecting a Type I distribution would make allowance for margins of errors associated with different sources of uncertainties (Duraõna, 2015).

In the meantime, new arguments regarding the importance of taking into account the existence of different meteorological phenomena, namely of resorting to models adequate for mixed wind climates, were advanced by Vickery (1979). Preoccupation with this problem in connection with thunderstorm winds had been expressed earlier by Gomes and Vickery (1978) and Riera et al., (1977). It is already widely recognized, on the other hand, that hurricane or tornado winds cannot be grouped together with winds generated by extratropical storms (Riera and Nanni, 1989).

As introduced before, like extra-tropical cyclones, thunderstorms also occur almost everywhere at the mid-latitudes causing extreme wind speeds that often exceed those of extra-tropical cyclones (Gomes and Vickery, 1976; Choi, 1999; Letchford et al., 2002). Their short duration, sporadic occurrence, and small size of thunderstorm cells make a limited data available, thus preventing a clear representation of these phenomena and the development of reasonable extreme wind speed analyses (Solari, 2014).

Gomes and Vickery (1977/1978) defined a mixed wind climate as a climatological condition in which different wind phenomena occur, in particular extra-tropical cyclones and thunderstorm outflows, and formulated a ground-breaking method to determine the extreme wind speed distribution in such a mixed condition. The technique required a separate extreme-value analysis of the values stemming from each significant wind-producing mechanism, followed by synthesis of the individual mechanisms into a composite extreme-value distribution (Cook et al., 2003). This pioneering work has become the de facto standard methodology, quoted frequently in research papers right up to the present day (Cook, 1985; Riera and Nanni, 1989; Choi, 2001).

Evolutions of this method were proposed by Twisdale and Vickery (1992), Cook et al.

(2003), and Harris (2017). The applications carried out by Riera and Nanni (1989), Kasperski (2002), and Lombardo et al. (2009) pointed out the shortcomings of separating different events based on a limited information, and of gathering a representative data related to mesoscale events. This thesis provides a preliminary but representative contribution to this topic as presented in **Chapter 6**, and tries to link these different types of research, and to present their results in the context of the current knowledge of the regional extreme wind climatology, giving also an innovative perspective of extreme wind events that have been documented in the northern Mediterranean.

1.4 Research aims and objectives

Despite a lot of research, literature lacks of a thunderstorm model shared by scientific community, consistent with physical properties and suitable for simple engineering evaluations. The main aims of the PhD research presented in this thesis are:

(1) Catalogue thunderstorm outflows and characterize them related to wind loading on structures;

(2) Carry out a preliminarily interdisciplinary research leaning thunderstorm outflow from both wind engineering and meteorology;

(3) Determine the extreme wind events with the dominant influence on the wind action on structures in this area.

(4) Evaluate if thunderstorms in different areas have similar properties.

To achieve these aims, a number of objectives were set and are presented as following:

(1) Conduct a check of the original dataset from the unprecedented European wind monitoring network and make sure the available data and the veracity of them.

(2) Separate and classify the dataset into different wind phenomena according to their properties for the targeted analysis in the mixed wind climate.

(3) Extract the thunderstorm outflow records and create a unique catalogue of them, which is the base of all the further study about this phenomena.

(4) A novel decomposition method is formulated. Thunderstorm outflow signals are decomposed into component functions and statistical averages will be evaluated.

(5) A wide collection of information will be gathered to classify the weather scenarios in which thunderstorms occur, which will be applied to the judgement of the whole catalogue. Research contributes to linking weather scenarios and wind speed data.

(6) Perform extreme wind value analysis on available wind data series of adequate length and quality, and estimate the frequency of occurrence of potential damaging wind events in the case of short records in this area considered.

(7) The main statistical characteristics of thunderstorm outflows obtained from different areas are analyzed and compared to clarify if they are similar.

1.5 Thesis structure

The thesis is organized into 8 chapters, including the current chapter, **Chapter 1**, which presents the background, literature review and general aims of this PhD research.
Chapter 2 describes the main in-situ monitoring network and wind databases analyzed in this research.

Chapter 3 presents the separation and classification procedure for separating the different phenomena according to their properties, and the thunderstorm extraction and cataloguing related to the duration of the passage of the gust front.

Chapter 4 presents the classical decomposition approach and formulates a novel directional decomposition approach. The results provided by them are first compared and elucidated with reference to a couple of real thunderstorm and synoptic wind velocity records. Later on, they are applied to a broad class of thunderstorm outflow records whose statistical properties are investigated.

Chapter 5 clarifies thunderstorm direction, seasonality, and hour of daily occurrence based on the measured data, then presents the field data analysis and weather scenario of a typical thunderstorm outflow in Livorno creating preliminarily a bridge between wind engineering and meteorology. The simplified analysis of weather scenario are carried out for three thunderstorm outflow corresponding to different families related to the duration of jump.

Chapter 6 discusses a preliminary but representative analysis of the extreme wind speed distribution, which are carried out in a mixed wind climate area frequently struck by thunderstorms considering the 6 year continuous high-frequency records registered in two Port areas of the northern Mediterranean Sea, confirming the dominant factor of thunderstorm outflows.

Chapter 7, the above analysis is first repeated and extended to the dataset detected by 9 anemometers in-stalled at different levels on the Beijing 325 m high meteorological tower studying the characteristics of thunderstorms here and comparing these with the northern Mediterranean ones.

Finally, **Chapter 8** presents the main conclusions of the research presented in this thesis and several recommendations for future work.

Overall, this PhD thesis tries to link these different types of research, and to present their results in the context of the current knowledge of the regional extreme wind climatology, giving also an innovative perspective of extreme wind events that have been documented in the northern Mediterranean and Beijing urban area.

2 Monitoring network and wind dataset

The wind monitoring and measurement through direct- and remote-sensing techniques is essential for a broad range of scientific disciplines including atmospheric physics, meteorology, climatology, wind, civil and environmental engineering. Besides, the analysis of wind data has an ever more extensive field of application in the interpretation of the wind phenomena that occurred in the past as well as in forecasting the future ones, in climatological analyses and in climate change surveys (Ortego et al., 2014; Dawkins et al., 2016), in the study of wind hazards, damage and risks to which buildings, infrastructures and human activities in contact with Earth's atmosphere are exposed, until pollutant dispersion and wind energy production.

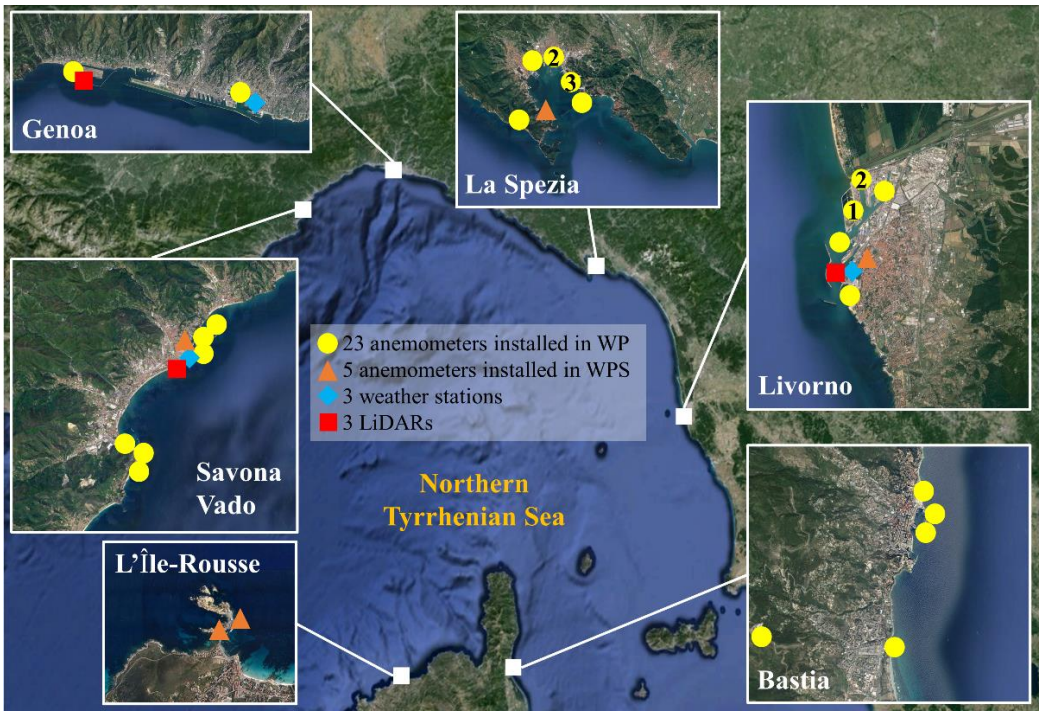

Figure 2.1 WP and WPS anemometric monitoring network.

Figure 2.1 shows an outline of the in-site wind monitoring network created by the "WP" (Solari et al., 2012) and "WPS" (Repetto et al., 2018) European Projects. The yellow circles correspond to the first 23 ultrasonic bi- or tri-axial anemometers, distributed in the Ports of Genoa (2), La Spezia (5), Livorno (5), Savona (6) and Bastia (5) in the course of the "WP" Project (the port area of Vado Ligure belongs to the Port of Savona). The orange circles refer to 5 new ultra-sonic anemometers mounted in the Ports of Savona (1), La Spezia (1), Livorno (1) and L'Île Rousse (2) during the "WPS" Project the port area of L'Île Rousse belongs to the Port of Bastia). Still in the frame of the "WPS" Project, the monitoring network has been enlarged by adding 3 weather stations (blue circles), each one including another ultra-sonic anemometer, one barometer, one thermometer and one hygrometer, and 3 LiDAR (Light Detection And Ranging) (red circles), which detect the wind velocity profile from 40 to 250 m above ground level (AGL). Other sensors autonomously installed

by single Port Authorities are in the stage of becoming integral parts of the “WP” and “WPS” network.

Figure 2.2 The Picture of Port of Livorno showing the positon of the anemometers. (Google earth)

The position of the anemometers was chosen in order to cover homogeneously the port areas involved in these projects and to register undisturbed wind velocity histories, for instance, the distribution of the 5 anemometers in the port of Livorno is presented in **Figure 2.2**.

Figure 2.3 Examples for the towers and antenna masts at the top of building.

The instruments are mounted on high-rise towers or on antenna masts at the top of buildings as the examples in **Figure 2.3,** paying attention to avoid local effects that may contaminate the quality of measurements. **Table 2.1** illustrates the most important features of the 31 anemometers that currently the "WP" and "WPS" network is made up of, *h* being their height AGL that varies from 10 m to 84 m. A description of LiDAR properties is given in (Repetto et al., 2018).

(a) (b)

Figure 2.4 Biaxial Sonic Anemometer (a) and triaxial sonic anemometer (b).

The ultra-sonic anemometric stations consist of bi-axial or three-axial sensors as shown in **Figure 2.4** that detect the wind speed and direction with a precision of 0.01 m/s and 1 degree, respectively. Their sampling rate is 10 Hz with the exception of one sensor installed in Savona, which samples at 1 Hz, and the sensors installed in the Ports of Bastia and L'Île-Rousse, whose sampling rate is 2 Hz.

The anemometric data, measured with a precision of 0.01 m/s, are stored in terms of their components (V_X, V_Y) for bi-axial anemometers or (V_X, V_Y, V_Z) for three-axial anemometers, according to the geophysical coordinate system (**Figure 2.5 (a)**), where V_X is directed from West to East, V_Y from South to North, and V_Z is vertical and positive upwards.

Focusing on the horizontal components of the wind speed (V_X, V_Y), they can also be expressed in terms of the resultant wind speed U and the wind direction α (**Figure 2.5 (b)**):

$$\begin{aligned} U(t) &= \sqrt{V_X^2(t) + V_Y^2(t)} \\ \alpha(t) &= 270 - \text{atan2}(V_Y(t)/V_X(t)) \\ \gamma\ (t) &= 270 - \alpha(t) \end{aligned} \tag{2.1}$$

where $\alpha \in [0:360]$ is a clockwise directional angle, computed from Y (North), referred to the geographical notation commonly used in atmospheric sciences, $\gamma \in [0:360]$ is an anti-clockwise directional angle, computed from X (East), frequently used in wind engineering.

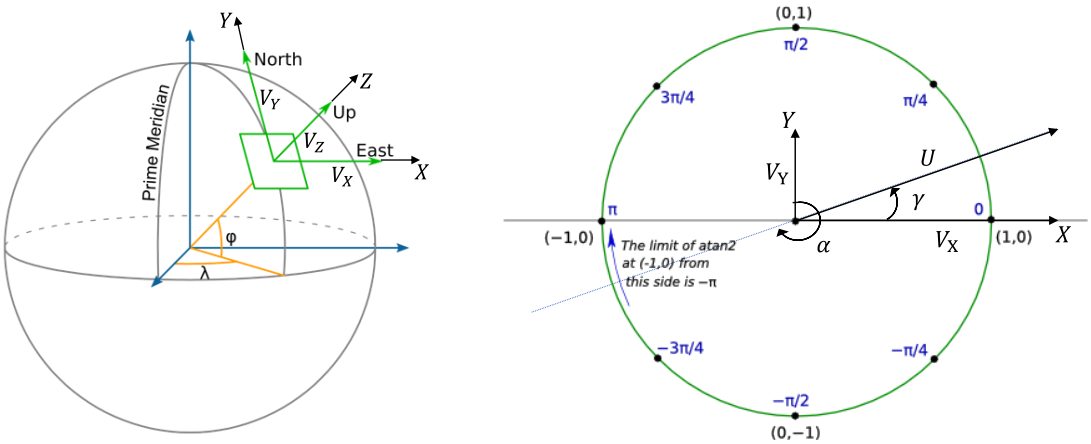

(a) (b)

Figure 2.5 (a) space coordinate system adopted for the anemometric measurements; (b) decomposition of the horizontal component of the wind speed and atan2 rationale.

As shown in **Figure 2.6**, a set of local servers placed in each Port Authority's headquarter receives the data recorded by anemometers and LiDARs in its own port area and elaborates the basic statistics on 10-min of averaging period, namely the mean and peak wind velocities and the mean wind direction. Each server automatically sends this information to the central server at the University of Genoa, which stores the data in a database through a four-step automatic procedure:

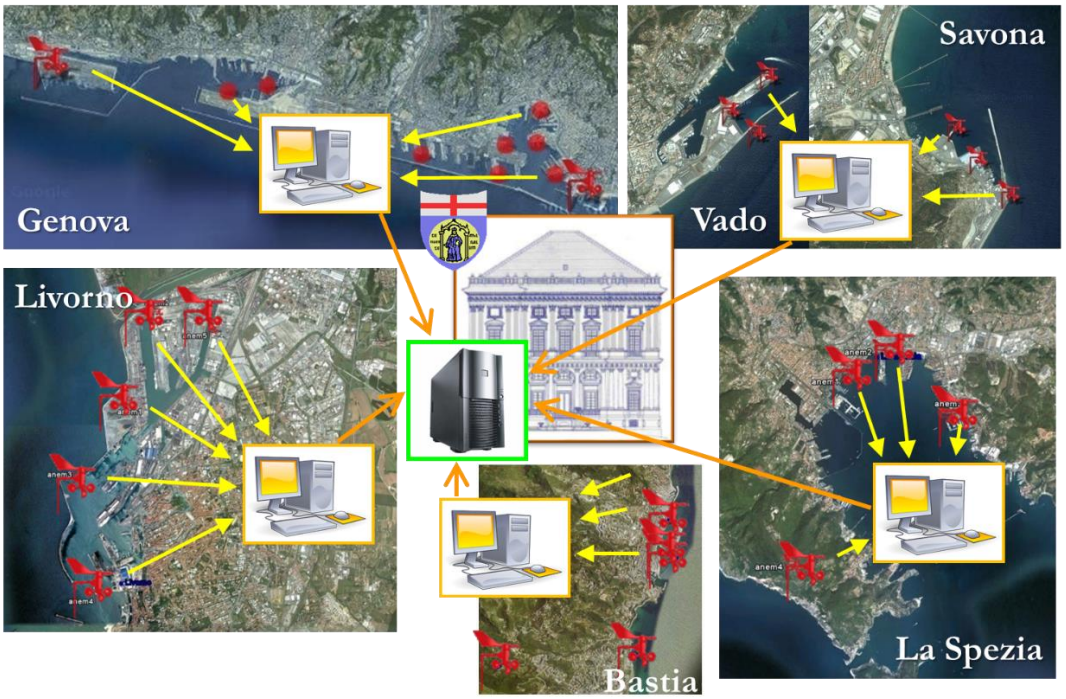

Figure 2.6 Schematic diagram of collecting data.

(1) raw data are systematically checked and validated;
(2) 10-min statistics, including turbulence intensity and gust factor, are evaluated from raw data and stored in the database;
(3) 1-min statistics, including turbulence intensity and gust factor, are evaluated and stored in the database;
(4) an automatic check report is produced and sent to Port Authorities daily.

Table 2.1 Main properties of the ultrasonic anemometers of the monitoring network.

Port	Anem. No.	*h* (m)	Type	Period of measurement	Period of analysis	Valid data (%)
Savona and Vado	0	84	tri-axial	2011.03.30-now	-	
	1	33.2			2014.12.01-2016.01.31	87%
	2	12.5			2014.12.01-2016.01.31	72%
	3	28			2014.12.01-2016.01.31	83%
	4	32.7			2014.12.01-2016.01.31	86%
	5	44.6			2014.12.01-2016.01.31	87%
	6	10	bi-axial	2014.04.05-now	-	
	7	35		2015.07.31-now		
Genoa	1	61.4	bi-axial	2011.03.30-2013.05.07	2011.03.30-2013.04.01	59%
	2	13.3		2010.10.12-2015.05.31	2010.10.12-2015.05.31	56%
	3	32		2015.04.16-now	-	
La Spezia	1	15.5	bi-axial	2010.10.29-now	-	
	2	13			2010.10.29-2015.12.31	88%
	3	10		2011.02.04-now	2011.02.05-2015.12.18	89%
	4	11		2011.04.14-now	-	
	5	10		2012.09.06-now		
	6	16		2015.01.23-now		
Livorno	1	20	tri-axial	2010.09.16-now	2010.10.01-2015.12.12	86%
	2	20			2010.10.01-2015.12.12	67%
	3	20		2010.09.16-2015.03.21	2010.10.01-2015.03.21	74%
	4	20		2010.09.16-now	2010.10.01-2015.12.12	60%
	5	75		2010.09.16-2014.08.25	2010.10.01-2014.08.25	69%
	6	12	bi-axial	2015.07.25-now	-	
	7	23.8				
Bastia	1	10	bi-axial	2011.11.17-now	-	
	2	10				
	3	13				
	4	10				
	5	10				
L'Île -Rousse	1	10	bi-axial	2015.06.03-now	-	
	2	10		2015.06.08-now		

These results are the main outcome transferred to Port Authorities for their institutional activity. At the same time, they represent the starting point for a broad range of researches carried out by the WinDyn Research Group.

In this regard, starting from the original database, a new one has been created that collects further statistical parameters of the anemometric measurements. In particular, one record for each subsequent $T = 10 - \text{min}$ period is stored that gathers such parameters into three groups:

(1) 1-s peak wind velocity $\widehat{U}$, mean wind velocity U_{m10}, mean wind direction α_{m10}, gust factor $G_{10} = \widehat{U}/U_{m10}$, turbulence intensity I_{10}, skewness γ_{10}, and kurtosis κ_{10} in the interval T;

(2) mean wind velocity U_{m60}, gust factor $G_{60} = \widehat{U}/U_{m60}$, turbulence intensity I_{60}, skewness γ_{60}, and kurtosis κ_{60} in the 1-h time interval centered around T;

(3) maximum mean wind velocity averaged over 1-min U_{m1} and gust factor $G_1 = \widehat{U}/U_{m1}$ in T.

Table 2.1 also shows periods of measurements varying from anemometer to anemometer. This depends, first of all, on the successive installation of the instruments. In addition, there are several periods in which measurements have been not carried out due to accidents or malfunctions of the instruments, these including some cases in which sensors have not been restored yet. Of course, there are also periods in which measurements have been not enough reliable to be examined (Cook, 2014a, b). Finally, taking into account the burden of the analyses described in this thesis, the data provided by several sensors has not been studied yet; more precisely, at present analyses have been carried out for 14 sensors out of 31 available. The last column of **Table 2.1** provides the percentage of the examined data for each examined instrument. Obviously, the correctness and reliability of the dataset is fundamental to carry out correct and reliable signal analyses.

This dataset represents the starting point for the separation and classification procedure described in the next chapter. And it provides a unique opportunity to extracting a number of thunderstorm outflow records and learn their property.

3 Separation and catalogue of thunderstorm outflows

It is now recognized that thunderstorms are crucial with respect to hazard assessments aimed at the safety of construction, infrastructure and territory, but they are often still undistinguished from extra-tropical cyclones in most cataloguing procedures (Stucki et al., 2014). Accordingly considering the mixed wind climates in the northern Mediterranean, it is the first step that the intense wind events are separated and classified into homogeneous families to determine the catalogue of thunderstorm outflows for the interested subsequent analysis. In order to achieve this goal efficiently, a semi-automatic procedure was implemented to recognize and extract these phenomena by De Gaetano et al. (2014), then it is improved by the author and a controlled catalogue of thunderstorm outflows is created, which is already described in the paper published in Journal of Probability Engineering Mechanics in 2018. Herein, **Section 3.1** illustrates in detail the separation and classification procedure applied in order to gather a rich sub-dataset of records labelled as thunderstorm outflows. **Section 3.2** provides a new procedure to extract and catalogue thunderstorm outflows with reference to their duration and intensity, these parameters being the key features for evaluating the wind loading of structures. This is fundamental for the further analysis.

3.1 Separation and classification procedure

A thorough examination of the huge amount of data collected during the “WP” and “WPS” Projects reveals that intense wind events can be separated and classified into three families characterized by different statistical properties (De Gaetano et al., 2014):

1) stationary Gaussian events with relatively large mean wind velocities and small gust factors; they usually correspond to synoptic neutral atmospheric conditions and are here referred to as extra-tropical cyclones or depressions as shown in **Figure 3.1**;
2) non-stationary non-Gaussian events with relatively small mean wind velocities, large and quite isolated peaks, and high gust factors; they are here referred to as thunderstorms outflows **Figure 3.2**;

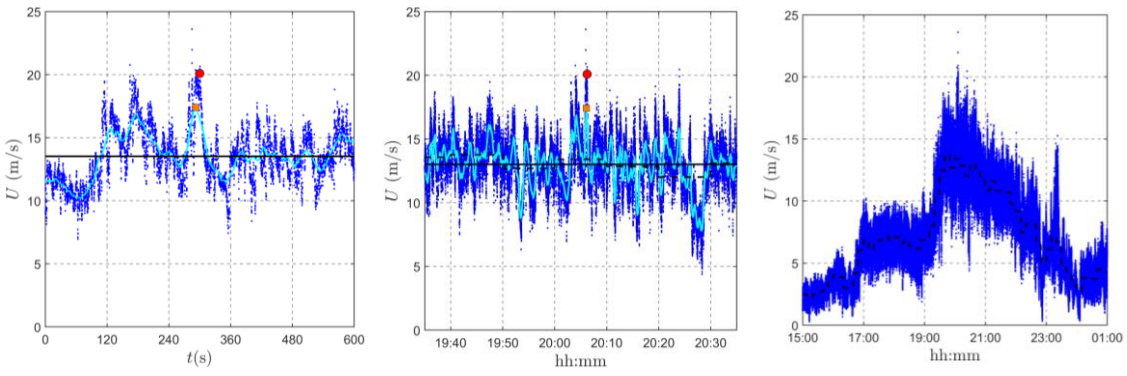

(a) (c) (e)

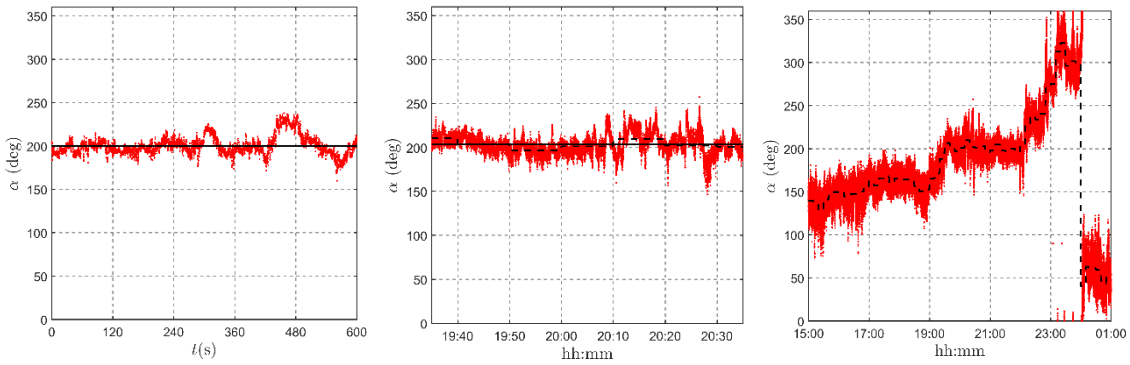

(b) (d) (f)

Figure 3.1 Extra-tropical cyclone recorded on 2nd March 2016 by the anemometer 03 of the Port of La Spezia: wind speed time-history in10-min (a), 1-h (c), and 10-h (e); wind direction time-history in 10-min (b), 1-h (d), and 10-h (f).

3) stationary non-Gaussian events with relatively small mean wind velocities, large and repeated peaks, and moderately high gust factors; they are here referred to as intermediate events as shown in **Figure 3.3** or gust fronts (Kasperski, 2002).

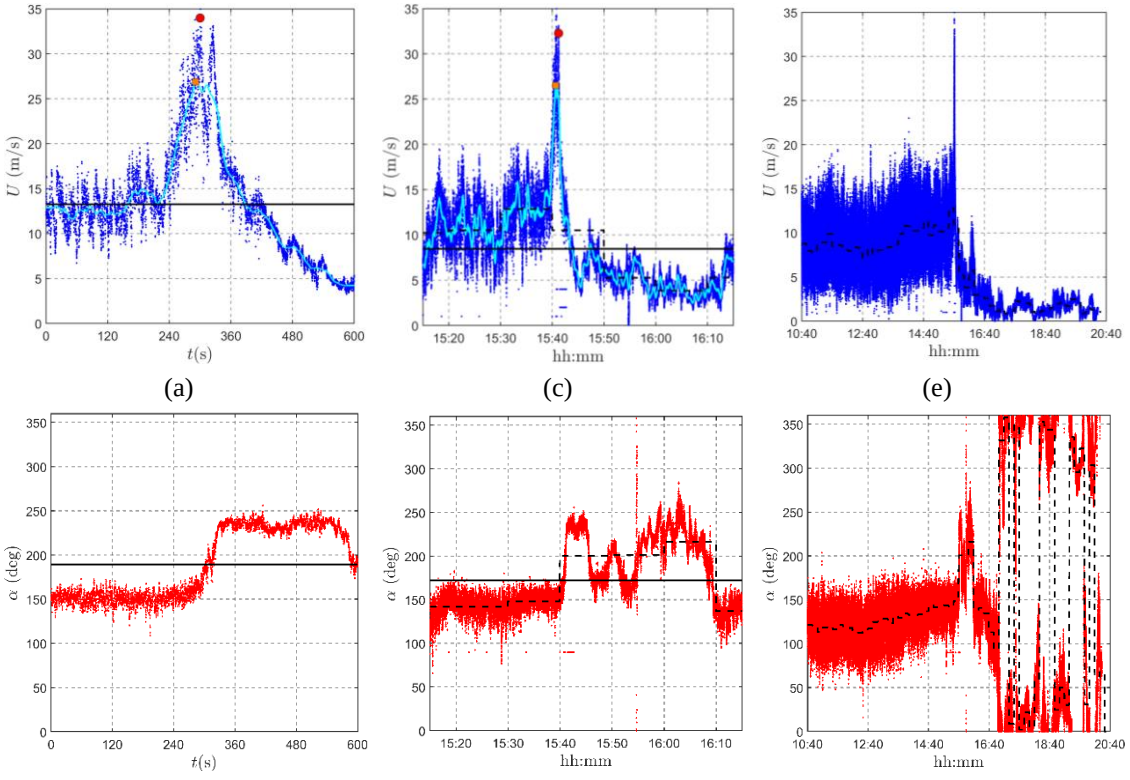

(a) (c) (e)

(b) (d) (f)

Figure 3.2 Thunderstorm outflow recorded on 25th October 2011 by the anemometer 03 of the Port of La Spezia: wind speed time-history in10-min (a), 1-h (c), and 10-h (e); wind direction time-history in 10-min (b), 1-h (d), and 10-h (f).

While waiting to carry out a systematic meteorological survey and interpretation of these events, it seems to be reasonable to advance the hypothesis that they are

associated to strongly unstable atmospheric conditions, or downslope winds, or recirculating vortices as well.

Coherently with modern trends in mixed wind climate conditions (Solari, 2014; Lombardo et al., 2009; Gomes and Vickery, 1977/1978; Kasperski, 2002), the separation and classification of intense wind events into homogeneous categories is a fundamental preliminary step to carry out refined analyses of different phenomena and of their loading and response of structures. In principle, this separation calls for the joint study of the records detected by a wind monitoring network and the weather scenarios in which such events take place; in the reality this approach is as powerful as burdensome and looks forward to future developments currently in the embryonic stage (Burlando et al., 2017a), which will be introduced in **Chapter 5**. This operation is clearly not possible when many instruments, many years of measurements, and many different events have to be examined as in this case. Accordingly, the process of wind velocity records by means of synthetic indicators and expert judgements is still the only reasonable pathway to separate and classify extensive amounts of data (Gomes and Vickery, 1976; Twisdale and Vickery, 1992; Choi, 1999; Lombardo et al., 2009; Choi, 2000; Dura ñona et al., 2007; Kasperski, 2002).

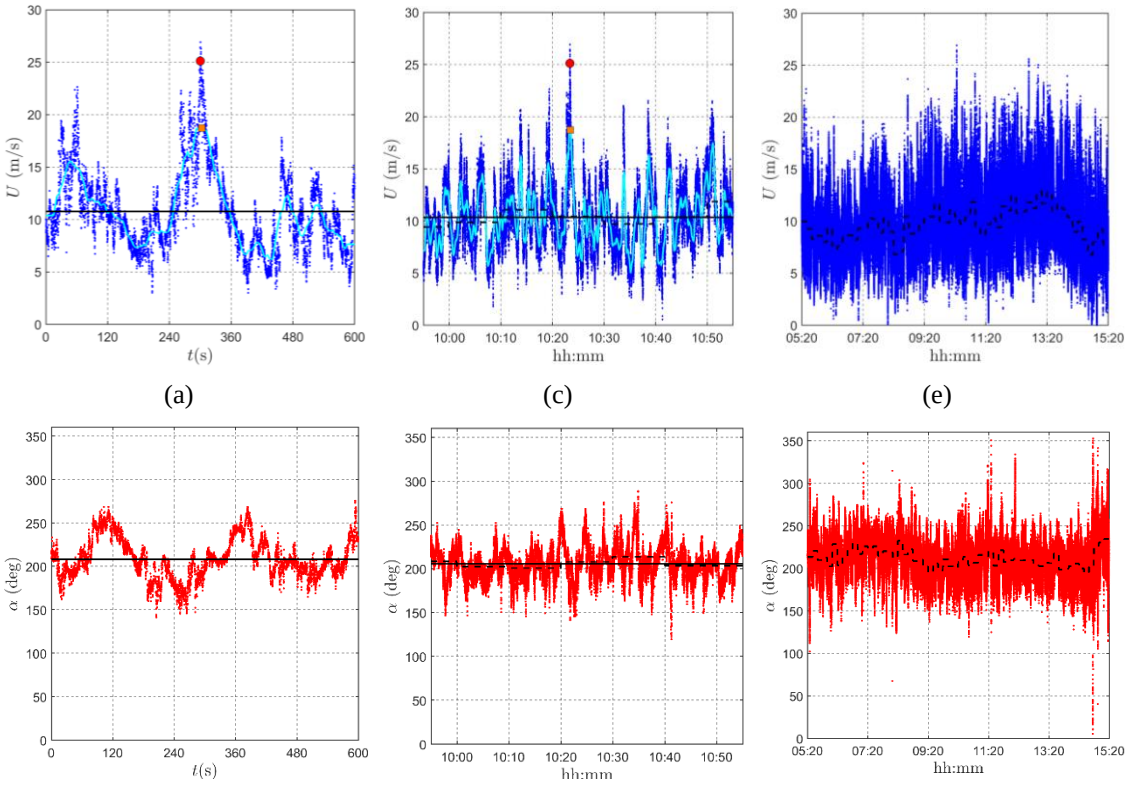

Figure 3.3 Intermediate event recorded on 16th December 2011 by the anemometer 03 of the Port of La Spezia: wind speed time-history in10-min (a), 1-h (c), and 10-h (e); wind direction time-history in 10-min (b), 1-h (d), and 10-h (f).

To achieve the separation and classification of different intense wind events as easily

and efficiently as possible, De Gaetano et al. (2014) developed a semi-automated procedure applied to the records with peak wind velocity $\widehat{U}$ greater than 15 m/s. This choice is coherent with thunderstorm analyses carried out by other authors (Choi, 2000; 2004; Durañona et al., 2007) and with the tradition of evaluating the parameters of synoptic events by collecting all records that satisfy the requirement of neutral atmospheric conditions (Solari and Piccardo, 2001; Solari and Tubino, 2002), these including several phenomena of limited engineering interest. The alternative approach of restricting analyses to thunderstorm outflows with higher peak values (Geerts, 2001; Lombardo et al., 2014) improves the information related to the phenomena of major engineering interest, but reduces the statistical representativeness of the results.

This semi-automated procedure involves a suitable mix of systematic quantitative controls and qualitative expert judgments. The quantitative controls are based on the comparison between the detected values of the gust factors, G_{60}, G_{10}, G_1, and their reference values, G_{60}^0, G_{10}^0, G_1^0, evaluated by means of numerical simulations (ESDU, 1993; Burlando et al., 2007; 2013) assuming that intense wind speeds occur in neutral atmospheric conditions during synoptic extra-tropical cyclones with stationary Gaussian properties. **Figure 3.4** shows the diagrams of the reference gust factors G_{60}^0, G_{10}^0 and G_1^0 as functions of the mean wind direction α_{m10} at the anemometers 1, 2 and 3 in the Port of La Spezia. These quantities are evaluated through the method proposed by Solari (1993). It is apparent that their values decrease when the wind blows from the sea.

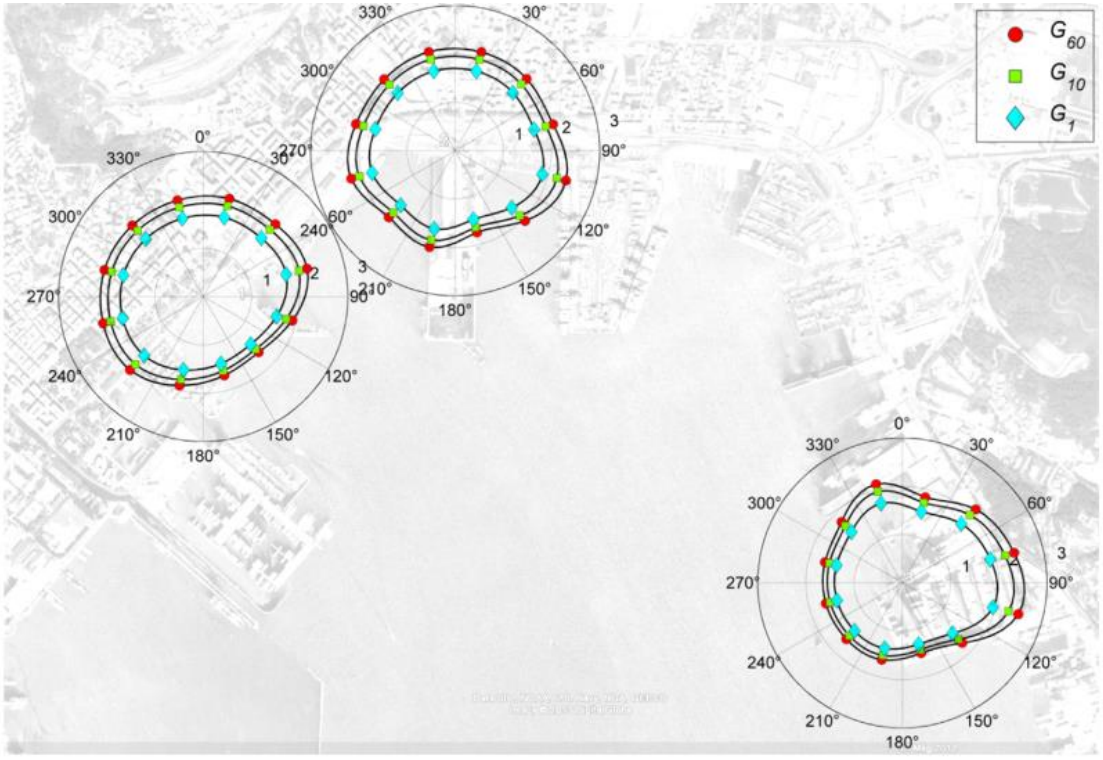

Figure 3.4 Reference gust factors G_{60}^0, G_{10}^0 and G_1^0 as functions of the mean wind direction at the anemometers 1, 2 and 3 in the Port of La Spezia.

Conceptually, a wind event is labeled as an extra-tropical cyclone if the ratios $G_{60}/G_{60}^{0},\ G_{10}/G_{10}^{0},\ G_{1}/G_{1}^{0}$ are small. Instead, it is labeled as a thunderstorm outflow or an intermediate event when the ratio G_{10}/G_{10}^{0} is large. In this way, De Gaetano et al. (2014) automatically identified as synoptic extra-tropical cyclones over 99.5% of the records related to intense wind events. The remaining ones were submitted to qualitative expert judgments as show in **Figure 3.5**. The procedure involves the following steps:

(1) Events for which the following rule applies are classified as depressions (D):

$$G_{60}/G_{60}^{0} \leq 1.10 \tag{3.1}$$

They are strongly stationary and Gaussian not only over 10-min intervals, but also over 1-h intervals.

(2) Events for which the following rule applies are classified as depressions (D):

$$G_{60}/G_{60}^{0} \leq 1.25 \cap G_{10}/G_{10}^{0} \leq 1.10 \tag{3.2}$$

They are strongly stationary and Gaussian over 10-min intervals, while they exhibit some variability over 1-h intervals.

(3) Events for which the following rule applies are classified as thunderstorms (T) or intermediate event/gust fronts (F):

$$G_{10}/G_{10}^{0} > 1.25 \tag{3.3}$$

The classification of such events into the category of thunderstorms (T) or intermediate event/gust fronts (F) is carried out through a qualitative control.

(4) Events for which the following rule applies are classified as depressions (D):

$$G_{60}/G_{60}^{0} < 1.25 \cap G_{1}/G_{1}^{0} > 0.80 \tag{3.4}$$

This procedure was applied in De Gaetano et al. (2014) to the 10-min records detected by 9 ultra-sonic anemometers in the period 2011-2012, whose 1-s peak was greater than 15 m/s. In that study, the use of synthetic parameters was mainly circumscribed to gust factors; the expert judgement involved the visual check of both 10-min and 1-h records centered around the peak. In De Gaetano et al. (2014), 93 transient velocity records related to convective conditions and thunderstorm outflows were extracted; this made possible to carry out preliminary statistical evaluations of their parameters.

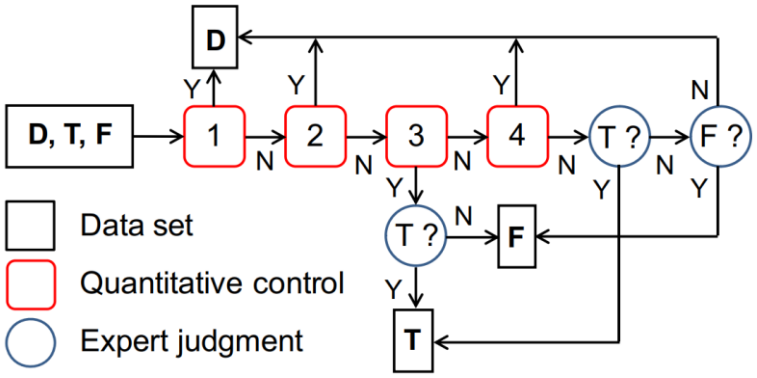

Figure 3.5 Flow-chart of the semi-automated algorithm by means of which depressions (D), thunderstorms (T) and gust fronts (F) are separated.

The above procedure is herein extended to the data recorded by 14 ultra-sonic anemometers (**Table 2.1**) (including the 9 previously studied) in the period 2010-2016. **Figure 3.6**, **Figure 3.7** and **Figure 3.8** show three typical 1-h long records registered by the anemometer 3 of the Port of La Spezia that correspond to an extra-tropical cyclone, a thunderstorm outflow and an intermediate event, respectively. The pictures **(a)** and **(b)** show the time-series of the wind speed and direction raw data, respectively. They also provide their mean values over 1-h, U_{m60} and α_{m60} (solid lines), and 10-min periods, U_{m10} and α_{m10} (dotted lines), and the 1-s peak wind velocity (red circles), which is obviously smaller than the instantaneous peak. The pictures **(c)** show the ratios G_{60}/G_{60}^0, G_{10}/G_{10}^0, G_1/G_1^0 over subsequent 10-min periods.

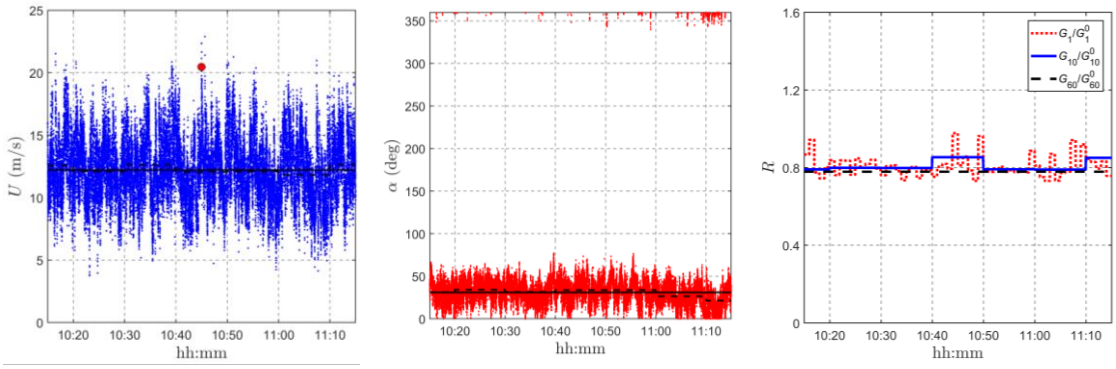

(a) (b) (c)

Figure 3.6 Extra-tropical cyclone recorded on 1 December 2013 by the anemometer 3 of the Port of La Spezia: (a) 1-h wind speed time-series; (b) wind direction time-series; (c) ratio of gust factors.

The extra-tropical cyclone record shown in **Figure 3.6** is characterized by a relatively high mean wind speed (U_{m10} = 12.04 m/s, U_{m60} = 12.21 m/s) and gust peak ($\widehat{U}$= 20.46 m/s). The gust factor (G_{10}= 1.70, G_{60}= 1.68) is rather high but typical of synoptic neutral atmospheric conditions. Likewise, the wind speed also the wind direction involves stationary features. The ratios G_{60}/G_{60}^0= 0.80, G_{10}/G_{10}^0= 0.85 and G_1/G_1^0= 0.85 are well below 1.

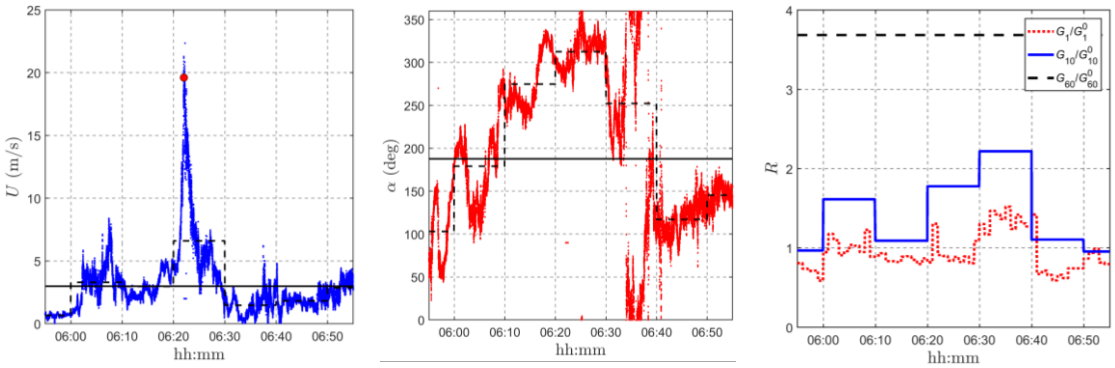

(a) (b) (c)

Figure 3.7 Thunderstorm outflow recorded on 25 June 2014 by the anemometer 3 of the Port of La Spezia: (a) 1-h wind speed time-series; (b) wind direction time-series; (c) ratio of gust factors.

The thunderstorm outflow record shown in **Figure 3.7** is characterized by a relatively low mean wind speed (U_{m10}= 6.60 m/s, U_{m60}= 2.99 m/s), a relatively high gust peak ($\widehat{U}$ = 19.61 m/s) and a very high gust factor (G_{10} = 2.97, G_{60} = 6.56). The ratio G_{60}/G_{60}^0= 3.69 exhibits a sudden increase in correspondence of the gust peak whereas the ratios G_{10}/G_{10}^0= 1.78 is well above 1 and G_1/G_1^0= 0.91 is larger than 0.80. The wind direction changes of almost 180 ° as usually occurs when a downburst passes over the anemometer (Orwig and Schroeder, 2007).

The intermediate event record shown in **Figure 3.8** is characterized by a relatively low mean wind speed (U_{m10}= 9.71 m/s, U_{m60}= 11.85 m/s) and a rather high gust peak ($\widehat{U}$ = 23.75 m/s); the gust factor (G_{10}= 2.45, G_{60}= 2.00) is much greater than the typical values in neutral atmospheric conditions, this being confirmed by the ratios G_{60}/G_{60}^0= 1.22, G_{10}/G_{10}^0= 1.58 and G_1/G_1^0= 1.17. Both the wind speed and the direction exhibit quite regular trends without apparent transient features.

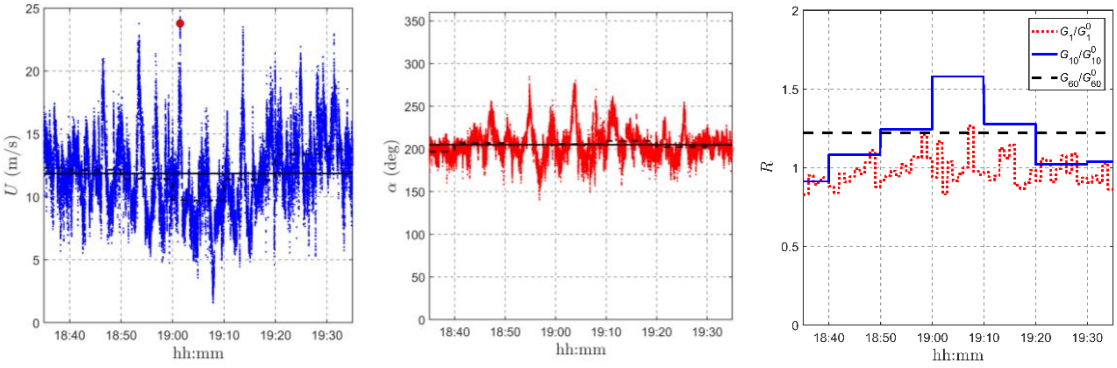

(a) (b) (c)

Figure 3.8 Intermediate event recorded on 10 October 2013 by the anemometer 3 of the Port of La Spezia: (a) 1-h wind speed time-series; (b) wind direction time-series; (c) ratio of gust factors.

It is worth noting that the records shown in **Figure 3.6**, **Figure 3.7** and **Figure 3.8** have clear trends that do not imply doubtful decisions. Unfortunately, this ideal condition does not always occur and the extraction of the thunderstorm outflows

carried out by De Gaetano et al. (2014) may give rise to controversial choices. On the other hand, though not availing of records detected with high sample rates, Durañona (2015) made a fine selection of the convective events that take place in Uruguay by inspecting 10-min mean and peak wind speeds over a period 10-h long. This study inspired a re-calibration of the procedure applied by De Gaetano et al. (2014) based on 10-min, 1-h and 10-h long records. Joined with the possibility of processing a more extensive set of measurements, this approach leads to a novel extraction and cataloguing procedure described in the next section.

3.2 Thunderstorm extraction and cataloguing

As mentioned in the previous section, the above procedure is firstly extended to the data recorded by 14 ultra-sonic anemometers in the period 2011-2016, including the nine anemometers previously inspected in the period 2011-2012 as well. Secondly, following the method suggested by Durañona (2015), the previous analyses have been improved by performing the qualitative selection of thunderstorm outflows based not only on 10-min and 1-h records as in De Gaetano (2014), but also inspecting the 10-h records centered around the peak wind speed.

Table 3.1 Number of thunderstorm events (NTE) and records (NTR) examined.

Port	Anem. No.	NTE	NTR	10min	1h	10h
Genoa	1	41	9	5	4	0
	2		34	11	18	5
Livorno	1	84	40	19	14	7
	2		20	8	9	3
	3		28	15	9	4
	4		39	18	19	2
	5		16	6	8	2
Savona and Vado	1	23	5	3	2	0
	2		3	1	2	0
	3		7	6	0	1
	4		10	7	2	1
	5		4	2	1	1
La Spezia	2	50	20	12	8	0
	3		42	28	10	4
Total	14	198	277	141	106	30
Percent	-	-	100%	50.9%	38.3%	10.8%

Table 3.1 shows a general framework of the anemometers. NTE = 198 and NTR = 277 are, respectively, the number of events and the number of records labelled as thunderstorms; NTR is always greater than NTE since the same thunderstorm event may be detected simultaneously by more than one anemometer.

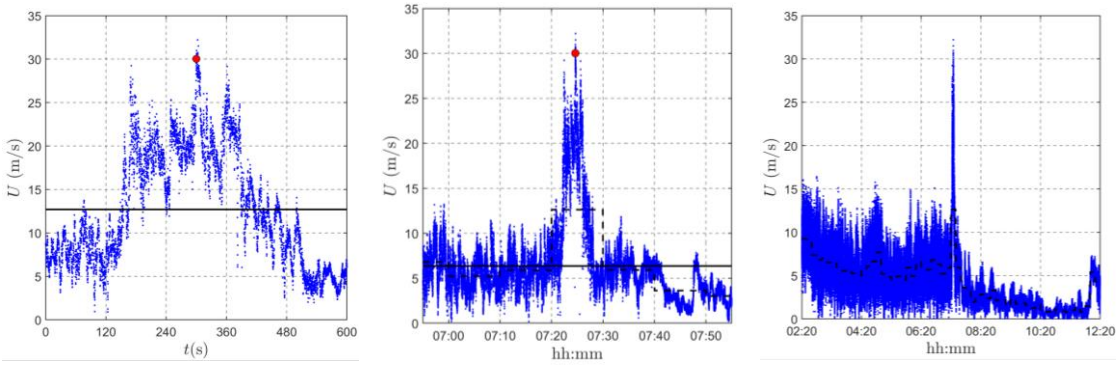

(a) (b) (c)

Figure 3.9 "10-min" thunderstorm outflow record (Anemometer 2, Port of La Spezia, 07:20, 11 April 2012): velocity in a 10-min period (a), in a 1-h period (b) and in a 10-h period (c).

It is worth noting that the percentage and the total amount of valid data are quite different at each experimental site. This depends first on the successive installation of sensors, then on the different periods in which measurements were not carried out due to accidents or malfunctions of instruments, these including some cases in which they have not been restored yet; there are also periods in which measurements have been judged not enough reliable to be examined and have been disregarded (Cook, 2014a，b). It is also worth noting that the databases of several anemometers have not been analyzed yet, that the monitoring network continuously produces new data and that new anemometers are progressively added to make the network richer and richer.

The analysis developed here involves not only the assemblage of a more comprehensive and controlled thunderstorm outflow dataset but, even more, a major advance in understanding the time-scale of transient events. Accordingly, it favors the classification and cataloguing of such events based on the duration of the transient peak and on the wind speed itself. This information is crucial to investigate the loading and response of structures.

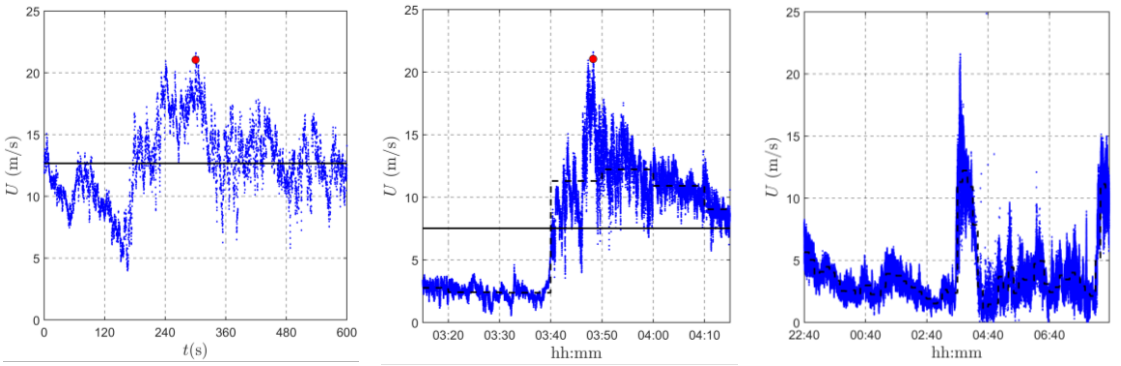

(a) (b) (c)

Figure 3.10 "1-h" thunderstorm outflow record (Anemometer 1, Port of Livorno, 03:40, 21 July 2014): velocity in a 10-min period (a), in a 1-h period (b) and in a 10-h period (c).

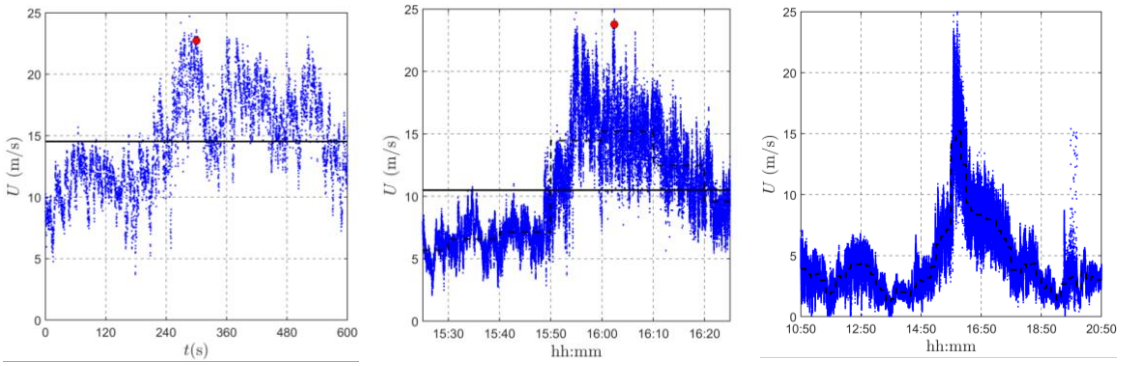

(a) (b) (c)

Figure 3.11 "10-h" thunderstorm outflow record (Anemometer 2, Port of Livorno, 15:50, 4 September 2011): velocity in a 10-min period (a), in a 1-h period (b) and in a 10-h period (c).

In this regard, transient records have been separated into three families depending on whether the presence of a ramp-up and the transient peak are clearly detectable in 10-min (**Figure 3.9**), 1-h (**Figure 3.10**) or 10-h (**Figure 3.11**) long records; for sake of simplicity they are referred to as "10-min", "1-h" and "10-h" events. It was found that 50.9 % of the extracted transient records are detectable on 10-min periods, 38.3 % of them can be recognized on 1-h periods whereas only 10.8 % are pointed out by inspecting 10-h records as show in **Table 3.1**. This aspect reflects on the duration of the ramp-up and has a key engineering role. As demonstrated by Kwon and Kareem (2009), the structural response increases on reducing the length of the impulse related to the passage of the gust front.

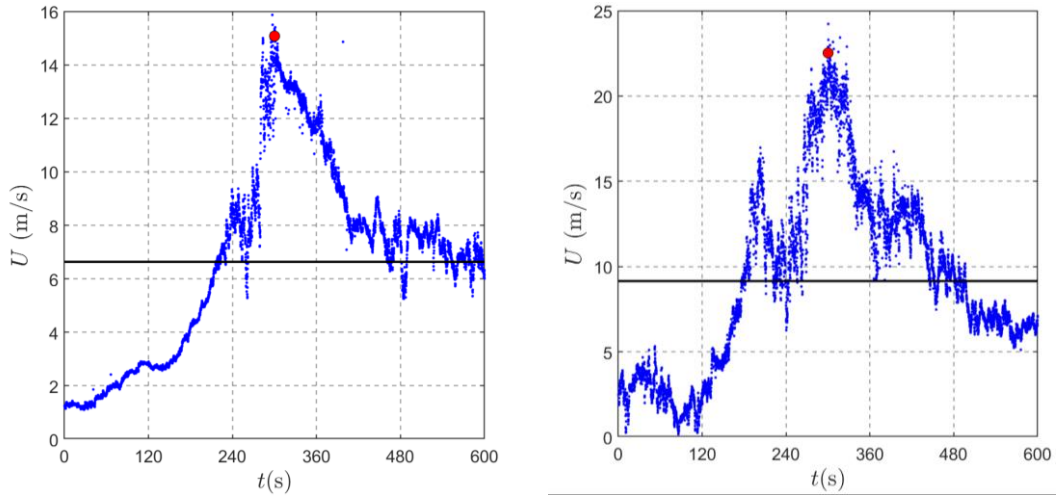

(a) (b)

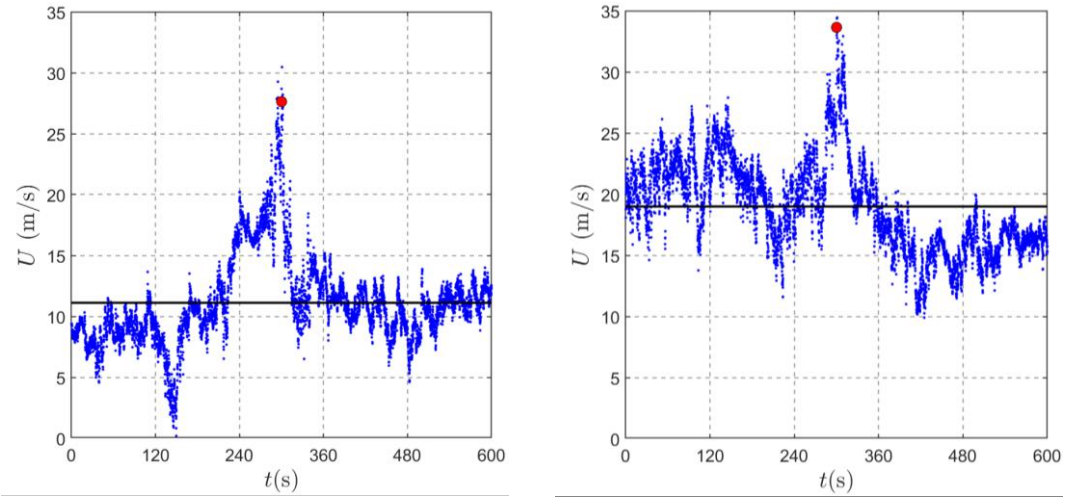

(c) (d)

Figure 3.12 Thunderstorm outflow records characterized by different wind speed classes (a) recorded on 25 August 2015 at 03:20 UTC by the anemometer 1 of the port of Livorno; (b) 15 October 2012 at 00:20 UTC by the anemometer 3 of the port of La Spezia; (c) 16 November 2010 at 02:00 UTC by the anemometer 5 of the port of Livorno; (d) 16 December 2011 at 22:50 UTC by the anemometer 1 of the port of Livorno.

Figure 3.9, Figure 3.10 and **Figure 3.11** show three typical events belonging to these three families, respectively. For each event the pictures **(a)**, **(b)** and **(c)** show, respectively, the time-history of the wind speed in a 10-min, 1-h and 10-h time period indicatively centered around the gust peak. In particular, picture **(a)** illustrates the mean velocity U_{m10} over a 10-min period (horizontal line) and the peak velocity $\hat{v}$ averaged on τ=1 s (circle) (obviously smaller than the instantaneous peak); picture **(b)** shows the mean velocity U_{m60} over a 1-h period (horizontal line), the variation of the mean velocity over 10-min subsequent periods (dotted line), and the 1-s peak (circle); picture **(c)** shows the evolution of the mean velocity over 10-min subsequent periods (dotted line).

The diversity between this approach and typical meteorological surveys is apparent. For instance, according to the Federal Meteorological Handbook No. 1 (NOAA, 2005), ‘‘the beginning of a thunderstorm is to be reported as the earliest time: (1) thunder is heard; (2) lightning is observed at the station when the local noise level is sufficient to prevent hearing thunder; or (3) lightning is detected by an automated sensor’’. Conversely, ‘‘the ending of a thunderstorm shall be reported as 15 minutes after the last occurrence of any of the above criteria’’. The gathering of high quality wind speed records makes it possible to introduce a diverse duration criterion that represents a key advance for hazard analyses, wind loading modelling, structural response and sensitivity to thunderstorm events.

Table 3.2 Classes of membership of the peak wind velocity of thunderstorms.

Duration	Port	15-20(m/s)	20-25(m/s)	25-30(m/s)	30-35(m/s)	Total
10min	GE	11	3	2	0	16
	LI	42	20	2	2	66

	SV	12	6	1	0	19
	SP	23	11	4	2	40
	Total	**88 (63%)**	**40(28%)**	**9(6%)**	**4(3%)**	**141**
1h	GE	19	3	0	0	22
	LI	40	16	3	0	59
	SV	5	0	2	0	7
	SP	14	3	1	0	18
	Total	**78(73%)**	**22(21%)**	**6(6%)**	**0(-)**	**106**
10h	GE	4	1	0	0	5
	LI	10	6	2	0	18
	SV	3	0	0	0	3
	SP	3	1	0	0	4
	Total	**20(67%)**	**8(27%)**	**2(7%)**	**0(-)**	**30**
NTR		186	70	17	4	277

In addition to the above classification criterion, transient records are separated into four groups as a function of the peak wind speed (in m/s), namely $15 \leq \widehat{U} < 20$, $20 \leq \widehat{U} < 25$, $25 \leq \widehat{U} < 30$, and $30 \leq \widehat{U} < 35$. This classification is aimed at recognizing the existence of any correlation between the duration of the gust front and its wind speed; of course, short-duration events with high wind speed are the most relevant hazard from a structural viewpoint. **Figure 3.12** shows the example of a thunderstorm record for each wind speed class. **Table 3.2** shows the results of intersecting the two classification criteria based on the duration and the wind speed pointing out, at least for the available data, no systematic correlation between the duration of the most intense part of the record and the peak wind speed. It is worth noting, however, that the four events whose peak wind speed exceeds 30 m/s are characterized by a limited duration. On the other hand, the 21 events whose peak wind speed exceeds 25 m/s are quite uniformly distributed over different durations.

3.3 Conclusions

Based upon the data detected by the monitoring network of the European Projects "WP" and "WPS" as introduced in **Chapter 2**, this chapter describes the separation of the different extreme wind storms and the extraction of 277 thunderstorm outflow records detected by 14 ultra-sonic anemometers in the period 2011-2016 according a semi-automated procedure proposed by De Gaetano et al. (2014) and improved by Zhang et al. (2018a) thanks to the new experience acquired in this topic carrying out by inspecting 10-min, 1-h and 10-h records centered around the peak wind speed; this approach pursues not only the creation of a more refined and controlled thunderstorm dataset but, even more, a major advance in the understanding of the thunderstorm time-scale and duration.

In this regard thunderstorm outflow records are separated into 3 families depending

on whether the presence of an evident peak associated with the gust front passage is clear in 10-min, 1-h or 10-h periods. In addition, thunderstorm outflows have been separated into 4 groups depending on their peak wind speed. Results show no clear correlation between the duration of the most intense part of the record and the peak wind speed. It is worth noting, however, that the four events whose peak wind speed exceeds 30 m/s have a limited duration.

The precious catalogue of the thunderstorm outflows is the base on understanding their properties and the foundation of the further research of thesis. In the **Chapter 4** the study of the statistical properties of the detected wind velocity signals is restricted to 141 10-min thunderstorms (1-h thunderstorms for the slowly varying mean velocity), thus excluding the 30 10-h thunderstorms (**Table 3.1**), whose duration is so long as to prevent significant transient effects on structures. Then, in **Chapter 5**, the characteristics of the thunderstorms belong to the three families in terms of direction of motion and seasonality/daily occurrence will be analysed. A typical thunderstorm event in Livorno and three events, each one representative of the corresponding class of duration, will be analysed from the meteorological point of view in order to investigate their physical nature. And in **Chapter 6**, considering the records registered in two Port areas, a preliminary but representative analysis of the extreme wind speed distribution is carried out in a mixed wind climate area frequently struck by thunderstorms. In C**hapter 7**, the author of this chapter is based on the Mediterranean Sea separating different winds events and extract the thunderstorm data, the method of application in the Beijing 325 m meteorological tower on the measured data, in order to ascertain the popularity of this method, and the analysis of the characteristics of wind and thunderstorms Beijing compared with Mediterranean thunderstorms, preliminary discovery in different places, whether thunderstorms have similar properties.

4 Characteristics relevant to the wind loading of structures

4.1 Introduction

Despite, as mentioned above, there are already some literatures about thunderstorm, due to the unique complexity, local and small size making very limited the available data, instantaneity and uncertainty of this phenomenon, the understanding, the representation and the modelling of thunderstorm outflows are still full of uncertainties and problems to be clarified (Gunter and Schroeder, 2015). Therefore, the large catalogue of thunderstorms obtained by the Mediterranean monitoring network supported by the European project "WP" and "WPS" described above provides us a unique opportunity to further understand the statistical characteristics of thunderstorms related to wind loading of structures.

Besides, the classical decomposition approach for thunderstorm signal expresses the horizontal component of the wind velocity as the sum of its slowly-varying mean part, averaged on a suitable moving average period, plus a residual fluctuation (Choi and Hidayat, 2002). And the slowly-varying mean wind velocity is modelled as the product of a function depending on space, provided by the previous time-independent analytical models (Oseguera and Bowles, 1988; Zhu and Etkin, 1985; Ivan, 1986; Vicroy, 1992), by a slowly-varying function of time (Chen and Letchford, 2004a, 2004b, 2007; Chay et al., 2006; Ponte and Riera, 2007, 2010; Holmes et al., 2008; Huang et al., 2015). The fluctuation, dealt with as non-stationary, was given by the product of its slowly-varying standard deviation by a random stationary Gaussian process with zero mean and unit standard deviation.

This classical signal decomposition method is diffused in wind engineering. And a relevant part of this research activity focused on how to separate the slowly-varying mean wind velocity from the residual fluctuation without availing of a clear spectral gap. In this framework, the slowly-varying mean wind velocity has been extracted by means of wavelets, empirical mode decomposition and kernel regression (Chen and Letchford, 2007; McCullough et al., 2014; Su et al., 2015) or, more easily, by a moving average filter (Choi and Hidayat, 2002), around which a huge discussion occurred on the most suitable choice of the moving average period (Choi and Hidayat, 2002; Chen and Letchford, 2005, 2006; Holmes et al., 2008; Orwig and Schroeder, 2007; Riera and Ponte, 2012; Lombardo et al., 2014; Solari et al., 2015a).

Very strangely, instead, nobody discussed, at authors' knowledge, a couple of relevant shortcomings involved by the classical decomposition rule rapidly become a sort of axiom. First of all, even if many papers provided a clear discussion on the sudden and large changes frequently exhibited by the wind direction in the course of thunderstorm outflows (Choi, 2000; Holmes et al., 2008; De Gaetano et al., 2014), the wind direction remained outside the decomposition rule from a quantitative viewpoint. In addition, in a totally different way from the classic analysis of synoptic winds, no decomposition was applied to separate the longitudinal turbulence from the lateral one. These aspects created at least three main shortcomings.

First, they caused a deep difference between the study of synoptic and thunderstorm wind speeds, making quite questionable any comparison between the properties of these two phenomena. Second, they oriented the literature on the dynamic response of structures to thunderstorm outflows towards the implicit assumption that the response occurred in the alongwind direction (Choi and Hidayat, 2002; Chen and Letchford, 2004b; Chen, 2008; Kwon and Kareem, 2009; Huang et al., 2013; Solari et al., 2015b; Solari, 2016; Solari et al., 2017; Solari and De Gaetano, 2018; Peng et al., 2018), precluding any chance to separate the alongwind response from the crosswind one, as it is classical, and, even more, to take into account the changes of the angle of attack jointly due to the turbulent fluctuations and to the rapid changes of the wind direction. Third, they did not provide any element to robustly take into account the change of direction in at least two relevant problems: the increase of the speed in thunderstorm outflows due to downburst translation and background flow (Miguel et al., 2018) and the reconstruction of these events through evolutionary models based on measurements and simulations (Abd-Elaal et al., 2013).

To overcome these shortcomings, a novel directional decomposition strategy of the wind speed is herein formulated that opens the doors to a robust comparison and parallel analyses of thunderstorm outflows and synoptic winds in terms of wind speed, wind loading and structural response. It also makes possible an appropriate treatment of all the problems in which the change of direction plays a significant role. This strategy is applied, in the framework of the "111 Project" and ERC Project THUNDERR (www.thunderr.eu), to the anemometric records detected during two previous European Projects, "Wind and Ports" (Solari et al., 2012) and "Wind, Ports and Sea" (Repetto et al., 2018) comparing with the classical decomposition approach and analysing the statistical characteristic of thunderstorm relevant to wind loading of structures. This part of work is already publicised in Journal of Wind Engineering and Industrial Aerodynamics (Zhang et al., 2019a) and Journal of Probability Engineering Mechanics (Zhang et al., 2018a).

In particular, **Sections 4.2.1** and **4.2.2** describe the classical decomposition rules commonly applied to synoptic and thunderstorm outflows, respectively, elucidating their properties through inspecting two typical recordings. **Section 4.2.3** introduces the new directional decomposition rule and compares it with the classical ones using as a reference the typical recordings analysed in the previous two sections. **Section 4.3** analyses an extensive set of thunderstorm outflow recordings using both the classical and the novel strategy in a statistical environment. Accordingly, **Sections 4.3.1**, **4.3.2** and **4.3.3** examine the slowly-varying mean wind velocity, the slowly-varying mean wind direction and the turbulence intensity, respectively. Then **Sections 4.3.4**, **4.3.5** and **4.3.6** illustrate the reduced turbulent fluctuations, integral length scale and power spectral density. **Sections 4.3.7** and **4.3.8** discuss the turbulence intensity modulation and the gust factor. Finally, **Section 4.4** summarizes the main conclusions.

4.2 Decomposition of wind velocity signals

4.2.1 Classical decomposition for synoptic winds

Adopting the classical decomposition rule for synoptic phenomena, the two horizontal components of the wind speed are usually expressed as (**Figure 4.1 (a)**):

$$\begin{aligned} V_{\mathrm{X}}(t) &= \bar{V}_{\mathrm{X}} + V'_{\mathrm{X}}(t) \\ V_{\mathrm{Y}}(t) &= \bar{V}_{\mathrm{Y}} + V'_{\mathrm{Y}}(t) \end{aligned} \tag{4.1}$$

where $t \in [0, \Delta T]$ is the time, being herein $\Delta T = 10$ min, $\bar{V}_{\mathrm{X}}$ and $\bar{V}_{\mathrm{Y}}$ are the mean values of V_{X} and V_{Y} over the time interval ΔT, V'_{X} and V'_{Y} are the residual turbulent fluctuations of V_{X} and V_{Y} with respect to $\bar{V}_{\mathrm{X}}$ and $\bar{V}_{\mathrm{Y}}$.
Based upon **Eq. (4.1)** the mean wind velocity and its direction are given by (**Figure 4.1 (a)**):

$$\begin{aligned} \bar{u} &= \sqrt{\bar{V}_{\mathrm{X}}^2 + \bar{V}_{\mathrm{Y}}^2} \\ \bar{\alpha} &= 270 - \operatorname{atan2}(\bar{V}_{\mathrm{Y}}/\bar{V}_{\mathrm{X}}) \\ \bar{\beta} &= 270 - \bar{\alpha} \end{aligned} \tag{4.2}$$

where $\bar{\alpha}, \bar{\beta} \in [0{:}\,360]$. Accordingly, V'_{X} and V'_{Y} are projected onto a new Cartesian reference system (*x*, *y*), where the *x*-axis coincides with the direction of the mean wind velocity $\bar{u}$ and is rotated $\bar{\beta}$ with respect to the fixed *X*-axis. Thus (**Figure 4.1 (b)**):

$$\begin{aligned} u'(t) &= V'_{\mathrm{X}}(t)\cos\bar{\beta} + V'_{\mathrm{Y}}(t)\sin\bar{\beta} \\ v'(t) &= -V'_{\mathrm{X}}(t)\sin\bar{\beta} + V'_{\mathrm{Y}}(t)\cos\bar{\beta} \end{aligned} \tag{4.3}$$

where u' and v' are the longitudinal and lateral turbulent components. **Eq. (4.3)** can also be re-written as:

$$\begin{aligned} u'(t) &= \sigma_u \tilde{u}'(t) \\ v'(t) &= \sigma_v \tilde{v}'(t) \end{aligned} \tag{4.4}$$

where σ_u and σ_v are the standard deviations of u' and v' over ΔT, $\tilde{u}'$ and $\tilde{v}'$ are the reduced longitudinal and lateral turbulence components. The latter terms are usually modelled as un-correlated stationary Gaussian random processes with zero mean and unit standard deviation (Solari and Piccardo, 2001).

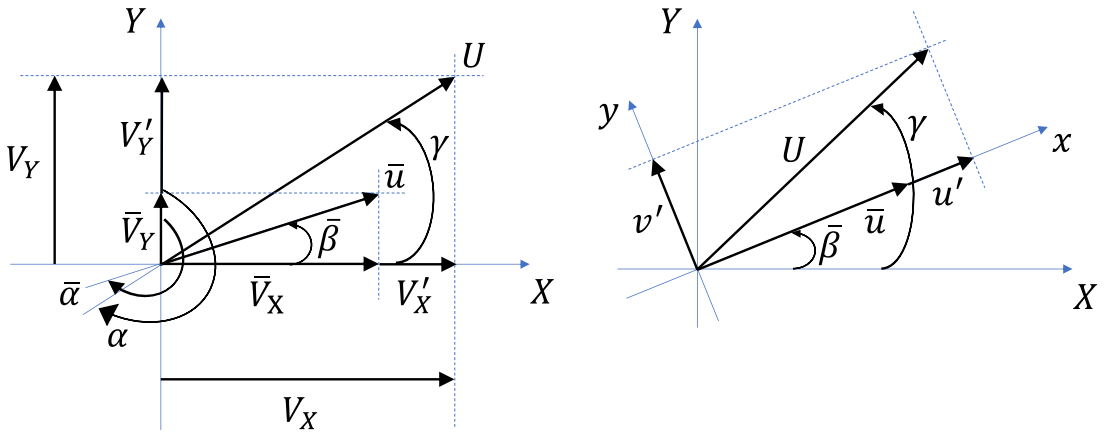

(a) (b)

Figure 4.1 Classical decomposition of the wind speed for synoptic phenomena.

Thanks to **Eqs. (4.2)** to **(4.4)** the longitudinal and lateral components of the wind velocity can be expressed as:

$$\begin{aligned} u(t) &= \bar{u} + u'(t) = \bar{u}[1 + I_u \tilde{u}'(t)] \\ v(t) &= v'(t) = \bar{u} I_v \tilde{v}'(t) \end{aligned} \tag{4.5}$$

where I_u and I_v are the longitudinal and lateral turbulence intensities:

$$\begin{aligned} I_u &= \sigma_u / \bar{u} \\ I_v &= \sigma_v / \bar{u} \end{aligned} \tag{4.6}$$

Literature is usual to assign $I_v / I_u = 0.75$ (Solari and Piccardo, 2001).
Finally, the gust factor is expressed as:

$$G_u = \hat{u} / \bar{u} \tag{4.7}$$

where $\hat{u}$ is the peak longitudinal velocity defined here as the maximum longitudinal wind velocity averaged over a τ = 1-s period.
Figure 4.2 shows the application of **Eqs. (4.1)** to **(4.3)** to the wind velocity of a synoptic extra-tropical cyclone recorded on July 8, 2014 by the anemometer 1 of the Port of Livorno; both the velocity components V_X and V_Y exhibit a typical stationary trend. In this case, $\bar{u}$ = 16.71 m/s, $\bar{\alpha}$= 251.51 degrees, I_u = 0.13, I_v = $0.10 = 0.76 I_u$, $\rho_{uv} = -0.11$, ρ_{uv} being the cross-correlation coefficient of u' and v'. In addition, the latter quantities have skewness values $\gamma_u = -0.40$ and $\gamma_v = 0.16$ whereas their kurtosis values are $\kappa_u = 2.65$ and $\kappa_v = 2.99$. All these values are coherent with those classically reported by the literature with regard to synoptic phenomena.

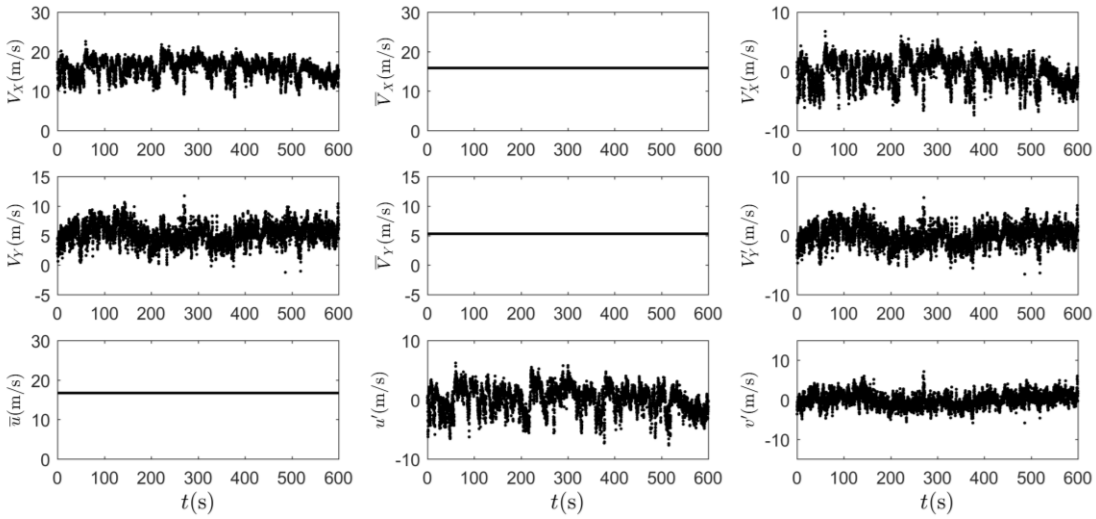

Figure 4.2 Application of Eqs. (4.1) to (4.3) to a typical synoptic extra-tropical cyclone.

It is worth noting, however, that having determined the mean wind velocity over ΔT, the residual fluctuations contain harmonic contents both in the low-frequency range (slowly-varying long waves) and in the high-frequency range (rapidly-varying short oscillations).

4.2.2 Classical decomposition for thunderstorm outflows

Let us consider the horizontal components of the wind velocity U and its direction γ or α as defined by **Eq. (2.1)** and **Figure 2.5 (b)**. It is worth noticing that most papers dealing with thunderstorm outflows provide diagrams of both the U and γ or α time-histories (Choi, 2000; Holmes et al., 2008; De Gaetano et al., 2014). However, while the velocity is later analysed in detail as described hereinafter, the direction is considered only on a qualitative level. Under this point of view, as an example, most research carried out on the dynamic response of structures to thunderstorm outflows (Choi and Hidayat, 2002a; Chen and Letchford, 2004b; Chen, 2008; Kwon and Kareem, 2009; Solari et al., 2015b; Solari, 2016; Solari et al., 2017; Solari and De Gaetano, 2018) implicitly deals with a sort of alongwind response, disregarding the fact that the wind direction often varies rapidly and thus produces alongwind and crosswind vibrations.

Based on this premise, as it is classical, let us express the wind velocity U of a thunderstorm outflow by the relationship (**Figure 4.3**):

$$U(t) = \overline{U}(t) + U'(t) \tag{4.8}$$

where $\overline{U}$ is the slowly-varying mean wind velocity extracted here by a running-mean filter with a moving average period T= 30 s, whereas U' is the residual turbulent fluctuation expressed as:

$$U'(t) = \sigma_U(t)\widetilde{U}'(t) \tag{4.9}$$

where σ_U is the slowly-varying standard deviation of U', $\widetilde{U}'$ is the reduced turbulent fluctuation. This latter quantity is usually modelled as a stationary Gaussian random process with zero mean and unit standard deviation (Chen and Letchford, 2004a; Holmes et al., 2008; Solari et al., 2015a).

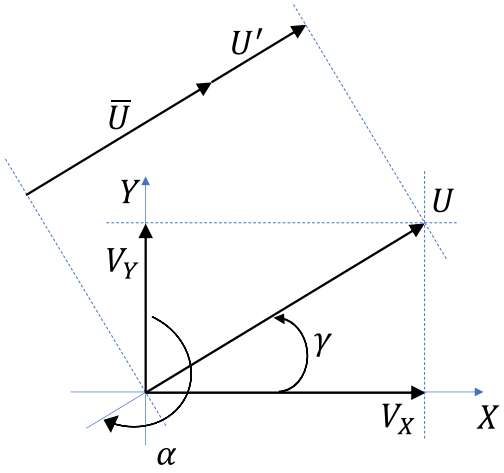

Figure 4.3 Classical decomposition of the wind speed for thunderstorm outflows.

Replacing **Eq. (4.9)** into **Eq. (4.8)**, the wind velocity U results:

$$U(t) = \bar{U}(t)\left[1 + I_U(t)\widetilde{U}'(t)\right] \tag{4.10}$$

where:

$$I_U(t) = \sigma_U(t)/\bar{U}(t) \tag{4.11}$$

is the slowly-varying turbulence intensity.
Let us now express the slowly-varying mean wind velocity and turbulence intensity as:

$$\bar{U}(t) = \bar{U}_{max}\gamma_U(t) \tag{4.12}$$

$$I_U(t) = \bar{I}_U\mu_U(t) \tag{4.13}$$

where $\bar{U}_{max}$ is the maximum value of $\bar{U}$ whereas γ_U is a non-dimensional function of t that describes the slow variation of $\bar{U}$, being $\gamma_{U,max} = 1$; $\bar{I}_U$ is the mean value of I_U over ΔT whereas μ_U is a non-dimensional function of t that describes the slow variation of I_U, being $\bar{\mu}_U = 1$.
Replacing **Eqs. (4.12)** and **(4.13)** into **Eq. (4.10)** the wind velocity may be re-written as:

$$U(t) = \bar{U}_{max}\ \gamma_U(t)\left[1 + \bar{I}_U\mu_U(t)\widetilde{U}'(t)\right] \tag{4.14}$$

Finally, the gust factor is expressed as:

$$G_U = \widehat{U}/\overline{U}_{max} \tag{4.15}$$

where $\widehat{U}$ is the peak wind velocity (τ = 1 s).
It is apparent that the above expressions are different from those described in **Section 4.2.1** not only because they disregard the wind direction. On assuming $T = \Delta T$, namely on identifying the moving average period with the 10-min average period traditionally used for synoptic winds, the model of the thunderstorm outflow depicted above does not provide the classical model of the synoptic wind, where the horizontal turbulent fluctuation is expressed in terms of its longitudinal and lateral components.

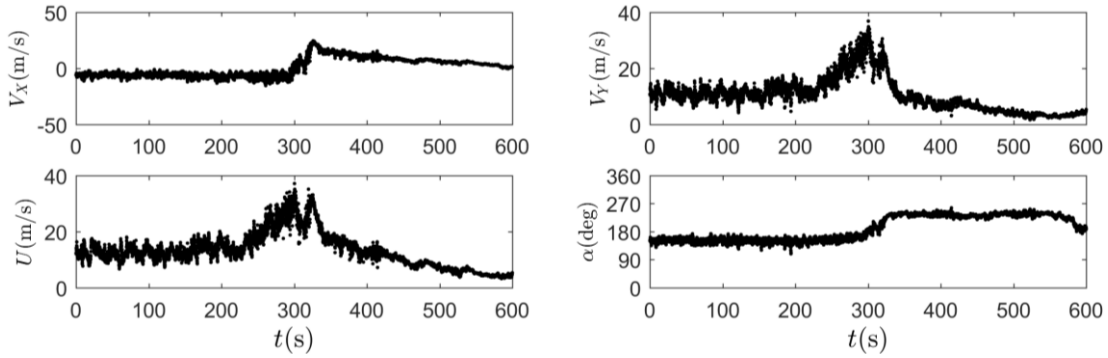

Figure 4.4 Application of Eq. (4.1) to a typical thunderstorm outflow.

Figure 4.4 shows the application of **Eq. (4.2)** to the wind velocity of a thunderstorm outflow recorded on October 25, 2011 by the anemometer 3 of the Port of La Spezia; the peak wind velocity is $\widehat{U} =$ 33.98 m/s. Both the velocity components V_{X} and V_{Y}, and thus the velocity U, exhibit typical non-stationary trends characterised by sudden simultaneous ramp-up phases in correspondence of which the wind direction changes of about 90 degrees.
Figure 4.5 shows the application of **Eqs. (4.8)** to **(4.11)** to the same recording. The maximum value of the slowly-varying mean wind velocity is $\overline{U}_{max} =$ 26.86 m/s. The slowly-varying turbulence intensity has a mean value $\bar{I}_U =$ 0.121; it exhibits a quite unusual decreasing trend. The reduced turbulent fluctuation has nearly zero mean and unit standard deviation; its skewness is $\gamma_U =$ 0.120 while its kurtosis is $\kappa_U =$ 2.895. As it is classical, the wind direction is no longer considered.

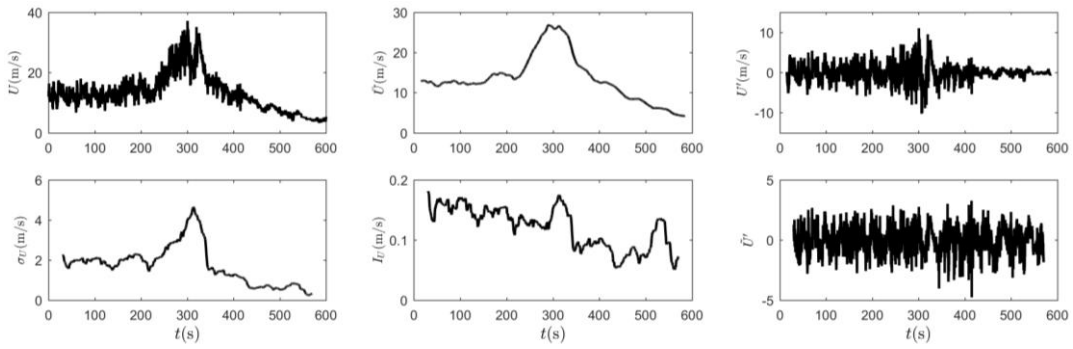

Figure 4.5 Application of Eqs. (4.8) to (4.11) to a typical thunderstorm outflow.

4.2.3 Novel directional decomposition approach

In order to overcome the above shortcomings and make the decomposition rule for thunderstorm outflows (**Section 4.2.2**) fully coherent with the one adopted for synoptic phenomena (**Section 4.2.1**), a novel decomposition strategy is herein formulated in which the variation of the wind direction is explicitly taken into account. In this framework, independently of whether the Aeolian phenomenon under examination is a synoptic event or a thunderstorm outflow, the two horizontal components of the wind speed are expressed as (**Figure 4.1 (a)**):

$$\begin{aligned} V_{\mathrm{X}}(t) &= \bar{V}_{\mathrm{X}}(t) + V'_{\mathrm{X}}(t) \\ V_{\mathrm{Y}}(t) &= \bar{V}_{\mathrm{Y}}(t) + V'_{\mathrm{Y}}(t) \end{aligned} \tag{4.16}$$

where $\bar{V}_{\mathrm{X}}$ and $\bar{V}_{\mathrm{Y}}$ are the slowly-varying mean wind velocity components extracted here by a running-mean filter with a moving average period T = 30 s, whereas V'_{X} and V'_{Y} are the residual turbulent fluctuations.

It is worth noticing that **Eq. (4.16)** identifies with **Eq. (4.1)** with the sole difference that the mean wind velocity components depend on time. The same property applies to the following equations in a generalised sense. Adopting this principle **Figure 4.1** can be retained as the reference scheme also for this section.

Based upon **Eq. (4.16)** the slowly-varying mean wind velocity and its slowly varying mean wind direction are given by (**Figure 4.1 (a)**):

$$\begin{aligned} \bar{u}(t) &= \sqrt{\bar{V}_{\mathrm{X}}^2(t) + \bar{V}_{\mathrm{Y}}^2(t)} \\ \bar{\alpha}(t) &= 270 - \mathrm{atan2}(\bar{V}_{\mathrm{Y}}(t)/\bar{V}_{\mathrm{X}}(t)) \\ \bar{\beta}(t) &= 270 - \bar{\alpha}(t) \end{aligned} \tag{4.17}$$

where $\bar{\alpha}, \bar{\beta} \in [0{:}\,360]$. Accordingly, V'_{X} and V'_{Y} are projected onto a new Cartesian reference system (x, y), where the x-axis coincides with the direction of $\bar{u} = \bar{u}(t)$ and is rotated $\bar{\beta} = \bar{\beta}(t)$ with respect to the fixed X-axis. Thus (**Figure 4.1 (b)**):

$$u'(t) = V'_{\mathrm{X}}(t)\cos\bar{\beta}(t) + V'_{\mathrm{Y}}(t)\sin\bar{\beta}(t)$$
$$v'(t) = -V'_{\mathrm{X}}(t)\sin\bar{\beta}(t) + V'_{\mathrm{Y}}(t)\cos\bar{\beta}(t) \quad (4.18)$$

where u' and v' are the longitudinal and lateral turbulent fluctuations. **Eq. (4.18)** can also be re-written as:

$$u'(t) = \sigma_u(t)\tilde{u}'(t)$$
$$v'(t) = \sigma_v(t)\tilde{v}'(t) \quad (4.19)$$

where σ_u and σ_v are the slowly varying standard deviations of u' and v', $\tilde{u}'$ and $\tilde{v}'$ are the reduced longitudinal and lateral turbulent components. The prosecution of this paper proves that these latter quantities can be modelled as un-correlated stationary Gaussian random processes with zero mean and unit standard deviation.
Thanks to **Eqs. (4.17)** to **(4.19)** the longitudinal and lateral components of the wind velocity can be expressed as:

$$u(t) = \bar{u}(t) + u'(t) = \bar{u}(t)[1 + I_u(t)\tilde{u}'(t)]$$
$$v(t) = v'(t) = \bar{u}(t)I_v(t)\tilde{v}'(t) \quad (4.20)$$

where I_u and I_v are the slowly-varying longitudinal and lateral turbulence intensities:

$$I_u(t) = \sigma_u(t)/\bar{u}(t)$$
$$I_v(t) = \sigma_v(t)/\bar{u}(t) \quad (4.21)$$

Eqs. (4.16) to **(4.21)** represent a full generalization of **Eqs. (4.1)** to **(4.6)** with the key remark that the mean quantities, the standards deviations and the turbulence intensities are now slowly-varying function of time as well as the direction of the mean wind speed. It follows that the longitudinal and lateral turbulence components of the wind velocity are aligned with a couple axes (*x*, *y*) whose direction is a slowly-varying function of time.
Likewise **Eqs. (4.12)** and **(4.13)**, the slowly-varying mean wind speed and the slowly-varying turbulence intensities can be expressed as:

$$\bar{u}(t) = \bar{u}_{max}\gamma_u(t) \quad (4.22)$$

$$I_u(t) = \bar{I}_u\mu_u(t)$$
$$I_v(t) = \bar{I}_v\mu_v(t) \quad (4.23)$$

where $\bar{u}_{max}$ is the maximum value of $\bar{u}$ whereas γ_u is a non-dimensional function of t that describes the slow variation of $\bar{u}$, being $\gamma_{u,max} = 1$; $\bar{I}_u$ and $\bar{I}_v$ are the mean values of I_u and I_v in ΔT, whereas μ_u and μ_v are non-dimensional functions of t

that describe the slow variation of I_u and I_v, being $\bar{\mu}_u = \bar{\mu}_v = 1$.
In a similar way to **Eq. (4.14)**, replacing **Eqs. (4.22)** and **(4.23)** into **Eq. (4.20)** the longitudinal and lateral components of the wind velocity may be re-written as:

$$\begin{aligned} u(t) &= \bar{u}(t)[1 + I_u(t)\tilde{u}'(t)] = \bar{u}_{max}\gamma_u(t)[1 + \bar{I}_u\mu_u(t)\tilde{u}'(t)] \\ v(t) &= \bar{u}(t)I_v(t)\tilde{v}'(t) = \bar{u}_{max}\gamma_u(t)\bar{I}_v\mu_v(t)\tilde{v}'(t) \end{aligned} \tag{4.24}$$

Finally, the gust factor is expressed by the relationship:

$$G_u = \hat{u}/\bar{u}_{max} \tag{4.25}$$

where $\hat{u}$ is the peak longitudinal velocity (τ = 1 s).
It is worth noting that, on assuming $T = \Delta T$, namely identifying the moving average period with the 10-min average period, this model provides the classical model for synoptic wind speeds as a particular case. In this case, $\bar{u}$, σ_u, σ_v, I_u and I_v are constant quantities whereas $\bar{u}_{max} = \bar{u}$, $\gamma = \mu_u = \mu_v = 1$.

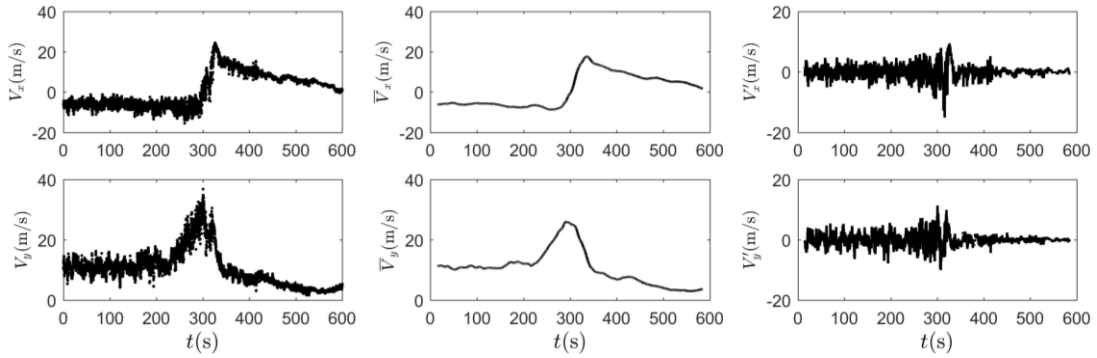

Figure 4.6 Application of Eq. (4.16) to the thunderstorm outflow examined in Section 4.2.2.

Figure 4.6 shows the application of **Eq. (4.16)** to the wind velocity of the thunderstorm outflow already analysed in **Section 4.2.2**. Similarly, **Figure 4.7** shows the application of **Eqs. (4.17)** to **(4.21)**. The maximum value of the slowly-varying mean wind velocity is $\bar{u}_{max} = 26.39$ m/s; it is slightly different from the value $\overline{U}_{max} = 26.86$ m/s provided by the classical approach. The mean values of the longitudinal and lateral turbulence intensities are $\bar{I}_u$ = 0.123 and $\bar{I}_v$ = 0.104, respectively; their ratio, $\bar{I}_v/\bar{I}_u = 0.85$, is greater than the reference value $I_v/I_u = 0.75$ commonly adopted for synoptic winds. The reduced longitudinal and lateral turbulence components have both nearly zero mean and unit standard deviation; their skewness values are γ_u = -0.129 and γ_v = 0.129 while the kurtosis values are κ_u = 2.924 and κ_v = 2.996; the cross-correlation coefficient is ρ_{uv} = -0.152.

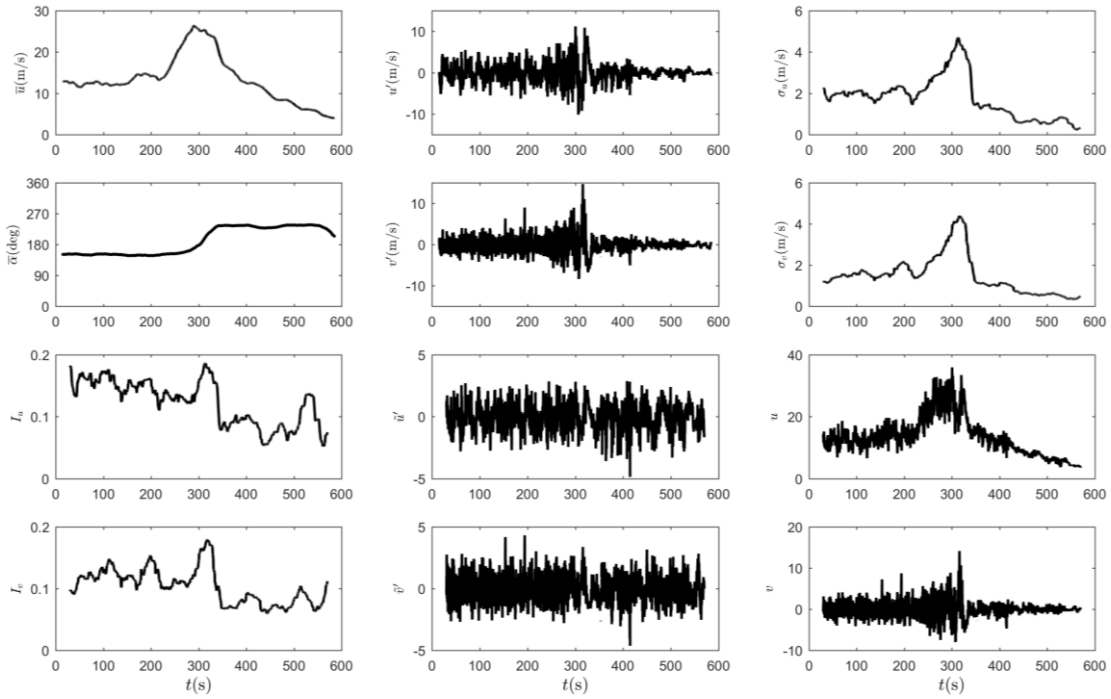

Figure 4.7 Application of Eqs. (4.17) to (4.21) to the thunderstorm outflow examined in Section 4.2.2.

Figure 4.8 shows the application of **Eqs. (4.16)** to **(4.21)** to the wind velocity of the synoptic extra-tropical cyclone already analysed in **Section 4.2.1**. In this case, the slowly varying mean wind velocity is characterised by a low-frequency harmonic content (slowly-varying long waves), previously embedded in the classical residual turbulent fluctuations, while the new residual turbulent fluctuations exhibit only a dominant high-frequency harmonic content (rapidly-varying short oscillations). The maximum value of the slowly-varying mean wind velocity is $\bar{u}_{max} =$ 16.80 m/s; as expected, it is slightly greater than the constant value $\bar{u} = 16.71$ m/s, since it takes into account the slowly-varying long waves previously embedded in the turbulent fluctuations. The mean values of the longitudinal and lateral turbulence intensities are $\bar{I}_u =$ 0.10 and $\bar{I}_v =$ 0.08, respectively; their ratio, $\bar{I}_v/\bar{I}_u =$ 0.82, is greater than the previous value $I_v/I_u = 0.76$ since excluding the slowly-varying long waves from the turbulent fluctuations they tend to the isotropic condition typical of the inertial sub-range. The reduced longitudinal and lateral turbulence components have nearly zero mean and unit standard deviation; their skewness and kurtosis values are $\gamma_u = -0.61$, $\gamma_v =$ 0.13, $\kappa_u = 3.45$, $\kappa_v = 3.58$; the cross-correlation coefficient is $\rho_{uv} =$ -0.03.

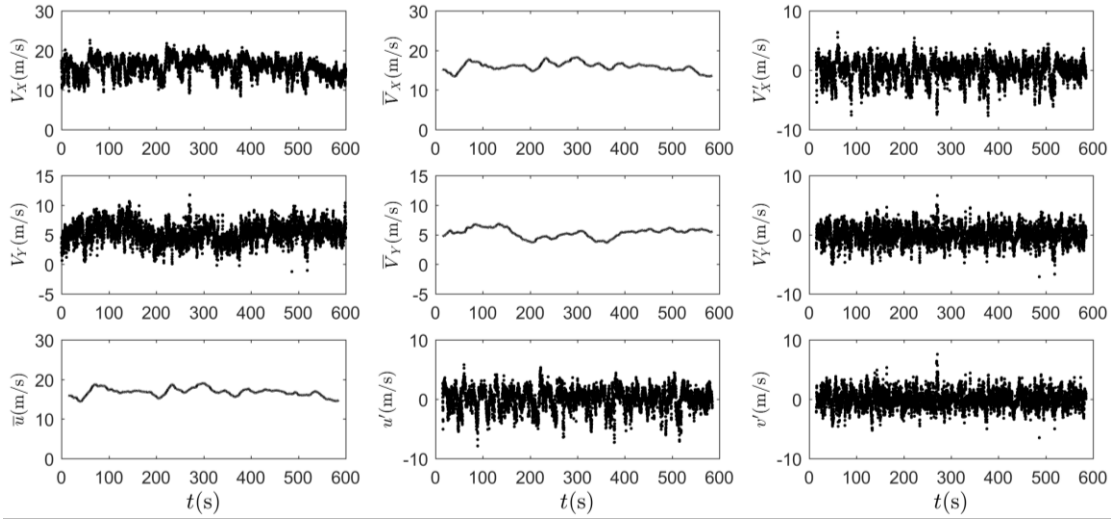

Figure 4.8 Application of Eqs. (4.16) to (4.21) to the synoptic extra-tropical cyclone examined in Section 4.2.1.

4.3 Statistical properties of the thunderstorm outflows

Having available 141 10-min and 106 1-h thunderstorm outflow records as shown in **Table 3.1** involving rapid variations in speed, each of them has been first decomposed into component signals whose properties have been examined by the classical rule first of all and there is no relevant difference between 10-min and 1-h thunderstorms except the slowly varying mean wind velocity (Zhang et al., 2018a). Therefore, only in **Section 4.3.1** both of these families are presented for learning their prominent peak. And then only the 141 intense thunderstorm records belong to 10-min family are decomposed by means of the classical (**Section 4.2.2**) and novel (**Section 4.2.3**) rules. Subsequently, these component properties have been analysed as a whole in statistical form. Finally, the results are compared and discussed. In this framework, the prosecution of this section deals with the slowly-varying mean wind speed (**Section 4.3.1**) and direction (**Section 4.3.2**), the turbulence intensity (**Section 4.3.3**), the reduced turbulent fluctuations (**Section 4.3.4**), their integral length scales (**Section 4.3.5**) and power spectral densities (**Section 4.3.6**), the turbulence intensity modulation (**Section 4.3.7**) and the gust factor (**Section 4.3.8**). It is worth noticing that the application of the classical method may involve some slight differences respect to the results obtained by Zhang et al. (2018a) and even more by Solari et al. (2015a); this happens because, on passing the time, the data and dataset have been progressively improved.

4.3.1 Slowly-varying mean wind velocity

The records labelled here as thunderstorm outflows are characterized by a prominent peak whose duration has a dominant role in the wind loading and response of structures (Kwon and Kareem, 2009); it corresponds to the gust front passage and it is classically described by the slowly varying mean wind velocity $\overline{U}(t)$ or, more

precisely, by the non-dimensional function $\gamma_U(t)$ (**Eq. (4.12)**) (Solari et al., 2015a).

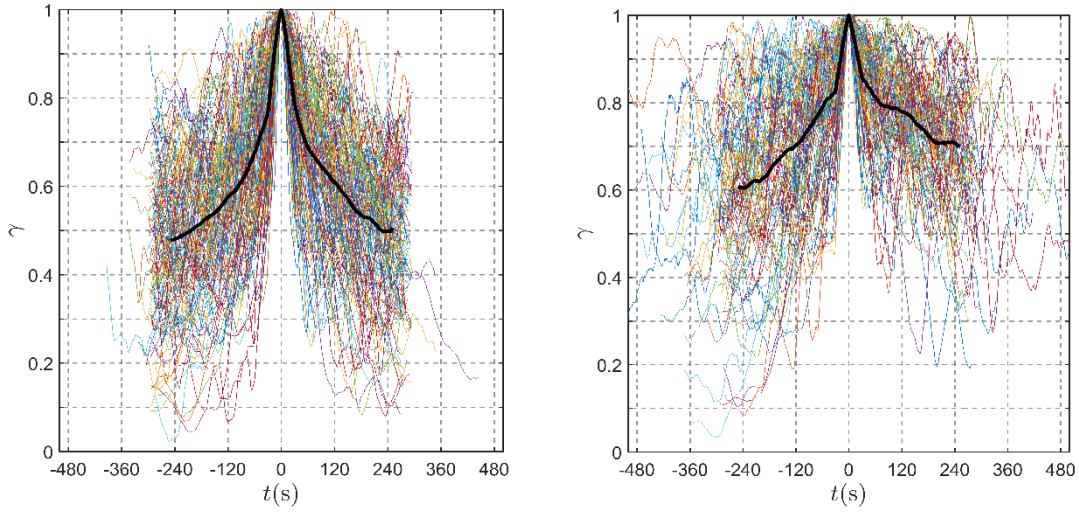

Figure 4.9 Ensemble of the diagrams of $\gamma_U(t)$ for all the 10-min (a) and 1-h (b) thunderstorm records investigated, and their mean value (thick line).

Figure 4.9 shows the ensemble of the diagrams of $\gamma_U(t)$ for all the 10-min (a) and 1-h (b) thunderstorm records investigated; the thick lines refer to the mean value of $\gamma_U(t)$ as a function of time. This figure confirms what was already noted in Solari et al. (2014): due to the great variability of the functions $\gamma_U(t)$, they can be regarded as samples of a non-stationary random process. The mean values of $\gamma_U(t)$ in the pictures (a) and (b) sums up the essential features of a sudden ramp-up and down in the wind speed; they are very similar in proximity of the peak whereas their difference is apparent far from it. In particular, the definition of the peak duration provided in Solari et al. (2014), namely the period in which $\gamma_U(t)$ is greater than or equal to 0.6, confirms that 1-h thunderstorms last clearly more than the 10-min ones. In both cases the inner envelopes of the $\gamma_U(t)$ diagram closely approximate the half-sine wave function introduced in Kwon and Kareem (2009) in order to model $\bar{U}(t)$.

The number of thunderstorm signals detected with a high sampling rate offers authors a unique opportunity to establish a preliminary description of the most recurrent shapes of the slowly-varying mean wind velocity time histories.

The family of the 10-min thunderstorm records presents a large variety of shapes, whose features could in principle affect the structural response. **Figure 4.10** depicts some examples of the dominant shapes, showing the 20-min time histories of the wind speed centered around the 1-s peak. The most frequent shape is similar to a single spike lasting 2 to 3-4 minutes approximately, as shown in **Figure 4.10 (a,b)**. Note that the highest slope of the spike can occur during the ramp-up (**Figure 4.10 (a)**) as well as during the drop-off, after the maximum (**Figure 4.10 (b)**). A second recurrent shape presents a plateau after a very steep ramp-up that lasts about 4-5 minutes, as shown in **Figure 4.10 (c,d)**. Instead of a single maximum, the plateau is characterized

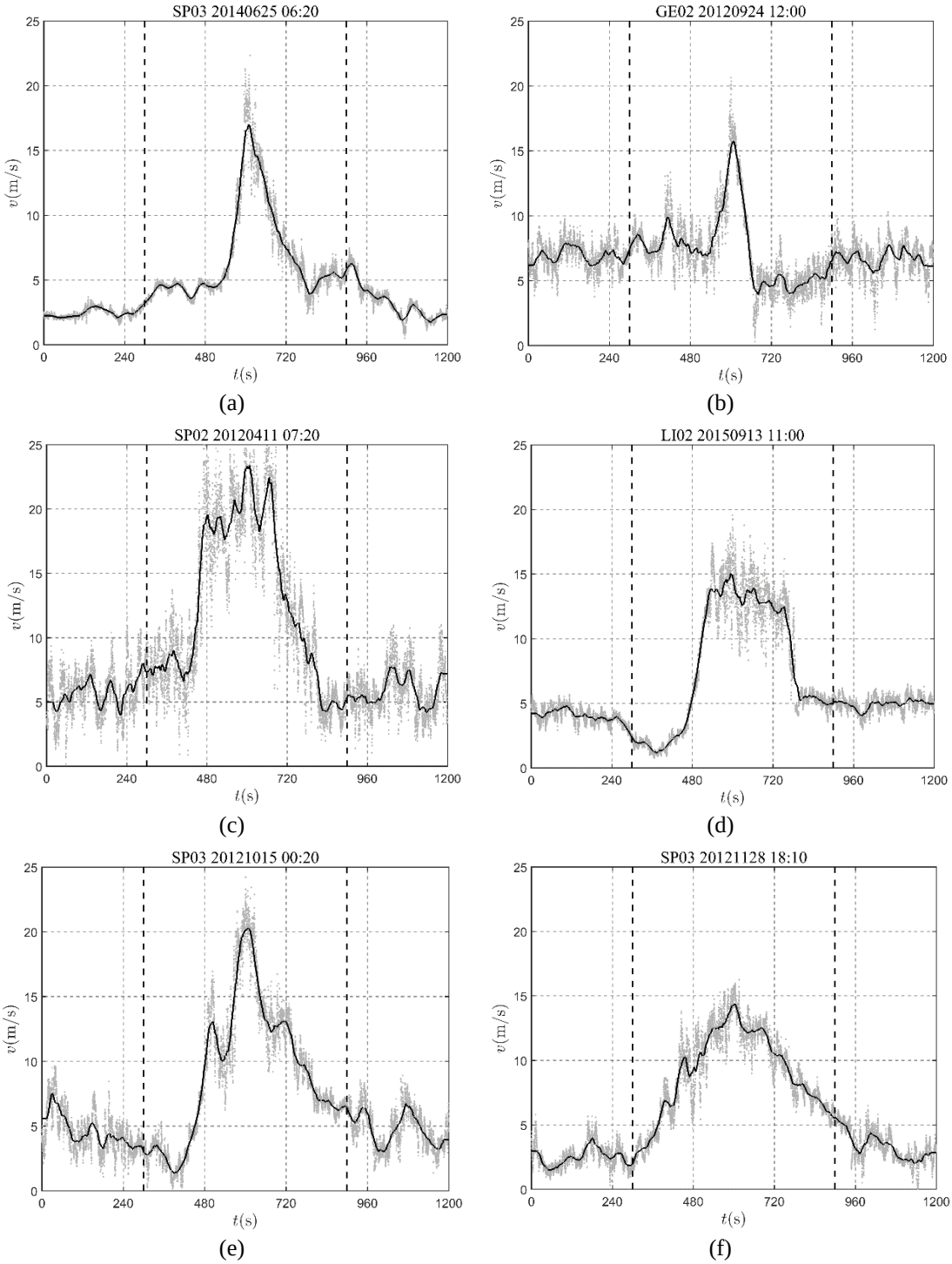

Figure 4.10 Examples of 10-min thunderstorm records that present wind gusts with different shapes (the gray points denote the 20min wind speed history; the black lines show the moving average wind speed; the vertical dashed lines include the 10-min time window around the peak).

by many secondary peaks. **Figure 4.10 (e,f)** shows less frequent shapes, characterized by two well distinguished peaks (**Figure 4.10 (e)**) or by relatively mild increasing /decreasing ramps (**Figure 4.10 (f)**). A common feature of all these 10-min signals is that they all have a lower background wind speed before and after the stronger event's occurrence, which represents the mean flow that these short-living thunderstorms are

embedded into.

The family of the 1-h thunderstorm records may be drawn back to some recurrent shapes depicted through the examples in **Figure 4.11**, which shows the 2-h time histories of the wind speed centered around the 1-s peak. The first group is characterized by a strong event lasting approximately 20-40 minutes as shown in **Figure 4.11 (a,b)**; also in these cases the highest slope of the spike can occur during the ramp-up (**Figure 4.11 (a)**) as well as during the drop-off, after the maximum (**Figure 4.11 (b)**). The second recurrent shapes presents a plateau after a very steep ramp-up, that lasts 30-50 minutes and is characterized by many peaks of the same order of magnitude (**Figure 4.11 (c)**) or by secondary maxima after the main peak's occurrence (**Figure 4.11 (d)**). **Figure 4.11 (e,f)** shows less frequent shapes, characterized by relatively slow increasing/decreasing ramps. Differently from the 10-min records, these events can also be subdivided according to the occurrence or not of a transition between different wind regimes during the 1-h period. **Figure 4.11 (a,c,e)** shows some examples of the no-transition case, in which the large short-lasting events are superimposed to a steady lower background flow. **Figure 4.11 (b,d,f)** shows some examples of transition cases between higher-to-lower (**Figure 4.11 (b,f)**) or between lower-to-higher (**Figure 4.11 (d)**) wind speed regimes. Such transitions can be due, for instance, to mesoscale meteorological structures like fronts, which represent the passage between two different air masses and are usually associated to an intense convective activity sometimes organized in multi-cell systems, e.g. squall lines.

Studies will be in illustrated in **Section 5.4** to inspect the meteorological phenomena that can be associated to different thunderstorm shapes as well as to evaluate the response of structures to 10-min and 1-h thunderstorm records in order to clarify the actual role of the gust front time passage.

During the study of the thesis, the novel directional decomposition approach is proposed as illustrated in **Section 4.2.3** and applied to the intense thunderstorm in 10-min family comparing with the results by classical decomposition method.

The comparison between the slowly-varying mean wind velocity evaluated by means of the classical, $\overline{U}_{max}$ (**Eq. (4.12)**), and directional, $\bar{u}_{max}$ (**Eq. (4.22)**), decomposition rules proves that they are, on average, very close to each other: the average value of their ratios over the ensemble of the analysed records is $< \bar{u}_{max}/\overline{U}_{max} >$ = 0.99. **Figure 4.12** shows the average value of the non-dimensional functions $\gamma_U(t)$ (**Eq. (4.12)**), black solid line) and $\gamma_u(t)$ (**Eq. (4.22)**, blue dashed line) over all the thunderstorm outflow records investigated; they are characterized by a prominent peak that sums up the essential features of the sudden ramp-up and slow-down of the wind speed corresponding to the passage of a gust front. It is apparent that the classical decomposition rule and the new directional one provide almost overlapped results in proximity of the peak whereas small differences occur on the tails.

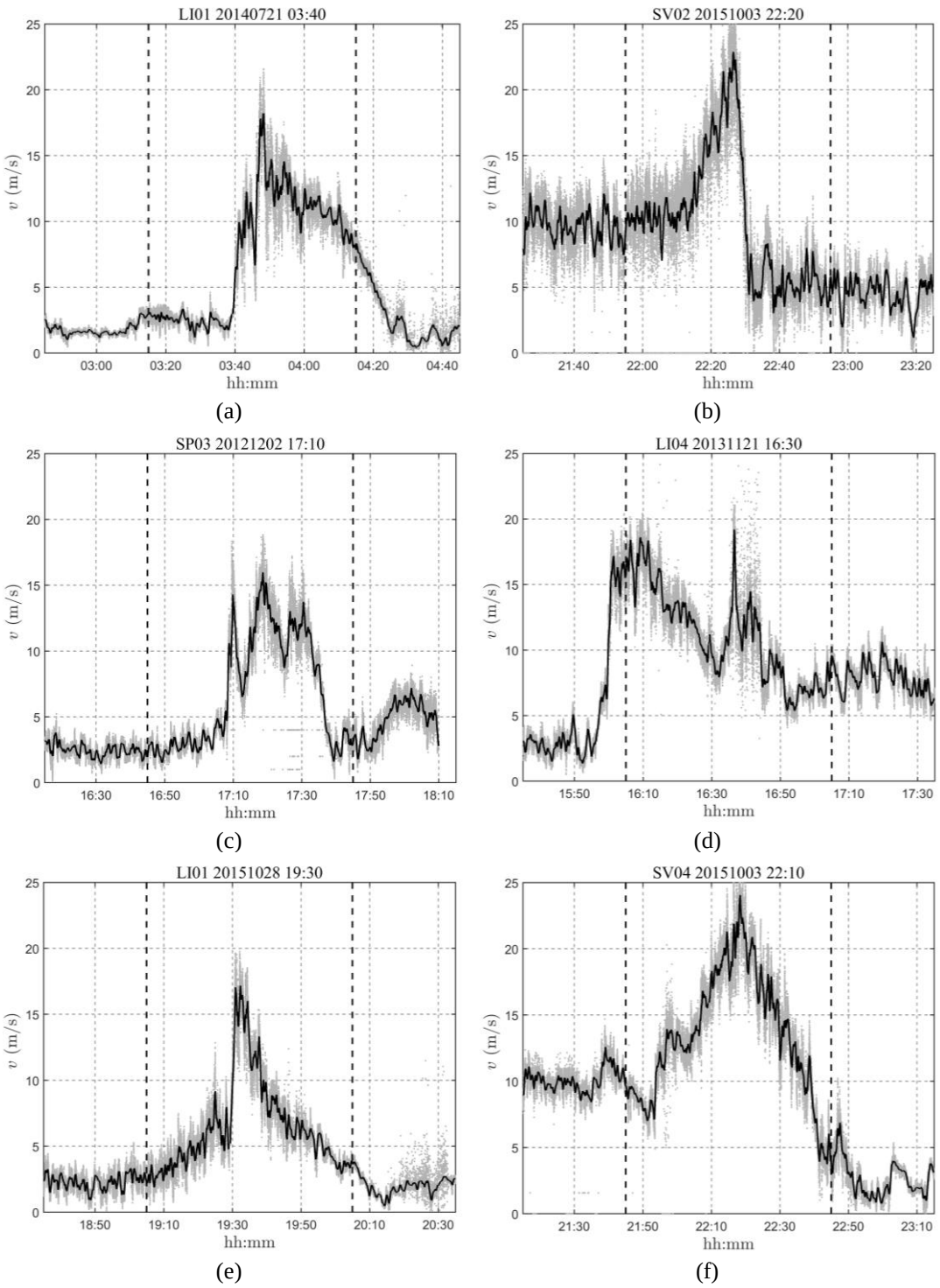

Figure 4.11 Examples of 1-h thunderstorm records that present wind gusts with different shapes (the gray points denote the 2h wind speed history; the black lines show the moving average wind speed; the vertical dashed lines include the 1-h time window around the peak).

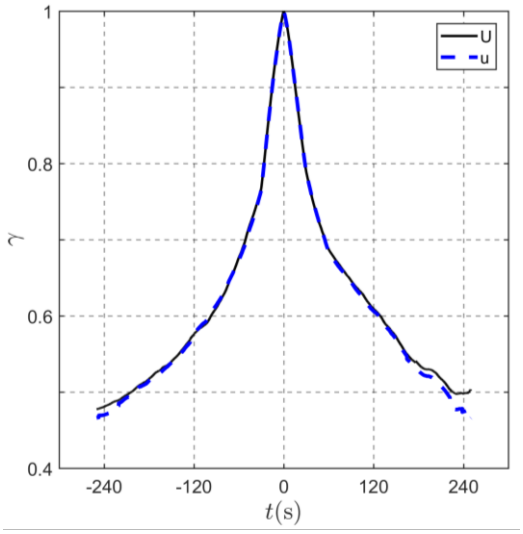

Figure 4.12 Ensemble mean value of the normalized slowly-varying mean wind velocity.

4.3.2 Slowly-varying mean wind direction

According to the classical decomposition rule, the wind direction of the thunderstorm outflows is usually examined qualitatively, but later disregarded quantitatively. This unavoidably leads to consider the wind direction, more or less implicitly, as invariant with time. The dominant property of the new decomposition strategy is its ability to extract and embed the slowly-varying mean wind direction $\bar{\alpha}$ or $\bar{\beta}$ **(Eq. (4.17))** within the wind velocity model.

Table 4.1 Number of thunderstorm outflows (%) characterised by given ranges of the maximum shift of the slowly-varying mean wind direction.

Maximum direction shift (deg)	Method 1	Method 2
$\Delta\bar{\alpha}_{max} \leq 45$	41 (29%)	92 (65%)
$45 < \Delta\bar{\alpha}_{max} \leq 90$	56 (40%)	35 (25%)
$90 < \Delta\bar{\alpha}_{max} \leq 180$	30 (21%)	10 (7%)
$\Delta\bar{\alpha}_{max} > 180$	14 (10%)	4 (3%)
All	141 (100%)	141 (100%)

This fact is relevant because, when a thunderstorm outflow occurs, the slowly-varying mean wind direction often changes suddenly, and the rate of this change depends on the translation of the thunderstorm cell with respect to the anemometer that registers the record as well as on the background wind speed – namely the wind speed associated with the synoptic weather condition in which the thunderstorm takes place – before and after the downburst, which in principle could be different from each other. This situation may make difficult to distinguish between the rate of change due to the thunderstorm outflow alone and the rate of change that occurs due to the evolution of the weather conditions.

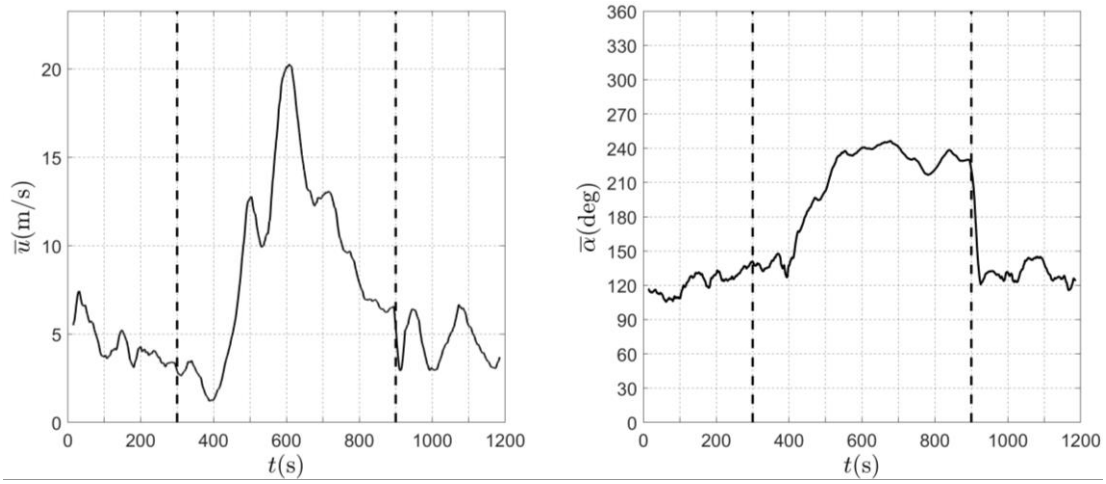

(a) **(b)**

Figure 4.13 20-min slowly-varying mean wind velocity (a) and direction (b) during a thunderstorm outflow occurred on October 15, 2012 in the Port of La Spezia (the vertical dashed lines include the 10-min period centred around the peak wind velocity).

The examination of the slowly-varying mean wind direction of the thunderstorm outflow records considered here depicts complex and varied trends that make anything but simple to classify these phenomena according to their shift in wind direction.

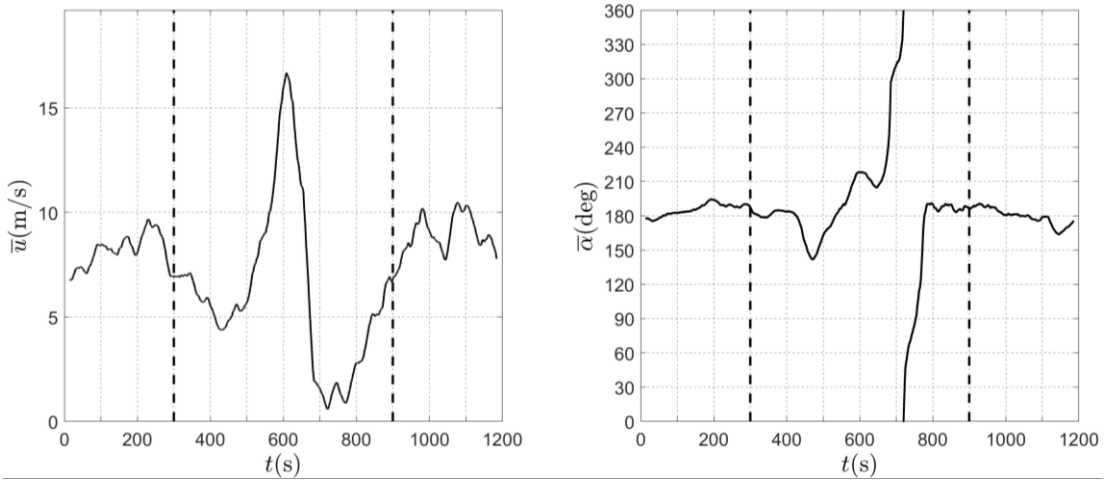

(a) **(b)**

Figure 4.14 20-min slowly-varying mean wind velocity (a) and direction (b) during a thunderstorm outflow occurred on January 18, 2014 in the Port of Livorno (the vertical dashed lines include the 10-min period centred around the peak wind velocity).

Figure 4.13 and **Figure 4.14** show two examples of thunderstorm outflows during which the background wind velocity is almost unchanged before and after the gust front passage; this can happen, as an instance, during fair weather conditions, when some forcing mechanism triggers the formation of a deep convective cell. In both cases the sudden jump of the slowly-varying mean wind velocity is accompanied by a relevant change of the slowly-varying mean wind direction. During the event depicted

in **Figure 4.13** the slowly-varying mean wind direction exhibits a rotation around 120 degrees, which mainly occurs before the peak wind speed. Conversely, the event depicted in **Figure 4.14** gives rise to a mean wind rotation 60 degrees before the peak wind speed; after such peak a mean wind rotation occurs around 360 degrees.

Table 4.1 implements a pair of conventional attempts to quantify the rate of change of the slowly-varying mean wind direction, $\Delta\bar{\alpha}$, by providing the number of events characterized by different ranges of this quantity. In the column referred to as Method 1, $\Delta\bar{\alpha} = \Delta\bar{\alpha}_1$ corresponds to the maximum shift of the wind direction in the 10-min period centred around the peak wind speed. In the column referred to as Method 2, $\Delta\bar{\alpha} = \Delta\bar{\alpha}_2$ corresponds to the maximum shift of the wind direction in the 5-min period preceding the peak wind speed. According to Method 1, most of the examined events (90%) has a rate of change $\Delta\bar{\alpha}_1$ in the range from 0 to 180 deg. According to Method 2, most of the examined events (90%) has a rate of change $\Delta\bar{\alpha}_2$ in the range from 0 to 90 deg. Moreover, it has been verified that most of the shift of the slowly-varying mean wind direction occurs during the ramp-up phase of the wind speed that characterises the passage of the gust front.

Figure 15(a) shows the peak wind speed $\hat{U}$ as a function of the direction shift $\Delta\bar{\alpha}_1$. Three remarks stand out: 1) none of the examined events is characterised by $\Delta\bar{\alpha}_1$ < 15 degrees, which corresponds to nearly straight winds; 2) a limited amount of events, 15%, involves $\Delta\bar{\alpha}_1$ > 135 degrees; none of them exceeds the peak wind speed $\hat{U}$ = 25 m/s; thus, they correspond to rather weak winds; 3) the largest amount of events, 85%, falls in the range $\Delta\bar{\alpha}_1$ between 15 and 135 degrees; here, no apparent correlation exists between $\hat{U}$ and $\Delta\bar{\alpha}_1$; despite this remark, the three most intense events, those exceeding $\hat{U}$ = 30 m/s, fall in the range $\Delta\bar{\alpha}_1$ between 50 and 90 degrees.

Figure 15(b) shows the peak wind speed $\hat{U}$ as a function of the direction shift $\Delta\bar{\alpha}_2$. The comparison with Figure 15(a) shows an apparent compaction of the data towards the smaller values of the direction shift. Also in this case, no apparent correlation exists between $\hat{U}$ and $\Delta\bar{\alpha}_2$; despite this remark, the three most intense events, those exceeding $\hat{U}$ = 30 m/s, fall in the range $\Delta\bar{\alpha}_2$ between 20 and 30 degrees.

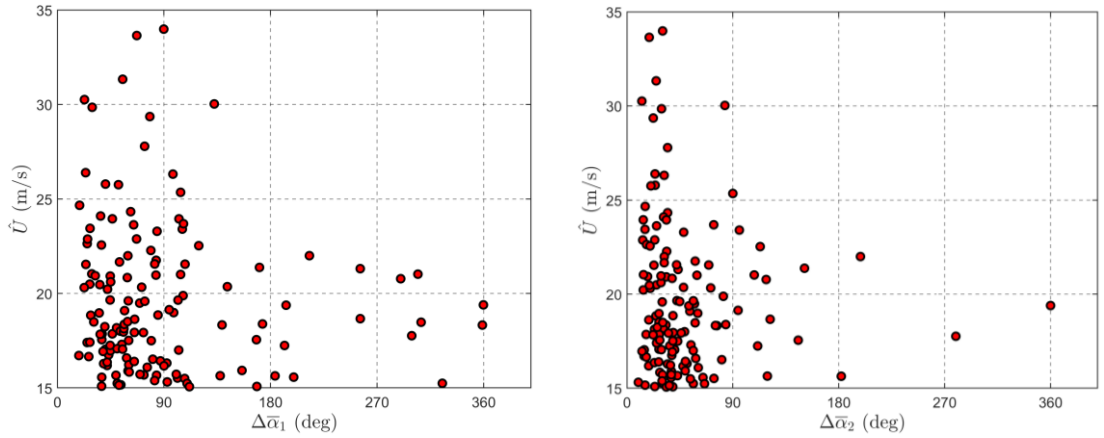

(a) (b)

Figure 4.15 Peak wind speed $\hat{U}$ as a function of the direction shift: (a) $\Delta\bar{\alpha} = \Delta\bar{\alpha}_1$; (b) $\Delta\bar{\alpha} = \Delta\bar{\alpha}_2$.

This matter deserves further studies with a prominent focus on separating the wind speed components related to the downdraft, to the background flow into which it is embedded and to the translational speed of the thunderstorm cell (Asano et al., 2019; Romanić et al., 2019), recognizing the interactions between the different components of the wind speed.

4.3.3 Turbulence intensity

As described in **Sections 4.2.2** and **4.2.3**, the longitudinal and lateral slowly-varying turbulence intensities, I_u and I_v, can be extracted by means of the directional decomposition rule through **Eq. (4.21)** whereas the turbulent intensity based on the classical method, I_U, can be evaluated by **Eq. (4.11)**. It is worth noting that in some cases the turbulent intensity time-histories exhibit abnormal large values and even sharp peaks in correspondence of very small values of the slowly-varying mean wind velocity, sometimes tending to zero. In this study, differently from the previous ones (Solari et al., 2015a; Zhang et al., 2018a), large turbulence intensities (greater than 0.2) related to small slowly-varying mean wind velocities (less than 5 m/s) have been disregarded.

Table 4.2 Ensemble mean value and cov of the turbulence intensity.

Port	Anem. No.	$\langle \bar{I}_U \rangle$	cov($\bar{I}_U$)	$\langle \bar{I}_u \rangle$	cov($\bar{I}_u$)	$\langle \bar{I}_v \rangle$	cov($\bar{I}_v$)
Genoa	1	0.09	0.33	0.09	0.34	0.09	0.32
	2	0.12	0.30	0.13	0.29	0.13	0.27
Livorno	1	0.09	0.26	0.09	0.26	0.09	0.31
	2	0.15	0.15	0.15	0.16	0.14	0.18
	3	0.08	0.22	0.08	0.22	0.08	0.27
	4	0.09	0.27	0.09	0.27	0.08	0.28
	5	0.12	0.28	0.12	0.29	0.12	0.21
Savona	1	0.14	0.19	0.15	0.20	0.13	0.17
	2	0.13	0.00	0.13	0.00	0.12	0.00
	3	0.13	0.41	0.13	0.43	0.14	0.41
	4	0.13	0.22	0.13	0.21	0.13	0.22
	5	0.13	0.40	0.13	0.40	0.13	0.27
La Spezia	2	0.16	0.15	0.17	0.15	0.17	0.18
	3	0.13	0.19	0.13	0.20	0.12	0.20
All ports		0.12	0.32	0.12	0.33	0.11	0.34

Table 4.2 shows the average values and the coefficients of variation (cov) of $\bar{I}_U$, $\bar{I}_u$ and $\bar{I}_v$ corresponding to the thunderstorm outflows belonging to 10-min family investigated. The ensemble values, shown in the last row, exhibit some relevant properties. First, the $\bar{I}_U$ and $\bar{I}_u$ values are very similar; thus the turbulence intensity

evaluated by the classical decomposition rule closely approximates the longitudinal turbulence intensity extracted through the new rule. Second, differently from classical analyses carried out for synoptic winds, the $\bar{I}_u$ and $\bar{I}_v$ values related to thunderstorm outflows are almost equal: $\langle \bar{I}_u \rangle$ is slightly greater than $\langle \bar{I}_v \rangle$ whereas cov($\bar{I}_u$) and cov($\bar{I}_v$) are nearly the same.

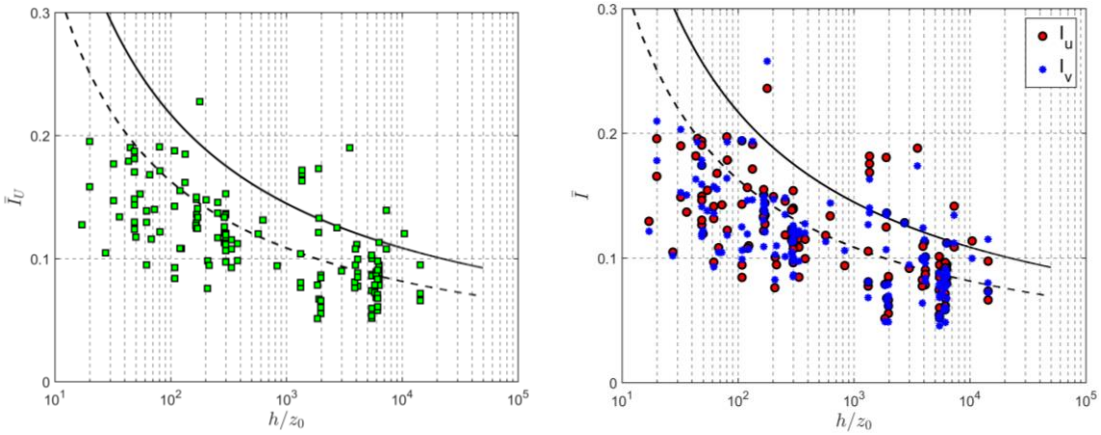

(a) (b)

Figure 4.16 Mean value of the turbulence intensity as a function of h/z_0: (a) $\bar{I}_U$; (b) $\bar{I}_u$ and $\bar{I}_v$.

This latter circumstance may be interpreted based on the remark that in the case of synoptic winds the residual turbulence derives from averaging the wind speed over a 10-min period, so it contains a relevant amount of low frequency harmonic content (**Section 4.2.1**). In the case of thunderstorm outflows (**Sections 4.2.2** and **4.2.3**) the use of a mobile mean wind speed with an averaging period T = 30 s elides the low frequency harmonic content and limits it, indicatively, to the inertial sub-range, where turbulence is locally isotropic.

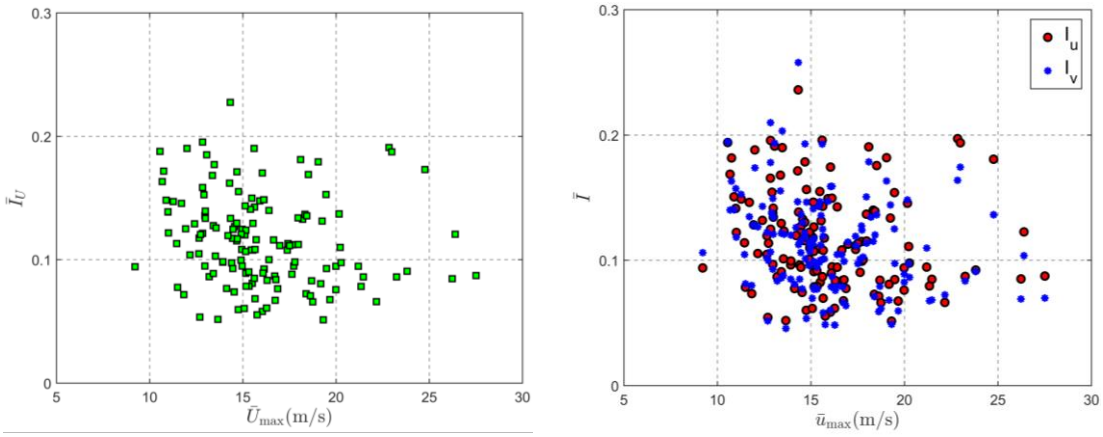

(a) (b)

Figure 4.17 Mean value of the turbulence intensity as a function of the maximum mean wind velocity: (a) $\bar{I}_U$; (b) $\bar{I}_u$ and $\bar{I}_v$.

In order to investigate the dependence of the mean value of the turbulence intensity of thunderstorm outflows on the height h AGL and on the roughness length z_0, (Xu

and Hangan, 2008; Lombardo et al., 2014), **Figure 4.16** shows $\bar{I}_U$, $\bar{I}_u$ and $\bar{I}_v$ as a function of h/z_0. Here, the z_0 values have been evaluated as described by Solari et al. (2015a), referring to neutral synoptic wind velocity profiles in equilibrium with the local topography and the upwind roughness features (ESDU, 1993; Castino et al., 2003; Burlando et al., 2013). The solid and dashed lines correspond, respectively, to the expressions $\bar{I}_u = 1/\ln(h/z_0)$ and $\bar{I}_v = 0.75\bar{I}_u$ commonly used for synoptic events and neutral conditions (Solari and Piccardo, 2001). It is worth noting, however, that these expressions are calibrated to fluctuations related to 10-min mean wind velocities whereas in **Figure 4.16** the fluctuations correspond to a mean wind velocity extracted through a moving average period T = 30 s. This is the main reason why turbulence intensity values related to thunderstorms are generally lower than these reference curves. It is also worth noting that $\bar{I}_U$, $\bar{I}_u$ and $\bar{I}_v$ exhibit similar values (**Table 4.2**) and trends characterized by a moderate decrease on increasing h/z_0; this trend was not present in Solari et al. (2015a) and only slightly evident in Zhang et al. (2018a); it is possible that the improved quality of the dataset and the removal of abnormally large values of the turbulence intensity reveal now a property that was, initially, not or slightly appreciable.

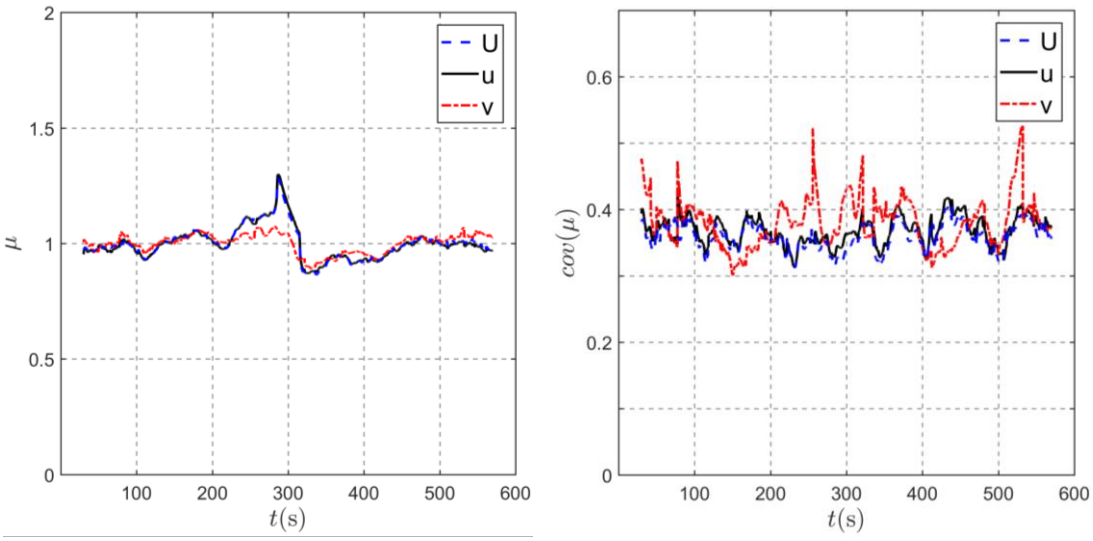

(a) **(b)**

Figure 4.18 Ensemble mean (a) and cov (b) values of μ.

Figure 4.17 shows that $\bar{I}_U$, $\bar{I}_u$ and $\bar{I}_v$ don't exhibit any relevant dependence on the maximum value of the slowly-varying mean wind velocity.

Figure 4.18 shows the ensemble average **(a)** and the cov **(b)** values of $\mu_U(t)$, $\mu_u(t)$ and $\mu_v(t)$. The diagrams related to $\mu_U(t)$ and $\mu_u(t)$ are almost perfectly overlapped; those corresponding to $\mu_v(t)$ shows limited detachments from the previous ones; all in all they are weakly dependent on time, with the exception of a small around of t = 300 s where $\mu_U(t)$ and $\mu_u(t)$ are significantly greater than 1. Thus, they may be reasonably regarded as sample functions of a stationary process.

As already noted by Zhang et al. (2018a) for the classical decomposition rule, also for the new directional one the probability density function (PDF) f of $\mu_U(t)$, $\mu_u(t)$ and

$\mu_v(t)$ are non-Gaussian. **Figure 4.19** elucidates this property by comparing the PDF of these quantities with reference Gaussian PDFs with the same mean and cov values. **Table 4.3** strengthens this remark by showing the mean value (Mean) and the standard deviation (Std) of the mean (m), standard deviation (σ), skewness (γ) and kurtosis (κ) of μ_U, μ_u and μ_v: the detachment of the skewness and kurtosis values from 0 and 3, respectively, is apparent.

Table 4.3 Ensemble Mean and Std of the mean, standard deviation, skewness and kurtosis (m, σ, γ κ) of μ_U, μ_u and μ_v.

	Parameter	m	σ	γ	κ
μ_U	Mean	1.000	0.353	0.744	3.431
	Std	0.000	0.099	0.537	1.275
μ_u	Mean	1.000	0.360	0.780	3.560
	Std	0.000	0.102	0.564	1.523
μ_v	Mean	1.000	0.368	0.752	3.520
	Std	0.000	0.111	0.595	1.873

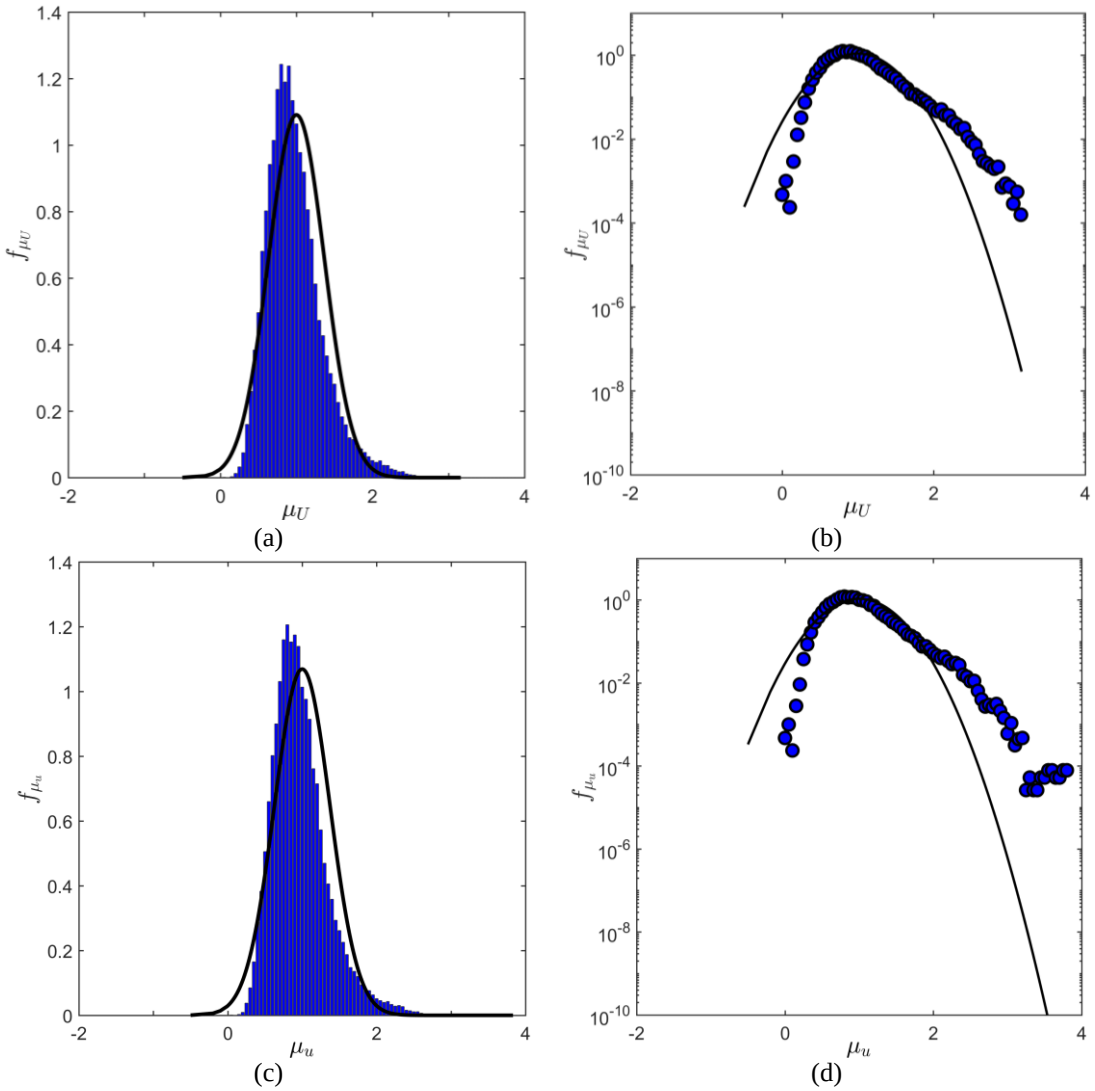

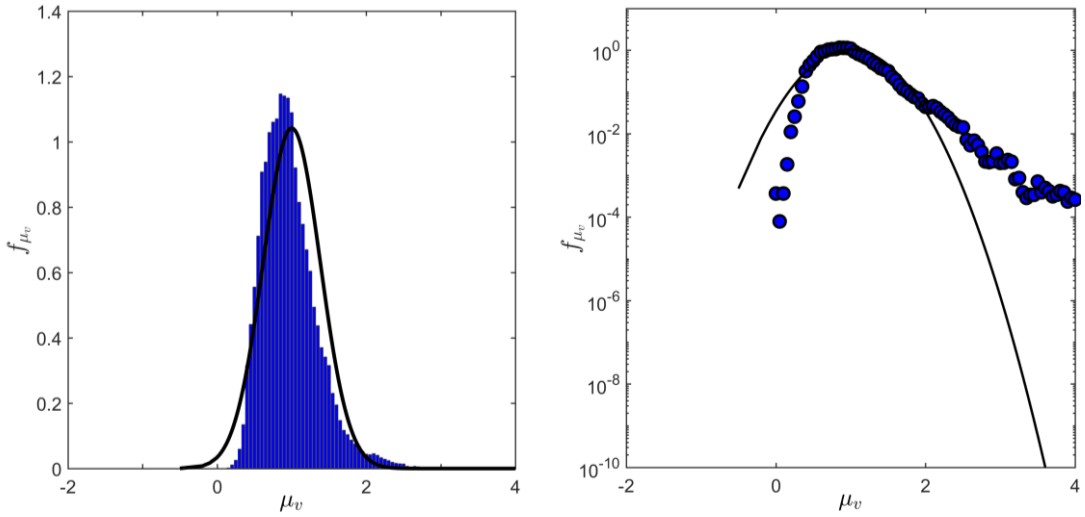

(e) (f)

Figure 4.19 PDF of μ_U, μ_u and μ_v: decimal (a) (c) (e) and logarithmic (b) (d) (f) ordinate.

4.3.4 Reduced turbulent fluctuations

Solari et al. (2015a) proved a result widely shared in literature: the reduced turbulent fluctuation $\widetilde{U}'(t)$ can be reasonably modelled as a stationary Gaussian random process with zero mean and unit standard deviation. The analysis of an enlarged dataset of thunderstorm outflows (Zhang et al., 2018a) confirmed this remark. The application of the novel directional decomposition rule to a refined dataset of events shows that the above property can be extended to the longitudinal and lateral reduced turbulence components $\tilde{u}'$ and $\tilde{v}'$ (**Figure 4.20** and **Table 4.4**). In addition, likewise for synoptic winds, **Table 4.5** shows that the longitudinal and lateral reduced turbulence components are, to a very good extent, un-correlated.

Table 4.4 Ensemble Mean and Std of the mean, standard deviation, skewness and kurtosis (m, σ, γ κ) of $\widetilde{U}'$, $\tilde{u}'$ and $\tilde{v}'$.

	Parameter	m	σ	γ	κ
$\widetilde{U}'$	Mean	-0.010	1.005	-0.068	2.835
	Std	0.020	0.012	0.153	0.255
$\tilde{u}'$	Mean	0.011	1.005	-0.089	2.843
	Std	0.023	0.011	0.153	0.263
$\tilde{v}'$	Mean	-0.001	1.001	0.018	3.000
	Std	0.018	0.010	0.123	0.504

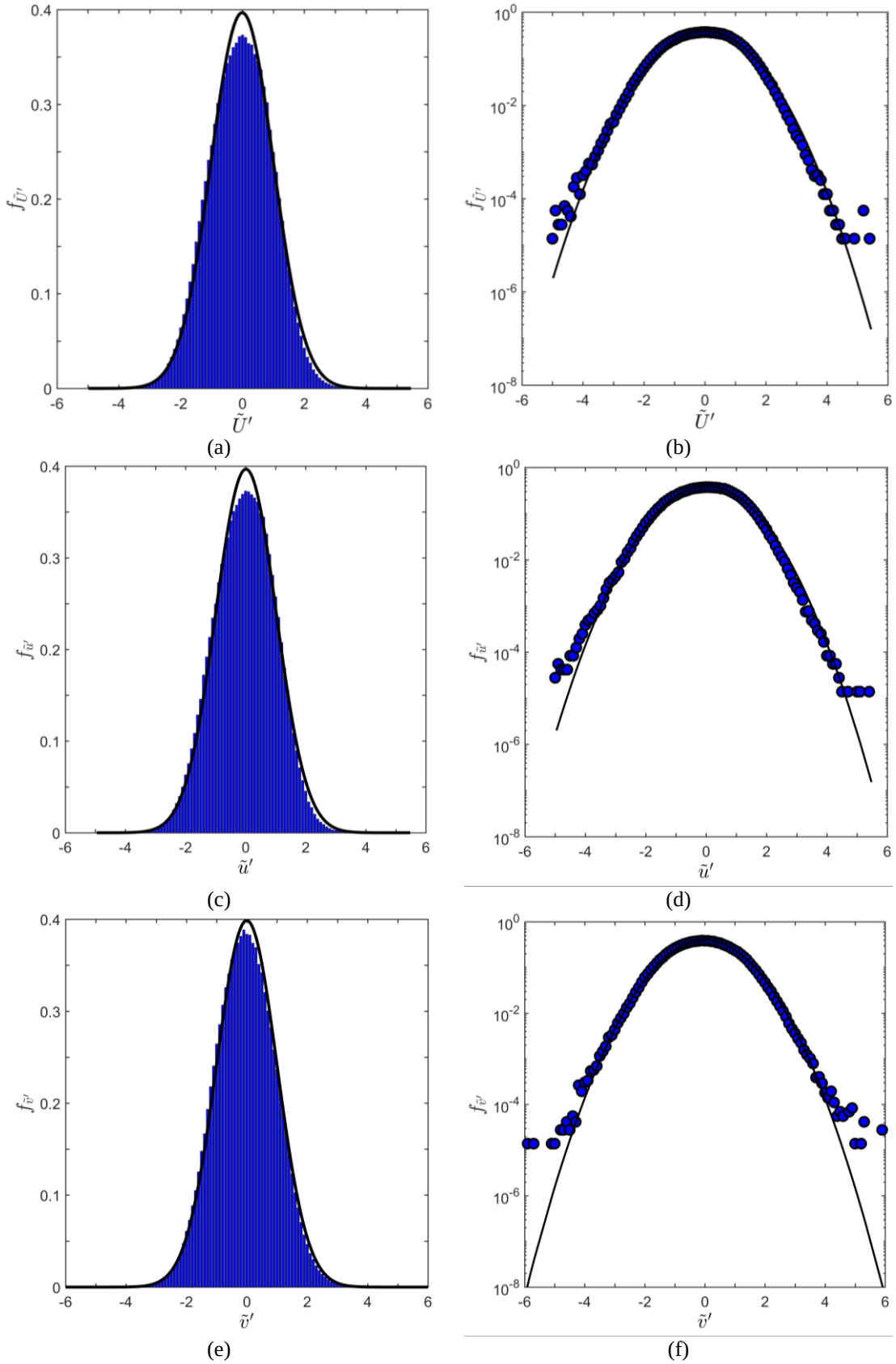

Figure 4.20 PDF of $\tilde{U}'$, $\tilde{u}'$ and $\tilde{v}'$: decimal (a) (c) (e) and logarithmic (b) (d) (f) ordinate.

Table 4.5 Ensemble coefficient of correlation of $\tilde{u}'$ and $\tilde{v}'$.

Port	Anem. No.	ρ_{uv}
Genoa	1	-0.14
	2	-0.03
Livorno	1	0.01
	2	0.01
	3	-0.01
	4	0.00
	5	-0.01
La Spezia	2	0.02
	3	-0.05
Savona	1	0.00
	2	-0.01
	3	0.00
	4	0.03
	5	0.04
	2	0.02
All ports		-0.01

4.3.5 Integral length scale

The integral length scale and the power spectral density (PSD) of the longitudinal and lateral reduced turbulence components, $\tilde{u}'$ and $\tilde{v}'$, are determined here for a highly controlled sub-set of 74 thunderstorm outflow records including an extremely low number of missing values; in the few points in which the time-histories are interrupted, their continuity is recovered through linear interpolation.

Table 4.6 shows the mean value and the cov of the integral length scales L_U, $L_u$and L_v of $\tilde{U}'$, $\tilde{u}'$ and $\tilde{v}'$ as detected by each anemometer and the whole network. Their time scales T_U, T_u and T_v have been first estimated by integrating the normalized auto-correlation functions from 0 until the time lag for which their values drop to 0.05 (Flay and Stevenson, 1988); the integral length scales are then determined by means of the Taylor's hypothesis: $L_U = \bar{U}_{max} T_U$, $L_u = \bar{u}_{max} T_u$ and $L_v = \bar{u}_{max} T_v$.

Table 4.6 Ensemble mean value and cov of the integral length scale of the reduced turbulent fluctuation.

Port	Anem.No.	$\langle L_U \rangle$ (m)	$\mathrm{cov}(L_U)$	$\langle L_u \rangle$ (m)	$\mathrm{cov}(L_u)$	$\langle L_v \rangle$ (m)	$\mathrm{cov}(L_v)$
Genoa	1	33.13	0.20	32.35	0.21	25.98	0.23
	2	23.47	0.35	22.73	0.33	18.65	0.46
Livorno	1	27.54	0.14	25.37	0.09	19.51	0.04
	2	24.33	0.24	22.96	0.23	17.34	0.17

	3	28.28	0.22	27.18	0.24	21.71	0.32
	4	29.94	0.13	29.27	0.13	23.56	0.27
	5	31.18	0.26	31.09	0.26	27.53	0.20
Savona	1	27.11	0.31	26.59	0.32	17.48	0.31
	2	-	-	-	-	-	-
	3	25.48	0.21	25.47	0.22	20.40	0.12
	4	25.23	0.07	24.86	0.07	20.57	0.07
	5	24.77	0.00	24.33	0.00	22.10	0.00
La Spezia	2	25.29	0.30	24.04	0.30	22.68	0.33
	3	25.66	0.23	23.81	0.23	18.41	0.28
All ports		26.78	0.23	25.66	0.24	20.83	0.29

In terms of ensemble mean values, $\langle L_U \rangle = 26.78$ m is similar to $\langle L_u \rangle = 25.66$ m, which is slightly greater than $\langle L_v \rangle = 20.83$ m. In terms of spread, $\mathrm{cov}(L_U) = 0.23$ is similar to $\mathrm{cov}(L_u) = 0.24$, which is slightly smaller than $\mathrm{cov}(L_v) = 0.29$.

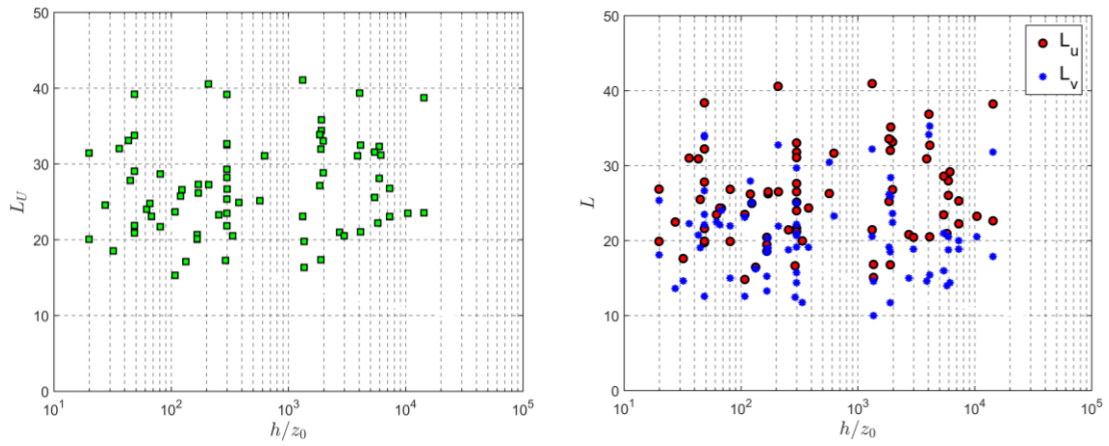

(a) (b)

Figure 4.21 Integral length scale as a function of h/z_0: (a) L_U; (b) L_u and L_v.

Figure 4.21 shows that L_U, L_u and L_v do not exhibit any significant dependence on h/z_0. **Figure 4.22** shows that L_U, L_u and L_v increase on increasing the maximum value of the slowly-varying mean wind velocity. This result matches with the one provided by ESDU (1993) for synoptic winds and neutral atmospheric conditions.

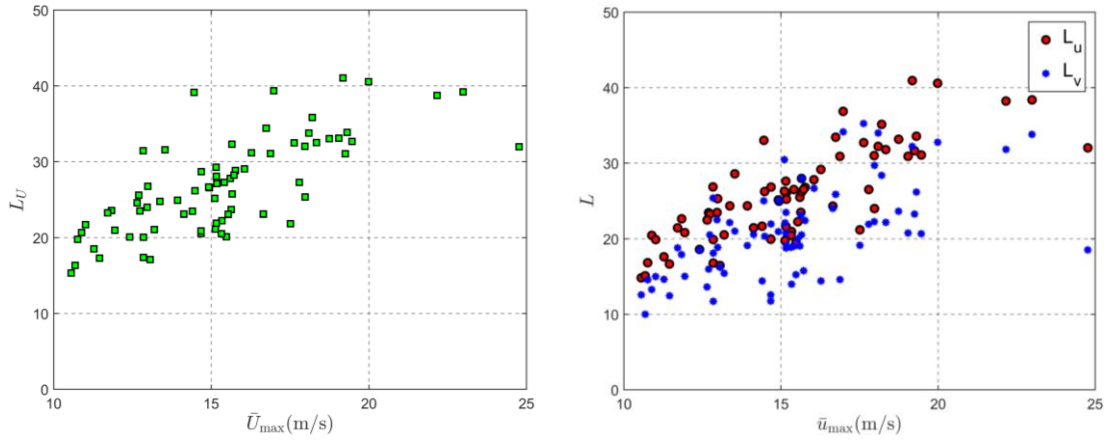

(a) (b)

Figure 4.22 Integral length scale as a function of the maximum value of the slowly-varying mean wind velocity: (a) L_U; (b) L_u and L_v.

4.3.6 Power spectral density

Approaching the thunderstorm outflow decomposition by means of the classical rule, Zhang et al. (2018a) demonstrated that expressing the PSD of $\tilde{U}'$ as a function of the reduced frequency $f_U = nz/\bar{U}_{max}$, being z the height of the anemometer, is not appropriate. Better results may be obtained by expressing such PSD as a function of the reduced frequency $f_U = nL_U/\bar{U}_{max}$, being L_U the integral length scale of $\tilde{U}'$ obtained through its auto-correlation function. The application of the novel directional decomposition rule shows that the same property is valid also for $\tilde{u}'$ and $\tilde{v}'$.

Figure 4.23 (a,b,c) show the PSD of $\tilde{U}'$, $\tilde{u}'$ and $\tilde{v}'$ as a function of $f_U = nL_U/\bar{U}_{max}$, $f_u = nL_u/\bar{u}_{max}$ and $f_v = nL_v/\bar{u}_{max}$, respectively; each scheme provides the mean PSD for every anemometer. **Figure 4.23 (d)** compares the PSD of $\tilde{U}'$, $\tilde{u}'$ and $\tilde{v}'$ averaged over the ensemble of all the anemometers. On the one hand they confirm the reliability of the parameterization adopted here and by Zhang et al. (2018a). On the other hand they show that the PSD of $\tilde{U}'$ is almost perfectly overlapped with the PSD of $\tilde{u}'$; the PSD of $\tilde{v}'$ exhibits some limited detachments from the previous ones.

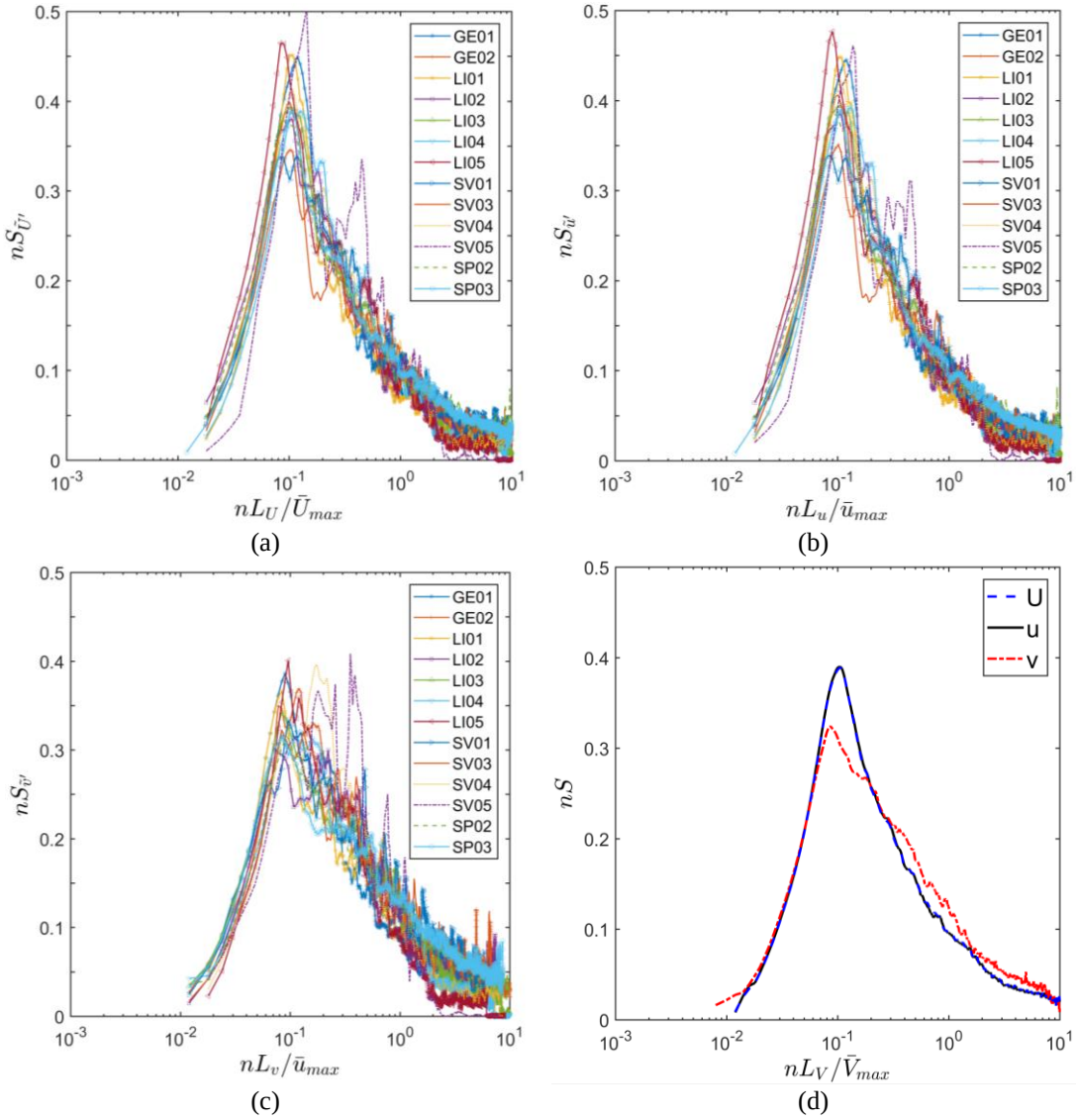

Figure 4.23 Ensemble mean values of the PSD of $\tilde{U}'$ (a), $\tilde{u}'$ (b), and $\tilde{v}'$ (c) for every anemometer; mean value of PSD of $\tilde{U}'$, $\tilde{u}'$ and $\tilde{v}'$ for all the records (d), being $V = U, u, v$.

4.3.7 Turbulence intensity modulation

Though $\tilde{U}'(t)$, $\tilde{u}'(t)$ and $\tilde{v}'(t)$ are well represented by Gaussian (rapidly-varying) random processes, according to **Eqs. (4.14)** and **(4.24)** they are modulated by the non-Gaussian (slowly-varying) random processes $\mu_U(t)$, $\mu_u(t)$ and $\mu_v(t)$. Therefore, $\mu_U(t)\tilde{U}'(t)$, $\mu_u(t)\tilde{u}'(t)$ and $\mu_v(t)\tilde{v}'(t)$ are non-Gaussian random processes. **Table 4.7** shows the mean value and the std of the mean, standard deviation, skewness and kurtosis of $\mu_U(t)\tilde{U}'(t)$, $\mu_u(t)\tilde{u}'(t)$ and $\mu_v(t)\tilde{v}'(t)$, exhibiting a relevant agreement between the statistical moments of $\mu_U(t)\tilde{U}'(t)$ and $\mu_u(t)\tilde{u}'(t)$; the statistical moments of $\mu_v(t)\tilde{v}'(t)$ show some differences. **Figure 4.24** points out the detachment between the PDF of $\mu_U(t)\tilde{U}'(t)$, $\mu_u(t)\tilde{u}'(t)$ and $\mu_v(t)\tilde{v}'(t)$ and the reference Gaussian models. **Figure 4.25** proves that the PSDs of $\mu_U(t)\tilde{U}'(t)$ and $\mu_u(t)\tilde{u}'(t)$ are almost exactly overlapped whereas the PSD of $\mu_v(t)\tilde{v}'(t)$ exhibits

some slight detachment from the previous ones. The PSDs of $\widetilde{U}'(t)$, $\tilde{u}'(t)$ and $\tilde{v}'(t)$ are very close to the PSDs of their modulations.

Table 4.7 Ensemble Mean and Std values of the mean, standard deviation, skewness and kurtosis (m, σ, γ κ) of $\mu_U(t)\widetilde{U}'(t)$, $\mu_u(t)\tilde{u}'(t)$ and $\mu_v(t)\tilde{v}'(t)$.

	Parameter	m	σ	γ	κ
$\mu_U\widetilde{U}'$	Mean	-0.013	1.082	-0.098	4.380
	Std	0.031	0.041	0.331	1.939
$\mu_u\tilde{u}'$	Mean	0.006	1.086	-0.119	4.376
	Std	0.038	0.045	0.337	1.194
$\mu_v\tilde{v}'$	Mean	0.000	1.085	0.006	4.802
	Std	0.023	0.048	0.325	1.886

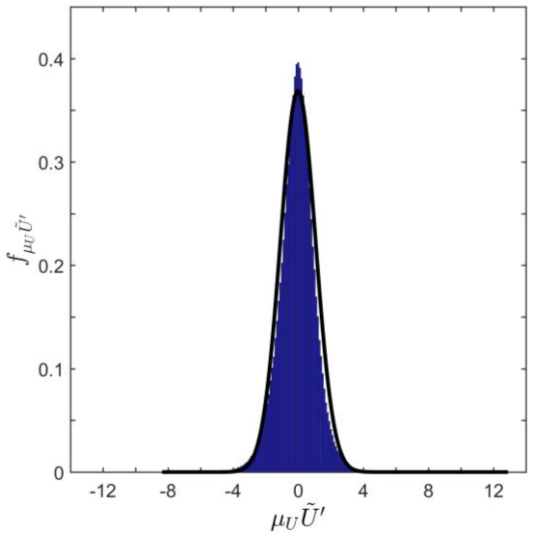

(a)

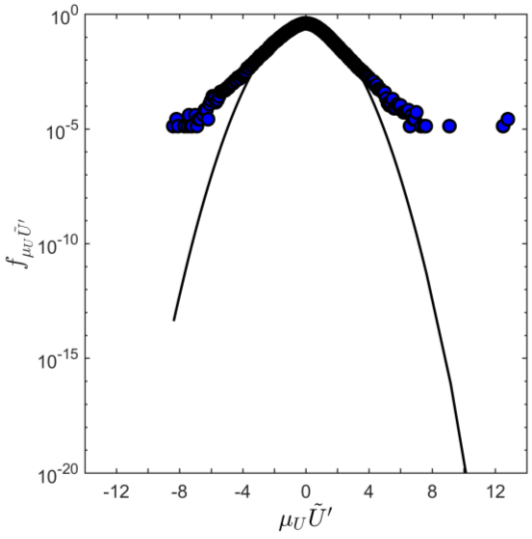

(b)

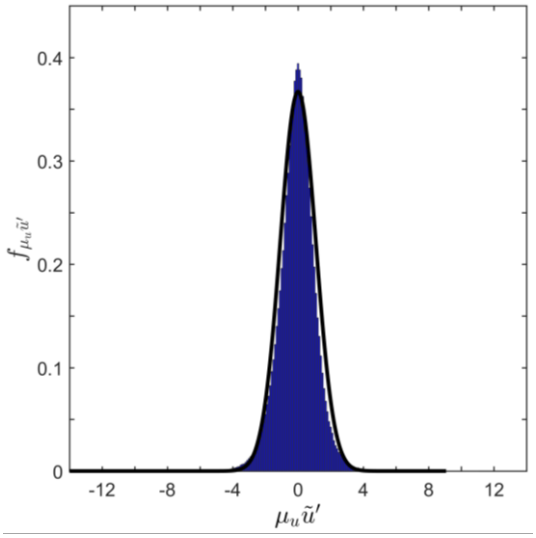

(c)

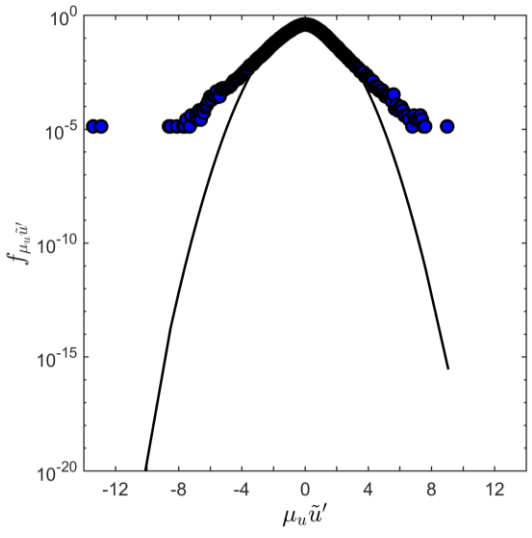

(d)

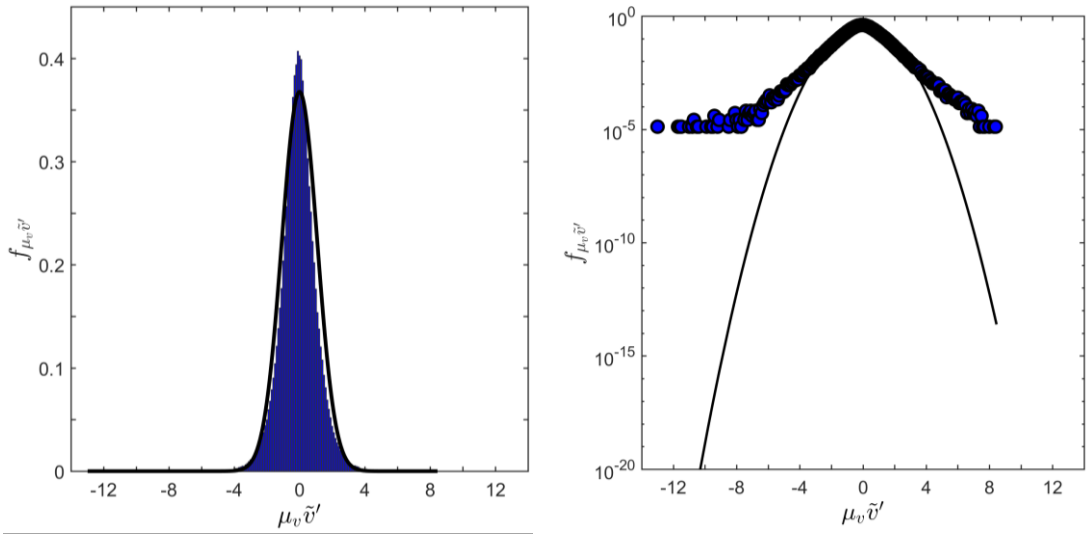

(e) (f)

Figure 4.24 PDF of $\mu_U(t)\widetilde{U}'(t)$, $\mu_u(t)\widetilde{u}'(t)$ and $\mu_v(t)\widetilde{v}'(t)$: decimal (a) (c) (e) and logarithmic (b) (d) (f) ordinate.

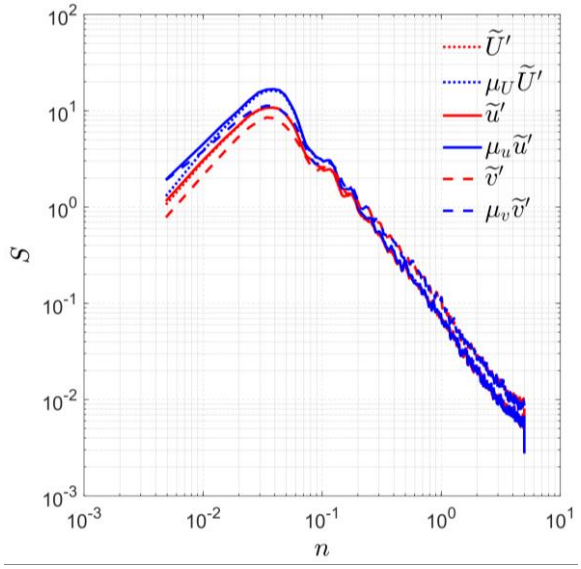

Figure 4.25 Ensemble PSD of $\widetilde{U}'$, $\mu_U\widetilde{U}'$, $\widetilde{u}'$, $\mu_u\widetilde{u}'$, $\widetilde{v}'$ and $\mu_v\widetilde{v}'$.

4.3.8 Gust factor

Gust factor plays a key role in the thunderstorm loading and response of structures (Solari et al., 2015a,b; Solari, 2016). **Table 4.8** summarizes the mean value and the cov of the gust factors G_U (**Eq. (4.15)**) and G_u (**Eq. (4.25)**), showing an almost perfect matching. Coherently with the results obtained by Zhang et al. (2018a), **Figure 4.26** shows that both gust factors do not exhibit any clear correlation with h/z_0. **Figure 4.27** shows that the same quantities slightly decrease on increasing the maximum value of the slowly-varying mean wind velocity.

Table 4.8 Ensemble mean and cov values of the gust factors.

Port	Anem. No.	$\langle G_U \rangle$	Cov(G_U)	$\langle G_u \rangle$	Cov(G_u)
Genoa	1	1.20	0.09	1.21	0.10
	2	1.26	0.08	1.26	0.08
Livorno	1	1.16	0.08	1.16	0.08
	2	1.26	0.09	1.27	0.09
	3	1.16	0.06	1.16	0.06
	4	1.15	0.06	1.15	0.06
	5	1.14	0.02	1.14	0.02
Savona	1	1.24	0.06	1.25	0.06
	2	1.49	0.00	1.50	0.00
	3	1.22	0.06	1.23	0.06
	4	1.25	0.06	1.25	0.06
	5	1.45	0.14	1.47	0.15
La Spezia	2	1.33	0.07	1.34	0.08
	3	1.26	0.08	1.28	0.08
All ports		1.22	0.09	1.23	0.09

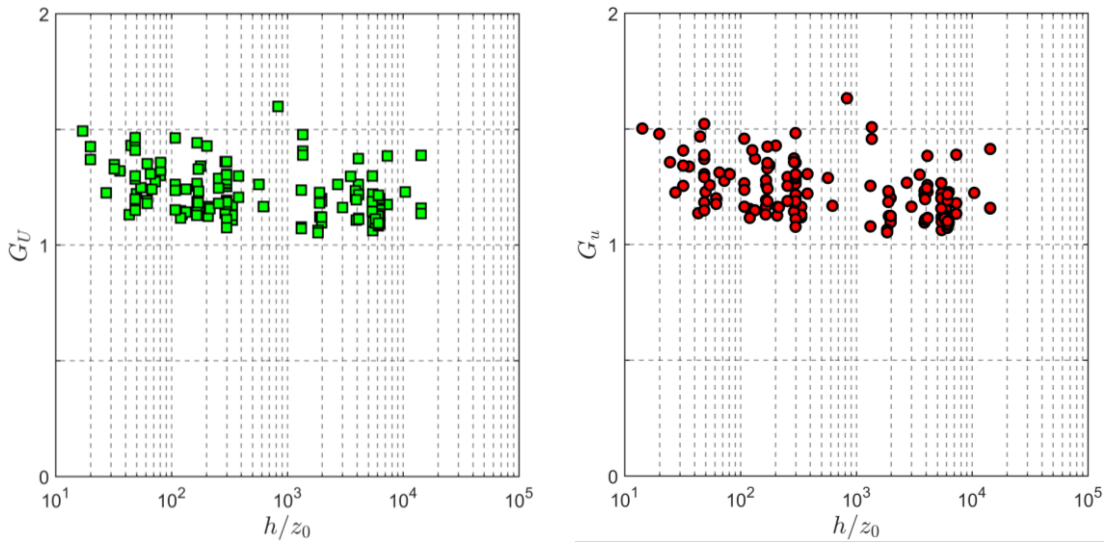

(a) (b)

Figure 4.26 Gust factor as a function of h/z_0: (a) G_U; (b) G_u.

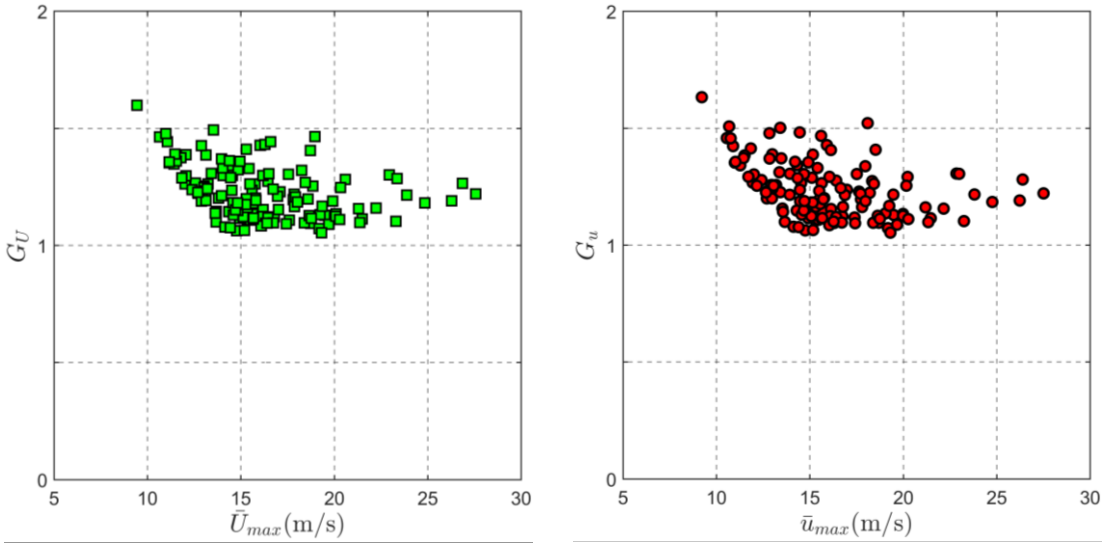

(a) (b)

Figure 4.27 Gust factor as a function of the maximum value of the slowly-varying mean wind velocity: (a) G_U; (b) G_u.

4.4 Conclusions

Up to now the study of thunderstorm outflows has followed the classical signal decomposition, different from the synoptic winds, according to which the horizontal resultant velocity is decomposed into a slowly varying mean part and a residual turbulent fluctuation. Also, the wind direction is defined from a qualitative viewpoint and the structural response is implicitly assumed in the alongwind direction. This framework is easy to apply and diffuses widely in wind engineering while precludes a parallel treatment and a robust comparison of the wind speed and of the structural response for thunderstorm outflows and synoptic winds.

This chapter proposes a novel decomposition rule of the horizontal component of the wind speed that can be used to analyse measured records and to develop analytical models. Likewise for synoptic winds, but diversely from the tradition in thunderstorm outflows, this rule takes explicitly into account the wind direction and decouples the turbulent fluctuations into longitudinal and lateral components. On the contrary, likewise for the methods classically applied to thunderstorm outflows, but diversely from the tradition in synoptic winds, this rule extract the mean wind velocity through a running-mean operator with a moving average period (here T = 30 s) shorter than the full length of the record (here ΔT = 10 minutes). Nevertheless, assuming $T = \Delta T$, the slowly-varying time-histories extracted by this procedure (i.e. the mean wind velocity, the standard deviation and the turbulence intensity) identify themselves with the constant values classically used for synoptic wind speeds. Under these viewpoints the new decomposition rule applies to both synoptic winds and thunderstorm outflows, contains the classical decomposition rule for synoptic winds as a particular case, provides a substantial generalisation of the decomposition rule classically applied to thunderstorm outflows.

A typical thunderstorm outflow record detected by one of the anemometers belonging to the monitoring network of the European Projects “Wind and Ports” and “Wind, Ports and Sea” is firstly examined to illustrate the improvement of the novel decomposition approach compared to the classical one. Then the spectral content of the new signals and a systematic investigation of their statistical properties with regard to 141 intense thunderstorm outflow records in the 10-min family detected by 14 ultra-sonic anemometers in the period 2011-2016 is carried out. Especially for the slowly-varying mean wind velocity, also the results related to the 1-h family records are presented here because the previous research found that the property of the two families appears obvious difference only on this aspect.

The extraction of the slowly-varying mean wind velocity and direction is a fundamental step towards the reconstruction of thunderstorm properties based on multiple thunderstorm records. Accordingly, the slowly-varying mean wind speed are examined normalizing by means of its maximum values. Despite their essential feature is a speed-up and -down of the wind speed, they exhibit an impressive spread. However, their mean values related to 10-min and 1-h thunderstorms are very similar in proximity of the peak whereas their difference is apparent far from it. These functions are crucial for defining quantitative criteria aiming to express the duration of the gust front passage likewise qualitative models to classify the different shapes of the thunderstorm outflow signature. And there is no doubt that the difference between the mean values of the slowly-varying mean wind speeds according to the classical and directional decompositions is not really relevant, and only a little bit difference appears near the tails.

Corresponding to the new decomposition approach, the moving average wind direction of every record can be presented giving an important contribution to learn the tendency of direction and the movement of thunderstorm outflows. It has been verified that most of the shift of the slowly-varying mean wind direction occurs during the ramp-up phase of the wind speed that characterises the passage of the gust front. Moreover, there is no apparent correlation exists between the peak wind speed and the direction shift. And this matter deserves further studies with a prominent focus on separating the wind speed components related to the downdraft, to the background flow into which it is embedded and to the translational speed of the thunderstorm cell, recognizing the interactions between the different components of the wind speed.

The longitudinal and lateral turbulences intensities of the intense thunderstorm outflows are decomposed by the novel approach and their mean values trend to the similar different with the synoptic winds. Both of them and the result by the classical method present the similar tendency with the referential synoptic events as a function of the ratio between the height above ground level and the roughness length which not presented in the previous research, and generally lower than these reference curves manly due to the different mean approach. While all of them don’t exhibit any relevant dependence on the maximum value of the slowly-varying mean wind velocity. As far as the ratio between the horizontal resultant, longitudinal and lateral slowly varying turbulence intensity and their mean value is concerned, the set of these signals

can be regarded as a random stationary non-Gaussian process. This remark confirms that the usual hypothesis adopted in literature to identify the turbulence intensity with its average value is quite questionable.

Then, based upon a sub-set of 74 thunderstorm outflow records including a very low number of missing values, it is fully confirmed that both the reduced longitudinal and lateral turbulent fluctuations are stationary Gaussian process. Then, the PSD as a function of the reduced frequency $nL/\bar{u}_{max}$ are presented. The integral length scale of the reduced turbulent fluctuation is almost independent of the ratio between the height and the roughness length, while increases on increasing the maximum value of the slowly-varying mean wind velocity. These are coincide with the results based on the classical decomposition approach.

Finally, also the gust factor is redefined related to the longitudinal wind velocity with the aim of estimating the wind loading and response of structures， which presents an almost perfect matching with the values related to the classic decomposition method. It does not exhibit any relevant dependence on the ratio between the height above ground and the roughness length of the terrain, while slightly decrease on increasing the maximum value of the slowly-varying mean wind velocity.

Summarily, a dominant property of the new decomposition rule is that it neither cancels nor distorts the knowledge acquired so far with regard to thunderstorms outflows, but extends the information relating thereto. More precisely, this chapter proves that the properties classically extracted from thunderstorm outflows with reference to the resultant wind speed – namely the slowly varying mean wind velocity, the turbulence intensity and its modulation, the reduced turbulent fluctuations, the integral length scales and the power spectral density, and the gust factor - are very close to the ones obtained through the new rule with reference to the longitudinal component of the wind speed. On the other hand the new rule furnishes a thorough information, usually disregarded when adopting the classical decomposition rule, with reference to the slowly-varying mean wind direction and the lateral turbulence component.

It is very worth noting that the properties of the lateral turbulence component of the thunderstorm outflows - i.e. its turbulence intensity and its modulation, the reduced turbulent fluctuations, the integral length scale and the power spectral density - are very similar to the analogous quantities that characterize the longitudinal turbulence component and, for the transitive property, to those that characterize the turbulence classically analyzed without decoupling its components. Also, the longitudinal and lateral turbulence components are nearly uncorrelated. These properties derive from the use of a mobile mean wind speed with an averaging period T = 30 s: it transfers the low frequency harmonic content to the slowly-varying mean wind velocity and limits the high-frequency harmonic content, indicatively, to the inertial sub-range, where turbulence is locally isotropic or quasi-isotropic.

5 Weather scenarios of thunderstorm outflows

5.1 Introduction

As introduced before, the analysis of these data detected by the in-situ monitoring network shows the presence of recordings due to wind phenomena of different nature, namely extra-tropical cyclones, thunderstorms outflows and intermediate events (**Chapter 3**). Thus, in order to focus on the study of intense thunderstorm outflows a semi-automatic procedure was implemented to recognize and extract these phenomena (De Gaetano et al., 2014; Zhang et al, 2018b) as shown in **Chapter 3**. This approach is consistent with previous procedures developed and calibrated in order to process a huge amount of data based on few synthetic elements derived from the sole anemometric recordings (Riera and Nanni, 1989; Twisdale and Vickery, 1992; Choi and Tanurdjaja, 2002; Kasperski, 2002; Durañona et al., 2007; Lombardo et al., 2009), without carrying out systematic and prohibitive meteorological surveys of the weather scenarios out of which they took place. According to this criterion, an extensive set of records labelled as thunderstorms has been gathered as illustrated in **Section 3.2** and subjected to probabilistic signal analyses aiming at evaluating their main properties relevant to the wind loading of structures as shown in **Chapter 4** (Solari et al., 2015a; Zhang et al., 2018b).

Despite its inherent advantages and merits, however, this approach suffers the main shortcoming of missing the knowledge of the weather scenarios that occur during events classified as thunderstorms without recognizing their actual meteorological nature. In order to make a first step towards filling this gap, **Section 5.2** furnishes additional elements on the direction, seasonality and hour of daily occurrence of these events. In **Section 5.3**, the thunderstorm downburst that occurred on 1 October 2012 over the City of Livorno, Italy is selected as a reference test case (Burlando et al., 2017a). Detailed analyses are carried out of the wind speed and direction records detected by the “WP” and “WPS” network. In parallel, the atmospheric conditions concurrent with this event are studied in great detail by gathering all the meteorological data available in this area, in particular model analyses, standard in-situ measurements (stations and radio-soundings), remote sensing techniques (radar and satellite), proxy data (lightning), and direct observations (from the European Severe Weather Database, Dotzek et al., 2009). This information leads to reconstruct the weather scenario, to classify this event as a wet downburst, to determine its space-time evolution, and to embed in this framework signal analyses aiming to extract the key parameters for determining the wind loading of structures. This part of research is already published in Journal of Monthly Weather Review (Burlando et al., 2017a).

From this point of view the above study may become a reference model to carry out comprehensive analyses of the major thunderstorm events recorded by the “WP” and “WPS” monitoring network and more in general by any network. This is relevant, however, only repeating such investigations for several events and elaborating the results in a probabilistic framework aiming to construct suitable models of the wind

field of thunderstorm outflows truly related to classes of meteorological events, to recognize clear precursors of these phenomena and their main parameters, to develop statistical analyses of their occurrence in terms of touch-down position, size, motion pattern and background flow. These data are in turn the key information to implement advanced thunderstorm models addressed to hazard and risk analyses for a broad spectrum of applications.

Unfortunately, the framework depicted above may represent a utopian prospect due to the burden of collecting so many data from different sources and performing their joint analysis for several events. Finding a reasonable balance between expeditionary evaluations based on the sole wind records detected and studies that encapsulate the above information within detailed meteorological surveys is a very difficult and ambitious aim. The **Section 5.4** represents a first step and a pilot attempt in this direction, which introduces a synthetic meteorological survey, coherent with but easier than the general methodology described in **Section 5.3**, of the weather scenarios corresponding to three events preliminarily labelled as “thunderstorms” and characterized by different lifetime-scales, which is already published in Journal of Natural Hazards and Earth System Sciences (Burlando et al., 2018).

Section 5.5 summarizes the main conclusions and highlights some prospects for future research.

5.2 Thunderstorm direction, seasonality, and hour of daily occurrence

As shown by **Figure 3.2**, the definition of the thunderstorm outflow direction is quite controversial. A thunderstorm cell may be classified as stationary or non-stationary depending on whether it is endowed with a translational motion. In the case of a stationary event the direction of the thunderstorm outflow, of radial nature, strictly depends on the position of the axis of the downdraft, usually assumed as vertical, with regard to the position of the sensor. In the case of a non-stationary event, the velocity and direction detected by the sensor is the vector composition of the velocity and direction of the thunderstorm cell, dealt with as stationary, and its translational components (Holmes and Oliver, 2000). The situation becomes more complex in the frequent case in which a thunderstorm cell is embedded in a background larger-scale boundary layer flow field, usually of synoptic type, or ever more in the case in which multiple downdraft are generated by single or multiple thunderstorm cells. In principle, all these situations may be treated by vector compositions of the velocity and direction of component flows; in reality, no proof exists that this approach is physically and mathematically suitable.

Lombardo et al. (2009) identified the thunderstorm outflow direction with its average value in a 5-s period centered around the peak wind speed. Solari et al. (2015a) defined it as the average value in a 30-s period centered around the gust peak. In this research, the period in which the wind direction is averaged is increased to the 1-min centered around the peak.

Figure 5.1 shows the distribution of the thunderstorm records reported in **Table 3.1**

with reference to the day of occurrence shown on the polar radius (1 relates to 1 January) and to the wind direction (0 ° refers to the north); the background of every diagram is the map of the port for roughly illustrating the relationship between the directions of intense outflows and geographic conditions. Most of the events (68 %) occurs in the months between September and January. Besides, most of the events (78 %) is characterized by wind directions coming from the sea.

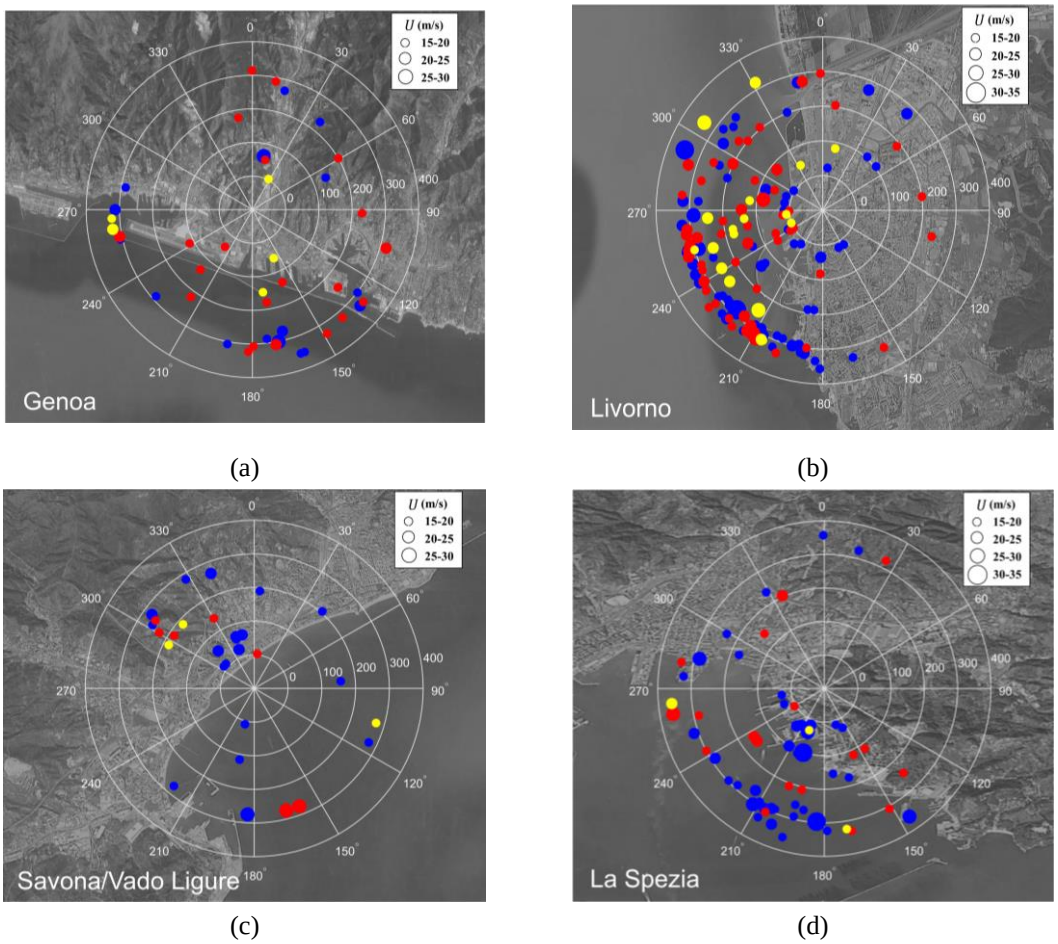

Figure 5.1 Day of the year (radial distance from the origin), direction of the thunderstorm outflows and peak wind speed (marker size). Blue triangles: 10-min family; red squares: 1-h family; yellow circles: 10-h family.

In the Port of Savona only one year of reliable data has been gathered, so the number of thunderstorm records is small and no definite trend is identified. It is possible, however, that the spread of these results may be due not only to the scarcity of data but also to the fact that the Port of Savona comprehends two different port areas: the one of Savona itself and that of Vado Ligure; though these areas are rather close, they have indeed peculiar different features. Also, the presence of intense downslope winds in Vado Ligure area (Burlando et al., 2017c) may contribute to increase the spread.

Figure 5.2 shows the distribution of thunderstorm records (NTR) corresponding to the three families defined before, namely 10-min, 1-h and 10-h events, reported in Table 2 with respect to the day time. Overall, for the area under study, 20 % of the

thunderstorms occur between 00:00 and 06:00 UTC, 24 % occur in the morning between 06:00-12:00 UTC, 30 % occur in the afternoon from 12:00 to 18:00 UTC and 26 % occur in the evening from 18:00 until 00:00 UTC. Therefore, at least in the monitored area, it seems that thunderstorm events are slightly more likely to occur in the warmer hours of the day, possibly because of the role of solar heating in triggering thermals from the earth's surface. The percentage of 1-h events grows in the afternoon with respect to the 10-min events, as well.

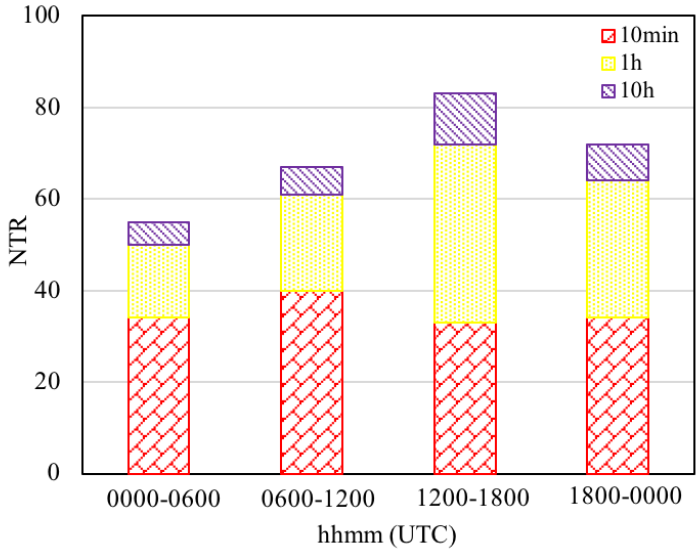

Figure 5.2 Number of thunderstorm outflow records detected at different hours of the day.

It is worth noting, however, that the occurrence of thunderstorms during night hours is an open topic that needs further study. These phenomena are most likely to form when the temperature of the air decreases with height pretty rapidly, i.e. when it is hot at the ground and cold aloft. Thunderstorms that form at night occur in the absence of heating at the ground by the sun, so that they are due to different forcing mechanisms.

5.3 A typical thunderstorm outflow event in Livorno

Here, the thunderstorm event that struck the Livorno coast on 1 October 2012 at about 1210 UTC (i.e., 1.10 p.m. local Italian time) identified in **Section 3.2**, measured by more than two anemometers in the only monitored area that is not topographically complex, is investigated as a test-case and a first step towards inspecting the potential of this combination. This study uniquely couples synoptic analysis, which describes the atmospheric conditions on large scales prior to and during the downburst event, with the near-surface statistical analyses of the anemometric records, which characterize the transient nature of the downburst on small scales.

5.3.1 Field measurements

The selected event was recorded by three of the five anemometers monitoring the

Livorno site (**Table 5.1**), as two instruments were out of order at that time. All the instruments are three-axial ultrasonic anemometers with a 10-Hz sampling rate and wind speed and direction precision of 0.01 m/s and 1 °, respectively. Their position was selected in order to register undisturbed wind velocity time histories. The locations of the three anemometers that recorded the event of 1 October (i.e., LI.01, LI.03, and LI.05) are shown in **Figure 5.3**.

Table 5.1 Full composition of the anemometric monitoring network in the Port of Livorno in 2012. The position of anemometers LI.01, LI.03, and LI.05 is indicated in Figure 5.3 (b).

Code	**Geographical coordinates** (λ,ϕ) (°E, °N)	**Position**	**Height above ground** (m)
LI.01	(10.301, 43.570)	Tower	20
LI.02	(10.307, 43.583)	Tower	20
LI.03	(10.290, 43.558)	Tower	20
LI.04	(10.294, 43.541)	Tower	20
LI.05	(10.319, 43.580)	Building [a]	75
[a] The anemometer is at the top of an antenna mast, 2.5 m above the building roof.			

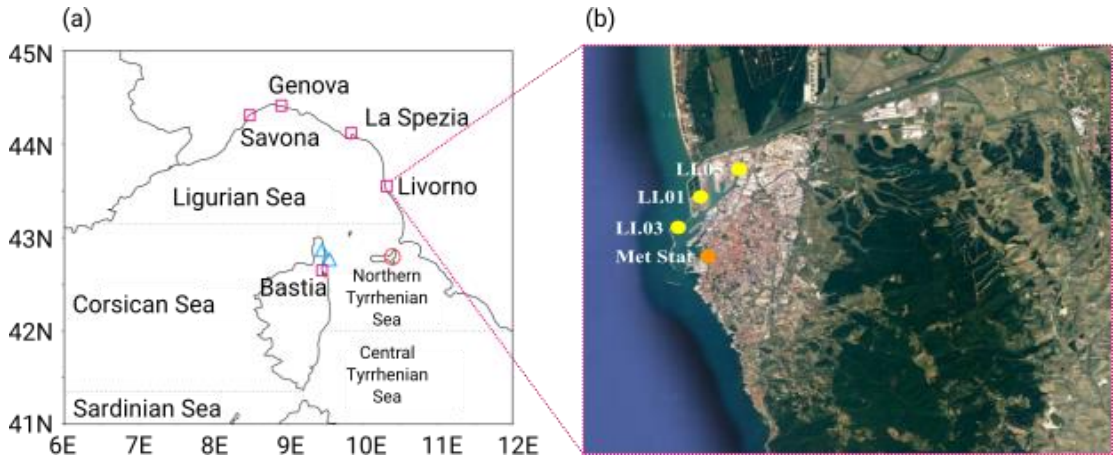

Figure 5.3 (a) Map of the northern Mediterranean basin with the international nomenclature of its subbasins, positions where waterspouts occurred on 1 Oct (blue triangles), location of the meteorological radar on Elba (red circle), and positions of cities that are part of the "WP" measurement network (magenta squares). (b) Map of Livorno with the locations of anemometers LI.01, LI.03, LI05 (yellow circles), and the Laboratorio di Monitoraggio e Modellistica Ambientale (LaMMA) meteorological station (orange circle). See Table 5.1 for anemometers' coordinates.

Figure 5.4 shows the time series of wind speed and direction recorded by these anemometers. The order (from top to bottom) of the time series has been chosen to follow the chronological occurrence of this meteorological event: the anemometer LI.03, which is the closest to the sea, was the first to measure the wind speed increase that occurred at around 1209 UTC, as indicated by the vertical dashed line in **Figure 5.4 (a)**; the anemometers LI.01 and LI.05, which are gradually farther from the coast (see **Figure 5.3**), measured the same ramp and peak at about 1211 UTC (**Figure 5.4 (c)**) and 1215 UTC (**Figure 5.4 (e)**), respectively. The steady increase in wind speed

before the downburst is due to the approach of a gust front that precedes the thunderstorm (Droegemeier and Wilhelmson, 1987; Mueller and Carbone, 1987). The first maximum value of the peak slightly decreases from the sea toward the land (i.e., from LI.03 to LI.05). The wind direction, which was about from the north until 1150 UTC, backed 90 ° (i.e., west) at the peak occurrence and then veered to the original direction. The entire event lasted about 20–30 min.

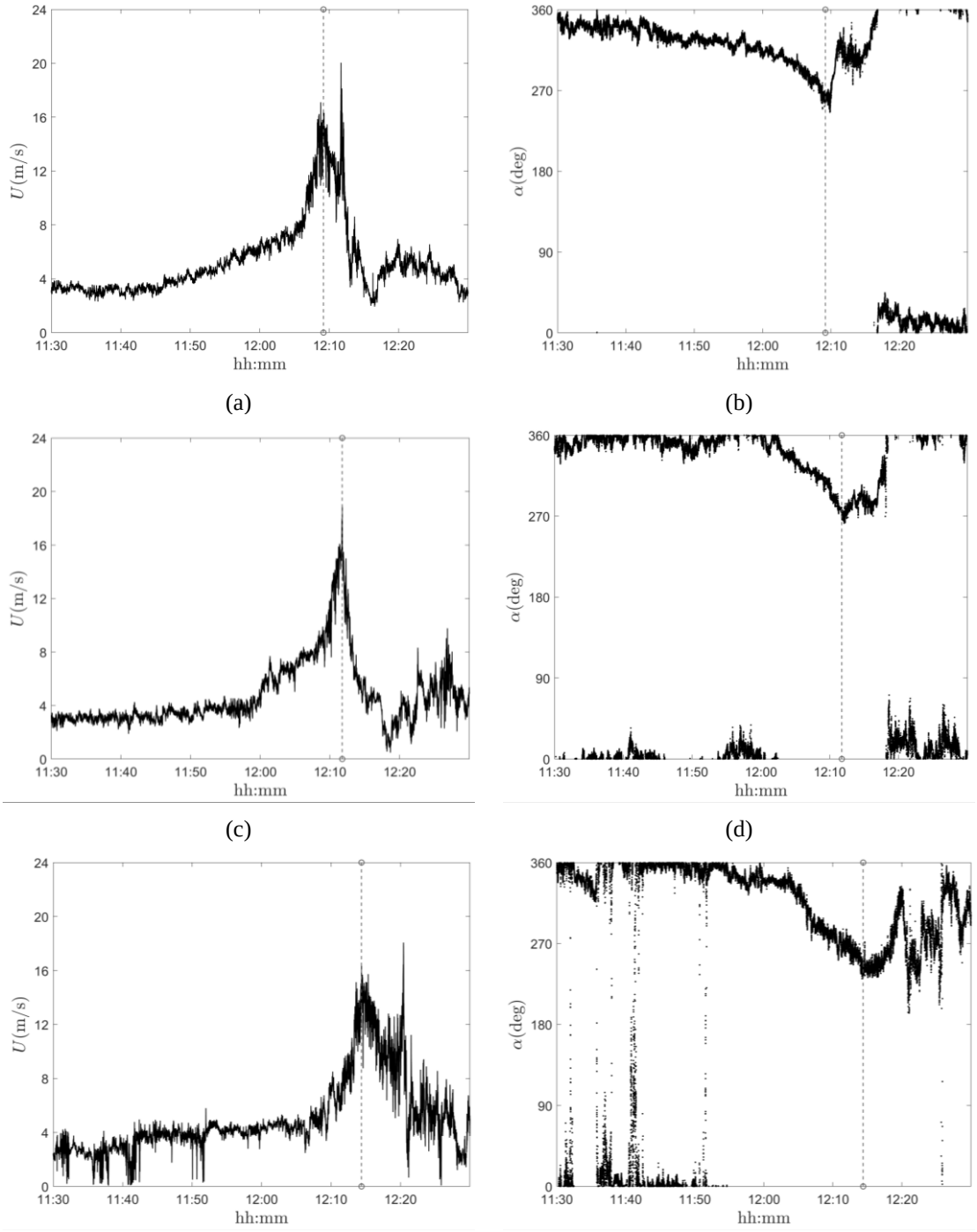

Figure 5.4 (left) Wind speed and (right) direction measured by the (a), (b) LI.03; (c), (d) LI.01; and (e), (f) LI.05 anemometers of the port of Livorno monitoring network from 1130 to 1230

UTC 1 Oct 2012. Vertical dashed lines show the approximate times of the gust front passage.

This description resembles a nonstationary event that originated over the sea, and moved inland east or northeastwardly. A spike stronger than the first peak occurred a few minutes after (at LI.03 and LI.05) or concurrent to the peak itself (at LI.01), which may be interpreted as a small-scale jet like downburst embedded the larger-scale main downdraft (Fujita, 1986; Sherman, 1987; Hjelmfelt, 1988). Most likely the spike is not caused by a local random fluctuation of wind speed since it is observed at all three stations and it is associated with an abrupt clockwise change in wind direction, as clearly illustrated in **Figure 5.4 (b)** and **(f)**. The wind direction shifts between the first peak and the spike are abrupt (Sherman, 1987) and approximately 90 °and 130 °at LI.03 and LI.05, respectively.

Despite the phenomenon considered here being a single event from the Mediterranean, it is worth comparing the records reported in **Figure 5.4** to downbursts measured in other parts of the world. The wind records from the United States (Goldman and Sloss, 1969; Charba, 1974; Wakimoto, 1982; Fujita, 1981, 1985; Gast and Schroeder, 2004; Holmes et al., 2008) and Singapore (Choi, 2004) seem to have either a constant background wind speed or a sudden drop in wind speed prior to the downburst. Conversely, the wind records in **Figure 5.4 (a)** and **(c)** are characterized by a steady increase in wind speed before reaching the downburst ramp up. In these two cases, the wind speed increased by approximately 5 m/s between 1145 and 1205 UTC and from 1200 to 1210 UTC, respectively. Simultaneously, the wind direction steadily shifted in a counterclockwise direction, reaching approximately 280–290 °before the ramp up at both anemometers (**Figure 5.4 (b)** and **(d)**).

The reported measurements in **Figure 5.4** seem to differ from downbursts measured across the continental parts of Europe as well (Järvi et al., 2007; Pistotnik et al., 2011). The downburst recorded in southern Finland (Järvi et al., 2007) was characterized by an intense gust front prior to the downburst, but it lacks the secondary peak in two out of three wind speed records. Surveying the fallen trees around the measuring site, Järvi et al. (2007) concluded that their instruments most likely did not capture the maximum velocities, therefore suggesting the existence of highly localized small-scale downbursts embedded within the parent downburst. Field measurements from Austria (Pistotnik et al., 2011) show two pronounced peaks in both mean and peak wind speeds, but the speed seems to rapidly decrease prior to the downburst. This deceleration of winds prior to the gust front occurs in situations when the front propagates into strong opposing winds (Mahoney, 1988). The background winds in the data reported by Pistotnik et al. (2011) were approximately 3 m/s larger than in the present case.

The anemometer records in **Figure 5.4**, instead, look very similar to the graphs of a weak downburst measured at a suburban area of Brisbane, Australia (Sherman, 1987). The wind speed and direction time series at LI.03 (**Figure 5.4 (a)**) are almost identical to the measurements reported by Sherman (1987) at 10 m AGL. Sherman also measured a temperature decrease of a few degrees Celsius concurrent to the ramp-up

time as well as rainfalls during the whole event, both very similar to the measurements presented in **Section 5.3.2.2**.

Wakimoto (1982) analyzed several data records of weak downbursts measured outside of Chicago, Illinois, using a Doppler radar, radiosondes, and a network of surface measurements. He classified the life cycle of a downburst into four stages (formative, early mature, late mature, and dissipative) and presented measurements for each of these stages. It seems that the reported event resembles downbursts at stages II and III, which are characterized by sudden shifts in wind directions before, during, and after the downbursts, as well as wind speeds between 10 and 30 m/s. However, his analysis also shows a noticeable decrease in wind speed prior to the arrival of the downburst with the first peak always being the most pronounced. None of these two features have been observed in the presented case.

The pronounced spike after the first well-defined peak (**Figure 5.4 (a)** and **(e)**) has been numerically simulated by Orf et al. (2012). Using a nonhydrostatic LES cloud model (Bryan and Fritsch, 2002), they showed a steady increase in wind speed prior to the nonsteady and highly fluctuating downburst peaks, similar to anemometer records in **Figure 5.4**. They reported the existence of a pronounced spike after the first downdraft at a reference point situated along the east flank of the downdraft, whereas the same pattern has not been observed along the west flank of the downdraft.

To inspect the characteristics of the wind speed records shown in **Figure 5.4** in brief, the classical decomposition rule of transient wind velocity signals (Choi and Hidayat, 2002a; Chen and Letchford, 2004a; Holmes et al., 2008; Kwon and Kareem, 2009; Solari et al., 2015a) as illustrated in **Section 4.2.2** is herein applied.

Table 5.2 shows some synthetic parameters of the wind velocity records. Here, $\widehat{U}$, $\overline{U}_{max}$, and $G = \widehat{U}/\overline{U}_{max}$ are the 1-s peak wind velocity, the maximum value of the slowly-varying mean wind velocity, and the gust factor associated with the primary peak, respectively, whereas the values related to the secondary peak, if present, are put in parentheses. $\bar{I}_U(1-\mathrm{hr})$ and $\bar{I}_U(10-\mathrm{min})$ are the average values of I_U over 1 hour and 10-min interval centered around $\widehat{U}$, and μ', σ', γ', κ', and L'_U are, respectively, the mean value, standard deviation, skewness, kurtosis, and the integral length scale of the reduced turbulent fluctuation $\widetilde{U}'$. The joint analysis of **Figure 5.5**, **Figure 5.6**, **Figure 5.7** and **Table 5.2** shows that the slowly-varying mean wind velocity $\overline{U}$ provides a very clear picture of the movement of the gust front from the sea to the inland. It is worth noting that the moving average does not filter out the secondary peak in the LI.03 and LI.05 records, confirming that this peak represents a dominant feature of the large scale flow. As opposed to the typically adopted wind tunnel modelling approaches, the residual fluctuation U' shows nonstationary random properties with large intensities and intermittency strongly correlated to the largest values of $\overline{U}$. This trend is confirmed by the slowly-varying standard deviation σ_U, which exhibits very large values corresponding to the secondary peak detected by the LI.03 and LI.05 anemometers. This observation does not alter the fact that this peak is a dominant

feature of the large scale flow, but points out that its large intensity is significantly enhanced by strong random fluctuations.

Table 5.2 Synthetic parameters of the wind velocity records. The values related to the secondary peak, if present, are in parentheses.

Parameter	*LI.03*	*LI.01*	*LI.05*
$\hat{U}$ (m/s)	15.81 (18.98)	18.00	15.45 (17.27)
$\bar{U}_{max}$ (m/s)	14.55 (13.89)	15.66	13.93 (12.46)
G	1.09 (1.37)	1.15	1.11 (1.39)
$\bar{I}_U(1-\text{hr})$	0.052	0.074	0.114
$\bar{I}_U(10-\text{min})$	0.070	0.065	0.085
μ'	-0.003	0.000	0.000
σ'	1.003	1.003	1.000
γ'	-0.032	-0.059	-0.125
κ'	2.914	2.863	3.178
L'_U (m)	26.44	28.71	27.08

The diagrams of the slowly-varying turbulence intensity I_U and its average values $\bar{I}_U$ over different time intervals (**Figure 5.6**) confirm that this quantity is not strongly time dependent, except for the presence of some spurious large values that occur when $\bar{U}$ is very small, like for instance the spike over 0.3 of LI.01 in correspondence of an almost null $\bar{U}$ value (**Figure 5.5**). In accordance with the results by Solari et al. (2015a) and Zhang et al. (2018a), $\bar{I}_U$ ranges between 0.05 and 0.12. Especially on the shorter time scale $\Delta T =$ 10-min, $\bar{I}_U$ does not show any significant growth from the sea to the inland. This provides a partial confirmation that the time evolution of a downburst is so rapid and short that its wind field does not reach an equilibrium condition over the roughness of the terrain, thus turbulence intensity is not much affected by this parameter.

The diagrams of the rapidly varying reduced turbulent fluctuation $\tilde{U}'$ in **Figure 5.7** exhibit the classical random stationary Gaussian features supported by many authors in literature (Chen and Letchford, 2004a; Holmes et al., 2008; Solari et al., 2015a). The Gaussian property of the three signals is confirmed by the good agreement between the histogram of $\tilde{U}'$ and the reference Gaussian PDF with $\mu' = 0$ and $\sigma' = 1$; the partial detachment, observed mostly for the middle and right side of the signal, is a consequence of skewness values γ' not exactly equal to 0 and kurtosis values κ' not exactly equal to 3. In addition, the PSD of $\tilde{U}'$ matches the results provided by Solari et al. (2015a). Around T = 30 s $S_{\tilde{U}'}$ shows a relative maximum and it decreases with the slope of $n^{-5/3}$ that is typical of the inertial subrange for synoptic-type winds. The integral length scale of turbulence L'_U has been determined by fitting the experimental PSD by the model proposed by Solari and Piccardo (2001); it is almost invariant from signal to signal and is fully coherent with the data reported by Solari et al. (2015a). Also, the gust factor G, between 1.11 and 1.39, is coherent with the data reported by Solari et al. (2015a). Slight departures from the universal equilibrium have been previously observed in parts of signals of flows that have sharp

interfaces and high intermittency (Braza et al., 2006). This matter deserves further investigations.

This information plays a key role in the evaluation of the behavior of the structures related to downbursts and nonsynoptic severe wind events (Kwon and Kareem, 2009; Solari, 2016). Unlike synoptic cyclones, where the stationary Gaussian properties of the wind velocity field are rather well known and whose impacts on structures are shared and codified in its essential elements (Davenport, 1961), the amount of data available is limited on the duration of the ramp up of the slowly varying mean wind velocity of transient thunderstorm outflows. Moreover, the harmonic content, turbulent fluctuations, and non-Gaussianity, as well as the parameterization of these quantities as functions of time and space, are still not well understood. The collection, interpretation, and modeling of these parameters first for single transient events then for ensembles of homogeneous phenomena are fundamental to filling this gap and opening new prospects aimed at increasing the safety and resiliency of the built environment.

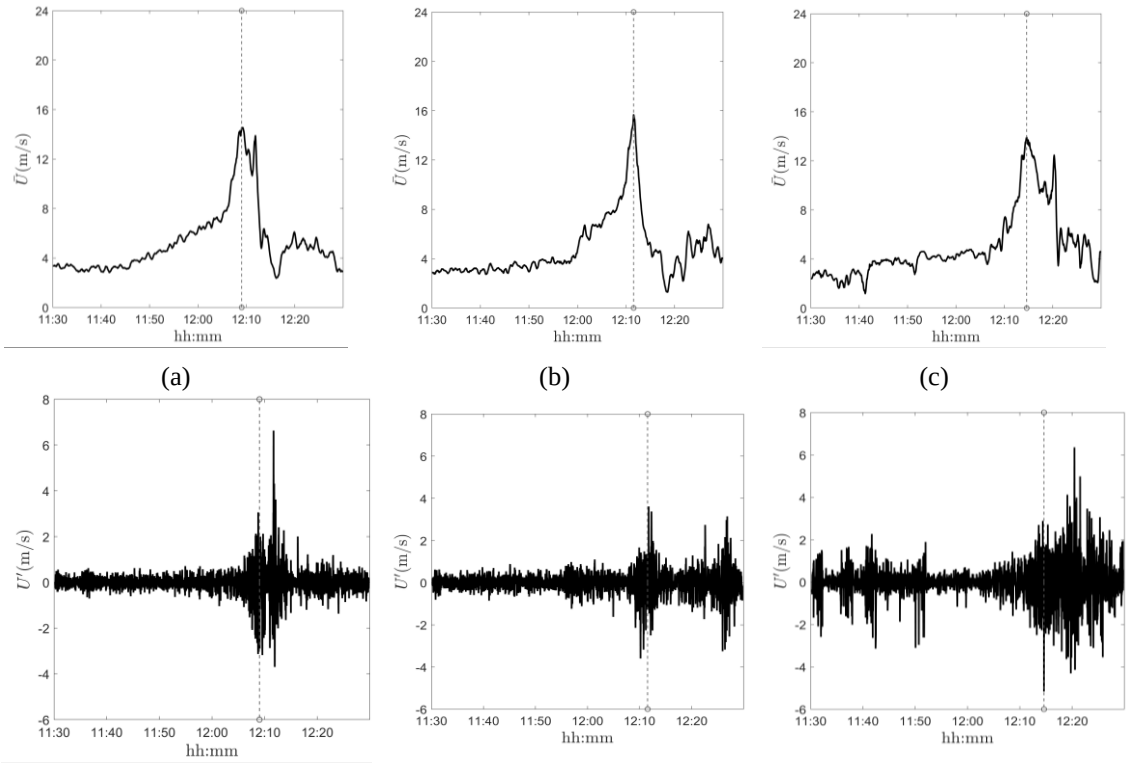

(a) (b) (c)

(d) (e) (f)

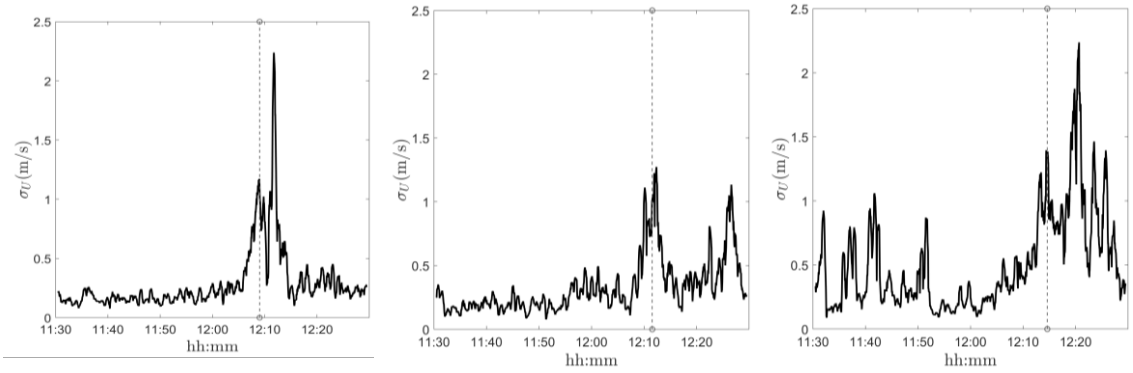

(g) (h) (i)

Figure 5.5 (top) Slowly varying mean wind velocity, (middle) residual fluctuation, and (bottom) slowly varying standard deviation, as extracted from the records detected by the (a), (d), (g) LI.03; (b), (e), (h) LI.01; and (c), (f), (i) LI.05 anemometers of the port of Livorno monitoring network from 1130 to 1230 UTC 1 Oct 2012. Vertical dashed lines show the approximate times of the gust front passage.

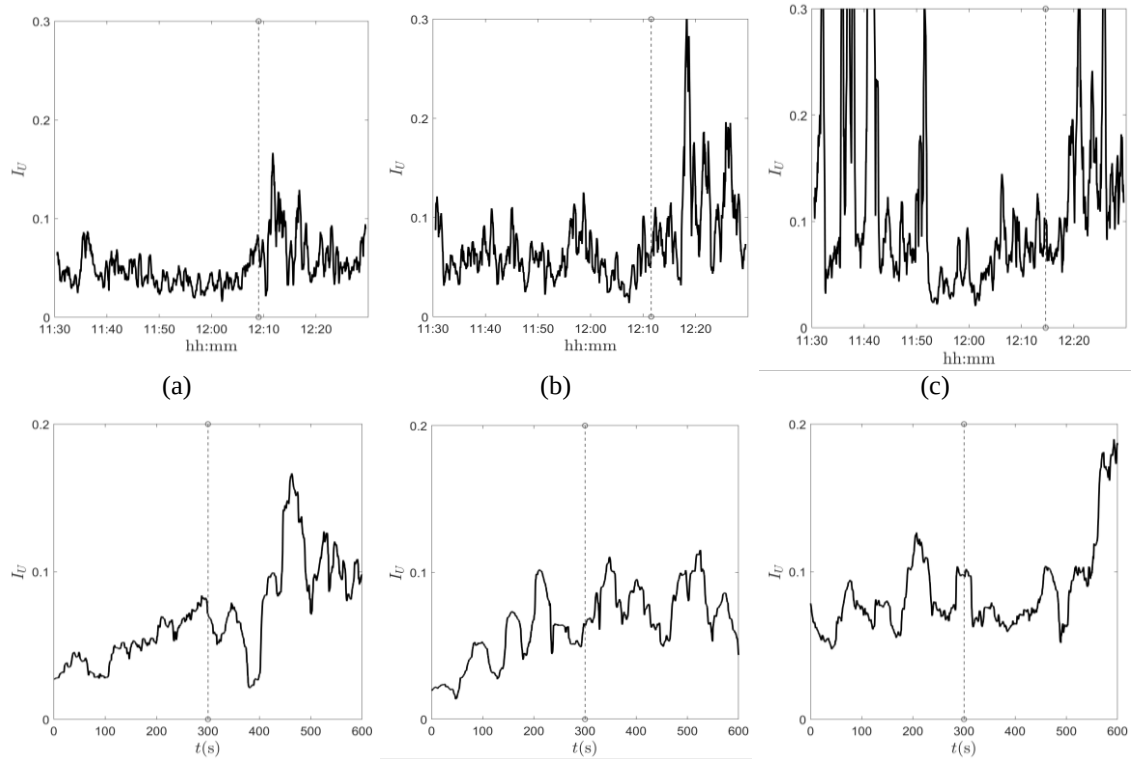

(a) (b) (c)

(d) (e) (f)

Figure 5.6 Slowly-varying turbulence intensity over $\Delta T = 1$ hour (top) and the 10-min interval centred around the time instant at which $\overline{U}_{max}$ occurs (bottom), as extracted from the records detected by the (a), (d) LI.03; (b), (e) LI.01; and (c), (f) LI.05 anemometers of the Port of Livorno monitoring network from 1130 to 1230 UTC 1 Oct 2012. Vertical dashed lines show the approximate time of the gust front passage.

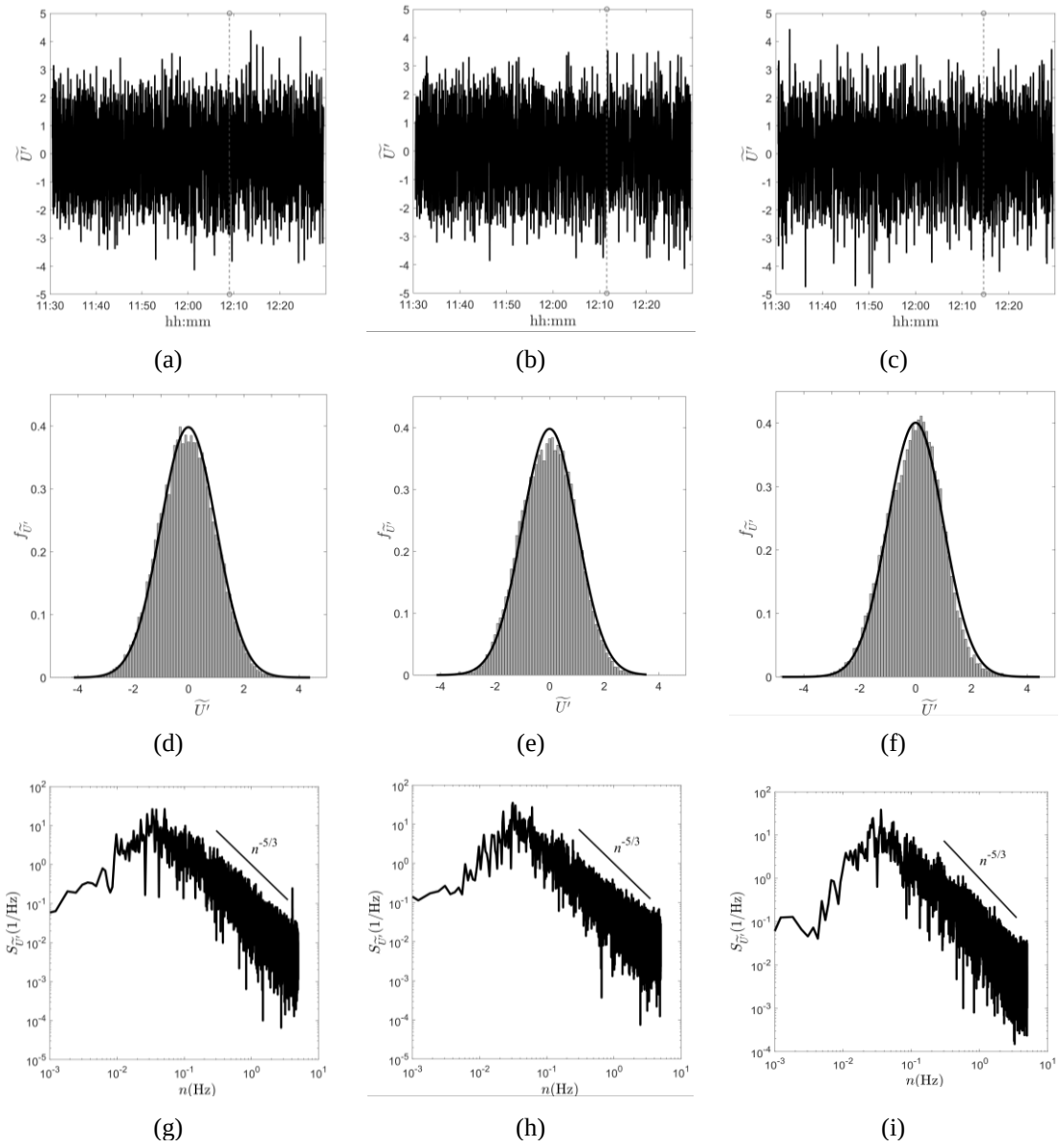

Figure 5.7 Rapidly-varying reduced turbulence fluctuation (top), histogram compared with a reference Gaussian PDF (thick line) (middle), and PSD (bottom), as extracted from the records detected by the (a), (d), (g) LI.03; (b), (e), (h) LI.01; and (c), (f), (i) LI.05 anemometers of the Port of Livorno monitoring network from 1130 to 1230 UTC on 1 Oct 2012.

5.3.2 Weather scenario and meteorological precursors

5.3.2.1 Synoptic dynamics

The synoptic conditions over Europe on 1 October 2012 are depicted along with the positions of cyclones and anticyclones at 0000 (**Figure 5.8 (a)**) and 1200 UTC (**Figure 5.8 (b)**). The data are obtained from the National Centers for Environmental Prediction's (NCEP) Global Forecast System (GFS) analyses, available on a 0.5°×0.5° grid. The meteorological situation over Europe was dominated by the presence of Extratropical Cyclone Marianne (following the naming convention used by the Institute of Meteorology of the Freie Universität Berlin, Berlin, Germany) southeast

of Iceland, with a surface low pressure minimum below 985 hPa and a trough aloft extending southward to the western Alps. To the east, the occluded front of Extratropical Cyclone Lulu developed on 25 September in the Labrador Sea and extended from northwestern Russia to north of the Sea of Azov. Finally, the 1025-hPa high pressure maximum associated with Anticyclone Harald, which was situated over central Europe a few days before, had moved over Poland and Ukraine, indicating a blocking situation (Rex, 1950).

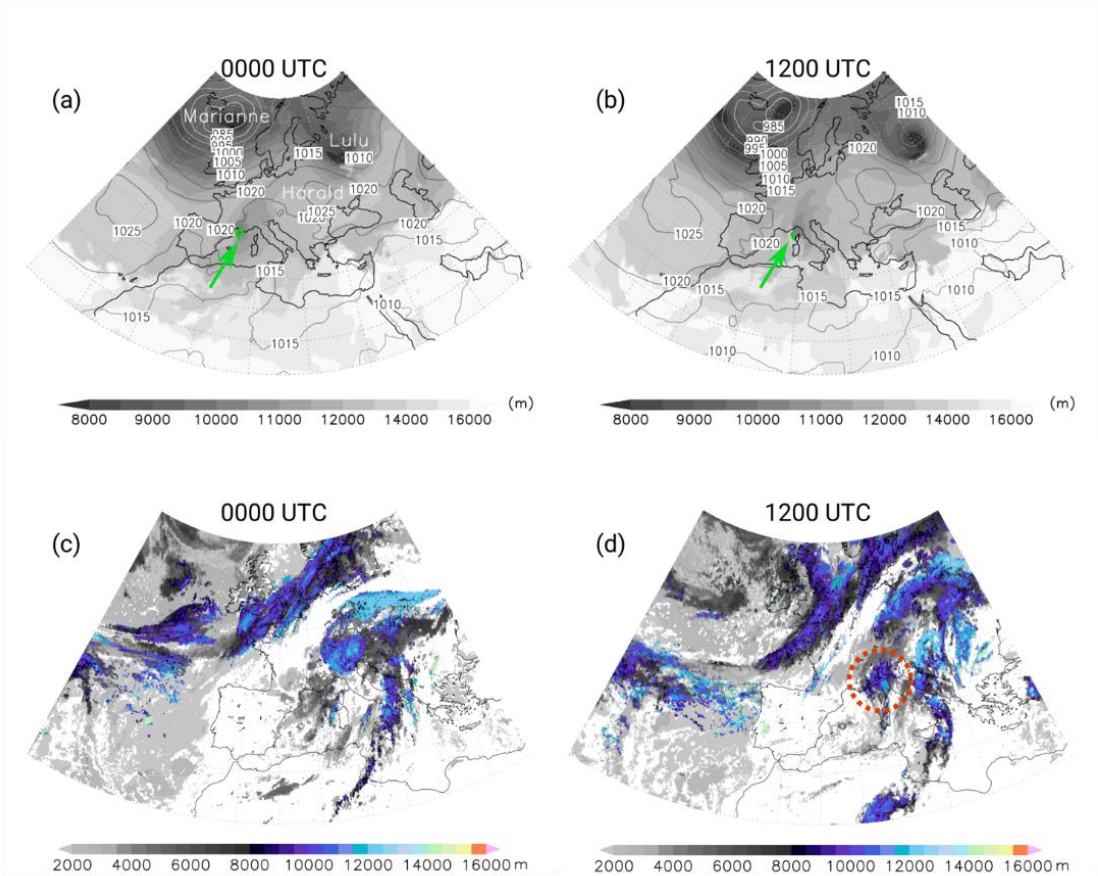

Figure 5.8 (a), (b) Mean sea level pressure (contours) and tropopause height (shaded contours) over Europe from GFS analyses. The green contour (indicated with the green arrow) corresponds to the minimum of the tropopause anomaly cutoff over the western Alps. (c), (d) Cloud-top height from Meteosat Second Generation (MSG) data. Results from (left) 0000 and (right) 1200 UTC 1 Oct. The red dashed circle in (d) shows the convective system that developed over the Gulf of Genoa during the morning of 1 Oct.

At 0000 UTC, the tropopause anomaly cut off had a relative minimum of 9870 m and it was located in the northern Mediterranean over the Gulf of Lion (France). The anomaly cutoff moved westward over the Gulf of Genoa at midday. This situation is depicted by the positioning of the 10 000-m height (green contours in **Figure 5.8 (a)** and **(b)**). According to GFS analyses, at 1200 UTC the tropopause height showed an abrupt discontinuity along a distance of about 100 km, spanning from less than 10 km

over the Gulf of Genoa to more than 13 km over the Corsican Sea (i.e., to the west of Corsica; see **Figure 5.3 (a)**), denoting the existence of a frontal zone beneath.

The distribution of cloud-top heights obtained from the cloud analysis performed by EUMETSAT (EUMETSAT, 2013; Derrien et al., 2013) also shows the presence of a smaller cyclone in the eastern Padan plain at 0000 UTC (**Figure 5.8 (c)**). The cyclone, which developed on 29 September as a secondary cyclogenesis event in the Gulf of Genoa (Trigo et al., 2002), had moved over the Balkans at 1200 UTC. However, **Figure 5.8 (d)** shows that a mesoscale convective system, which was only in its embryonic stage at 0000 UTC, developed rapidly over the Gulf of Genoa during the morning. This mesoscale convective system is the main contributor responsible for the strong wind event described in **Section 5.3.1**.

Both an upper-level trough upstream of the Alps, like the one of Cyclone Marianne, and a low-level frontal system impinging on the Alps, as denoted by the tropopause discontinuity mentioned above, are considered indispensable meteorological precursors to lee cyclogenesis. These factors play a fundamental role during the rapid trigger phase as a result of the interactions between the frontal zone and mountains (Buzzi and Tibaldi, 1978). During this stage, the cyclone deepens while remaining quasi stationary, the upper-level trough fills north of the Alps and deepens to the south, and the jet stream splits northwest of the Alps into a secondary branch over the Mediterranean before reconnecting to the main branch to the north of the Black Sea (**Figure 5.9**). Many different and partially concurrent mechanisms have been proposed for lee cyclogenesis during the trigger phase (Buzzi and Tibaldi, 1978; McGinley, 1982; Mattocks and Bleck, 1986; Bluestein, 1995; McTaggartCowan et al., 2010a,b). The absolute vorticity fields at the 300-hPa level over Italy at 0000 and 1200 UTC on 1 October are depicted in **Figure 5.10 (a)** and **(b)**, respectively. Only contours higher than 0.00025 s^{-1} are drawn to indicate the position of the trough (**Figure 5.8 (a)** and **(b)**) and its movement from upstream of the Alps to the lee side, where secondary cyclogenesis took place. The conditions favorable for intensification of lee cyclones during their trigger phase (Bluestein, 1995; Mattocks and Bleck, 1986) were present over the Corsican Sea at 0000 UTC and over the Ligurian Sea at 1200 UTC when the relative humidity at 700 hPa (**Figure 5.10 (a)** and **(b)**) exceeded 99%. At midday, high clouds covered the whole Ligurian Sea and a deep convective system with cloud-top heights above 10 000 m formed and extended from northeast of Corsica to the coast of Tuscany.

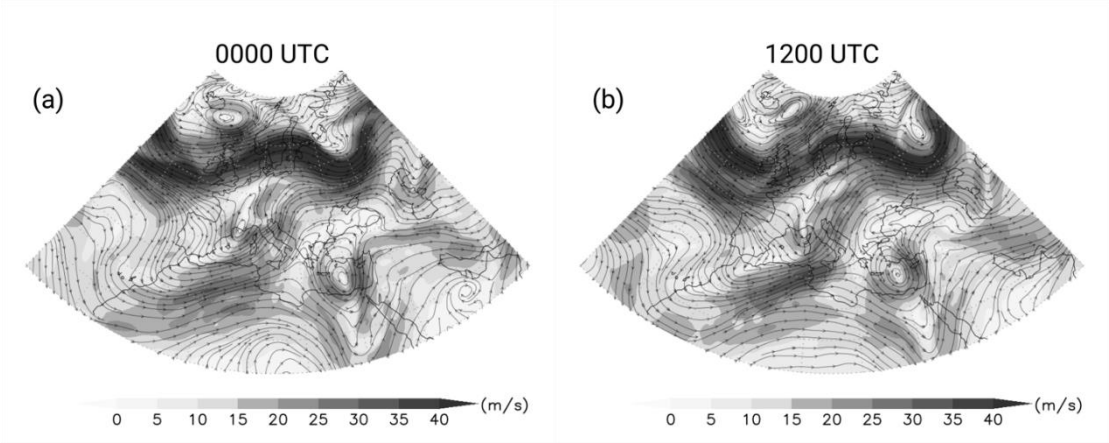

Figure 5.9 Wind speed (shaded contours) and streamlines at 300 hPa at (left) 0000 and (right) 1200 UTC 1 Oct.

Figure 5.10 (a) and **(b)** show the mean storm motion (vectors), which is calculated as an integral measure of the wind velocity variation between 0 and 6000 m above sea level (ASL). This parameter is very useful for predicting the spatial evolution of thunderstorms inside complex convective systems. In the present case, the mean storm motion at 1200 UTC in the eastern Ligurian Sea and northern Tyrrhenian Sea (**Figure 5.10** (**b)**) was almost purely zonal with an average magnitude of about 6 m/s to the east. This value is the result of the wind field shift from south-southeast in the lower troposphere (at 925 hPa) to southwest aloft (at 400 hPa). The updrafts turn clockwise as they rise and their corresponding gust fronts occur prevailingly on the eastern side of the convective cells, where new updrafts form (Weisman and Klemp, 1982; Fovell and Ogura, 1989). The multicell system is driven by the lifting of warm air along the gust front and the system shifts eastward under such wind shear conditions. The storm-relative helicity (SRH), calculated in a layer from 0 to h = 3000 m ASL, is another important parameter that helps in determining the type of thunderstorms (Davies-Jones et al., 1990) by measuring the vertical transfer of energy due to the wind shear:

$$\mathrm{SRH} = -\int_0^h \boldsymbol{k} \cdot (\boldsymbol{V} - \boldsymbol{C}) \times \frac{d\boldsymbol{V}}{dz}\, dz, \tag{5.1}$$

where $\boldsymbol{V}$ is the environmental wind vector, $\boldsymbol{C}$ is the storm's translation velocity, and $\boldsymbol{k}\times\mathrm{d}\boldsymbol{V}/\mathrm{dz}$ is the horizontal vorticity with $\boldsymbol{k}$ being the unit vector in the vertical (z) direction. This index reached the maximum value of 116 m^2s^{-2} (not shown) 25 km to the west-southwest of Livorno. According to Rasmussen and Blanchard (1998), the calculated values of the mean storm motion and SRH correspond to nonsupercell thunderstorm conditions. It is worth noting, however, that the maximum SRH is above the 75th percentile of the SRH distribution of nonsupercell thunderstorms and very close to the median (124 m^2s^{-2}) of the SRH distribution of supercells without tornadoes. Therefore, the possibility of supercell-like thunderstorms off the coast of Livorno cannot be completely excluded. The SRH, however, should always be

interpreted with caution since the values above 350 m^2s^{-2} were observed in intense low-level jets and stable stratification (Romanić et al., 2016).

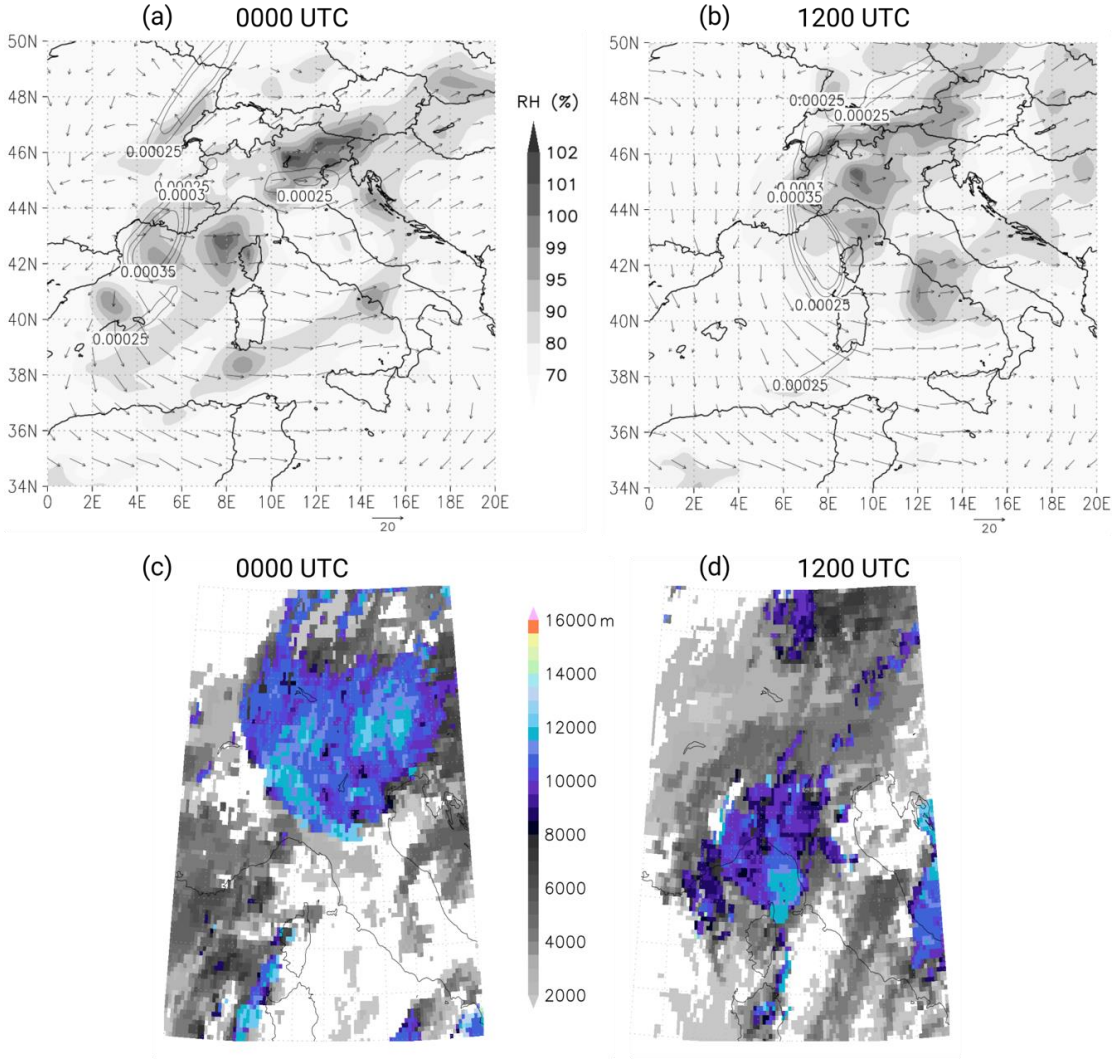

Figure 5.10 (a), (b) Relative vorticity (contours) at 300 hPa, relative humidity (shaded contours) at 700 hPa, and mean storm motion (vectors) from GFS analyses. (c), (d) Cloud-top height from MSG data. Results are from (left) 0000 and (right) 1200 UTC 1 Oct.

5.3.2.2 Local-scale observations

According to satellite images (not shown), the deep convective system shown in **Figure 5.8 (d)** started growing to the northeast of Corsica between 0900 and 1000 UTC on 1 October. As reported in the European Severe Weather Database (Dotzek et al., 2009), two waterspouts were observed at 0900±15 min UTC and 1000±15 min UTC at Pietracorbara and Santa Maria di Lota (Corsica), respectively. Their positions are shown in **Figure 5.3 (a)**. Later on, the convective system grew as a multicell complex of thunderstorms positioned along a rather straight line [i.e., a squall line; Zipser (1977)].

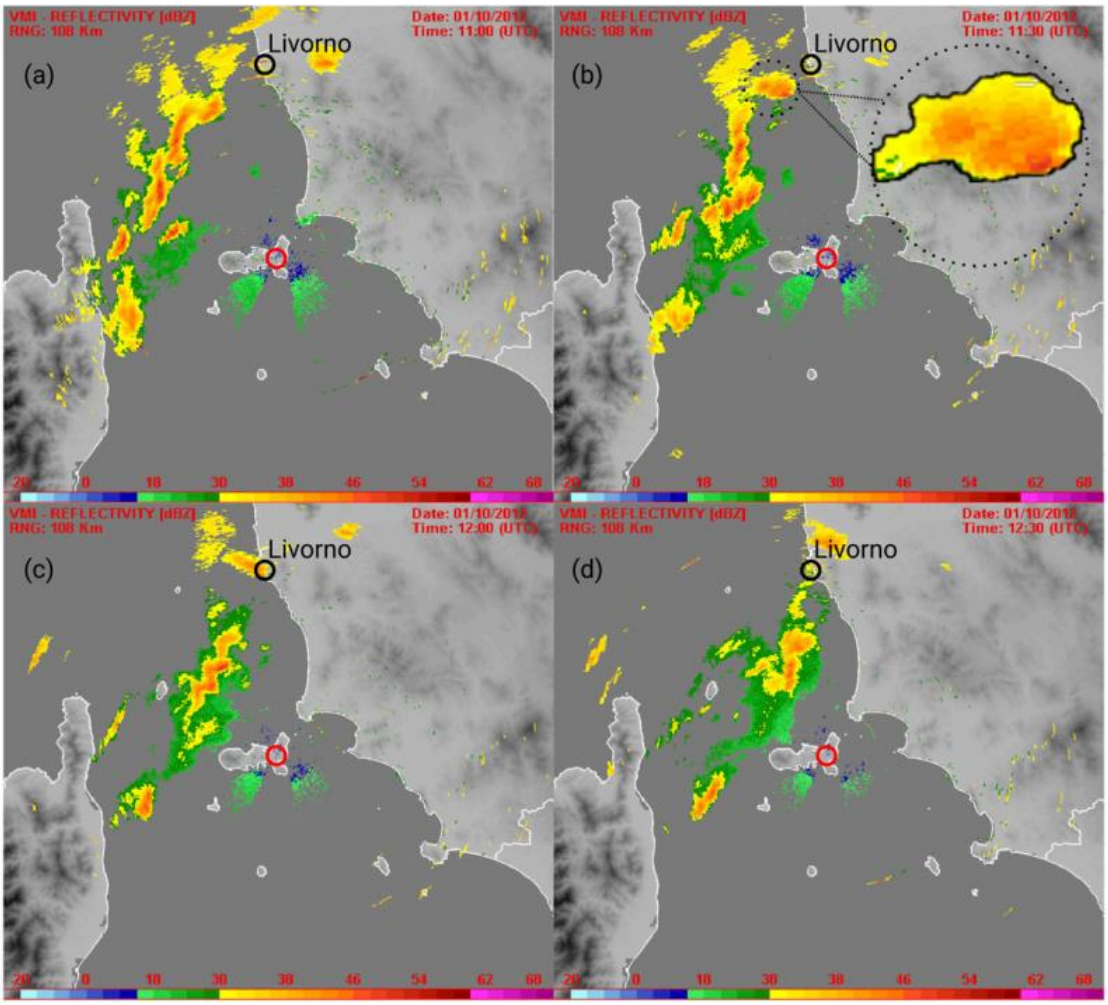

Figure 5.11 Reflectivity (dBZ, vertical maximum intensity) measured by the meteorological X-band radar, installed at Cima di Monte (Elba) at 480 m ASL at (a) 1100, (b) 1130, (c) 1200, and (d) 1230 UTC. The location of the meteorological radar on Elba is indicated with a red circle. (Courtesy of the LaMMA Consortium.)

Figure 5.11 shows the reflectivity measured by the meteorological radar installed on the island of Elba, which spans a circular area with radius of about 108 km: **Figure 5.11 (a–d)** show the time evolution of the convective system from 1100 to 1230 UTC with a 30-min time step. At 1100 UTC, the values of radar reflectivity around 30 dBZ show the position of scattered thunderstorms organized along a straight line from Corsica to Tuscany, which slightly shifts to the northeast during the next hour. This observation seems to be coherent with the mean storm motion obtained from the GFS analyses mentioned in the previous section, as the thunderstorms develop new cells to the right of the mean flow, which is about northward. At 1130 UTC (**Figure 5.11 (b)**), a roughly circular blob appears to the west-southwest of Livorno, in the same position where the maximum SRH value was observed. This convective thunderstorm arrived at 1200 UTC in Livorno (**Figure 5.11 (c)**) and is very likely responsible for the strong wind event depicted in **Section 5.3.1**. Unavailability of radar velocity data prevents any firm statement on the existence of a rotating updraft. At 1230 UTC (**Figure 5.11**

(d)), the convective cell had already moved to the north of Livorno. The recorded wind directions during the downburst event (**Figure 5.4 (b)**, **(d)** and **(f)**), supplemented with the results in **Figure 5.11 (c)** and **(d)**, suggest that the downburst was spawned in the north part of the convective system. Interestingly, this region is not characterized by the highest radar reflectivity. Takayama et al. (1997) also found that the strongest winds in the mature stage of downburst were located northwest from the strongest radar reflectivity. The confirmation of this finding is important for downburst forecasting.

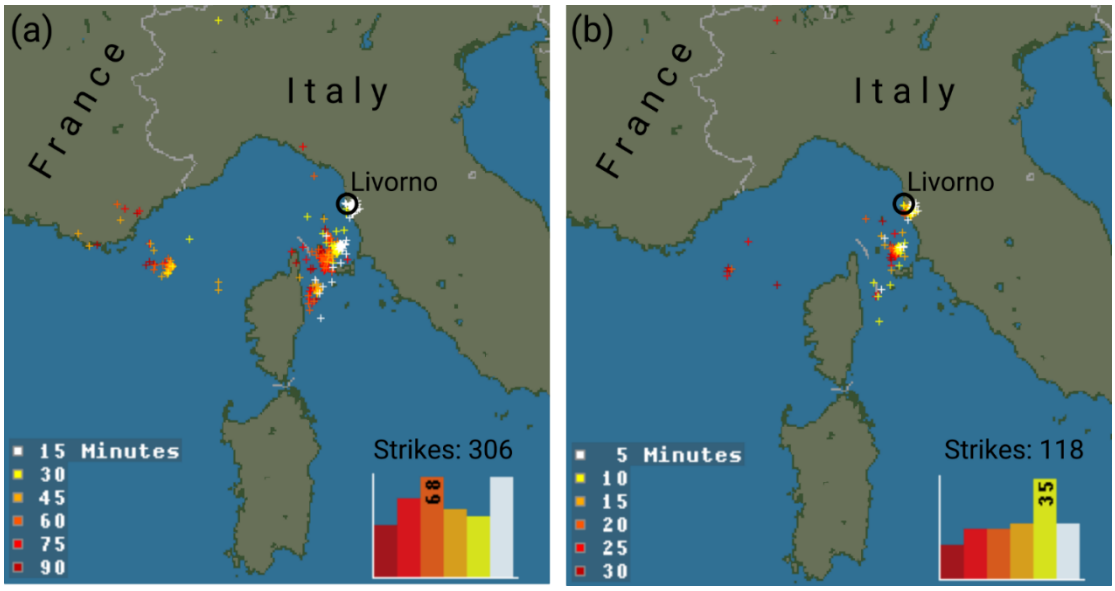

Figure 5.12 Strikes recorded (left) from 1100 to 1230 UTC and (right) from 1200 to 1230 UTC 1 Oct by means of the Blitzortung network for lightning and thunderstorms, retrieved through the online archive. (Courtesy of Blitzortung.org.)

The intense convective activity that occurred over the area from Corsica and Tuscany during the morning of 1 October is confirmed by the large number of lightning strikes registered by the Blitzortung network for lightning and thunderstorms (**Figure 5.12**). Lightning strikes were localized in the southern part of the convective system, which is the area populated with the deepest (**Figure 5.8 (d)** and **Figure 5.10 (d)**) and most intense convection (**Figure 5.11 (c)**). Lightning strikes were observed in Livorno during this event.

Finally, the weather station located in the city center (**Figure 5.3 (b)**) measured several important parameters during the thunderstorm with a sampling rate of 15 min. The records of wind speed and direction, temperature, solar radiation, and precipitation are reported in **Figure 5.13**. The station measured quite a low mean and maximum wind speed with the prevailing and gust wind directions from the northern sector, as shown in **Figure 5.13 (a)** and **(b)**. The only wind speed anomaly was registered at 1215 UTC, when both the mean and maximum speeds spiked to 8.5 and 15.8 m/s, respectively. The temperature also decreased by more than 3 °from 21.9 °at 1200 UTC to 18.6 °at 1230 UTC. At the same time, solar radiation dropped from its

daily maximum of 1082 W m^{-2} at 1100 UTC to 11.2W m^{-2} at 1215 UTC, and the rain gauge registered 10.6mm of precipitation between 1200 and 1215 UTC and 5.6 mm between 1215 and 1230 UTC. The local observations combined with the anemometer records in **Figure 5.4** confirm that the studied event was a wet downburst (Wakimoto, 1982; Atkins and Wakimoto, 1991). The pronounced decrease in solar radiation indicates the existence of well-developed and deep thunderstorm clouds in the area.

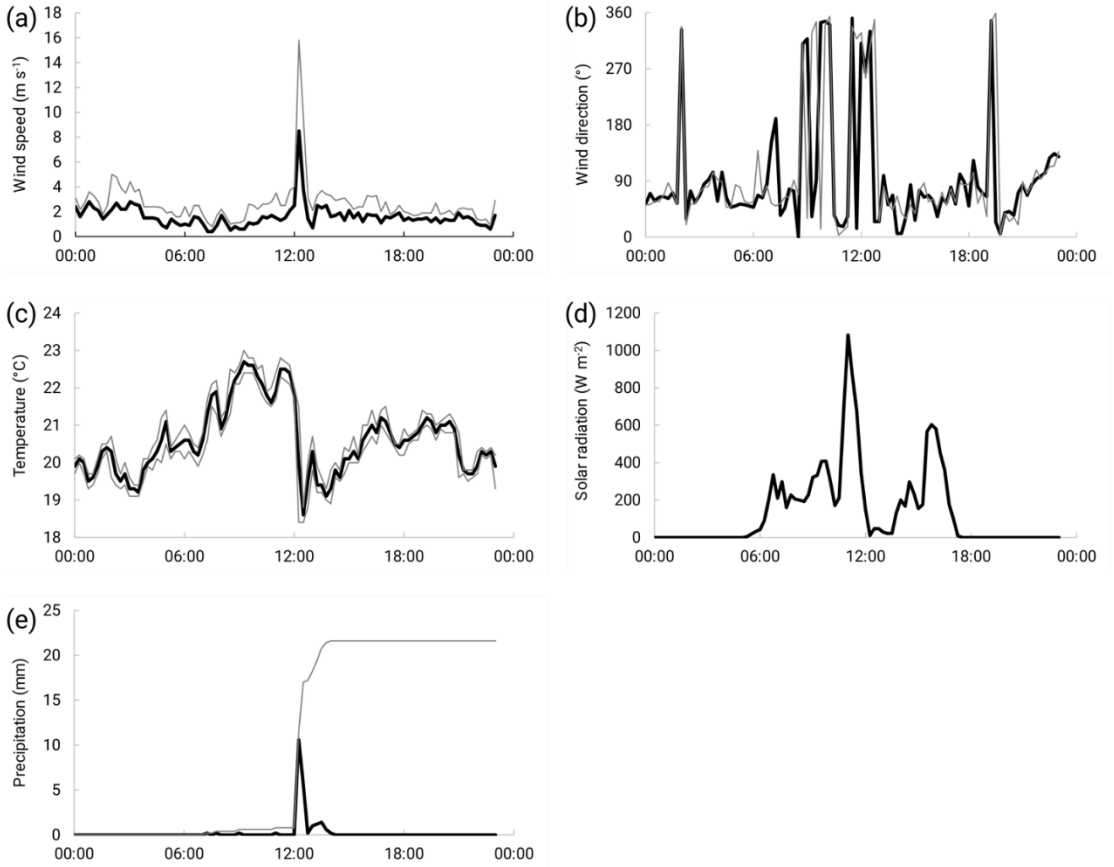

Figure 5.13 Measurements from the LaMMA meteorological station in Livorno: (a) mean (black) and maximum (gray) wind speed (m/s), (b) prevailing (black) and gust (gray) wind directions ( ), (c) temperature (black) and its variability (gray) (°C), (d) maximum solar radiation (black) (W m^{-2}), and (e) precipitation (black) and daily cumulated rain (gray) (mm). Data are available every 15 min. (Courtesy of the LaMMA Consortium.)

5.2.2.3 Instability indices

In the case of small-scale convective phenomena, many instability indices exist that are intended to provide some deterministic or probabilistic information about the occurrence of severe weather conditions [lifted index (LI), Showalter index, total totals, K index, the severe weather threat index (SWEAT), bulk Richardson number, convective available potential energy (CAPE)]. Three instability indices particularly important for wet downdrafts are the wind index (WINDEX), which can be interpreted as a direct measure of downdraft intensity; LI; and CAPE, which are widely used as measures of updraft intensity. Following the work of Proctor (1989) and Wolfson (1990), McCann (1994) proposed the following expression for WINDEX (WI):

$$\mathrm{WI} = 5\sqrt{H_M R_Q(\Gamma^2 - 30 + Q_L - 2Q_M)}, \tag{5.1}$$

where H_M is the height of the melting level above ground (in km), R_Q = min(Q_L/12, 1), Q_L is the mixing ratio in the first 1 km above the surface, Γ is the temperature lapse rate from the surface to the melting point (in °Ckm^{-1}), and Q_M is the mixing ratio at the melting level. This parameter tends to replicate the peak wind velocity [in knots (kt, where 1 kt = 0.5144 m/s)].

The WINDEX values calculated at 1200 UTC from GFS data over the Ligurian Sea and northern Tyrrhenian Sea are shown in **Figure 5.14 (a).** The index is missing where the lapse rate is lower than about 5.5 °Ckm^{-1}, which occurs over the Alps and the eastern Ligurian Apennines. In Livorno, the WINDEX is between 35 and 40, which is similar to the peak velocities (in kt) presented in **Figure 5.4**. The LI and CAPE results at 1200 UTC from GFS data are shown in **Figure 5.14 (b)** and **(c)**, respectively. Because of the low values of LI (Peppier, 1988) and the relatively high values of CAPE, thunderstorms were expected to occur over Corsica, the central Tyrrhenian Sea, the southwestern Alps, and the eastern Padan plain.

The atmospheric soundings from the three stations indicated in **Figure 5.14 (a)** and **(b)** were also analyzed and the corresponding skew T–logp diagrams are presented in **Figure 5.14 (d) and (f)**. The WINDEX values evaluated from TEMP messages are 39.5 and 33.5 for LIML (Milan Linate airport) and LIRE (Pratica di Mare Air Force base, Rome), respectively, whereas values were not calculated for LFKJ (airport of Ajaccio, Corsica) as the lapse rate is equal to -5.37°Ckm^{-1}. The LI results based on radiosoundings are -0.74, -0.70, and -2.07 for LFKJ, LIML, and LIRE, respectively, whereas the CAPE results based on the virtual temperature are 493.4 J kg^{-1} for LFKJ, 315.5 Jkg^{-1} for LIML, and 670.9 Jkg^{-1} for LIRE.

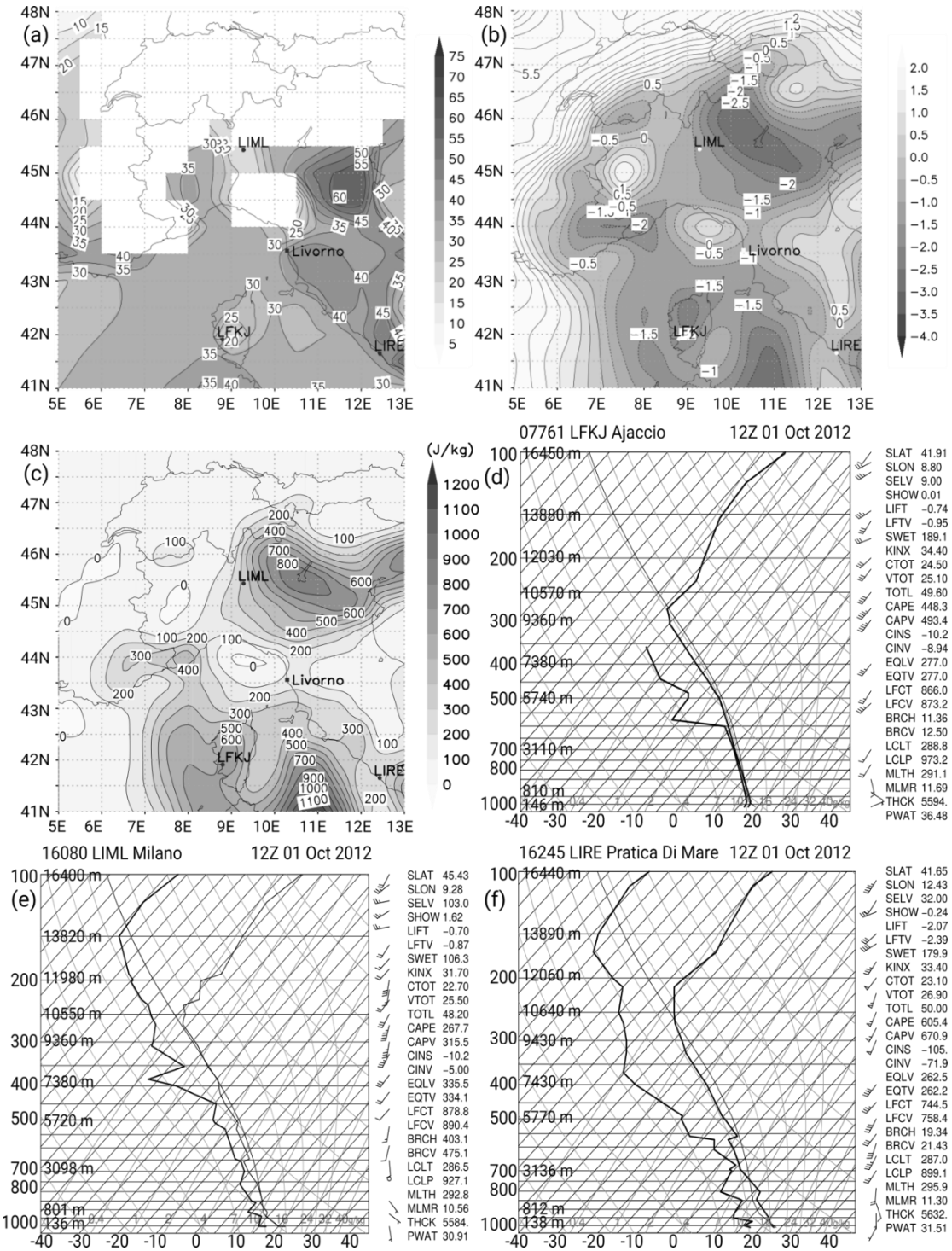

Figure 5.14 (a) WINDEX, (b) LI, and (c) CAPE from GFS analyses. Skew T–logp thermodynamic diagrams at (d) Ajaccio, (e) Milan, and (f) Rome. All panels refer to 1200 UTC 1 Oct. (Diagrams courtesy of the University of Wyoming.)

5.4 Three thunderstorm outflow events related to three families

As previously noted, the procedure in **Section 5.3** may represent a reference model to carry out comprehensive analyses of the major thunderstorm events. However, its burden is so high that it makes this procedure realistically unusable for systematic

analyses of historical series of such events. Hence, the need arises, or at least the objective, to develop an faster approach that integrates the data provided by an anemometric network such as the "WP" and "WPS" ones, with few essential meteorological information that may qualify, albeit preliminarily, the transient intense wind events detected by the network.

In this spirit, making treasure of the experience matured during the detailed analysis of several downbursts, in particular the one that stroke Livorno on 1 October 2012, this section describes simplified meteorological surveys and preliminary reconstructions of the weather scenarios that occurred during the three events presented in **Figure 5.15**, **Figure 5.16** and **Figure 5.17**. In which, the pictures **(a) (b)**, **(c) (d)** and **(e), (f)** refer to 10-min, 1-h and 10-h long records, respectively, centered around the gust peak; pictures **(a), (c), (e)** and **(b), (d), (f)** correspond to wind speed and direction, respectively. In all these diagrams the time variation of the wind direction reflects the time variation of the wind speed, exhibiting a change that may be perceived at the same time-scale in which the ramp-up and the transient peak are perceived.

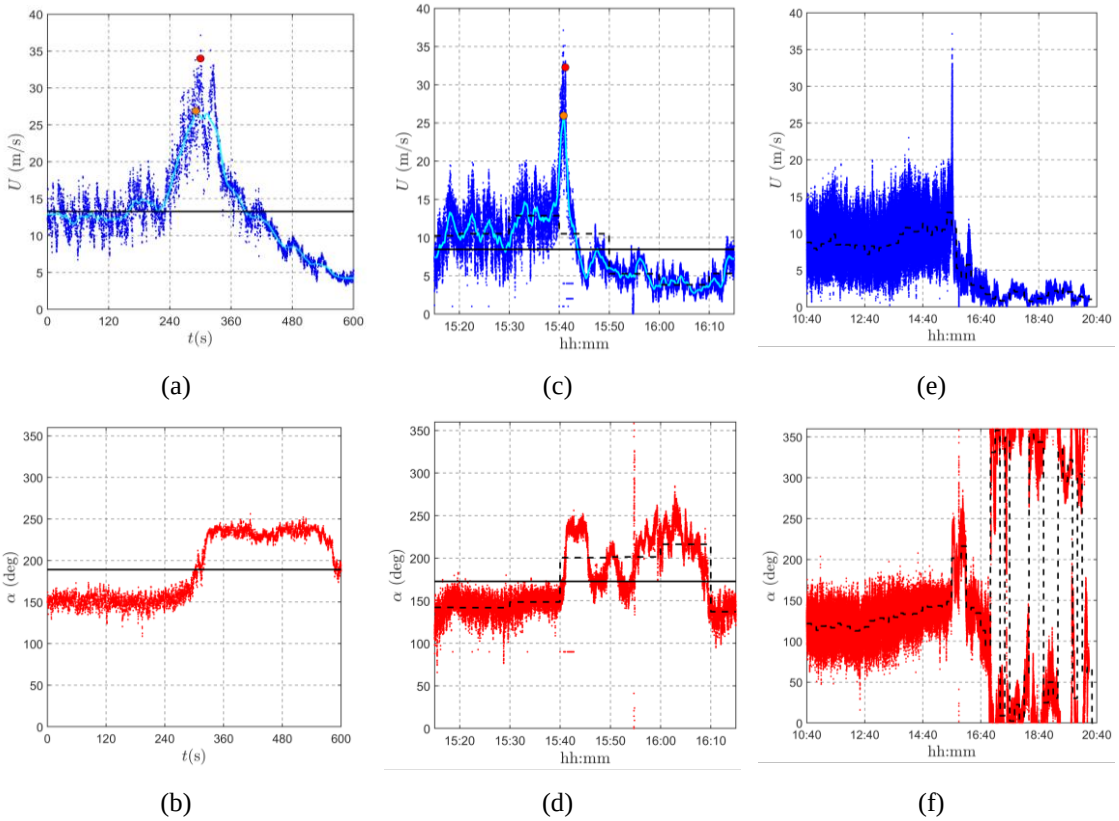

Figure 5.15 Thunderstorm outflow recorded on 25 October 2011 at about 15:40 UTC by the anemometer 3 of the Port of La Spezia: wind speed time-series in10-min (a), 1-h (c), and 10-h (e); wind direction time-series in 10-min (b), 1-h (d), 10-h (f).

In the following three subsections, the meteorological conditions that brought about all these intense wind events, whose characteristic lifetime-scales is 10-min, 1-h, and

10-h, are briefly reported one by one. The analysis is performed at two spatial scales: the meteorological conditions at the synoptic-scale are firstly inspected in order to evaluate the pattern of cyclones, anticyclones, and fronts that determined instability and cloudiness in the atmosphere; the phenomena possibly occurring at the meso-scale that developed over the areas of interest are then investigated in order to understand the specific convective structures present during the events under consideration. The whole analysis is based primarily on the following data: the Global Forecast System (GFS) analyses, obtained from the National Center for Environmental Prediction (NCEP) through the National Centers for Environmental Information database; the cloud top height, obtained from the cloud analysis performed by Eumetsat (EUMETSAT, 2013; Derrien et al., 2013) based on infrared measurements collected by SEVIRI (Spinning Enhanced Visible & Infrared Imager) on board Meteosat Second Generation (MSG) satellites; the lightning strikes, obtained from the Blitzortung database.

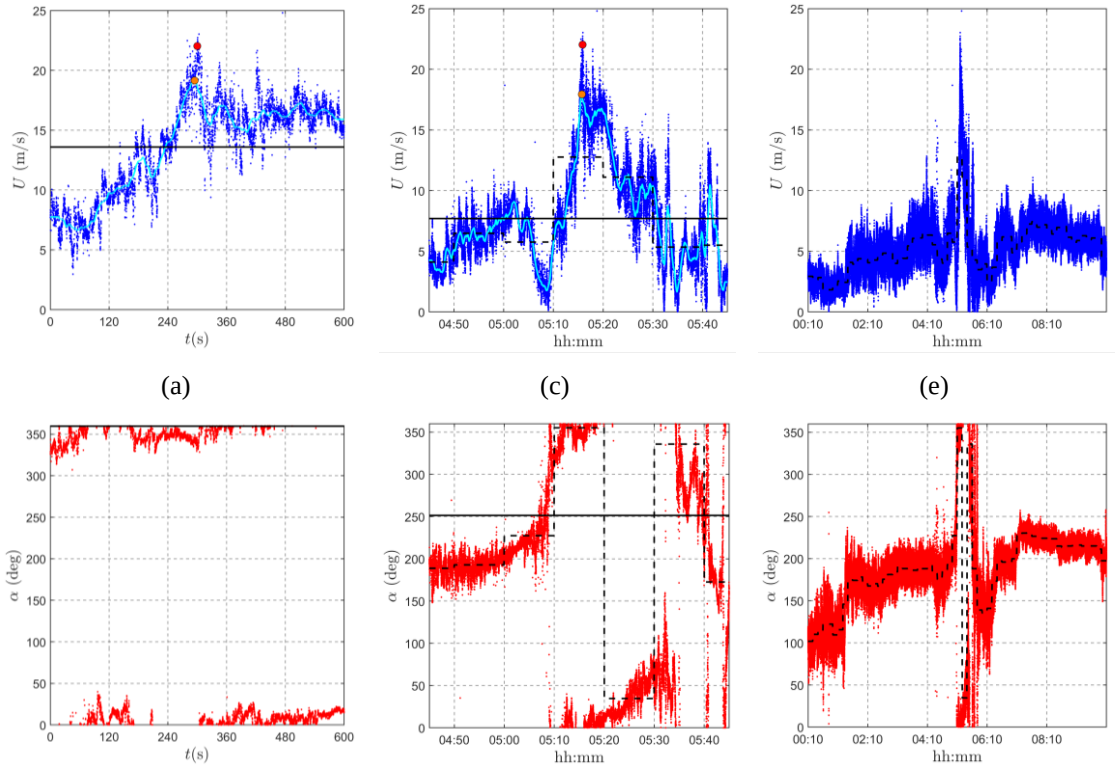

Figure 5.16 Thunderstorm outflow recorded on 4 October 2015 at about 05:15 UTC by the anemometer 1 of the Port of Livorno: wind speed time-series in 10-min (a), 1-h (c), and 10-h (e); wind direction time-series in 10-min (b), 1-h (d), and 10-h (f).

GFS analyses are available worldwide on a 0.5 ºby 0.5 ºgeographical grid with 6-hour time step; these spatial and temporal resolutions are suitable to evaluate the movement of the large-scale structures that determine the evolution of the weather conditions. The satellite measurements of Meteosat 10, which is the one used here, are available every 15 minutes as a full disk imagery centred at 0 degrees of longitude and latitude,

with a spatial resolution over Europe of a few kilometres. The spatial and temporal resolution of such data allows to distinguish the convective structures at the meso-scale and their evolution in time with sufficient accuracy also in case of thunderstorms, whose typical scales are of the order of 10 km and 1 h. Finally, the lightning strikes are used to confirm whether the convective activity can be associated to cumulonimbus clouds, which are typical of thunderstorms, or not.

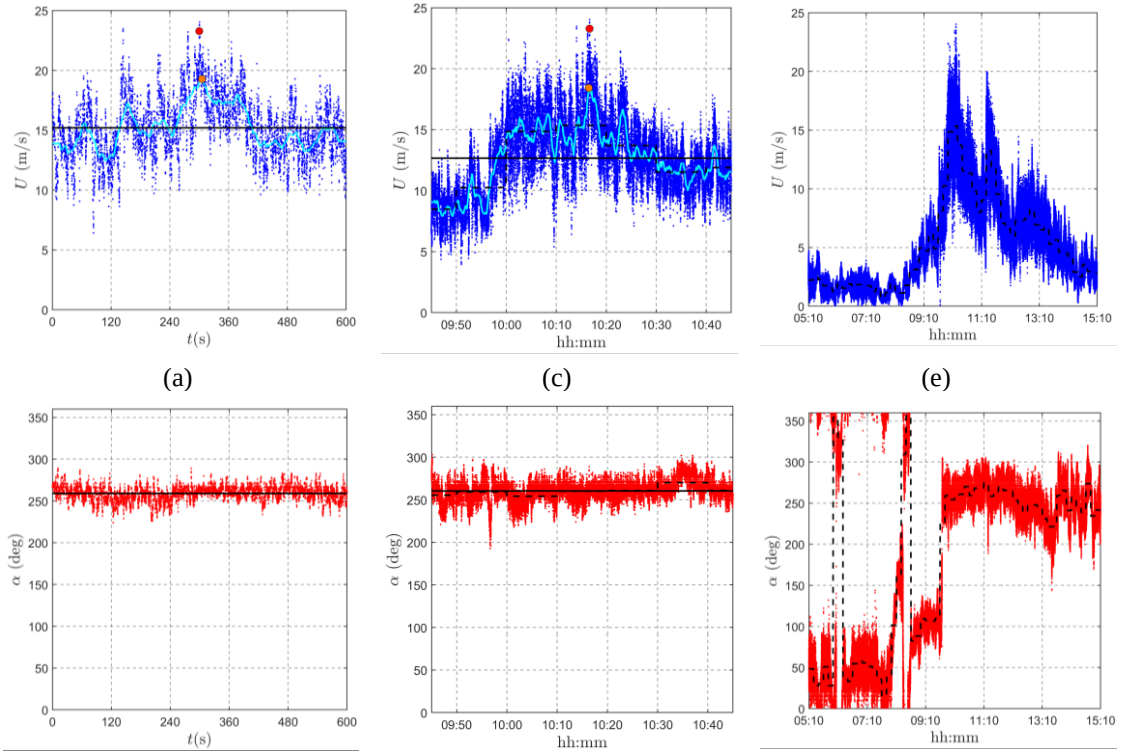

Figure 5.17 Thunderstorm outflow recorded on 21 November 2013 at about 10:15 UTC by the anemometer 2 of the Port of Genoa: wind speed time-series in 10-min (a), 1-h (c), and 10-h (e); wind direction time-series in 10-min (b), 1-h (d), and 10-h (f).

The meteorological analysis based on such data cannot provide precise information concerning the very small-scale structure of the thunderstorm considered, like the shape of its gust front or the area covered by heavy precipitations. This information can be obtained using higher resolution measurements like radar imagery or finer monitoring networks (Burlando et al., 2017a), and possibly high resolution numerical simulations (Lompar et al., 2017). However, as shown in the next sections, the meteorological analysis described above may be sufficient to state the nature, i.e. convective or synoptic, of the transient intense wind events investigated, which is the main focus of the present paper.

5.4.1 The 10-minute event on 25 October 2011 in La Spezia

On 25 October 2011, the exceptionally large Anticyclone Ulla (names given by the Institute of Meteorology of the Freie Universität Berlin, Germany) located over

Eastern Europe, with pressure maxima greater than 1030 hPa, determined the blocking of the zonal shift of Cyclone Meeno, which remained approximately stationary to the west of Ireland, extending its low-pressure minimum of 985 hPa northward to Iceland, as shown in **Figure 5.18 (a)**. The cold front of Cyclone Meeno, which extended meridionally to northern Africa passing over the Alps, was slightly moving westward over the Mediterranean during the day. The warm sector uplift ahead of Meeno's cold front due to the south-easterly winds forced over southern Italy and the Adriatic Sea by the extension of the influence of Ulla to the Balkans Region, determined a wide area of cloudiness all over northern and central Italy, shown in **Figure 5.18 (b)**. The distribution of cloud top heights in this figure shows that the prevailing southerly flow of warm and humid air from the Mediterranean favoured the development of strong instability associated to deep convection, which in turn determined locally very intense thunderstorm events.

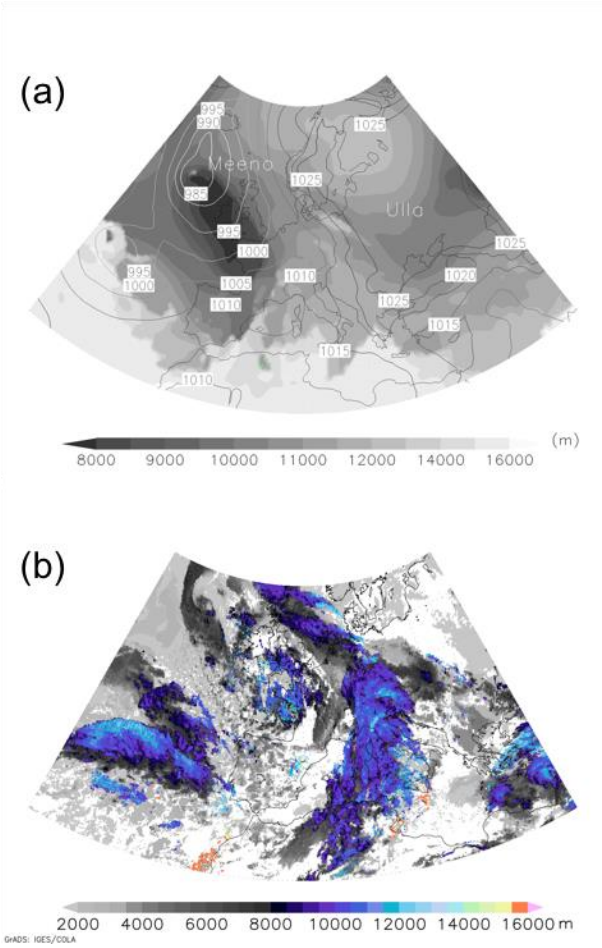

Figure 5.18 Top panel (a): mean sea level pressure (contours) and tropopause height (shaded contours) over Europe from GFS analyses on 25 October 2011 at 18:00 UTC. Bottom panel (b): cloud top height from MSG data on 25 October 2011 at 15:45 UTC.

The advection and uplift of moist air from the southern quadrants in the lee of the Alps is confirmed by values of relative humidity higher than 100 % over great part of the Padan Plain, the eastern Liguria and southward along a convergence line which

corresponds approximately to the frontal zone beneath. According to the GFS analysis, **Figure 5.19 (a)** shows that saturated air conditions, i.e. RH values (shaded contours) equal to 100%, were occurring exactly above La Spezia, at 1800 UTC. Moreover, the values of mean storm motion in the 0-6000 m AGL in the same area were between 10 and 15 m/s from south or southwest. According to satellite measurements, **Figure 5.19 (b)** shows that a deep convective cloud with the top at about 12000 m above the sea level (ASL) occurred at around 1545 UTC over La Spezia, indeed. However, during the morning of 25 October, a series of thunderstorms developed slightly to the northwest of La Spezia because of the orographic forcing determined by the south-eastern flow, as measured by the anemometers in the Port of La Spezia (see **Figure 5.15 (e)** and **(f)**). In that area, many meteorological stations of the Liguria Region (e.g. Monterosso, Serò di Zignago, Levanto S. Gottardo, Brugnato) reported precipitation rates larger than 50 and even 100 mm h^{-1} from 9:00 UTC to 15:00 UTC. The thunderstorm over La Spezia at 15:40 UTC was the last of this series, just before the wind shifted to the north when the cold front overcame the Western Alps. The sudden change in wind speed and direction reported in **Figure 5.15** represent the transition between these higher-to-lower wind speed regimes. It is worth noting that, as reported in Zhang et al. (2018a), the transition between this kind of wind regimes is usually slower, so that these events are often classified as 1-h events. In the present case, the dynamics of the transition is particularly fast so that the event is classified as a 10-min one.

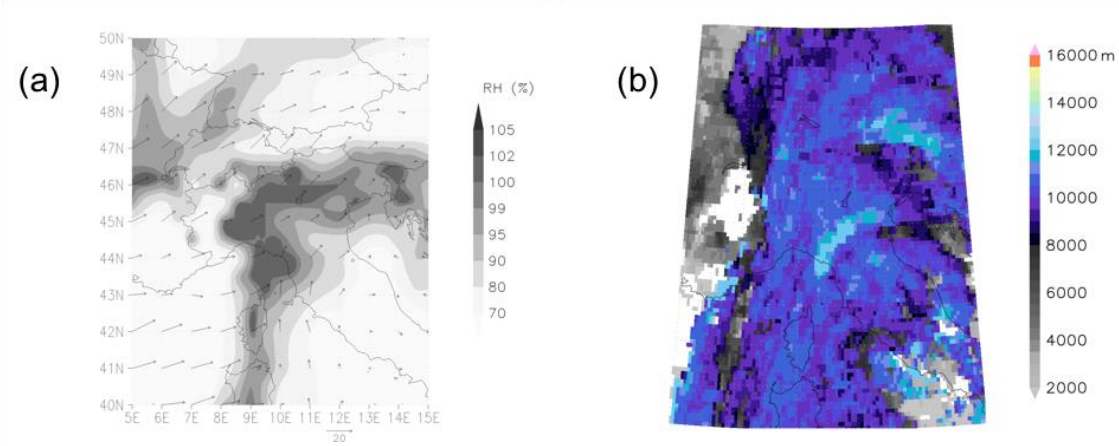

Figure 5.19 Panel (a): relative humidity (shaded contours) at 700 hPa and mean storm motion (vectors) from GFS analyses on 25 October 2011 at 18:00 UTC. Panels (b): cloud top height from MSG data on 25 October 2011 at 15:45 UTC.

As far as the cloud-ground strikes measured by the Blitzortung network are concerned, this convective cell showed only a moderate lightning activity, which confirms the convective nature of this phenomenon. The lightning occurrence on 25 October 2011, shown in **Figure 5.20**, in the interval from 15:25 to 15:55 UTC (half an hour centred with respect to the maximum wind speed recorded during this event) was 164 strikes, with a slightly increasing frequency during the first 25 minutes.

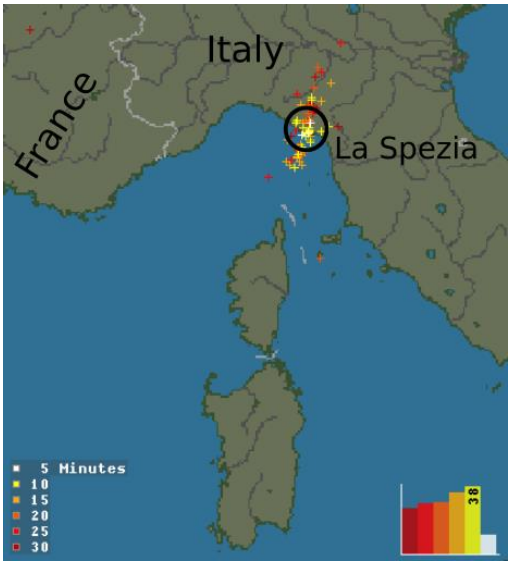

Figure 5.20 Strikes recorded on 25 October 2011, from 15:25 to 15:55 UTC, by means of the Blitzortung network for lightning and thunderstorms, retrieved through the on

5.4.2 The 1-hour event on 4 October 2015 in Livorno

Figure 5.21 (panels **(a)-(b)**) depicts the synoptic condition over Europe on 4 October 2015, showing the position of cyclones and anticyclones **(a)** and the cloud cover **(b)** at 06:00 UTC. The meteorological situation over Europe was dominated by the presence of the anticyclone Netti, with its high-pressure maximum of 1025 hPa situated over Ukraine and Russia, indicating a blocking condition (Rex, 1950). The cyclone Quirin, which was born on 2 October to the north of the Pyrenees, where a strong thermal contrast between a colder maritime Atlantic air mass to the north and the much warmer and moist tropical air to the south occurred, had slightly moved its low-pressure minimum north-eastward over the northern France on 3 October and Belgium on 4 October. According to GFS analyses, at 06:00 UTC the tropopause height showed an abrupt discontinuity to the north of the Alps with a roughly meridional gradient ranging from a maximum 14214 m to a minimum 9119 m, denoting the existence of a frontal zone beneath consisting of a warm core of tropical air southward (red contour reported in **Figure 5.21 (a)**) and a colder core of Atlantic air northward (blue contour in **Figure 5.21 (a)**). Cyclone Quirin, which was relatively small but very active because of the strong thermal gradients between Atlantic and tropical air masses, led to intense local thunderstorms and heavy precipitations in the southern France and northern Italy during the night between 3 and 4 October. The distribution of cloud top heights shows clearly the presence of the cyclone Quirin, with its surface low-pressure minimum located over Belgium at 06:00 UTC on 4 October (**Figure 5.21 (b)**) and the occluded front extending southward to the Adriatic Sea.

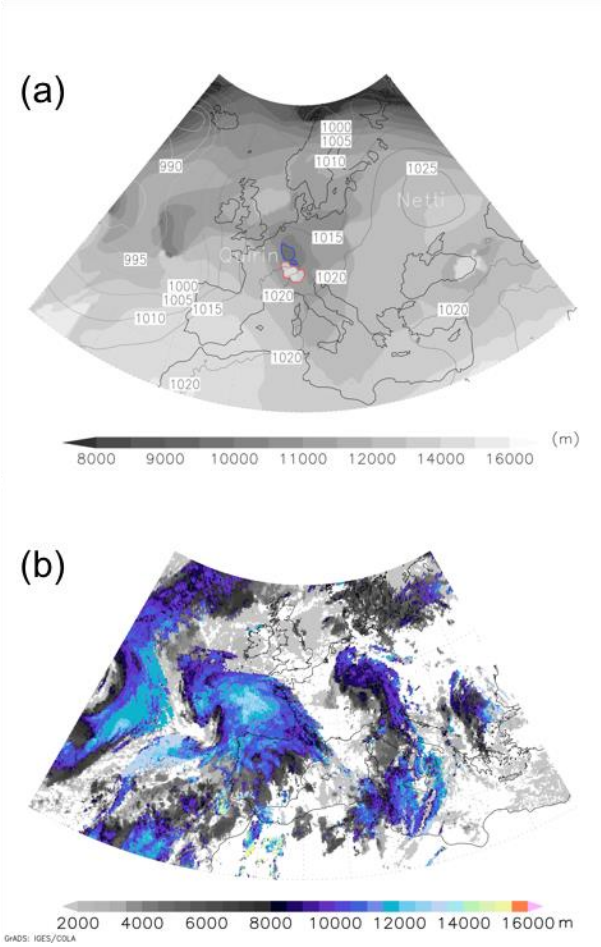

Figure 5.21 Top panel (a): mean sea level pressure (contours) and tropopause height (shaded contours) over Europe from GFS analyses. The red (blue) contour corresponds to the tropopause height equal to 12000 m (10000 m) to the north of the Alps. Bottom panel (b): cloud top height from MSG data. Both panels correspond to 4 October 2015 at 06:00 UTC.

In the lee side of the western Alps, the presence of a cold front extending from the Gulf of Genoa to the aforementioned occluded front in the northern Adriatic Sea is revealed by high relative humidity values in the lower troposphere due to the forced lift of the warmer and humid air over the Ligurian and Tyrrhenian Sea by the colder air flow from the north-western quadrant. **Figure 5.22 (a)** shows that RH values (shaded contours) close to saturation that occurred along a narrow band in the northern Tyrrhenian Sea, according to the GFS analysis at 0600 UTC. Vectors in **Figure 5.22 (a)**, which represent the mean storm motion in the 0-6000 m AGL, show that a storm developing along the frontal boundary would eventually move from the sea towards the coast of Tuscany at approximately 5 m/s or less. This is the case of the thunderstorm shown in **Figure 5.16** that developed on 4 October early in the morning off the coast of Livorno. The sequence of three satellite images reported in **Figure 5.22 (b)-(d)** resembles the development of a single-cell thunderstorm caused by a cumulonimbus cloud that started developing its cumulus stage around 0430 UTC (**Figure 5.22 (b)**) over Livorno City, then reached the mature stage with a cloud top

height of about 12000 m ASL at 05:15 UTC (**Figure 5.22 (c)**), and finally gradually dissipated while moving slowly farther inland (**Figure 5.22 (d)**). Because of the low storm advection from sea to land, the anemometric signals recorded in the Port of Livorno have caught the whole three stages of the thunderstorm evolution on a time scale, i.e. 1 hour, which is approximately coincident to the typical order of magnitude of a single-cell thunderstorm life-cycle.

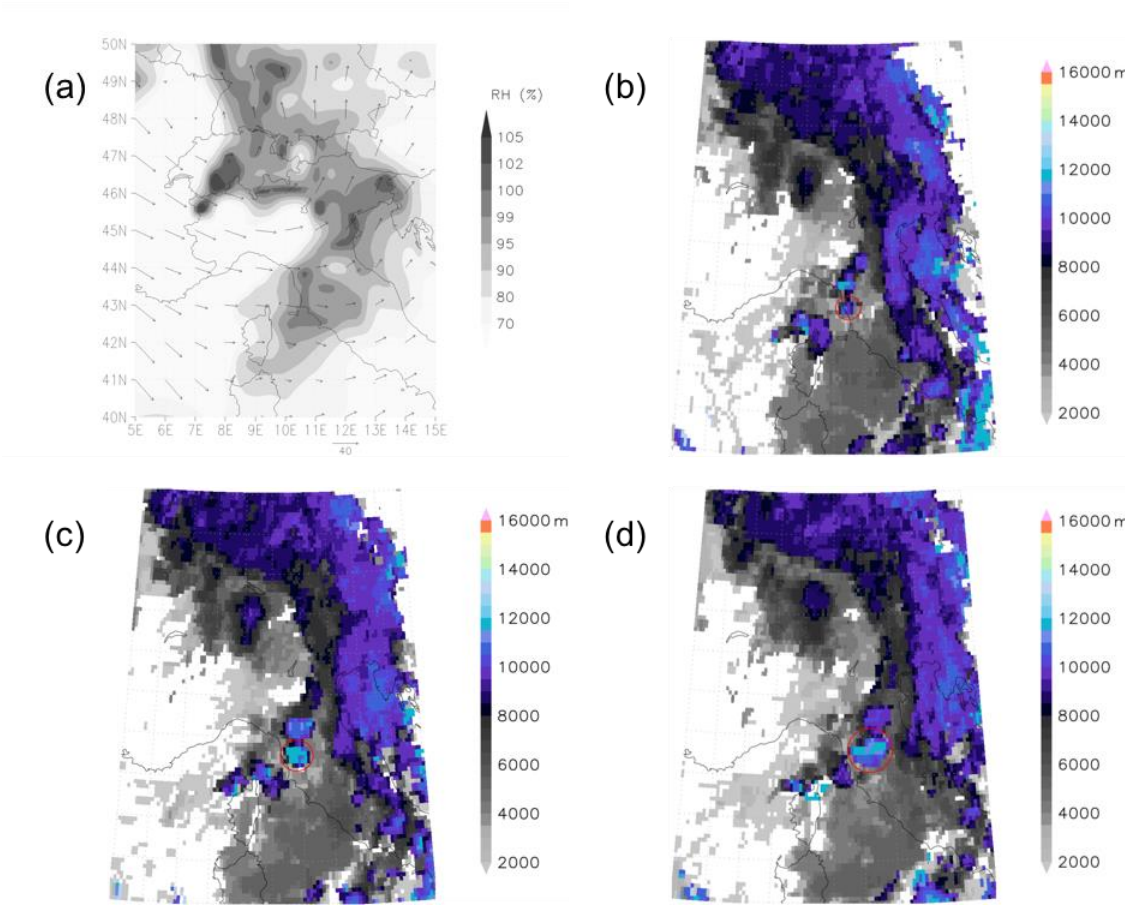

Figure 5.22 Panel (a): relative humidity (shaded contours) at 700 hPa and mean storm motion (vectors) from GFS analyses on 4 October 2015 at 06:00 UTC. Panels (b-d): cloud top height from MSG data on 4 October 2015 at 04:30 (b), 05:15 (c), and 06:00 UTC (d). Red circles indicate the thunderstorm position and extension.

The intense convective activity that occurred in the surroundings of Livorno City because of this thunderstorm is confirmed by the great number of lightning strikes registered by the Blitzortung network, as reported in **Figure 5.23**. The lightning occurrence from 0500 to 0530 UTC was almost 1500 strikes, quite regularly distributed during the 30 minutes (see the frequency histogram in the bottom right corner). Note that over Livorno the whitish symbols, which correspond to times closer to 05:30 UTC, are slightly shifted eastward with respect to the reddish ones, according to the slow thunderstorm advection from sea to land.

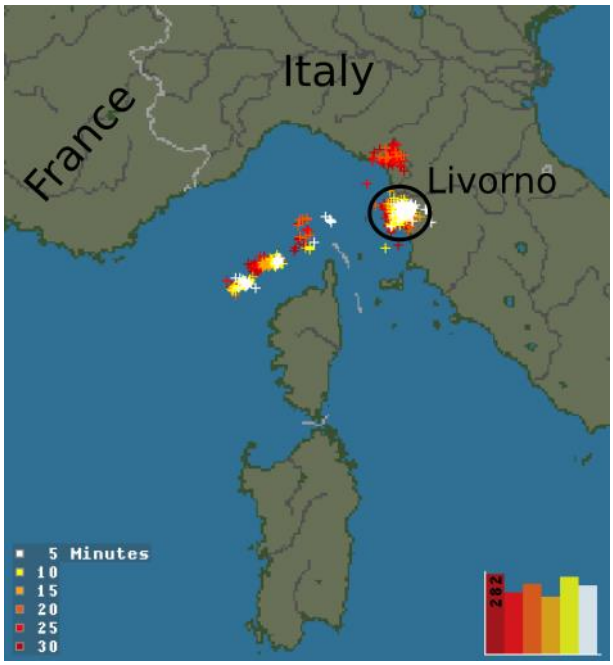

Figure 5.23 Strikes recorded on 4 October 2015, from 05:00 to 05:30 UTC, by means of the Blitzortung network for lightning and thunderstorms, retrieved through the online archive. Courtesy Blitzortung.org.

5.4.3 The 10-hour event on 21 November 2013 in Genoa

The low-pressure system known as Quentin was born on 18 November 2013 in the Baffin Bay, between Canada and Greenland, and moved zonally to the north of England. During the 20 November, it moved south-eastward under the influence of anticyclone Susanne I, located at mid-latitudes over the Atlantic Ocean, and approached Belgium on 21 November at about 0000 UTC. Then, it moved farther to the south and determined a low-pressure minimum of 995 hPa in the lee side of the Alps that was over the Ligurian Sea at 1200 UTC, as shown in **Figure 5.24 (a)**. The cold core aloft of Quentin, i.e. tropopause heights (shaded contours) below 8000 m, over France determined strong atmospheric instability and caused high precipitation rates in Belgium, Holland and France while advecting meridionally during the day. In the lee of the Alps, however, the south-eastward motion of the cold front of Quentin did not induce very deep convection over Liguria, as demonstrated by the relatively low values of the cloud top shown in **Figure 5.24 (b)**, which are between 8000 and 10000 m ASL.

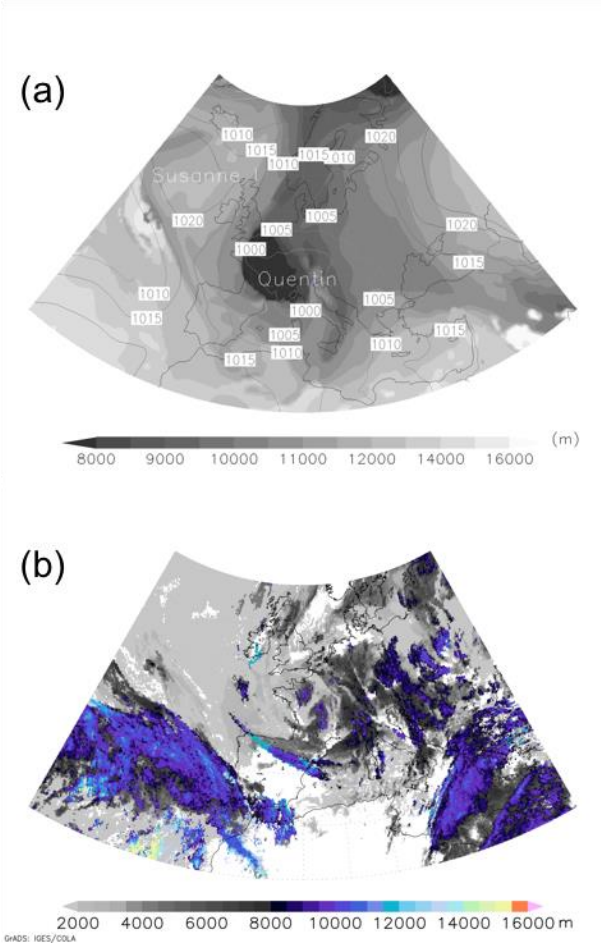

Figure 5.24 Top panel (a): mean sea level pressure (contours) and tropopause height (shaded contours) over Europe from GFS analyses on 21 November 2013 at 12:00 UTC. Bottom panel (b): cloud top height from MSG data on 21 November 2013 at 10:15 UTC.

The position of the cold front at the surface in the lee of the Alps at 12:00 UTC is indicated by the high-RH values that extends as an arc-shaped band from the eastern Liguria to the west of Sardinia Island, shown in **Figure 5.25 (a)**. On 21 November in the morning, the front had just passed over the Alps and the secondary pressure minimum aloft determined the wind rotation from north to southwest over the Ligurian Sea. The mean storm motion (vectors in **Figure 5.25 (a)**), which in this case corresponds approximately to the mean flow in the lower half of the troposphere as the directional wind shear from 0 to 6000 m ASL was rather low, was about 20-25 m s^{-1} from southwest, indeed. The strong forcing aloft was likely the main reason for the relatively sudden increase of wind speed recorded by anemometer 2 of the Port of Genoa (**Figure 5.17**) rather than some deep convective phenomenon that did not seem to occur according to the top height of clouds obtained from satellite data (**Figure 5.25 (b)**). This is also confirmed by means of the Blitzortung network that didn't record any strike in this area in between 0600 and 1400 UTC.

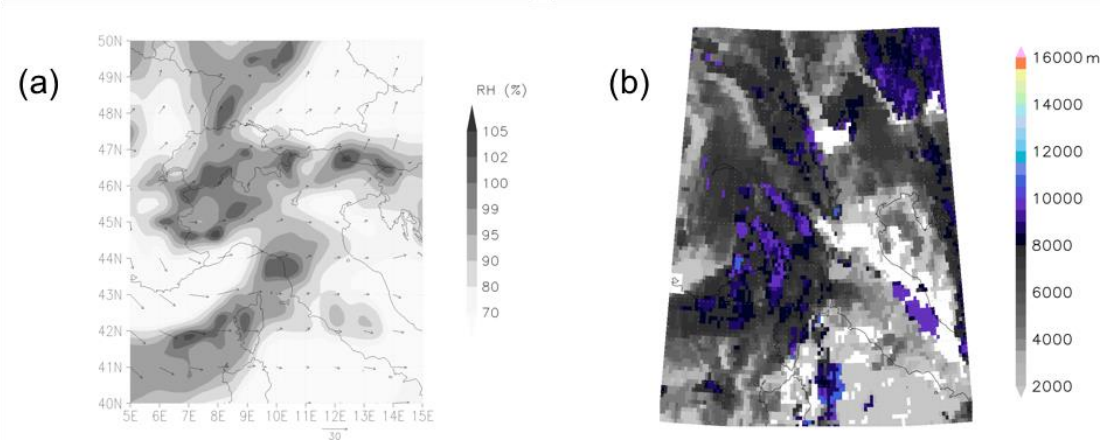

Figure 5.25 Panel (a): relative humidity (shaded contours) at 700 hPa and mean storm motion (vectors) from GFS analyses on 21 November 2013 at 1200 UTC. Panels (b): cloud top height from MSG data on 21 November 2013 at 1015 UTC.

5.5 Conclusions

Within the framework of a wide research program dealing with thunderstorm and nonsynoptic severe wind events, this study pursues a double purpose. First, it provides a meteorological survey of several nonstationary transient phenomena widely investigated in many parts of the world but rarely inspected in the Mediterranean. Second, the several events have been chosen as test cases with the aim of establishing their real meteorological properties with the potential to improve our understanding, characterization, and modeling of thunderstorms for wind engineering applications. In the first part of this chapter, analyses related to speed, direction, seasonality and hour of daily occurrence are also presented. It confirms that most of the local thunderstorm events occurred between September and January, and from the ocean direction. And thunderstorm events are now likely to occur at warmer times of day.

The **Section 5.3** provides a comprehensive description and interpretation of the field measurements and weather scenario associated with a transient event that struck the Livorno coast of Italy at about 1210 UTC (i.e., 1310 local time) on 1 October 2012.

The wind speed records detected by three ultrasonic anemometers of the monitoring network created for the European “WP” and “WPS” projects have been analyzed and decomposed into component parts to inspect the main features of this event. A statistical analysis for nonstationary wind events has been applied for this case and the resulting components have been discussed both individually and together. In addition, the joint analysis of different decomposed signals provides some interesting results.

Despite some peculiar aspects of this event, such as the double peak registered by the anemometric sensors, its properties match rather closely with the basic features of the entire database collected by the monitoring network. The set of the slowly varying mean wind velocity components provides a clear picture of the movement of the gust front from the sea to the land. In addition, the results support a robust separation

between the dominant features of the large-scale flow and the random turbulent fluctuations. Although the residual fluctuations have strongly nonstationary random properties, the set of diagrams of the slowly varying turbulence intensity confirms that this quantity is not time dependent. The probability density functions of the rapidly varying reduced turbulent fluctuation exhibit classical Gaussian features and its power spectral density tends to decrease in the high-frequency range with a slope that is typical of the inertial subrange of synoptic-type winds.

The analysis of the meteorological conditions concurrent with this event has been carried out by gathering all the meteorological data available in this area and making use of model analyses, standard in situ measurements (surface-observing stations and radio soundings), remote sensing techniques (radar and satellite), proxy data (lightning), and direct observations (from the European Severe Weather Database). All this information contributed to a reconstruction of the weather scenario that occurred on 1 October 2012, over Livorno, confirming that the strong wind event detected by the high-sampling-rate anemometers of the local monitoring network was a wet thunderstorm downburst.

This finding is an important result as it demonstrates the role of specific synoptic-scale conditions over western Europe (e.g., the formation of a secondary cyclone in the lee of the Alps) as an important and common meteorological precursor to the occurrence of localscale convectively forced severe wind events in the northern Mediterranean. High values of storm-relative helicity and negative values of the lifted index were good indicators of severe weather in the region. The WINDEX values and their location match the thunderstorm downburst observations well.

The third part of this chapter takes cue from the above detailed meteorological survey of the wet thunderstorm downburst in Livorno. Since the burden of this approach prevents its realistic application within systematic analyses of historical series of similar phenomena, an expeditionary procedure is codified and proposed herein to integrate the anemometric records with few essential meteorological features that at least qualify the convective or synoptic nature of different detected events. This procedure has been applied to three sample events referred to as 10-min, 1-h and 10-h long records.

The analysis of the two shorter events have confirmed their convective nature. These thunderstorms, however, have different triggering mechanisms. The 10-min event was determined by the mechanical lift of maritime air exerted by the orography; its transition between higher-to-lower wind speed regimes corresponds to the passage of the cold front. The 1-h event was most probably brought about by the mechanical lift due to the cold front southeastward movement. These remarks may provide preliminary motivations to the different temporal scales of fast transient events and stimulate research towards the comprehension of this delicate issue.

Conversely, the longer event, i.e. the 10-h one, turned out to be a synoptic phenomenon, endowed with a rapid evolution, initially misclassified as a potential thunderstorm, and it should be likely catalogued as an extra-tropical cyclone-related windstorm instead (Roberts et al., 2014). Even if this result cannot be generalized to

the whole family of 10-h intense wind events, it raises the question whether in some particular cases these phenomena can really have a convective genesis. This question remains open and will deserve further and more systematic investigations in the future.

The meteorological analysis of the three events considered here may result helpful also clarifying the relation between the shape of anemometric signals, discussed in the **Section 3.2** and **Section 4.3.1**, and the underlying meteorological phenomena. It is worth noting, however, that each particular shape could be determined in principle by more than one phenomenon, especially if different locations are considered. In perspective, therefore, this analysis should become more systematic and should be repeated for different databases of recordings taken at different latitudes and in geographical contexts different from the coastal area considered here.

6 Extreme wind speed distribution in a mixed wind climate

6.1 Introduction

The studies carried out in this thesis originate from "WP" (Solari et al., 2012) and "WPS" (Repetto et al., 2017, 2018), two European Projects carried out between 2009 and 2015 with the aim of forecasting the wind for the safe management of seaport areas. These areas often have a conflictual relationship with the wind. Overlooking the sea, they are lashed by more intense winds than those experienced in protected areas; in cases in which the ports are surrounded by mountainous reliefs, they are also subject to intense channeling phenomena. These elements are crucial as ports are home to a variety of activities the safe conduct of which essentially depends on the actions and effects of wind. In particular, wind gusts, combined with waves generated by them, affect the entry and docking of ships in ports and terminals operability; port structures, especially cranes, container unloaders, light towers and wind turbines are often damaged and sometimes disrupted; stacked containers can be overturned by wind.

In order to cope with this reality, among many other actions an extensive in-situ wind monitoring network has been set in the main commercial ports of the Upper Tyrrhenian Sea. This network is made up of about 40 ultrasonic anemometers, for some of which the duration of the data logging is now over 6 years as introduced in **Chapter 2**. Thanks to the continuous operating mode with high sampling frequency, this set of sensors offers a huge and perhaps unprecedented amount of high quality data. This creates a unique opportunity to obtain a large amount of high resolution wind records and to open the doors to refined analyses of extreme wind speed distribution in a mixed climate.

(a) (b)

Figure 6.1 Position of the anemometers selected for this analysis (basic pictures extracted from Google Earth): (a) Livorno; (b) La Spezia.

This thesis provides a preliminary but representative contribution to this topic. In order to establish a preliminary but robust procedure and discuss its outcomes concisely, the analyses carried out in this chapter are limited to the data gathered by

anemometers 01 and 02 in the port of Livorno (LI) and by anemometers 02 and 03 in the port of La Spezia (SP) (**Figure 6.1**). The main properties of these anemometers are shown in **Table 6.1**, in which h is the height of sensors AGL. It is worth noting that, despite the anemometers have been installed for more than 6 years, the period for which valid data is available is shorter (on average 80%). This is due to periods during which measurements were not taken out due to accidents or malfunctioning of instruments, as well as to the existence of periods in which recordings were not reliable enough to be examined (Cook, 2014a,b).

Table 6.1 Main properties of the anemometers selected to perform statistical analyses.

Port	Anemometer No.	*h* (m)	Type	Period of analysis (days)	Valid data (%)
LI	01	20	tri-axial	2010.10.01-2017.03.05 (2348)	81%
	02	20	tri-axial	2010.10.01-2017.03.05 (2348)	71%
SP	02	13	bi-axial	2010.10.29-2016.10.22 (2186)	87%
	03	10	bi-axial	2011.02.05-2016.09.16 (2051)	84%

Herein, **Section 6.2** illustrates the procedure applied to separate the data gathered during different intense wind events into selective homogeneous datasets; it also describes the difficulties encountered due to the presence of intermediate events; it goes on to discuss the creation of historical series of independent extreme wind speeds related to extra-tropical cyclones, thunderstorm outflows and intermediate events. **Section 6.3** evaluates the extreme wind speed distributions by means of various criteria. **Section 6.4** discusses the evaluation of the extreme wind speed distribution of the thunderstorm outflows by making recourse, comparatively, to peak wind speeds and to the maximum values of the slowly-varying mean wind velocity multiplied by an average gust factor (Holmes et al., 2008; Kwon and Kareem, 2009; Lombardo et al., 2014; Solari et al., 2015). **Section 6.5** compares the results provided by this study with the extreme wind speed values assigned by codes or obtained in previous investigations carried out disregarding the issue of mixed statistics. **Section 6.6** summarizes the main conclusions. This part of research is already published in Journal of Wind Engineering and Industrial Aerodynamics (Zhang et al., 2018b).

6.2 Separation of the dataset into selective sub-datasets

In order to carry out an appropriate statistical analysis of the extreme wind speed in a mixed climate, intense wind events should be extracted from the original dataset including all data, and they should be allocated to selective sub-datasets covering homogeneous families of wind events (Thom, 1968b; Gomes and Vickery, 1977/1978). This operation was done here in two successive steps. Firstly, only records with 1 s peak wind speed $\widehat{U}$ greater than 18–20 m/s were extracted from the whole dataset.

The actual censoring threshold was chosen in order to obtain a reasonable number of extreme wind speeds, for each family of homogeneous events. Secondly,

extra-tropical cyclones or depressions (D), thunderstorm outflows (T) and intermediate events (IN) were separated using the semi-automatic procedure described by De Gaetano et al. (2014). This procedure implies a mix of a massive number of quantitative checks, and a few qualitative expert judgments. The former compares the ratio between the peak wind speed $\widehat{U}$ and the mean wind speed over different time intervals, with the classic gust factor for synoptic wind speeds (Solari, 1993). The latter was refined here by selecting thunderstorm outflows based not only on 10 min and 1 h duration records, but also on 10 h records centred around the 10 min record selected (Duraõna, 2015; Zhang et al., 2018a).

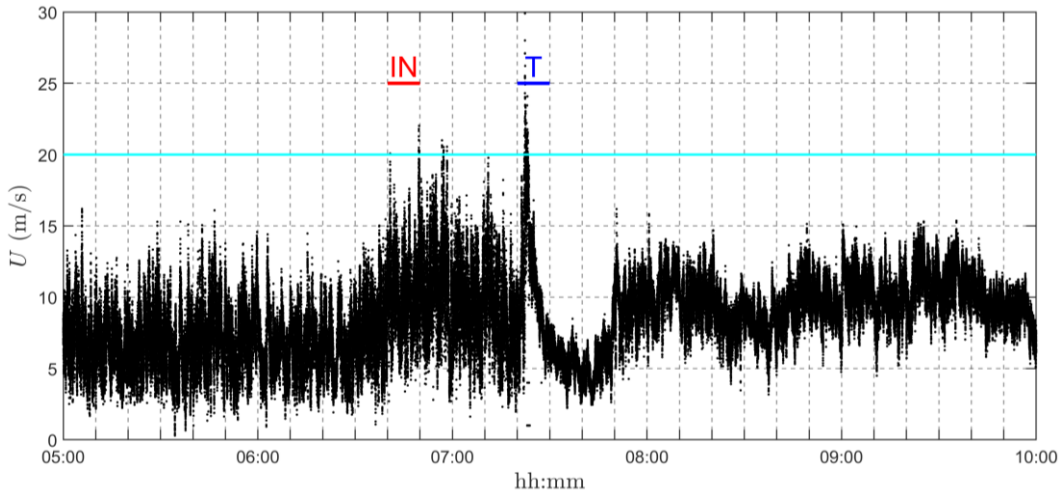

Figure 6.2 5-h wind speed time-history measured on Dec. 26 2013 by the anemometer 03 of the Port of La Spezia.

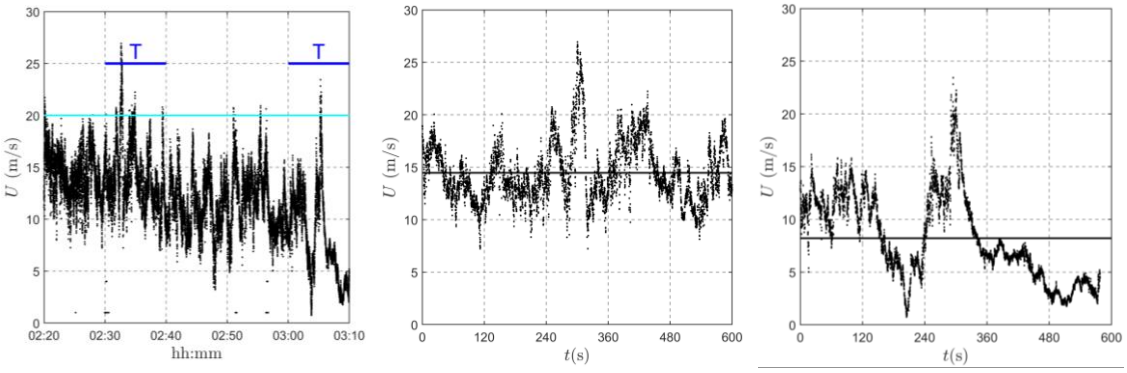

(a) (b) (c)

Figure 6.3 (a) 50-min wind speed time-history measured on Feb. 9 2014 by the anemometer 03 of the Port of La Spezia; (b, c) subsequent 10-min intervals in which two transient events occur.

Once highly controlled selective sub-datasets have been generated, independent extreme wind speeds are extracted in terms of the following criterion: Extra-tropical cyclones and intermediate events are considered as independent provided they are separated by a time interval longer than 3 days and 1 day, respectively. Thunderstorms are considered as independent if they are separated by an interval longer than 4 times their duration (Solari et al., 2015). This criterion works in most cases, except for some

complex situations in which two or three different types of events occur close to one another. In some cases this happens only due to actually different independent events occurring at the same time (**Figure 6.2** and **Figure 6.3**). In other cases the separation criterion provided by De Gaetano et al. (2014) results in the creation, within the same record, of an unrealistic sequence of alternating different events (**Figure 6.4**, **Figure 6.5** and **Figure 6.6**). Fortunately, this is not very frequent.

Figure 6.2 shows an intermediate event followed by a thunderstorm outflow, both of which with peak wind speed greater than the censoring threshold. In this case both the maximum peak wind speeds of these events are included in the appropriate series of the independent extreme values.

Figure 6.3 shows two intense events, labelled as thunderstorm outflows, which occurred quite close to one another. They are taken as being independent due to their short duration. Following the separation procedure, a qualitative expert judgement was required for the former, and it was labelled as a thunderstorm outflow after having ascertained the presence of lightning and thunder over La Spezia during its occurrence.

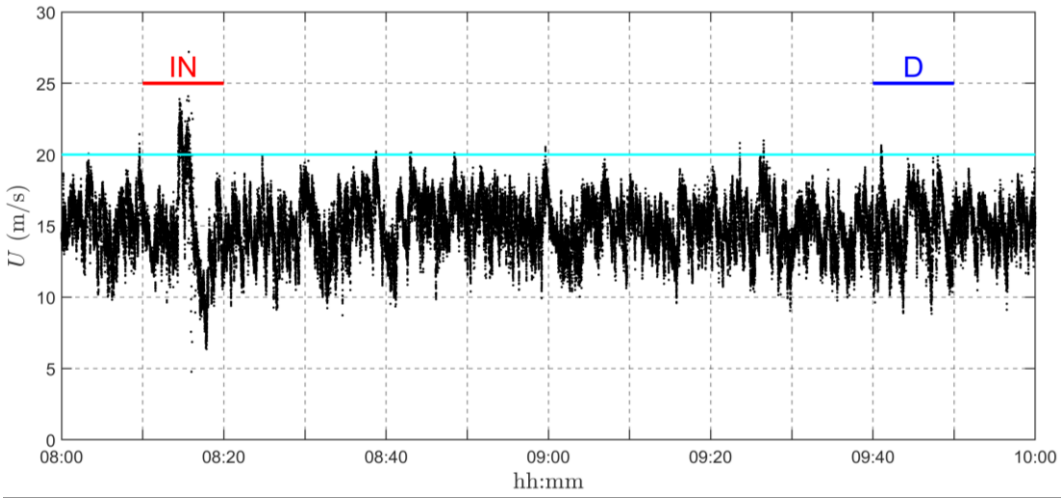

Figure 6.4 2-h wind speed time-history measured on Nov. 26 2010 by the anemometer 01 of the Port of Livorno.

Figure 6.4, **Figure 6.5** and **Figure 6.6** show three wind speed time-histories characterised by a sequence of records labelled as depressions and intermediate events. **Figure 6.4** depicts a case in which an intermediate event seems to be embedded within an extra-tropical cyclone. Accordingly, both the maximum peak wind speeds for these events are retained in the series of independent extreme values. **Figure 6.5** shows a sequence of alternating records labelled as depressions and intermediate events. Observing that the 10 min mean wind speed is relatively large for the entire intense part of this event, almost 20 m/s, the maximum peak wind speed for this sequence is labelled as a depression. Similarly, **Figure 6.6** shows a sequence of alternating records labelled as depressions and intermediate events. Unlike the previous case, however, the 10 min mean wind speed oscillates between 5 and 10 m/s.

Accordingly, the maximum peak wind speed for this sequence is labelled as an intermediate event.

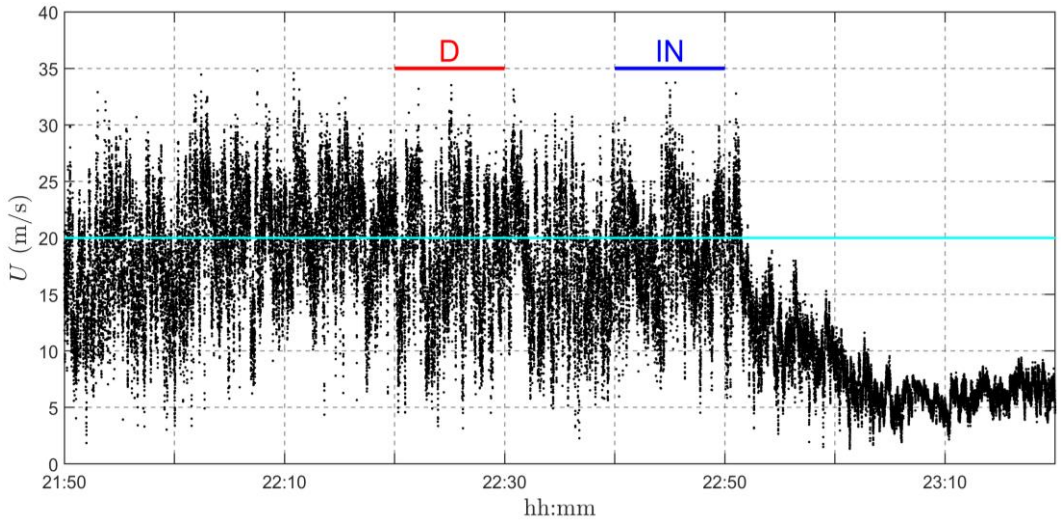

Figure 6.5 1 and a half-h wind speed time-history measured on 16 December 2011 by the anemometer 02 of the Port of Livorno.

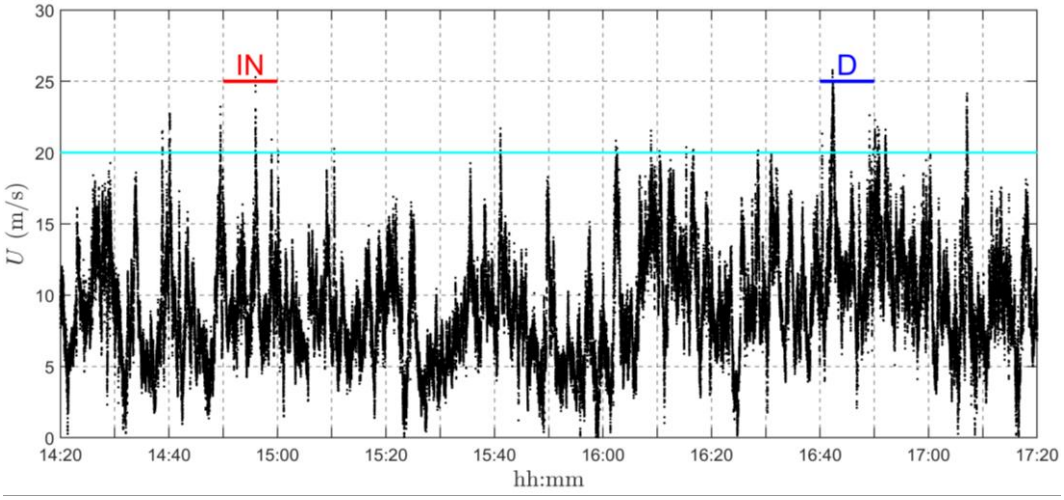

Figure 6.6 3-h wind speed time-history measured on 8 November 2010 by the anemometer 02 of the Port of La Spezia.

Table 6.2 and **Table 6.3** summarize, the number of data and the maximum value in each series of the peak wind speeds related to the 3 phenomena (D, T, IN) and to the 4 anemometers (LI_01, LI_02, SP_02, SP_03) examined, respectively. The full series of the peak wind speed values $\widehat{U}$ and of the corresponding maximum values of the slowly varying mean wind speeds $\overline{U}_{max}$ are provided in **Table 1**-**Table 4** detected during extra-tropical cyclones, in **Table 5**-**Table 8** detected during thunderstorm outflow and in **Table 9**-**Table 12** detected during intermediate events in the Appendix A.

Table 6.2 Number of data in each series of peak wind speed values.

Anemometer \ Event	D	T	IN
LI_01	47	19	17
LI_02	44	10	12
SP_02	10	9	20
SP_03	15	16	19

Table 6.3 Maximum value of the peak wind speed $\widehat{U}$ (m/s) in each series.

Anemometer \ Event	D	T	IN
LI_01	33.01	33.65	24.23
LI_02	31.49	29.44	26.47
SP_02	25.97	30.03	26.94
SP_03	26.54	33.98	25.60

6.3 Extreme wind speed distribution

The extreme wind speed distribution in a mixed climate should be evaluated by firstly investigating each wind phenomenon that strikes that area separately, with the aim of obtaining its own extreme distribution. Then, depending on their use, these distributions can be included in a comprehensive model referred to as a mixed extreme distribution (Gomes and Vickery, 1977/1978), or they can be kept separate, in order to provide independent wind loading conditions for each wind phenomenon (Solari, 2014).

Within the framework of a preliminary study still based on a limited number of years of acquisition, the use of advanced models (Harris, 2014; Torrielli et al., 2013, 2014) may prove to be disproportionate to the actual data available and, in addition, it may lead to results that are distorted or endowed with a false level of accuracy. Hence, the extreme distribution of the peak wind speed is reported here as being classic Fisher-Tippett Type I or Gumbel distribution for all the phenomena involved in the mixed climate.

In addition, since the limited number of the available years of wind measurements makes it impossible regress each extreme value distribution by its yearly maxima series, based on the monthly maximum (Simiu et al., 1982) and storm (Cook, 1982) methods, the cumulative distribution function (CDF) for the yearly maximum peak wind speed for each wind phenomenon is given by:

$$F_{\widehat{U}}^{(K)}(\widehat{U}) = \left[F_{\widehat{U},e}^{(K)}(\widehat{U})\right]^{N_K} \tag{6.1}$$

$$F_{\widehat{U},e}^{(K)}(\widehat{U}) = exp\{-exp[-a_K(\widehat{U} - u_K)]\} \tag{6.2}$$

where K = D, T, IN denotes the wind phenomenon, N_K is the average number of independent extreme peak wind speed values in one year for the K phenomenon, $F_{\hat{U},e}^{(K)}$ is the CDF for the extreme peak wind speed of the K phenomenon, and u_K and a_K are the mode and the scale factor for type I distribution.

The u_K and a_K parameters are inferred here using the measured data and the order statistics method. Accordingly, the series of the extreme peak wind speeds is ordered from the smallest $\hat{U}_1$ to the greatest $\hat{U}_{N_K}$ value and the empirical estimate for $F_{\hat{U},e}^{(K)}(\hat{U}_m)$, referred to as the plotting position, is determined based on the ranked position of $\hat{U}_m$(Guo, 1990) by means of the equation:

$$F_{\hat{U},e}^{(K)}(\hat{U}_m) = \frac{m}{N_K+1} \tag{6.3}$$

where m is the ranking of each value in the population (Cook, 1982). The estimation of the u_K and a_K parameters is done using the least squares technique, so that **Eq. (6.2)** best approximates **Eq. (6.3)** in a "Gumbel probability paper", that is, in a diagram in which the coordinate axes are such that **Eq. (6.2)** becomes linear. Also, in this case different weights are not applied to the sequence of the ordered values, nor are refined inference methods (Lieblein, 1974; Hoaglin et al., 1983) used, due to the limited number of data. **Table 6.4** shows the values of the u_K and a_K parameters together with the N_K values estimated by taking the actual number of valid data into account (**Section 6.1**, **Table 6.1**).

Table 6.4 Model parameters of the CDF of different wind phenomena.

Anemometer	K wind phenomenon	a_K (s/m)	u_K (m/s)	N_K
LI_01	*D*	0.49	21.40	9.02
	T	0.32	22.08	3.65
	IN	0.56	19.17	3.26
LI_02	*D*	0.49	21.83	9.63
	T	0.28	20.10	2.19
	IN	0.45	19.92	2.63
SP_02	*D*	0.62	21.82	1.92
	T	0.28	22.14	1.73
	IN	0.49	21.35	3.84
SP_03	*D*	0.51	21.40	3.18
	T	0.30	21.90	3.39
	IN	0.58	21.73	4.03

Figure 6.7-**Figure 6.10** show the CDF for the maximum yearly peak wind speed as detected by the 4 anemometers (LI_01, LI_02, SP_02, SP_03) respectively. Schemes **(a)**, **(b)**, **(c)** refer to the D, T and IN events, respectively. Each diagram is a Gumbel

plot that provides the peak wind speed $\widehat{U}$ as a function of the return period $R = 1/[1 - F_{\widehat{U}}(\widehat{U})]$. Type I distribution (solid lines) represents a reasonable fit for the experimental points (circles) except for the presence of a clear outlier, the maximum value of the peak wind speed in **Figure 6.7 (a)** (LI_01, D) and of two other suspicious bits of data, the maximum values for the peak wind speed in **Figure 6.7 (b)** (LI_01, T) and in **Figure 6.10 (b)** (SP_03, T). The correctness of the above data has been carefully checked with regard to both the individual records from which they were extracted and the records registered simultaneously by other anemometers in the monitoring network in the same port area, including those not examined in this chapter. In the case of the peak wind speed $\widehat{U}$ = 33.01 m/s in **Figure 6.7 (a)** (LI_01, D), the other four anemometers in the port of Livorno detected similar wind conditions, with peak wind speeds always higher than 30 m/s. In the case of the peak wind speed $\widehat{U}$ = 33.65 m/s in **Figure 6.7 (b)** (LI_01, T), the corresponding record shows a transient event embedded in an intense synoptic condition. The other four anemometers in the port of Livorno detected similar synoptic conditions without clear transient events as for LI_01, this having been probably caused by a local phenomenon. In the case of the peak wind speed $\widehat{U}$ = 33.98 m/s in **Figure 6.10 (b)** (SP_03, T), this refers to an isolated transient gust front. SP_02 detected a similar situation, delayed by about 5 min, with a lower peak wind speed of the order of 20 m/s.

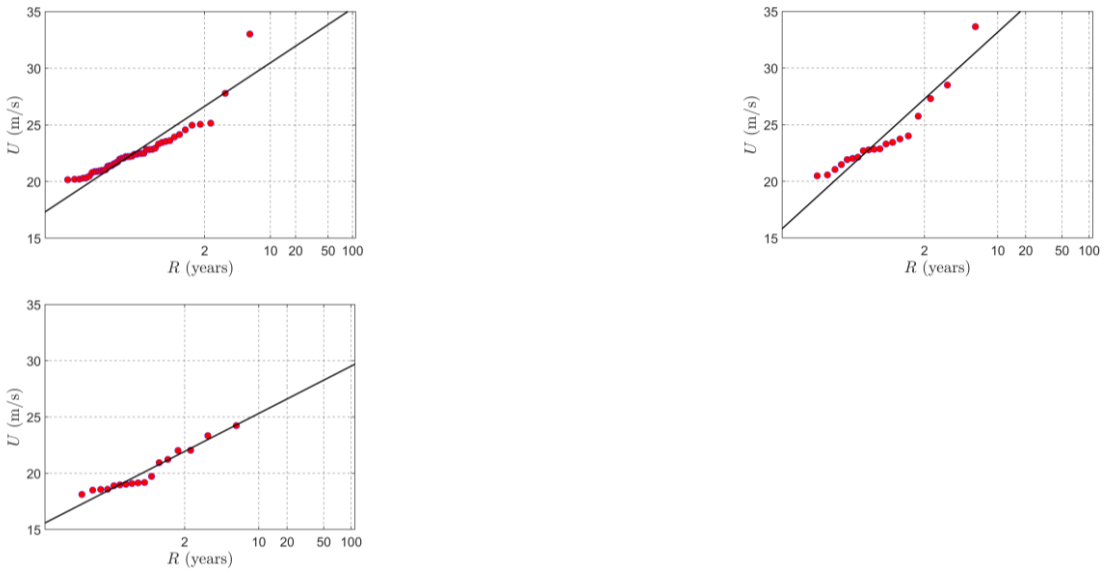

(a) (b) (c)

Figure 6.7 Plotting positions and fitting line for the extra-tropical depressions (a), thunderstorm outflows (b), and intermediate events (c) detected by the anemometer 01 in the Port of Livorno.

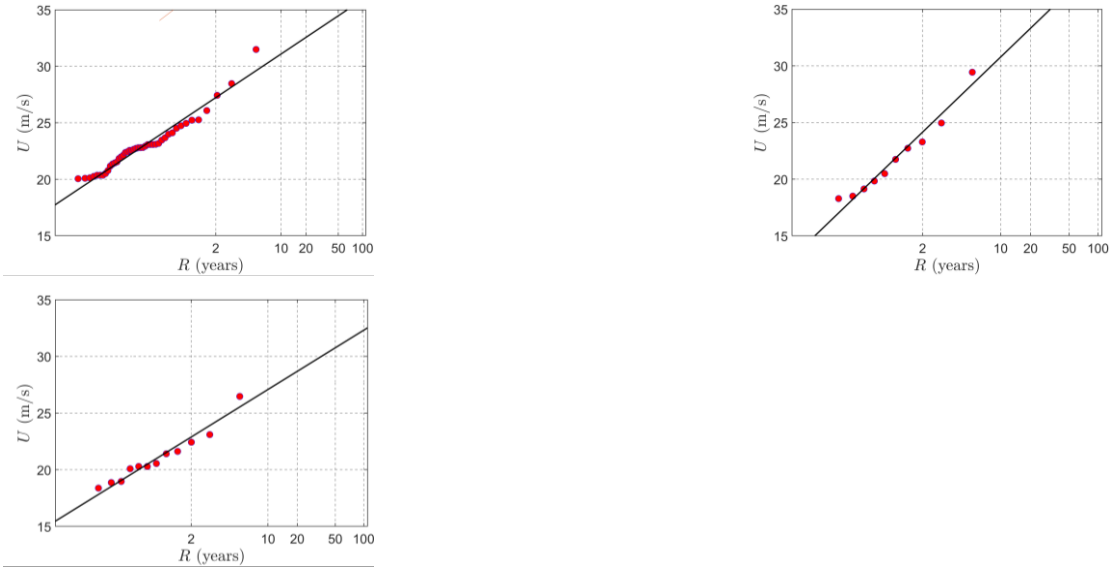

(a) (b) (c)

Figure 6.8 Plotting positions and fitting line for the extra-tropical depressions (a), thunderstorm outflows (b), and intermediate events (c) detected by the anemometer 02 in the Port of Livorno.

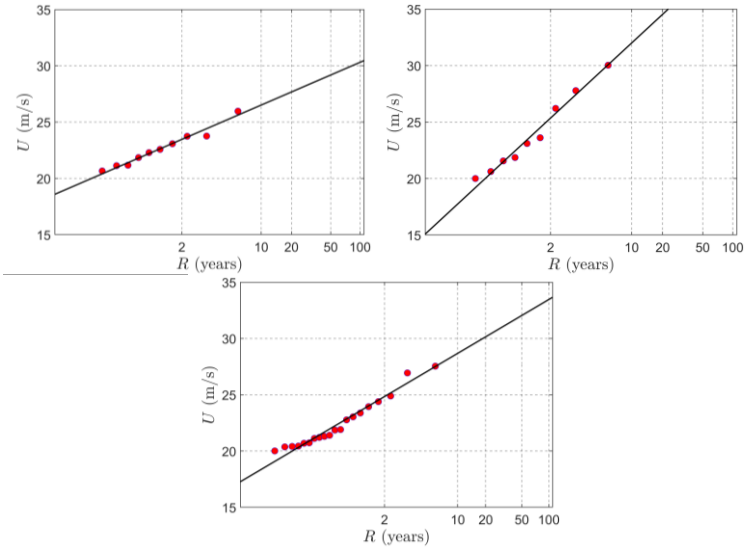

(a) (b) (c)

Figure 6.9 Plotting positions and fitting line for the extra-tropical depressions (a), thunderstorm outflows (b), and intermediate events (c) detected by the anemometer 02 in the Port of La Spezia.

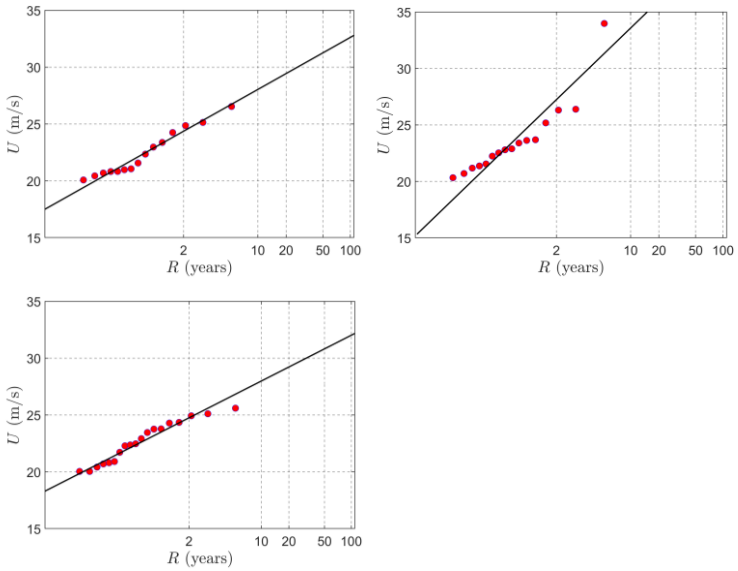

(a) (b) (c)

Figure 6.10 Plotting positions and fitting line for the extra-tropical depressions (a), thunderstorm outflows (b), and intermediate events (c) detected by the anemometer 03 in the Port of La Spezia.

Figure 6.11 shows the CDF of the maximum yearly peak wind speed detected by the 4 anemometers, for each wind phenomenon. The statistical analysis of depressions highlights rather good agreement between different anemometers in the same area. Small differences can be related to the local roughness of the terrain around the anemometric stations. On the other hand, significant differences occur between the areas of Livorno and La Spezia despite their proximity (about 75 km). This is probably due to the different properties of the two sites both in terms of orography and of roughness length: Livorno, which is characterised by higher wind speed values, has the sea to the west and a flat open area all around it, whereas La Spezia is surrounded by the mountain range of the Liguria Apennines in all directions, apart a small sector facing the sea towards the south. The situation is different for thunderstorm outflows, where data gathered by different anemometers in different areas lead to similar results: This may be due to the fact that thunderstorm cells frequently move from the sea towards inland and the roughness length plays a secondary role (Solari et al., 2015; Zhang et al., 2017). Intermediate events are characterised by intermediate properties.

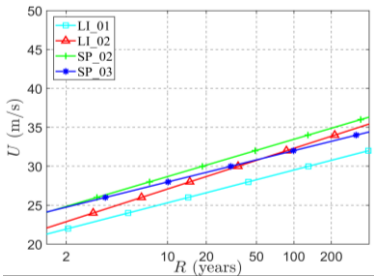

(a) (b) (c)

Figure 6.11 CDF of the yearly maximum peak wind speed for extra-tropical depressions (a), thunderstorm outflows (b), and intermediate events (c) in correspondence of the 4 anemometers analysed.

Once the CDF for the maximum yearly peak wind speed has been evaluated for each wind phenomenon at each anemometer, the method of mixed statistics (Gomes and Vickery, 1977/1978) provides a tool for estimating a comprehensive CDF for the maximum yearly peak wind speed at each anemometer. Assuming that the extreme wind speeds of different wind phenomena are statistically independent, the mixed (M) CDF for the maximum yearly peak wind speed is given by:

$$F_{\hat{U}}^{(M)}(\hat{U}) = F_{\hat{U}}^{(T)}(\hat{U}) \cdot F_{\hat{U}}^{(D)}(\hat{U}) \cdot F_{\hat{U}}^{(IN)}(\hat{U}) \tag{6.4}$$

$F_{\hat{U}}^{(K)}$ (**Eq. (6.1)**) being the CDF for the maximum yearly peak wind speed for the *K* phenomenon.

For each anemometer, **Figure 6.12** and **Figure 6.13** show the CDF for the maximum yearly peak wind speed for each phenomenon (D, T, IN) and for mixed statistics (M). In addition, following Lombardo et al. (2009), the results obtained by gathering the ensemble (E) of all the extreme values into a single set are also shown as a reference. **Table 6.5** provides a synthetic overview of these results.

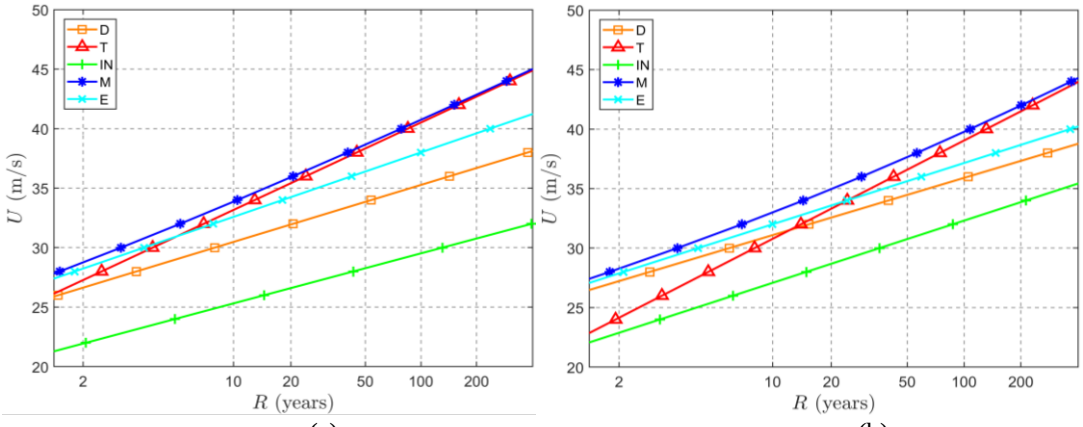

(a) (b)

Figure 6.12 Peak wind speed as a function of the return period for the anemometers 01 (a) and 02 (b) of the Port of Livorno.

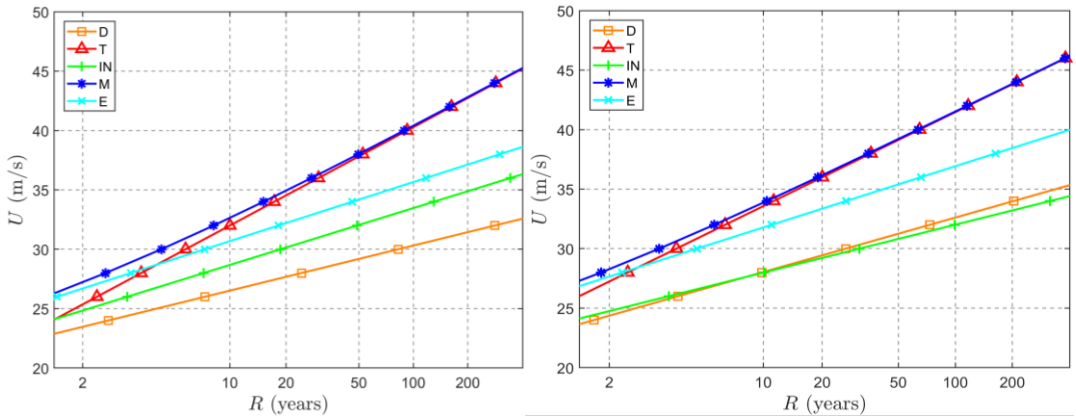

(a) (b)

Figure 6.13 Peak wind speed as a function of the return period for the anemometer 02 (a) and 03 (b) of the Port of La Spezia.

Figure 6.12, **Figure 6.13** and **Table 6.5** point out that wind events with a high return period, which are the most important for structural safety, are always related to thunderstorms. This finding confirms, at least in the area examined here, similar results reported worldwide (Whittingham, 1964; Davenport, 1968; Thom, 1968c; Gomes and Vickery, 1976; Twisdale and Vickery, 1992; Choi, 1999; Letchford et al., 2002; Lombardo et al., 2009). On the other hand, contrary to what was observed by Kasperski (2002) in Germany, intermediate events do not seem to have a determinant role in extreme wind speeds. In every case, gathering the ensemble of all extreme values into a single set leads to underestimating the mixed CDF especially for high return periods, where the mixed CDF tends to coincide with that for thunderstorms.

Table 6.5 Peak wind speed (m/s) as a function of the return period.

Analysis	Anemometer	*R* (years)					
		2	5	10	20	50	100
D	LI_01	26.64	28.95	30.48	31.95	33.85	35.27
	LI_02	27.23	29.55	31.09	32.56	34.47	35.90
	SP_02	23.47	25.30	26.51	27.68	29.18	30.31
	SP_03	24.36	26.57	28.03	29.44	31.25	32.61
T	LI_01	27.27	30.82	33.17	35.42	38.33	40.52
	LI_02	24.15	28.14	30.78	33.31	36.59	39.04
	SP_02	25.35	29.35	32.00	34.54	37.82	40.28
	SP_03	27.24	31.05	33.57	35.99	39.13	41.48
IN	LI_01	21.94	23.97	25.31	26.60	28.27	29.52
	LI_02	22.89	25.41	27.08	28.68	30.76	32.31
	SP_02	24.84	27.15	28.68	30.15	32.05	33.47
	SP_03	24.75	26.70	27.98	29.22	30.82	32.01
E	LI_01	28.24	30.85	32.58	34.24	36.39	38.00
	LI_02	27.88	30.36	32.00	33.58	35.62	37.15
	SP_02	26.69	29.09	30.68	32.21	34.18	35.66

	SP_03	27.65	30.14	31.78	33.36	35.40	36.93
M	LI_01	28.75	31.77	33.86	35.92	38.65	40.74
	LI_02	28.27	31.04	32.99	34.95	37.64	39.77
	SP_02	27.22	30.37	32.64	34.93	38.03	40.41
	SP_03	28.27	31.55	33.86	36.16	39.21	41.52

Coming to a more detailed examination of the two port areas examined here, the wind climate of the Port of Livorno is dominated by thunderstorm outflows, depressions are usually secondary, and intermediate events definitely have a marginal role. However, while for LI_01 thunderstorm outflows dominate depressions for any return period over 1 year, for LI_02 thunderstorm outflows exceed extra-tropical depressions in terms of importance, only for return periods over about 20 years.
As far as the wind climate of the Port of La Spezia is concerned, this is dominated by thunderstorm outflows for any return period over 1 year, whereas intermediate events are comparable with depressions for SP_03 and slightly exceed the same for SP_02.

6.4 Extreme mean VS peak wind speed distribution

The assignment of the extreme wind speed for synoptic extra-tropical cyclones is a key topic in wind engineering in relation to research, applications and codes. In some cases, the extreme wind speed is evaluated in terms of mean values usually averaged over a time interval ΔT = 10 or 60 min. In other cases, such as in this paper, it is carried out in terms of peak values averaged over a time interval τ = 1 or 3 s (in this paper τ = 1 s). In both cases, the passage from one evaluation to the other occurs by means of a velocity gust factor referred to as the ratio between the peak and the mean wind speed (Durst, 1960; Greenway, 1979; Solari, 1993; Holmes et al., 2014; Kwon and Kareem, 2014). The longstanding literature on this topic bears testimony to the inherent achievement of a relevant level of confidence in the application of this procedure.
The situation is quite different for thunderstorm outflows. Firstly, due to their transient character, the mean wind speed is no longer representative and should be replaced by a suitable value for the time-varying mean wind speed (Chay et al., 2008; Holmes et al., 2008; Lombardo et al., 2014). Since this quantity depends on the moving average period *T*, the gust factor of thunderstorm outflows is in turn a function of T (Choi, 2000; Choi and Hidayat, 2002b; Holmes et al., 2008; Lombardo et al., 2014). Solari et al. (2015) defined three noteworthy velocity ratios that play a key role in thunderstorm loading and response of structures. In this context, the ratio between the peak wind velocity $\widehat{U}$ and the maximum value of the slowly-varying mean wind velocity $\overline{U}_{max}$ corresponds to the most common definition of the gust factor for a thunderstorm outflow:

$$G_U = \widehat{U}/\overline{U}_{max} \tag{6.5}$$

Table 6.6 shows the mean values for the gust factors of the thunderstorm outflows recorded by each of the four anemometers examined here.

Table 6.6 Mean value of the gust factor of the thunderstorm outflows.

Anemometer	LI_01	LI_02	SP_02	SP_03
$\langle G_U \rangle$	1.14	1.27	1.34	1.27

Despite these definitions and the values for the gust factors estimated being rather recent, they are shared by the wind engineering community more and more. However, to the Authors' knowledge, no evaluation has been carried out to evaluate the reliability of using G_U in order to move from the extreme wind speed distribution in terms of $\widehat{U}$ to the one based on $\overline{U}_{max}$, and vice-versa.

In order to fill this gap and to provide some preliminary remarks on this issue, the CDF for the yearly maximum value of $\overline{U}_{max}$ (dotted blue line in **Figure 6.14**) is estimated for each anemometer using the method described in **Chapter 5** with regard to $\widehat{U}$ (full red line in **Figure 6.14**). In addition, the CDF for the yearly maximum value of $\widehat{U}$ is determined by multiplying the extreme values of $\overline{U}_{max}$ by the gust factors in **Table 6.5** (dashed and dotted black line in **Figure 6.14**). The agreement between these two methods is excellent. Also, this procedure is easy to apply due to the weak dependence of the thunderstorm gust factor on roughness length.

The persisting limited knowledge of intermediate events prevents development of similar studies in their regard.

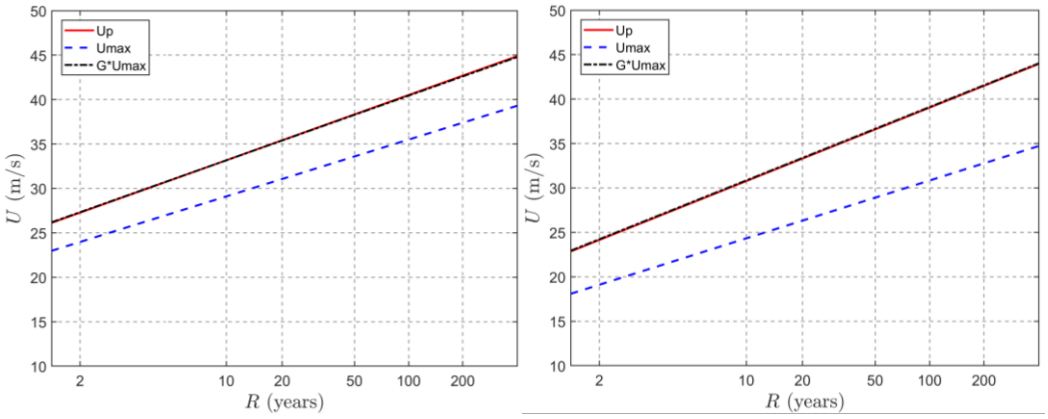

(a) (b)

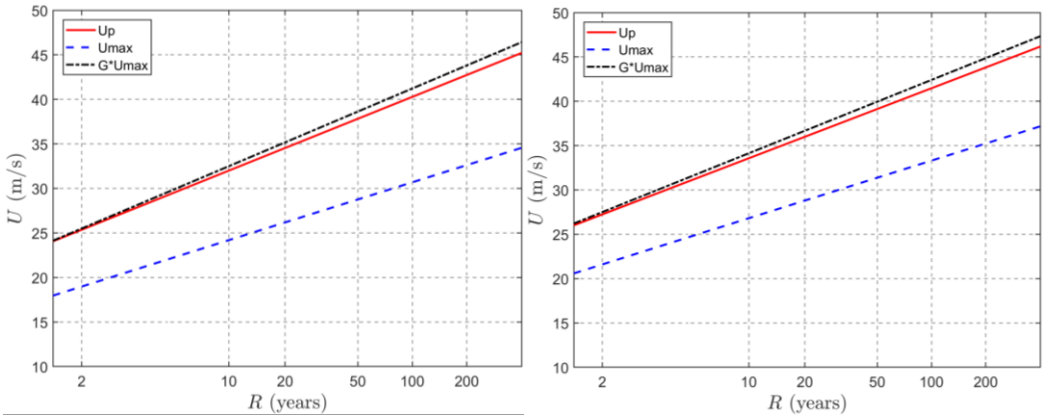

(c) (d)

Figure 6.14 Extreme mean vs peak wind speed distributions of thunderstorm outflows: anemometers 01 (a) and 02 (b) of the Port of Livorno; anemometers 02 (c) and 03 (d) of the Port of La Spezia.

6.5 Comparison with classic analyses

The results described in **Section 6.4** are compared with the extreme wind speed values provided by the Italian Guide for Wind Actions and Effects on Structures (CNR-DT 207/2008, 2008) in the two areas examined here. In addition, a comparison is carried out with the results of some detailed analyses of the wind climate of Pisa (Ballio et al., 1999), 20 km from Livorno, and of La Spezia (Castino et al., 2003). All these studies concern the historical ensemble of the mean wind speed values over 10 min periods, so they are based on many more years of measurements than those considered here. On the other hand they do not take into account either the occurrence of thunderstorms or mixed statistics.

Using the Italian Guide for Wind Actions and Effects on Structures (CNR-DT 207/2008, 2008), the Port of Livorno lies in Area 3 (Tuscany Zone) at sea level, so its basic reference wind velocity, i.e. the mean wind velocity over a 10 min interval at a height of 10 m above flat homogeneous open terrain with roughness length z_0 =0.05 m and return period $R = 50$ years, is $U_b = 27$ m/s. This document also provides the return coefficient c_r that multiplied by U_b provides the reference wind velocity U_r as a function of R. Besides, it assigns exposure category II to the seaport area of Livorno. Accordingly, the mean wind velocity at anemometers at a height z = 20 m (**Table 6.1**) is $U_m = 1.138 \cdot U_r$, whereas the peak wind velocity is the mean wind velocity multiplied by the gust factor $G_U = 1.471$, namely $U_p = 1.674 \cdot U_r$.

Similarly, the Port of La Spezia lies in Area 7 (Liguria Zone) at sea level, so U_b = 28 m/s. This makes it exposure category III. Accordingly, the mean wind velocities at anemometers at a height z_2 = 13 m and z_3 = 10 m (**Table 6.1**) are $U_{m2} = 0.973 \cdot U_r$ and $U_{m3} = 0.921 \cdot U_r$, respectively, whereas the gust factors are $G_{U2} = 1.572$ and $G_{U3} = 1.603$; thus, $U_{p2} = 1.530 \cdot U_r$ and $U_{p3} = 1.476 \cdot U_r$.

The wind climate of Pisa, extrapolated here from the seaport area of Livorno, was determined during the studies that led to the Italian wind map (Ballio et al., 1999) still

provided by the Italian wind code (CNR-DT 207/2008, 2008). The wind climate of La Spezia was evaluated in the framework of a pilot study for micro-zoning of the Liguria Region (Castino et al., 2003). These investigations, which took wind directionality effects into account, provided U_b = 24.7 m/s and U_b = 25 m/s, respectively. The local wind velocities at the anemometers have been scaled accordingly.

Figure 6.15 compares the above results with those provided in **Section 6.3** based on mixed statistics. Firstly, at least in the areas examined here, the Italian code (CNR-DT 207/2008, 2008) provides conservative estimates of the extreme wind speed. A comparison between the results of previous analyses based on long historical series but ignoring thunderstorms, and the new investigations based on a limited number of years but taking thunderstorms into account, shows different trends in Livorno and La Spezia. In Livorno (**Figure 6.15 (a)**), the results by Ballio et al. (1999) are always cautious when compared with the evaluations here. In La Spezia (**Figure 6.15 (b)**), the occurrence of intense thunderstorm outflows leads to equating (anemometer 02) or exceeding (anemometer 03), the results of the micro-zoning analysis performed by Castino et al. (2003), for high medium return periods. In any case, further analyses are necessary.

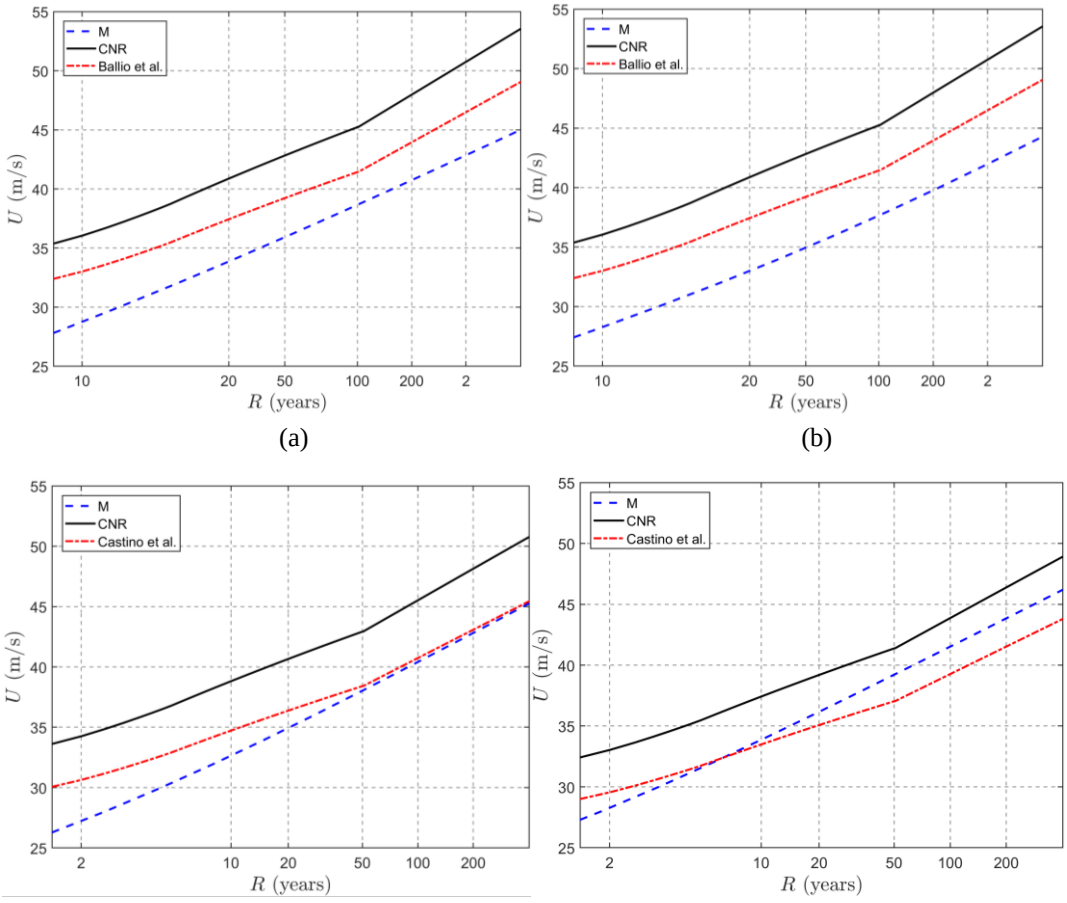

(a) (b)

(c) (d)

Figure 6.15 Peak wind velocity extreme distributions for the anemometer 01 (a) and 02 (b) of the Port of Livorno, and the anemometers 02 (c) and 03 (d) of the Port of La Spezia.

6.6 Conclusions

Extra-tropical cyclones are the most typical events that strike midlatitude areas. Thunderstorms, like extra-tropical cyclones, occur almost everywhere in these areas. The European wind climate and that of many other parts of the world is dominated by these two phenomena. In addition, intermediate events occur. In such a genuine multi-mechanism mixed wind climate, a reasonable extreme wind speed analysis cannot be done without separating the data related to different phenomena. How this data is combined in a mixed statistical scheme depends on the aim of the analyses to be carried out.

In this chapter, preliminary statistical analyses of the extreme peak wind speed recorded by the continuous high-frequency monitoring system of the "WP" and "WPS" Projects are done over a 6 year period, with regard to anemometers 01 and 02 of the Port of Livorno and to anemometers 02 and 03 of the Port of La Spezia. Firstly, records with a peak wind speed greater than a given censoring threshold are extracted from the data population. Secondly, depressions, thunderstorm outflows and intermediate events are separated and stored in selective datasets. Thirdly, independent extreme wind speeds are selected based on the time interval that separates successive extremes. Fourthly, the extreme distribution of the peak wind speed for each wind phenomenon is given by the Type I extreme value model. Finally, the information on the extreme distribution of the peak wind speed is completed by mixed statistics and by gathering the ensemble of all the extreme values into a single set.

At least in the seaport areas examined here, the results show that wind events with a high return period, the most important for structural safety, are always related to thunderstorm phenomena. Depressions play a relevant role only in some cases and always with reference to low return periods related to serviceability analyses. Intermediate events are still very uncertain phenomena. According to this study, however, they do not seem to be so relevant for assessing extreme wind speeds. The mixed extreme distribution asymptotically tends to coincide with thunderstorm distribution for high return periods and always provides the highest extreme wind speed values. In every case, gathering the ensemble of all the extremes into a single set leads to underestimating the extreme peak wind speed especially for high return periods.

As with synoptic depressions, for thunderstorm outflows too the passage from the distribution of the peak wind speed to the distribution of the maximum value of the slowly varying mean wind speed, and viceversa, may be suitably performed using appropriate velocity gust factor. In the case of thunderstorms this procedure is even easier due to the weak dependence of the gust factor on the roughness length, which

means that directionality effects can be disregarded, despite being very important for synoptic depressions.

The results provided by mixed statistics are compared with the extreme wind speed values taken from the Italian Guide for Wind Actions and Effects on Structures, and with the results of previous wind climate analyses concerning the historical ensemble of the wind speeds averaged over 10 min periods. These results derive from many more years of measurements than those considered in this paper. On the other hand they do not take into account either thunderstorms or mixed statistics.

The Italian Guide provides estimates of the extreme wind speed that are so conservative that they protect designers against thunderstorms as well. Previous analyses of the local wind climate provide extreme wind speeds that are always lower than those indicated in the Italian Guide. In Livorno, where thunderstorms seem to be less intense than in La Spezia, these results are also conservative compared to these evaluations. In La Spezia, on the other hand, the occurrence of intense thunderstorms leads to results that equate or exceed those provided by micro-zoning analyses done ignoring these phenomena, for high return periods. This finding confirms the risks involved in relation to studies based on data or on methods that are not suitable for recognizing or evaluating the occurrence of thunderstorms.

7 Characteristic of thunderstorm in Beijing urban area

7.1 Introduction

China, a country in East Asia having the world's largest population and covering approximately 9,600,000 square kilometres, is also frequently experiencing intense thunderstorms. For instance, at about 2132 BT, June 1, 2015, the 'Oriental Star' cruise from Nanjing to Chongqing suffered a severe stormy weather, which was confirmed to be a sudden squall line of downbursts, when it was sailing in the Yangtze River near Jianli County, resulting in 442 people killed (Duan et al., 2017). Thunderstorms represent also the main disastrous weather bringing strong winds in the national capital Beijing (Fu et al., 2007). In July 22, 1997, 27 houses were destroyed and dozens of trees up to 40cm in diameter were blown up by a thunderstorm downburst (Liu, 2001). This sudden thunderstorm that struck Beijing with hailstones and the peak wind speed of more than 20 m/s at around 2000 BT, August 23, 2001 interrupted the Chinese and English football match of the World University Games, besides it also brought serious damage to facilities and disruptions in electric power (Qin et al., 2006; Fu et al., 2007).

Meteorologists have made some achievements in the study of this phenomenon in Beijing. Based on the observational data of meteorological instruments, the thunderstorms in Beijing have strong local features, which mainly arise from the intense development of local convection systems, while large scale thunderstorm winds caused by large scale weather systems are rare. Besides, the occurrence of thunderstorms in Beijing area is restricted by topography, namely they are more likely to occur in wide, flat areas than near mountainous areas (Qin et al., 2006). Based on local statistics, for 134 thunderstorm gales from 1998 to 2007 in Beijing area, it is known that most of them were accompanied by downbursts and some of them broke out while hails were falling (Liao et al., 2009).

Despite these and many other analyses, at authors' knowledge, the research about the properties of thunderstorms relevant to the wind loading of structures in Beijing is still lacking. The Beijing 325 m high meteorological tower (Li et al., 2009; Tian et al., 2011; Hui et al., 2017) - along which 11 ultrasonic anemometers are mounted at nine different heights from 8 m to 280 m, detecting high-resolution data with 10 Hz sampling frequency from 2013 - provides a unique opportunity to shed new light on this crucial issue, to detect thunderstorm records, and to study their characteristics from the perspective of wind engineering. Besides, the presence of anemometers installed at different levels on the same tower makes it possible to study the time evolution of the wind speed profile related to thunderstorm outflows, a topic limitedly investigated in the Mediterranean due to the dominant presence of single anemometers. This part of research was submitted to the Journal of Wind Engineering and Industrial Aerodynamics (Zhang et al., 2019b).

In this framework, **Section 7.2** illustrates the main properties of the measurement site and observations. The characteristics of the Beijing climate and the wind speed statistical properties based on the ultra-sonic anemometers on the tower are

introduced briefly in **Section 7.3**. **Section 7.4** describes the criterion by means of which different intense wind events are separated and thunderstorm outflows are extracted and catalogued; it also provides additional elements on the direction, seasonality and hour of daily occurrence of these events. According to the directional method as introduced in **Section 4.2.3**, **Section 7.5** analyzes the slowly-varying mean wind speed and direction, the turbulence intensity, the reduced turbulent fluctuations, the integral length scale and the power spectral density, the turbulence intensity modulation and the gust factor, aiming to study these properties in a statistical environment coherent with that traditionally used for synoptic winds; in this stage of the research, likewise in the Mediterranean area, the examined records are dealt with as disjoint from each other. **Section 7.6** describes the time evolution of the wind speed and direction profile with reference to a thunderstorm test case event. **Section 7.7** summarizes the main conclusions and draws some prospects for the prosecution of this research, first of all with reference to a systematic analysis and interpretation of the most relevant thunderstorm outflows as simultaneously detected by the anemometers installed at 9 different levels along the tower.

7.2 Measurement Site and Observations

Beijing is one of the largest cities in the world; since 1978, its urban area and population exhibited an exponential growth according to which, by 2016 it reached 21.73 million residents. The 325 m high meteorological tower (39°58’N，116°2’E) is a guyed mast with regular triangle cross-section; it is situated between the Northern 3rd Ring Road and the Northern 4th Ring Road of Beijing city; it was set up in 1978 by the Institute of Atmospheric Physics (IAP) of the Chinese Academy of Sciences (CAS). The height of its base is about 48.63 m above the sea level. **Figure 7.1** shows the picture of the meteorological tower where a number of anemometers was installed **(a)** and the satellite picture of landforms around it (the red circle) **(b)**. As shown in **Figure 7.1 (b)**, there is almost no high rise structures within 1 km range of the tower, except for some residential buildings, about 60 m high, which are located 100 m away from the tower in the south direction. The site around the tower can be regarded as terrain C (urban area) according to the Chinese National Load Code (GB50009-2012).

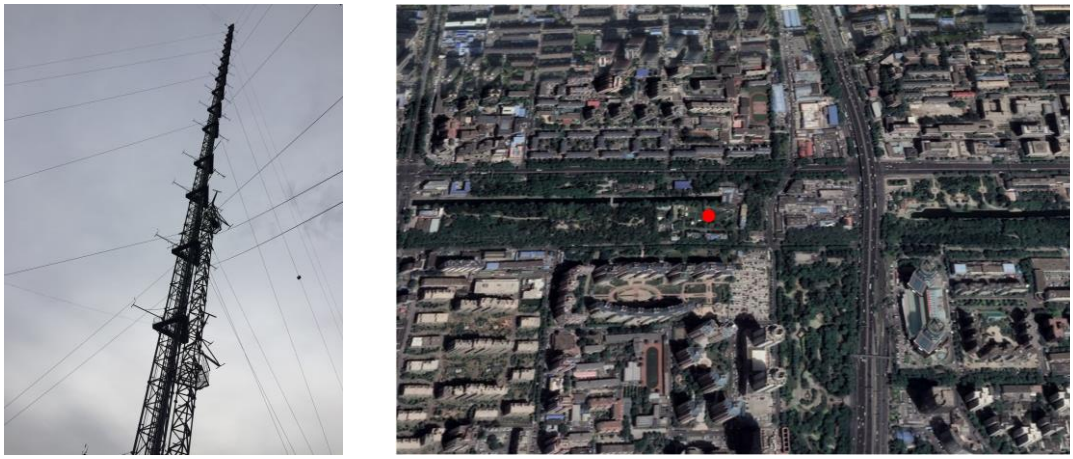

(a) (b)

Figure 7.1 Picture of the Beijing 325m meteorological tower (a) and satellite picture of landforms around it (b).

As shown in **Figure 7.2**, thirty vane anemometers (EC9-1 with high resolution, 0.1 m/s, produced by the Changchun Meteorological Instrument Research Institute, China) were installed on the tower at fifteen different levels in order to measure the mean wind speed data with a sampling rate of 0.05 Hz; besides, there are eleven three-channel ultrasonic anemometers mounted at nine different heights along the tower, namely 8, 16, 32, 47, 64, 80, 140, 200, and 280 m (Xu and Zhang, 2019). At 32 and 64 m height there is a couple of ultrasonic anemometers mounted at the same heights with different orientations (north and west), for validating the measured fluctuating speeds. To check the reliability of instruments, the measured wind speeds at each height are firstly averaged within 10-min periods and compared with the results provided by the cup-type anemometers; thus, the fidelity of instruments is well examined. To avoid the interference effects of the tower itself on the wind, the anemometers are fixed 1.5 m away from the tower on the north side, which is exposed to the dominant synoptic winds in Beijing during winter and spring. Hence, this meteorological tower is the best observation station to study the urban boundary layer and the urban most intense storms in Beijing city.

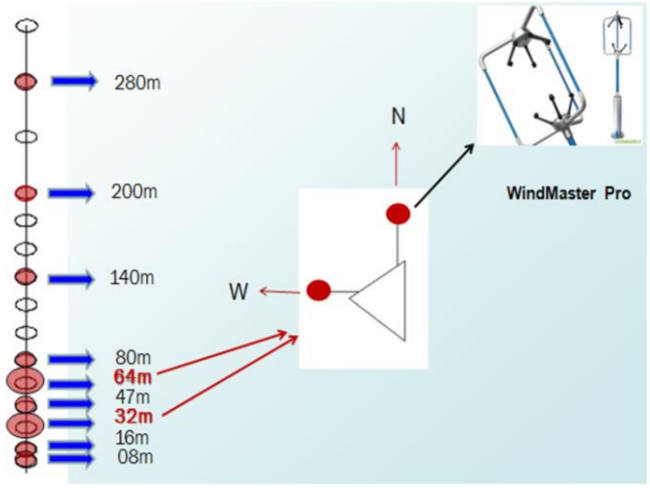

Figure 7.2 Arrangement of ultrasonic anemometers on the Beijing 325m high meteorological tower.

The anemometric data of the database is stored in terms of three instantaneous wind speed components (V_X, V_Y, V_Z) for the three-axial ultrasonic anemometers according to the geophysical coordinate system, where V_X is directed from South to North, V_Y from East to West, and V_Z is vertical and positive upwards. All these ultrasonic anemometers continuously collect wind speed data simultaneously with a sampling rate of 10 Hz.

7.3 Beijing wind climate

There are two main characteristics of China's climate: the climate is complex and diverse, and the monsoon climate is remarkable. Due to the vastness of China, its climate is manly divided into 5 areas as shown in **Figure 7.3**. The typical monsoon climate region in the eastern part of China is characterized by a temperate monsoon climate, a subtropical monsoon climate, and a tropical monsoon climate from north to south. The temperate continental climate is distributed in the Northwest China. The Tibetan Plateau is characterized by a plateau mountain climate.

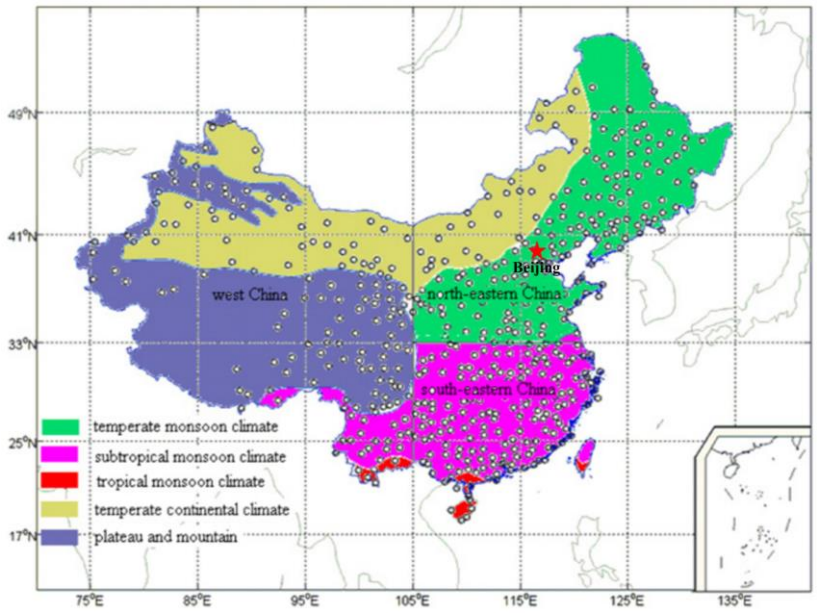

Figure 7.3 Distribution of climate regions in China. (Song et al., 2011)

Beijing, the capital of China, lies northwest of the north China plain with a total area of 16,410.54 square kilometres, as shown in the pentagram in **Figure 7.3**. The wind system of this city is dominated by the monsoon-influenced humid continental climate, characterized by hot, humid summers due to the East Asian monsoon, and by cold, windy, dry winters that reflect the influence of the vast Siberian anticyclone. Spring and autumn are seasons of transition and minimal precipitation. The monthly daily average temperature in January is -5~-4 ℃, while in July it is 26.2 ℃ for the plain region. The spatial distribution of annual precipitation is uneven, and the precipitation is close to 3/4 of the annual precipitation from June to August.

This area is not affected by typhoons and tornados. On the other hand, there are

frequent occurrences of thunderstorms. The winds produced by thunderstorm events are relatively stronger and more turbulent than those produced by monsoon winds and extra-tropical cyclones. Therefore, thunderstorm winds are important sources of strong winds in Beijing, and their main characteristics related to the wind loading of structures are dominant for the structure design.

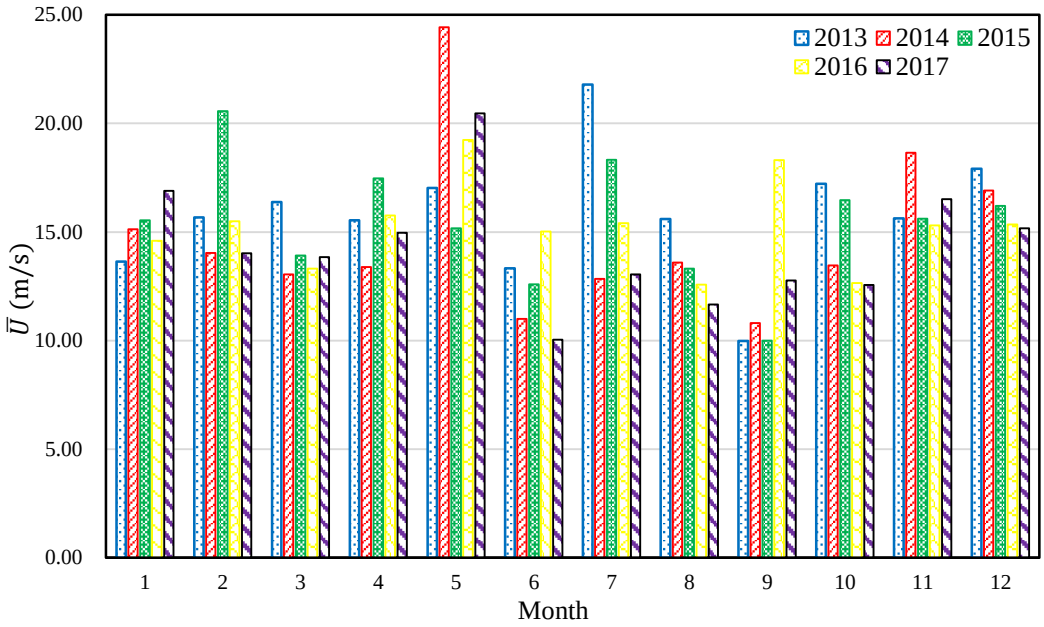

Figure 7.4 Monthly maximum mean wind speed.

The data detected by the 140 m anemometer on the Beijing 325 m high meteorological tower in 2013-2017 is used to preliminarily learn the local statistical properties of the wind speed. Based on it, the monthly maximum mean wind speeds in 10-min time intervals are shown in **Figure 7.4**. Their range is between 10 and 25 m/s. The maximum 10-min mean wind speeds occur generally in May for 2014, 2016 and 2017. On the other hand, for 2013 and 2015, they occurred in July and February, respectively. The overall values are relatively higher in spring and winter, which is coherent with the long-term meteorological statistical results.

Horizontal wind roses for different seasons according to the data detected by the anemometer at 140 m height in 2013 are shown in **Figure 7.5**. It shows that the dominant wind direction is northwest and southeast, which is consistent with the characteristics of Beijing's climate; almost all the strong winds larger than 8 m/s come from the northwest direction; strong winds frequently occur in spring and winter, while in summer the wind is weak; the northwest wind is dominant in spring, autumn and winter, while the southeast wind occurs more frequently in summer than in the other seasons.

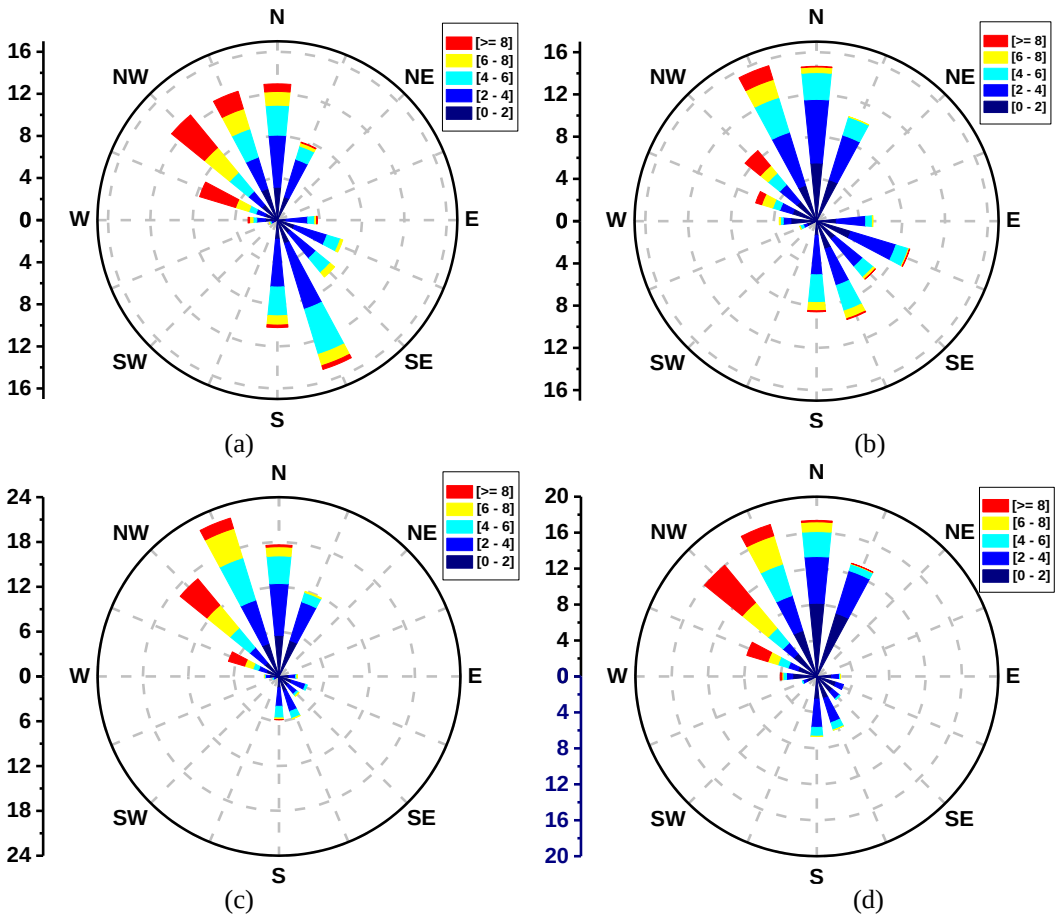

Figure 7.5 Horizontal wind roses in different seasons at 140 m in 2013: (a) Spring; (b) Summer; (c) Autumn; (d) Winter.

7.4 Separation and classification of thunderstorm outflows

Based on the characteristics of the Beijing wind climate described in the previous section, typhoons never occur in this area and thunderstorms are among the most frequent disastrous weather phenomena, especially in summer (Liao et al., 2009). A thorough examination of the huge amount of the collected data reveals that intense wind events can be separated and classified into three families characterized by different statistical properties similar to the ones that occur in the mid-latitude region in the northern Mediterranean (De Gaetano et al., 2014; Zhang et al., 2018a and 2018b):

1) stationary Gaussian events with relatively large mean wind velocities and small gust factors; they usually correspond to synoptic neutral atmospheric conditions and are here referred to as synoptic storms, namely monsoons and extra-tropical cyclones or large depression systems;
2) non-stationary non-Gaussian events with relatively small mean wind velocities, large and quite isolated peaks, and high gust factors; they are here referred to as thunderstorms outflows;
3) nearly-stationary non-Gaussian events with relatively small mean wind velocities,

large and repeated peaks, and moderately high gust factors; they are here referred to as intermediate events or gust fronts (Kasperski, 2002). While waiting to carry out a systematic meteorological survey and interpretation of these events, it seems to be reasonable to advance the hypothesis that they are associated to unstable atmospheric conditions.

The separation of intense wind phenomena into homogeneous families is a fundamental preliminary step to interpret the events of engineering interest and to deal with them by models coherent with their physical reality. It is found that the above semi-automatic procedure proposed by De Gaetano et al. (2014) and improved by Zhang et al. (2018b) is appropriate for the measured data in Beijing. It is also applied to the records with the horizontal 1-s peak wind velocity $\widehat{U}$ greater than 15 m/s.

As mentioned in the previous section, there are 11 ultra-sonic anemometers installed at nine different heights along the tower. The above procedure is applied to the data recorded by the 9 ultra-sonic anemometers on the north side of the tower during the period 2013-2017. After quantitative controls, over 97.5% of the records related to intense wind events are automatically identified as synoptic events. The remaining ones are submitted to qualitative expert judgments, in which the extraction of thunderstorm outflow records is mainly based on 10-min, 1-h and 10-h records centred around the peak wind speed. The information about temperature makes a great contribution to this judgement, since it generally presents a clear decrease during the passage of the gust front of a thunderstorm outflow (Huang et al., 2019). In addition, the availability of generalized weather records in Beijing is used as a reference information. Accordingly, thunderstorm outflows and intermediate events are separated successfully.

Three typical 1-h time history records registered by the 280m anemometer high, which correspond to a synoptic storm ($\widehat{U}$=23.01 m/s), a thunderstorm outflow ($\widehat{U}$=29.80m/s) and an intermediate event ($\widehat{U}$=16.20 m/s), are shown in **Figure 7.6, Figure 7.7 and Figure 7.8,** respectively. The pictures **(a)**, **(b)** and **(c)** show the time-series of the wind speed, wind direction and temperature raw data, respectively, and their mean values over 1-h (solid lines) and 10-min (dotted lines) periods. In pictures **(a)**, the 1-s peak wind speed (red circles) is also shown, which is obviously smaller than the instantaneous peak.

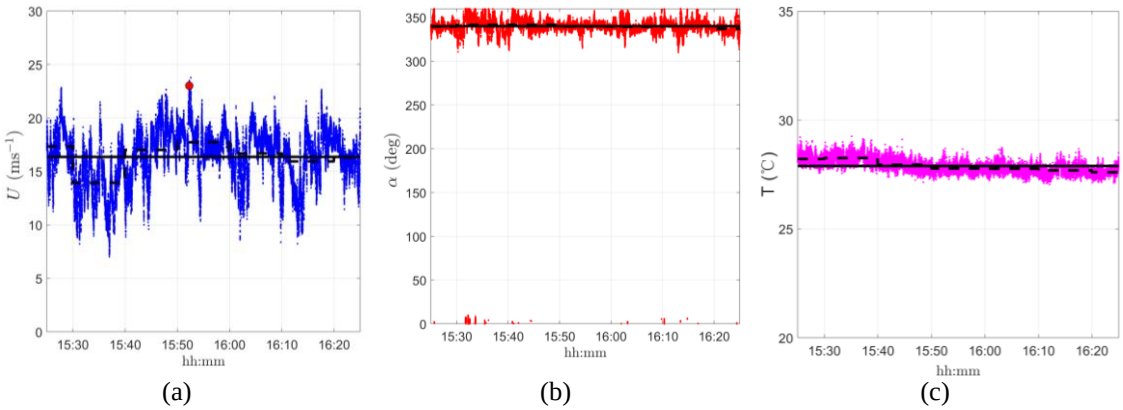

(a) (b) (c)

Figure 7.6 Synoptic wind recorded on 11 May 2017 by the 280m anemometer: (a) 1-h wind speed time-series; (b) wind direction time-series; (c) 1-h temperature time-series.

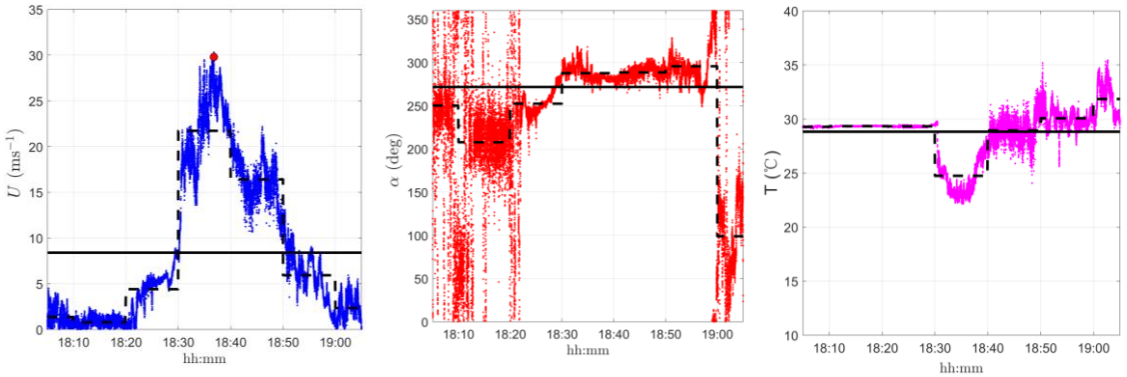

(a) (b) (c)

Figure 7.7 Thunderstorm outflow recorded on 07 September 2016 by the 280m anemometer: (a) 1-h wind speed time-series; (b) wind direction time-series; (c) 1-h temperature time-series.

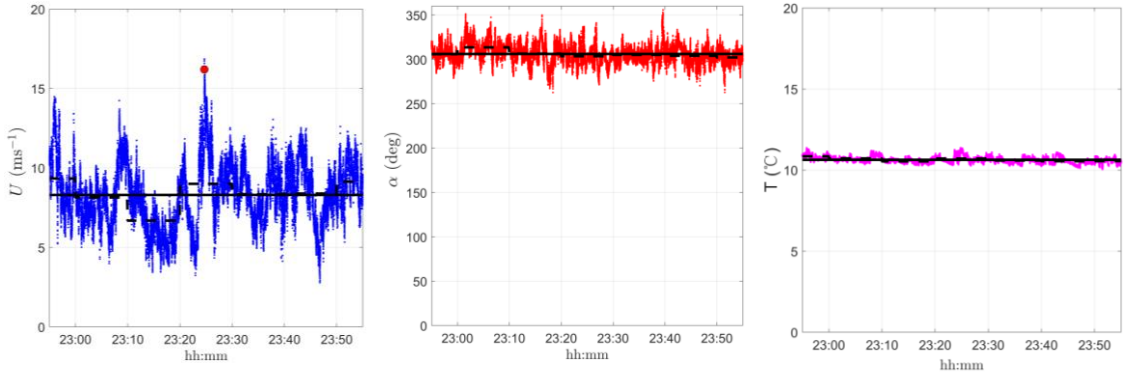

(a) (b) (c)

Figure 7.8 Intermediate event recorded on 02 December 2015 by the 280m anemometer: (a) 1-h wind speed time-series; (b) wind direction time-series; (c) 1-h temperature time-series.

On the whole, dealing with single records as disjoint from each other, this approach led to extract NTR = 314 strongly non-stationary records that can be traced back to convective conditions and thunderstorm outflows. Of course, since the same thunderstorm event may be detected by several anemometers simultaneously, the number of thunderstorm events NTE = 70 is smaller than NTR = 314.

This analysis points out a main difference respect to the analogous study carried out in the Northern Mediterranean area: in the Mediterranean the anemometers are distributed in different positions whereas in Beijing they are put along the same tower. This condition gives rise to a delicate issue: during a thunderstorm event, not all the wind speed records, analysed above separately, usually pass the control of possessing a peak wind speed above 15 m/s and a strongly non-stationary character. Accordingly, the overall number of the records detected during thunderstorm events, NTO = 630, is greater than NTR = 314.

This aspect unavoidably leads to a complication: the study of the most relevant thunderstorm records dealt with as disjoint includes NTR = 314 signals; the study of the most relevant thunderstorm events necessarily involves the consideration of all the records detected at different heights independently of their singular properties.

Table 7.1 summarizes the selected records and points out the above remarks. The columns "10-min", "1-h" and "10-h" provide, for each anemometer height, the number of events that can be recognized as non-stationary on 10-min, 1-h and 10-h periods respectively (Burlando et al., 2018).

Table 7.1 Number of thunderstorm events and records examined.

Anem. No.	h (m)	10-min	1-h	10-h	NTR	NTE	NTO
1	8	5	5	0	10	70	70
2	16	7	8	1	16		70
3	32	12	12	1	25		70
4	47	11	19	2	32		70
5	64	16	24	1	41		70
6	80	12	25	3	40		70
7	140	10	38	3	51		70
8	200	8	38	1	47		70
9	280	5	45	2	52		70
Total		86	214	14	314	70	630

A preliminary comparison between the data provided in **Table 7.1** for the Beijing urban area and the analogous data provided by **Table 3.1** for the Mediterranean area globally indicates, in this latter area, a major number of short events. In reality, this latter data derive from measurements mostly performed in the first 10-30 m above the ground level (AGL). Limiting the comparison to the same atmospheric range, the typical duration of the gust front passage in Beijing seems to be only slightly longer than that in the Mediterranean.

In order to complete the information provided in **Table 7.1**, the transient records are separated into five groups as a function of the 1-s peak wind speed (m/s), namely $15 \leq \widehat{U} < 20$, $20 \leq \widehat{U} < 25$, $25 \leq \widehat{U} < 30$, $30 \leq \widehat{U} < 35$ and $35 \leq \widehat{U} < 40$, as shown in **Table 7.2**. It points out, at least for the available data, that the thunderstorm outflow records whose 1-s peak wind speed exceeds 20 m/s can be found for all the anemometers from 8 m to 280 m and only the anemometers higher than 64 m detect thunderstorm outflow records whose 1-s peak wind speed exceeds 30 m/s.

Table 7.2 Classes of membership of the peak wind velocity of thunderstorms.

Anemometer (m) / $\widehat{U}$ (m/s)	8	16	32	47	64	80	140	200	280	ALL
15-20	7	12	16	22	30	25	27	26	31	196
20-25	3	3	7	8	7	12	14	11	12	77
25-30	-	1	2	2	3	2	7	7	6	30
30-35	-	-	-	-	1	1	2	2	2	8
35-40	-	-	-	-	-	-	1	1	1	3
ALL	10	16	25	32	41	40	51	47	52	314

The distribution of the 70 thunderstorm events reported in **Table 7.1** with respect to the daily Beijing time is shown in **Figure 7.9**. Overall, for the area under study, 8% of the thunderstorms occur between 00:00 and 06:00, 3% in the morning between 06:00-12:00, 33% in the afternoon from 12:00 to 18:00, and 56% in the evening from 18:00 until 24:00. So, thunderstorm events frequently occur in the afternoon and in the first half of the night. Therefore, at least in the tower site, they are slightly more likely to occur in the warmer hours of the day, which is similar to the conditions in which thunderstorm outflows occur in the northern Mediterranean (Burlando et al, 2018).

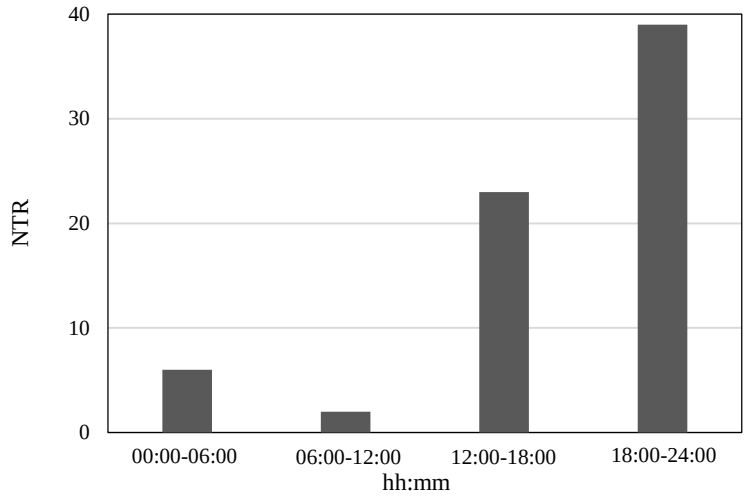

Figure 7.9 Number of thunderstorm outflow records detected at different hours of the day.

7.5 Statistical properties of the thunderstorm outflows

There are 314 thunderstorm outflow recordings available now, based on the Beijing meteorological tower described in **Section 7.4**. Each one of them has been first decomposed into component signals by means of the rule described in **Section 4.2.3**. Subsequently, the components signals have been analysed statistically, both considering the single anemometers at different heights and the whole of the registrations. The final aim of this study is to inspect the most relevant properties of the thunderstorm outflows detected in the Beijing urban area and to compare this information with the properties of the thunderstorm outflows detected in the northern Mediterranean area.

This comparison is quite delicate due to the different properties of the two datasets. Independently of the different geographical positions, the neighboring terrains are totally diverse. In Beijing the tower is placed in a flat urban area whereas in the Mediterranean the anemometers are distributed along the coast, with the sea on one side, over which most of the thunderstorm are originated, and an urban exposure inland, often involving also complex topographic features. In addition, in Beijing the anemometers are uniformly distributed between 8 and 280 m height whereas in the Mediterranean most of them are placed between 10 and 30 m height, with only a few

ones between 30 and 80 m height. Under this point of view the most probative comparison with the Mediterranean dataset should be limited to the 3-4 Beijing anemometers closest to the ground.
In this framework, the prosecution of this section deals with the slowly-varying mean wind speed (**Section 7.5.1**) and direction (**Section 7.5.2**), the turbulence intensity (**Section 7.5.3**), the reduced turbulent fluctuations (**Section 7.5.4**), their integral length scales and power spectral densities (**Section 7.5.5**), the turbulence intensity modulation (**Section 7.5.6**), and the gust factor (**Section 7.5.7**).
It is worth noticing that the above sections provide and discuss data dealt with as disjoint, putting together records detected during the same thunderstorm event with data detected in different events. Accordingly, such data should be interpreted in a probabilistic framework, height by height, without any attempt to speculate on the reconstruction of the vertical profile. This latter issue is discussed in **Section 7.6** with reference to a thunderstorm test case whereas a detailed investigation and discussion about the evolution of the wind speed and direction profile is postponed to future papers currently in progress.

7.5.1 Slowly-varying mean wind velocity

The records labelled here as thunderstorm outflows are characterized by a prominent peak whose duration has a dominant role in the wind loading and response of structures (Kwon and Kareem, 2009). Such peak is best described by the slowly varying mean wind velocity $\bar{u}(t)$ or, even better, by the non-dimensional function $\gamma_u(t)$ (**Eq. (4.22)**).
Figure 7.10 shows the mean value of the non-dimensional function $\gamma_u(t)$ for the thunderstorm records detected by each anemometer. The full lines correspond to the first 4 anemometers, at heights comparable with those of the anemometers in the Mediterranean area, whereas the dashed lines correspond to higher instruments. All the diagrams gathered for this analysis identify the essential features of a ramp-up and -down in the wind speed corresponding to the passage of a gust front. The duration of this passage is similar to that observed in the northern Mediterranean close to the ground. On increasing the height above the ground, as already pointed out by **Table 7.1**, the duration of the most intense part of the thunderstorm outflows increases. This aspect deserves further investigations.

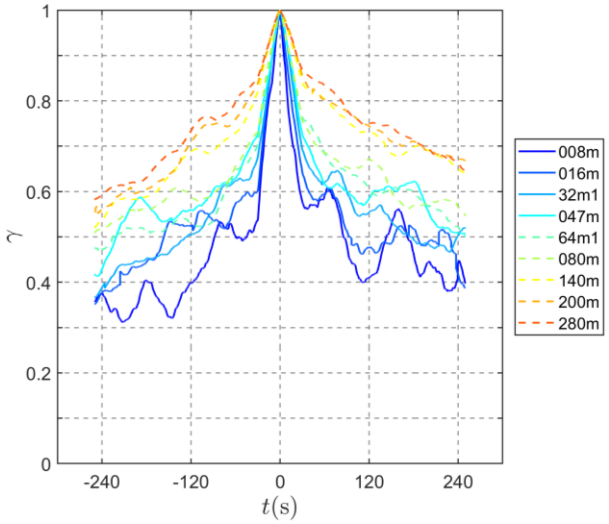

Figure 7.10 Mean values of the normalized slowly-varying mean wind velocity for each anemometer.

7.5.2 Slowly-varying mean wind direction

Based on the novel directional decomposition approach adopted here, the slowly-varying mean wind direction $\bar{\alpha}$ or $\bar{\beta}$ (**Eq. (4.17)**) can be extracted and embedded within the wind velocity model.

The examination of the slowly-varying mean wind direction of the thunderstorm outflow records considered herein exhibits complex and varied trends. By way of example, **Figure 7.11 (a)** shows a slowly-varying mean wind speed record, $\bar{u}(t)$, in which a rapid variation takes places for a relatively short time period. On the other hand, **Figure 7.11 (b)** shows that the corresponding slowly-varying mean wind direction, $\Delta\bar{\alpha}$, exhibits a sudden shift that anticipates the peak and lasts for a longer time period.

Referring to the ensemble of the transient records herein analysed, **Table 7.3** provides an attempt to quantify the maximum rate of change of the slowly-varying mean wind direction, $\Delta\bar{\alpha}$, in the 30-min period centred around the maximum wind speed. Most of the examined events (67%) has a rate of change $\Delta\bar{\alpha}$ larger than 90 deg. The choice of the most effective period in which the directional shift has to be evaluated calls for further studies.

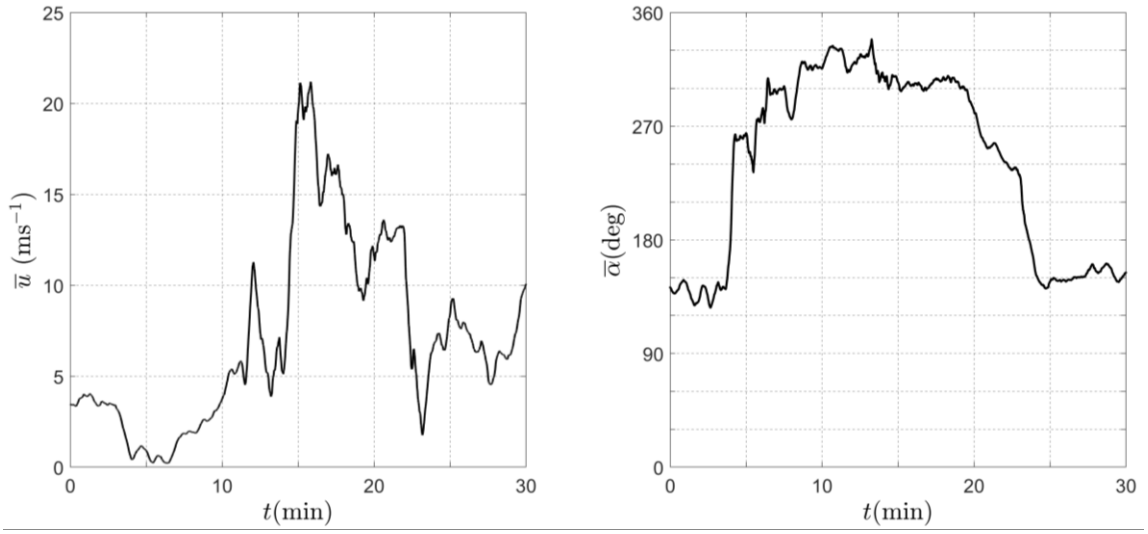

(a) (b)

Figure 7.11 30-min slowly-varying mean wind velocity (a) and direction (b) centred around the peak wind velocity during a thunderstorm outflow occurred on June 10, 2016 as detected by the anemometer at 80 m height.

Table 7.3 Classes of membership of the maximum shift of the slowly-varying mean wind direction in the 30-min period centred around the peak wind speed.

	Maximum direction shift (deg)				
h (m)	$\Delta\bar{\alpha} \leq 45$	$45 < \Delta\bar{\alpha} \leq 90$	$90 < \Delta\bar{\alpha} \leq 180$	$\Delta\bar{\alpha} > 180$	All
8	0	0	3	7	10
16	0	4	3	9	16
32	1	4	7	13	25
47	0	8	15	9	32
64	2	4	21	14	41
80	2	8	18	12	40
140	5	18	22	6	51
200	2	19	18	8	47
280	5	20	13	14	52
All	17 (6%)	85 (27%)	120 (38%)	92 (29%)	314

Figure 7.12 shows the peak wind speed $\widehat{U}$ as a function of the direction shift $\Delta\bar{\alpha}$. Three remarks stand out: 1) none of the examined events is characterised by $\Delta\bar{\alpha} < 15$ deg, which corresponds to nearly straight winds; 2) only one record exceeds the peak wind speed $\widehat{U}$ = 30 m/s in the range of $\Delta\bar{\alpha} > 145$ deg; 3) no apparent correlation emerges between $\widehat{U}$ and $\Delta\bar{\alpha}$. Despite this remark, 10 of the 11 most intense events, those exceeding $\widehat{U}$ = 30 m/s, involve directional shifts in the range between 35 and 145 deg.

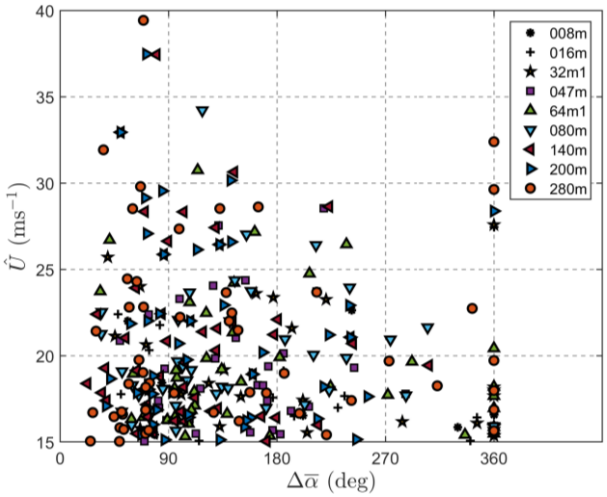

Figure 7.12 Peak wind speed $\hat{U}$ as a function of the direction shift in 30 min.

7.5.3 Turbulence intensity

The turbulence intensity is a key parameter for describing the fluctuating characteristics of wind flows. According to **Eq. (4.21)**, the longitudinal and lateral slowly-varying turbulence intensities, I_u and I_v, can be extracted by the directional decomposition rule. Note that at times the turbulent intensity time-histories exhibit abnormal large values and even sharp peaks in correspondence of very small slowly-varying mean wind velocity values, sometimes tending to zero. Accordingly, the large turbulence intensities (greater than 0.2) related to singular values (less than 5 m/s) are ignored in the following analyses (Zhang et al., 2019).

Table 7.4 shows the mean values and the coefficients of variation (cov) of the average longitudinal and lateral slowly-varying turbulence intensities, $\bar{I}_u$ and $\bar{I}_v$, for the thunderstorm outflows detected by each anemometer. The mean values of $\bar{I}_u$ and $\bar{I}_v$ decrease on increasing the height whereas their cov values increase on increasing the height. $\langle\bar{I}_u\rangle$ and $\langle\bar{I}_v\rangle$ assume quite similar values because they have been deprived by their low-frequency harmonic content through the mobile mean operator (Zhang et al., 2019). Despite this, $\langle\bar{I}_u\rangle$ is slightly larger than $\langle\bar{I}_v\rangle$.

It is relevant to point out that the values of $\langle\bar{I}_u\rangle$ and $\langle\bar{I}_v\rangle$ detected by the anemometers 1-4 of the Being Tower, the ones close to the ground, are much larger than those related to the thunderstorm outflows detected at similar heights in the northern Mediterranean. As better discussed below, this may be due to the fact that in the latter case the thunderstorm outflows mainly come from the sea whereas the Beijing tower is embedded in an urban area. In addition, the Mediterranean thunderstorms examined by Zhang et al. (2019) were limited to 10-min rapid events whereas those investigated in this paper include slower 1-h and 10-h events for which more time is available in order to create a boundary layer flow in equilibrium with the local roughness. Also this topic deserves further investigations.

Table 7.4 Ensemble mean value and cov of the turbulence intensity.

Anemometer No.	h (m)	$\langle \bar{I}_u \rangle$	cov($\bar{I}_u$)	$\langle \bar{I}_v \rangle$	cov($\bar{I}_v$)
1	8	0.34	0.12	0.30	0.12
2	16	0.27	0.14	0.25	0.17
3	32	0.22	0.22	0.20	0.17
4	47	0.21	0.39	0.19	0.29
5	64	0.20	0.42	0.17	0.24
6	80	0.18	0.34	0.16	0.26
7	140	0.12	0.34	0.10	0.29
8	200	0.10	0.35	0.09	0.33
9	280	0.11	0.88	0.08	0.41

Figure 7.13 (a) shows the average values of the turbulence intensity of the thunderstorm outflows as a function of h/z_0 (Xu and Hangan, 2008; Lombardo et al., 2014), where h is the height AGL and z_0 is the roughness length; the latter quantity is estimated referring to neutral synoptic conditions, taking into account the local topography and the upwind roughness features, and using the classic tools for synoptic winds (GB50009-2012; ESDU, 1993). The difference between the longitudinal and the lateral turbulence intensity is not relevant for most of the records, while the former is definitely larger than the latter for a few isolated thunderstorm outflow records. Similar to the results provided by Zhang et al. (2019), $\bar{I}_u$ and $\bar{I}_v$ decrease on increasing h/z_0; in addition, focusing on turbulence intensities associated with similar values of h/z_0, between 10^1 and 10^2, the agreement with the Mediterranean outcomes is definitely better. Also the decrease of $\bar{I}_u$ and $\bar{I}_v$ on increasing $\bar{u}_{max}$ possess strong analogies with the trend provided by Zhang et al. (2019) for the thunderstorms in the northern Mediterranean.

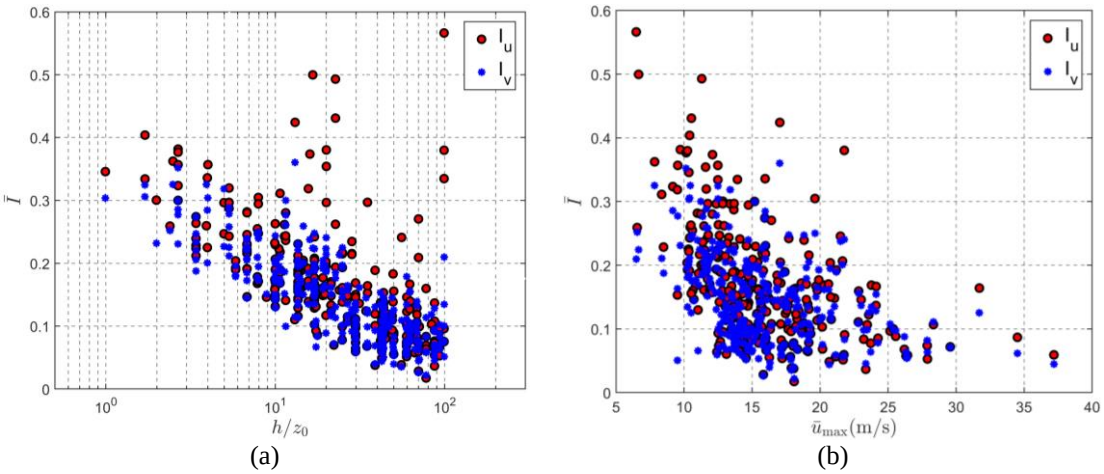

(a) (b)

Figure 7.13 Average turbulence intensity as a function of h/z_0 (a) and $\bar{u}_{max}$ (b).

The ensembles of the diagrams of μ_u and μ_v (**Eq. (4.23)**) for all the thunderstorm records investigated are illustrated in **Figure 7.14 (a)** and **(c)**. The cov values of μ_u and μ_v as a function of t are provided in **Figure 7.14 (b)** and **(d)**. Similar to the results

related to the thunderstorm outflows in the northern Mediterranean, both the mean value and the cov of μ_u and μ_v are weakly dependent on time; this means that μ_u and μ_v can be regarded, in simplified terms, as stationary processes. On the other hand, the μ_u and μ_v sample functions are not symmetric with respect to the mean, so their ensemble constitute a non-Gaussian process. **Figure 7.15** confirms this remark showing the detachment of the probability density function (pdf) of μ_u (**(a)** and **(b)**) and μ_v (**(c)** and **(d)**) from the reference Gaussian model. **Table 7.5** illustrates, for all the thunderstorm records considered, the mean value (Mean) and the standard deviation (Std) of the mean value (m), the std (σ), the skewness (γ) and the kurtosis (κ) of μ_u and μ_v. This strengthens the above remark by pointing out the detachment of the skewness and kurtosis of μ_u and μ_v from 0 and 3, respectively. All these results closely match the ones obtained by Zhang et al. (2019) in the Mediterranean area.

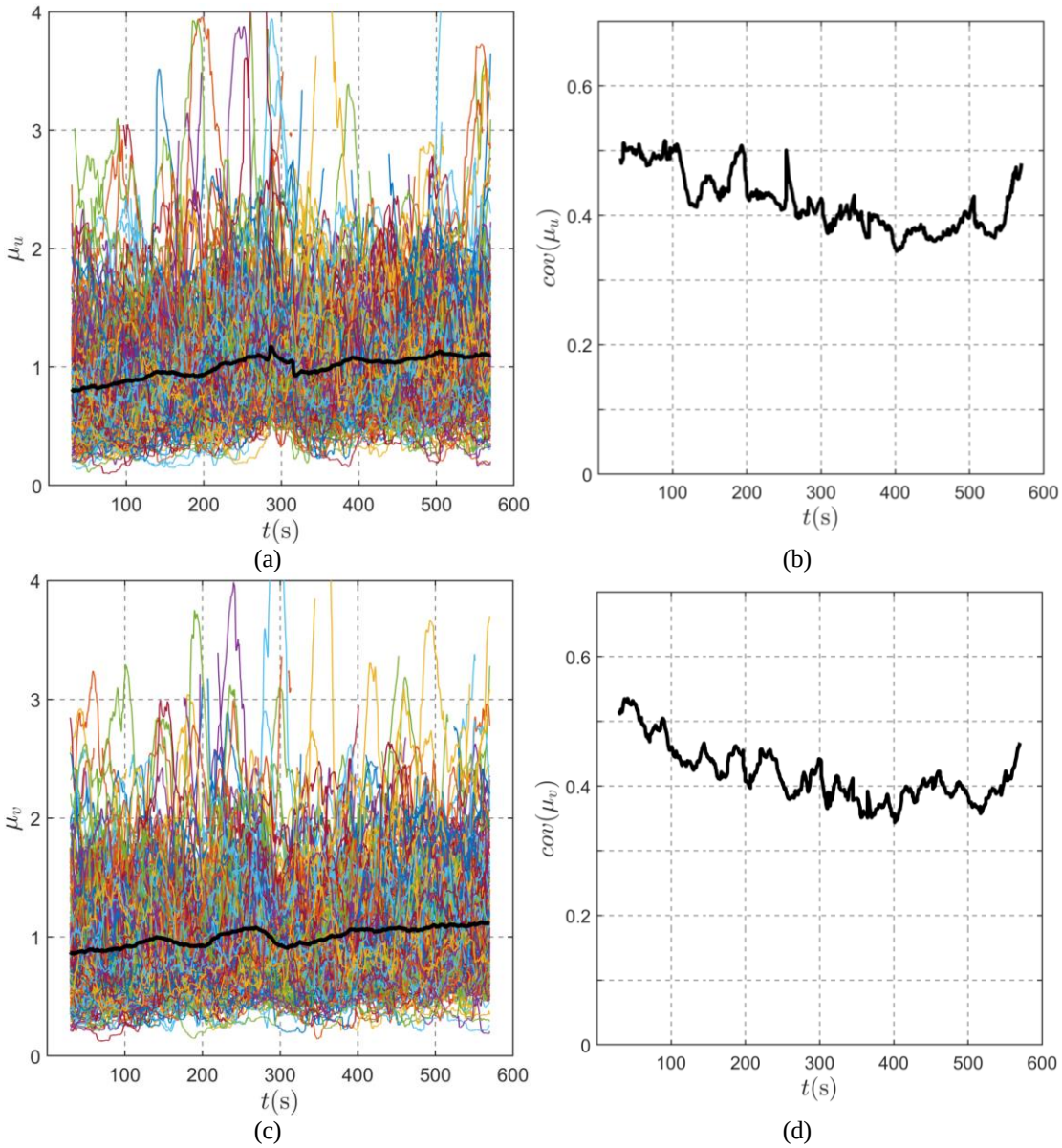

Figure 7.14 (a) (c) Ensemble of of the diagrams of μ_u and μ_v for all the thunderstorm records

investigated and their mean value (thick line); (b) (d) coefficient of variation of μ_u and μ_v.

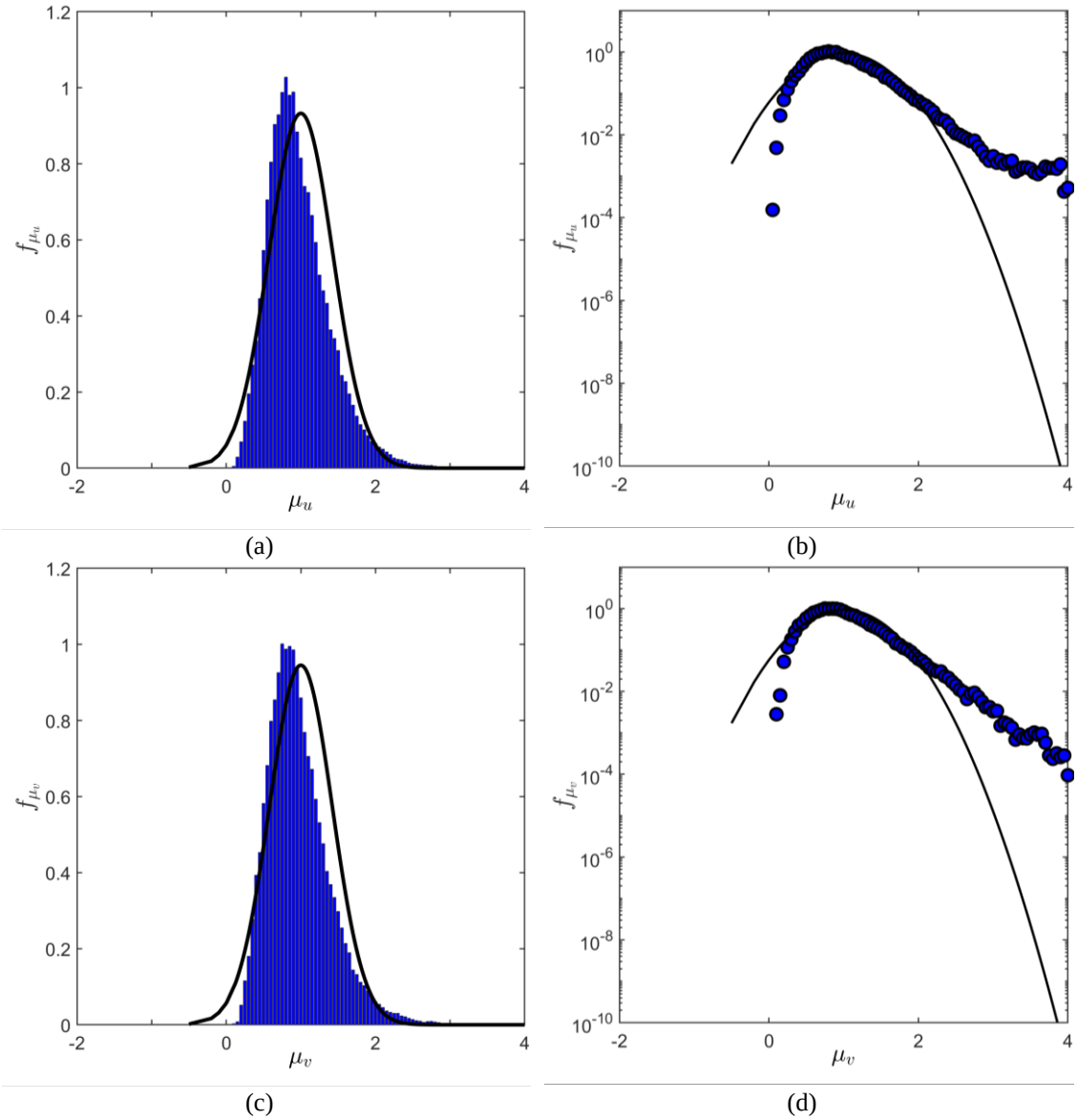

Figure 7.15 Probability density function of μ_u and μ_v for all the thunderstorm outflow records investigated: (a) (c) decimal ordinate; (b) (d) logarithmic ordinate.

Table 7.5 Mean value, standard deviation, skewness and kurtosis of μ_u and μ_v.

	Parameter	m	σ	γ	κ
μ_u	Mean	1.000	0.404	0.753	3.399
	Std	0.000	0.132	0.582	1.959
μ_v	Mean	1.000	0.397	0.745	3.366
	Std	0.000	0.128	0.536	1.430

7.5.4 Reduced turbulent fluctuations

The longitudinal and lateral reduced turbulent fluctuations are extracted according to the directional decomposition rule (**Eq. (4.19)**). **Table 7.6** shows, for all the thunderstorm records considered, the mean value (Mean) and the standard deviation (std) of the mean value (m), the std (σ), the skewness (γ) and the kurtosis (κ) of the longitudinal and lateral reduced turbulent fluctuations, $\tilde{u}'$ and $\tilde{v}'$, for T = 30 s. **Figure 7.16** highlights the good agreement between the pdf of $\tilde{u}'$ (**(a)** and **(b)**) and $\tilde{v}'$ (**(c)** and **(d)**) and the reference Gaussian pdf with zero mean and unit standard deviation. **Table 7.7** shows the correlation coefficient of $\tilde{u}'$ and $\tilde{v}'$ for all the thunderstorm records considered. Independently of height, its nearly zero value everywhere confirms that $\tilde{u}'$ and $\tilde{v}'$ are almost fully un-correlated. All these results are perfectly consistent with the outlines of the analyses carried out by Zhang et al. (2019) in the northern Mediterranean.

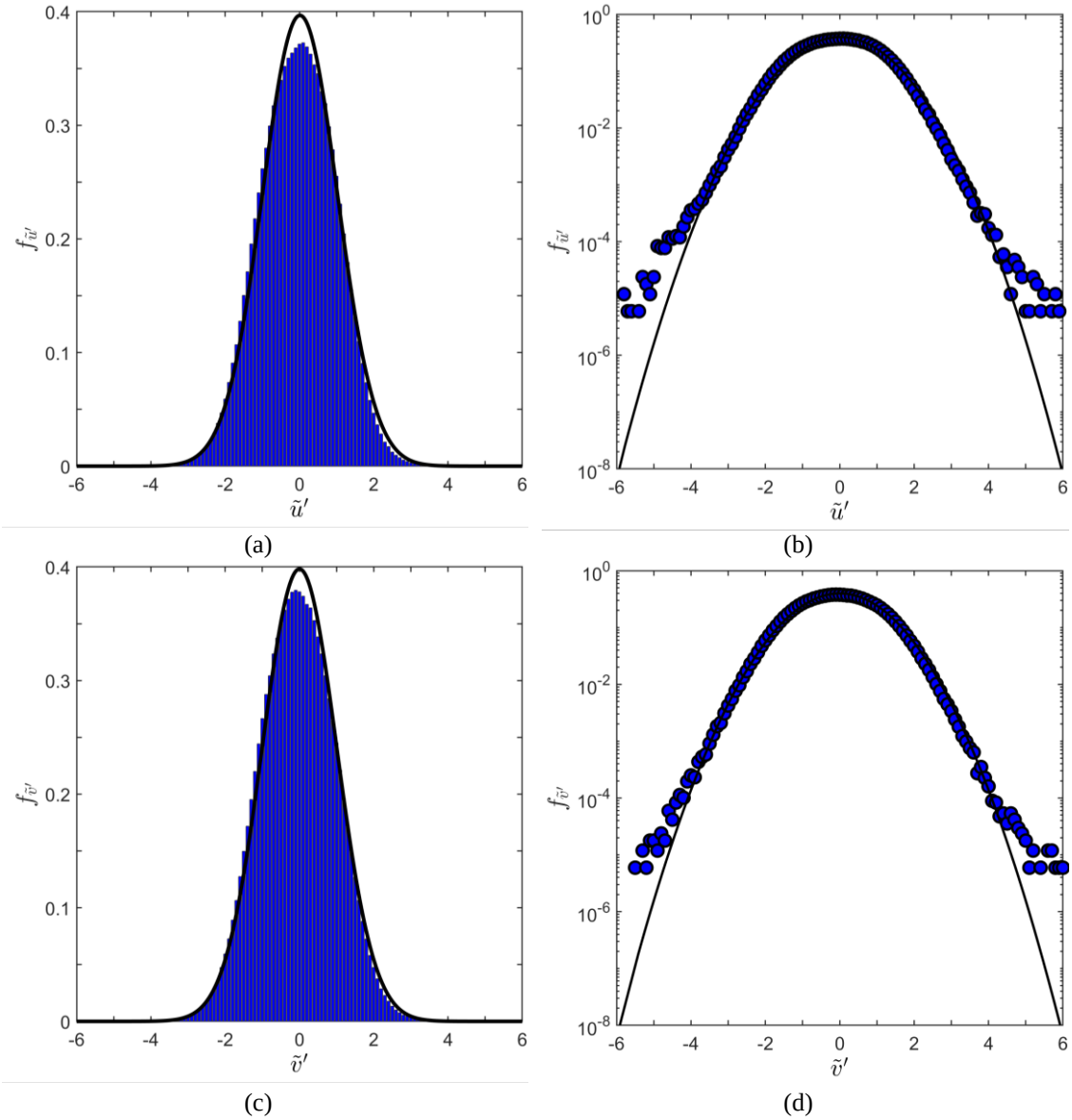

(a) (b)

(c) (d)

Figure 7.16 Probability density function of $\tilde{u}'$ and $\tilde{v}'$ for the thunderstorm outflow records

considered: (a) (c) decimal ordinate; (b) (d) logarithmic ordinate.

Table 7.6 Mean and std values of m, σ, γ and κ for the thunderstorm records.

	Parameter	m_c	σ_c	γ_c	κ_c
c=$\tilde{u}'$	Mean	0.013	1.005	-0.037	2.895
	Std	0.023	0.012	0.188	0.426
c=$\tilde{v}'$	Mean	0.000	1.002	0.005	2.909
	Std	0.018	0.010	0.135	0.291

Table 7.7 Correlation between $\tilde{u}'$ and $\tilde{v}'$ for the thunderstorm records.

Anem.No.	1	2	3	4	5	6	7	8	9	All
h (m)	8	16	32	47	64	80	140	200	280	-
Cor($\tilde{u}'\tilde{v}'$)	0.000	-0.032	-0.054	-0.034	0.024	0.049	0.004	0.020	0.048	0.003

7.5.5 Turbulence integral length scale and power spectral density

For the integral length scale and power spectral density (PSD) of the longitudinal and lateral reduced turbulent fluctuations, $\tilde{u}'$ and $\tilde{v}'$, a more controlled sub-set of 307 thunderstorm outflow records including an extremely low number of missing values are determined and applied; in the very few points in which the time series is interrupted, its continuity is obtained though linear interpolation.

As far as concerns the integral length scale and the power spectral density (PSD) of the longitudinal and lateral reduced turbulent fluctuations, $\tilde{u}'$ and $\tilde{v}'$, a more controlled sub-set of 284 thunderstorm outflow records, including an extremely low number of missing values, has been extracted and investigated; in the very few points in which the time series is interrupted, its continuity has been obtained though linear interpolation.

The longitudinal and lateral integral length scales of the reduced turbulent fluctuations, L_u and L_v, are determined from the auto-correlation function of $\tilde{u}'$ and $\tilde{v}'$ (Zhang et al., 2018a), using the method proposed by Flay and Stevenson (1988). **Table 7.8** compares the mean value and the cov of L_u and L_v as detected by each anemometer. The mean values of both these scales increase on increasing the height AGL whereas their cov exhibit a less regular trend. L_v is slightly lower than L_u. All these estimates are consistent with those obtained in the Mediterranean area (Zhang et. al, 2019).

Table 7.8 Mean value and cov of the integral length scale of the reduced turbulent fluctuation.

Anem. No.	h (m)	Mean(L_u) (m)	Cov(L_u)	Mean(L_v) (m)	Cov(L_v)
1	8	16.05	0.24	13.51	0.22
2	16	21.41	0.19	17.19	0.20
3	32	23.68	0.29	19.60	0.27
4	47	23.69	0.29	20.91	0.26
5	64	27.33	0.23	23.75	0.21
6	80	27.70	0.24	23.69	0.22

7	140	30.56	0.31	27.92	0.23
8	200	32.68	0.28	29.65	0.27
9	280	33.49	0.31	32.19	0.31

Figure 7.17 shows L_u and L_v as a function of h/z_0 **(a)** and $\bar{u}_{max}$ **(b)**. L_u and L_v exhibit a slight increase with h/z_0, which was not pointed out by the thunderstorm outflows detected in the northern Mediterranean; it is possible that such trend at the Beijing Tower is made clear by the presence of anemometers up to 280 m height. The Beijing data also show a clear increase of L_u and L_v on increasing $\bar{u}_{max}$; this result matches with the classical results for synoptic winds and neutral atmospheric conditions and also with the results obtained in the Northern Mediterranean area with regard to thunderstorms (Zhang et al., 2019).

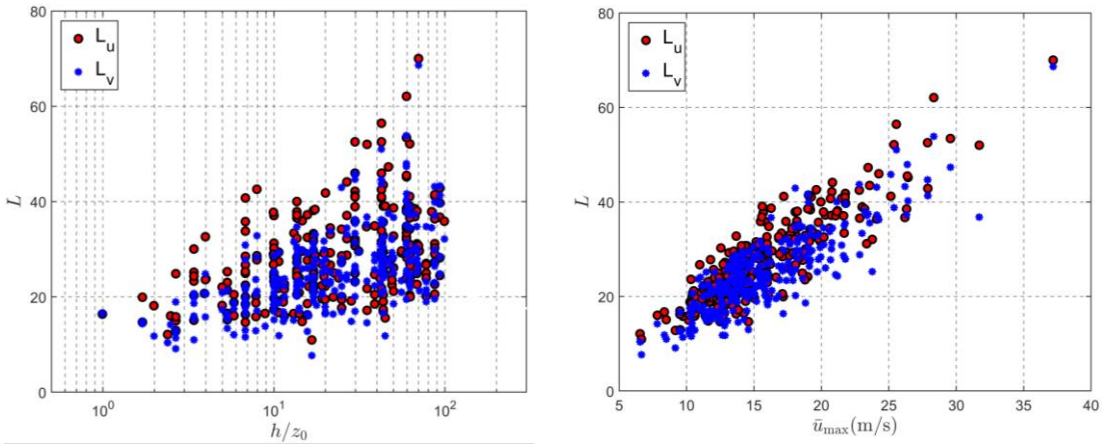

(a) (b)

Figure 7.17 Integral length scale as a function of h/z_0 (a) and $\bar{u}_{max}$ (b).

Figure 7.18 (a) and **(c)** show the PSD of $\tilde{u}'$ and $\tilde{v}'$ as a function of the reduced frequency $f = nL/\bar{u}_{max}$, in which $\bar{u}_{max}$ is the maximum value of the slowly-varying mean wind velocity, confirming the reliability of the parameterization previously adopted by Zhang et al. (2018b and 2019). This fact is enhanced by **Figure 7.18 (b)** and **(d)** that, despite the presence of anemometers located in a broad range of different heights, the mean values of the PSD related to each height exhibit one dominant peak whose position is very close to the one determined for the thunderstorm outflows in the northern Mediterranean. **Figure 7.19** compares the PSD of $\tilde{u}'$ and $\tilde{v}'$ as averaged over the ensemble of all the anemometers. It is worth noting that they exhibit an almost perfect superposition, even better than the one obtained with regard to the thunderstorms in the northern Mediterranean.

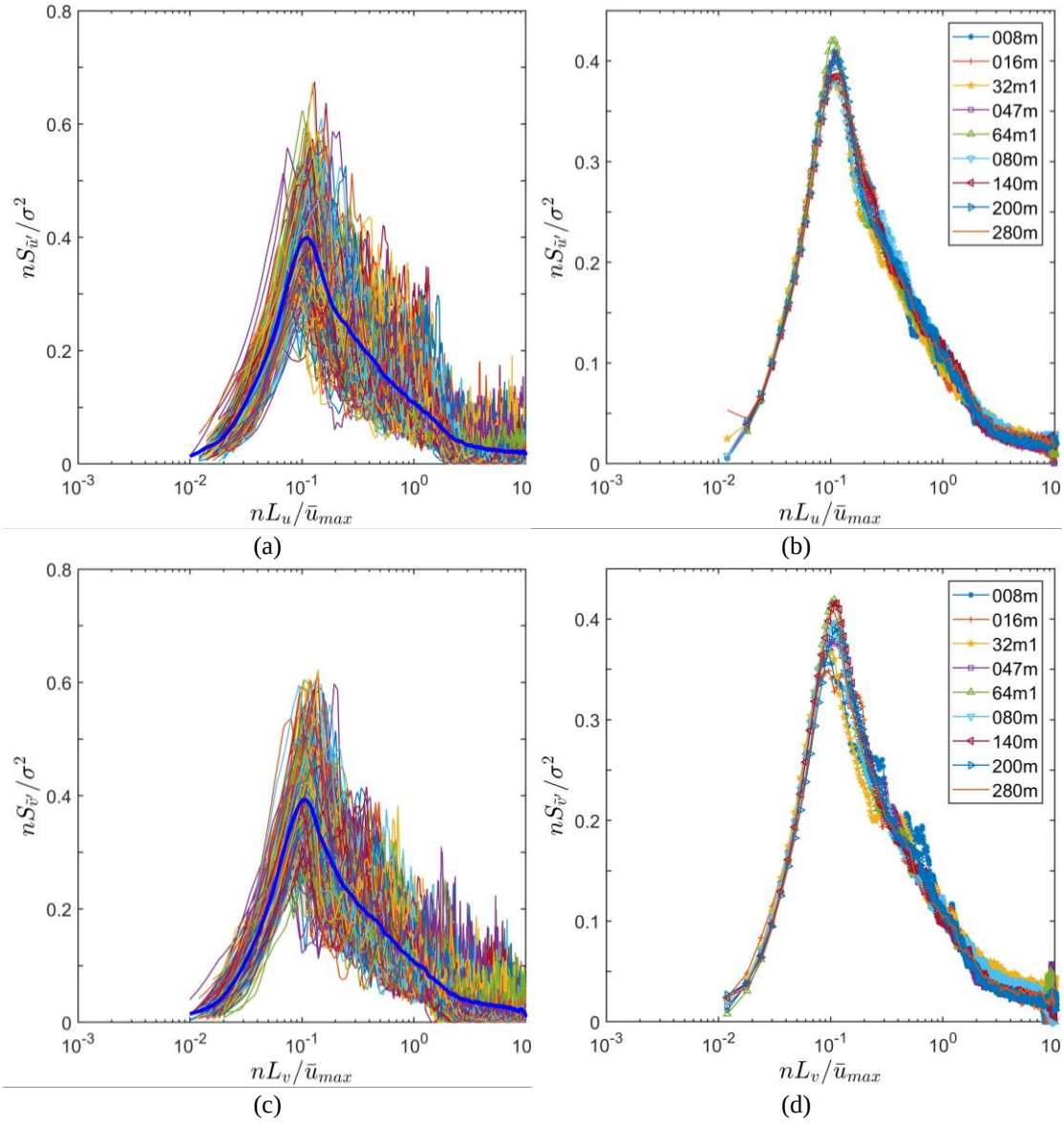

Figure 7.18 PSD of $\tilde{u}'$ (a, b) and $\tilde{v}'$ (c, d) for different records (a) (c) and their mean value (b) (d) for every anemometer as a function of $f = nL/\bar{u}_{max}$.

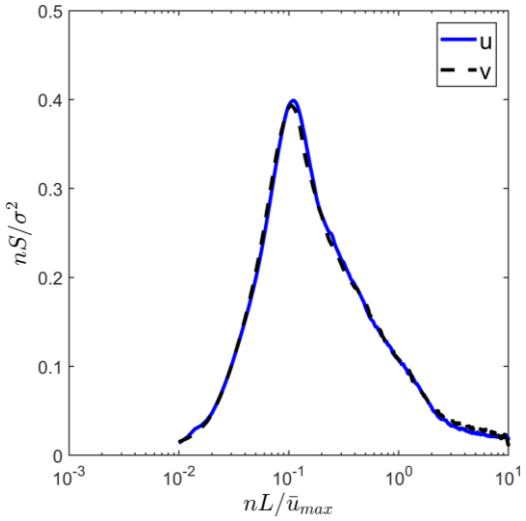

Figure 7.19 Mean value of PSD of $\tilde{u}'$ and $\tilde{v}'$ for different records as a function of $f = nL/\overline{u}_{max}$.

7.5.6 Turbulence intensity modulation

In the light of **Eq. (4.24)**, though $\tilde{u}'(t)$ and $\tilde{v}'(t)$ are well represented by Gaussian (rapidly-varying) random processes, $\mu_u(t)\tilde{u}'(t)$ and $\mu_v(t)\tilde{v}'(t)$ are non-Gaussian random processes due to their factorization by means of the non-Gaussian (slowly-varying) random processes $\mu_u(t)$ and $\mu_v(t)$. The mean value and the std of the mean, standard deviation, skewness and kurtosis of $\mu_u(t)\tilde{u}'(t)$ and $\mu_v(t)\tilde{v}'(t)$, shown in **Table 7.9**, exhibiting some differences between their statistical moments. **Figure 7.20** illustrates the detachment between the PDF of $\mu_u(t)\tilde{u}'(t)$ and $\mu_v(t)\tilde{v}'(t)$ and the reference Gaussian models. **Figure 7.21** shows that the PSD of $\mu_u(t)\tilde{u}'(t)$ exhibits some slight differences from the PSD of $\mu_v(t)\tilde{v}'(t)$, mostly limited to the low-frequency harmonic content. The PSDs of $\tilde{u}'(t)$ and $\tilde{v}'(t)$ are very close to the PSDs of their modulations. These results perfectly match the results obtained for the thunderstorm outflows in the northern Mediterranean.

Table 7.9 Ensemble Mean and Std values of the mean, standard deviation, skewness and kurtosis (m, σ, γ, κ) of $\mu_u(t)\tilde{u}'(t)$ and $\mu_v(t)\tilde{v}'(t)$.

	Parameter	m	σ	γ	κ
$\mu_u\tilde{u}'$	Mean	0.009	1.106	-0.150	4.874
	Std	0.047	0.064	0.437	2.502
$\mu_v\tilde{v}'$	Mean	-0.003	1.098	-0.026	4.694
	Std	0.030	0.059	0.300	1.483

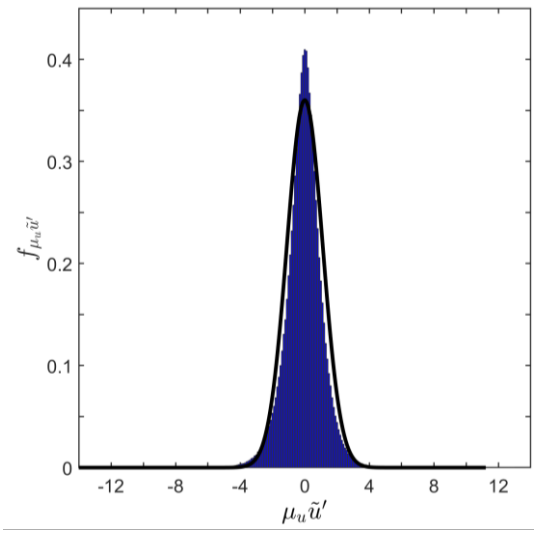

(a)

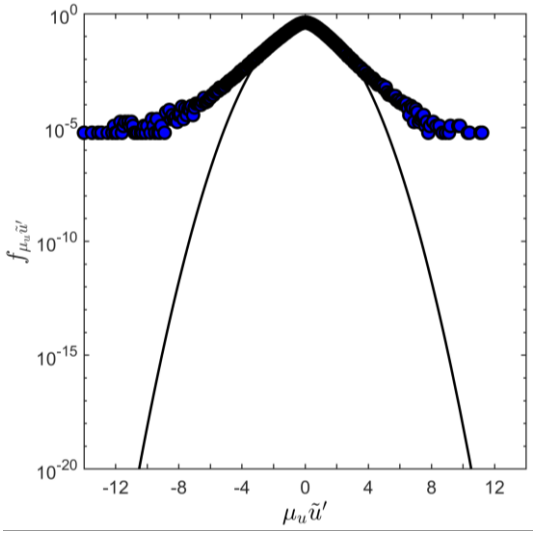

(b)

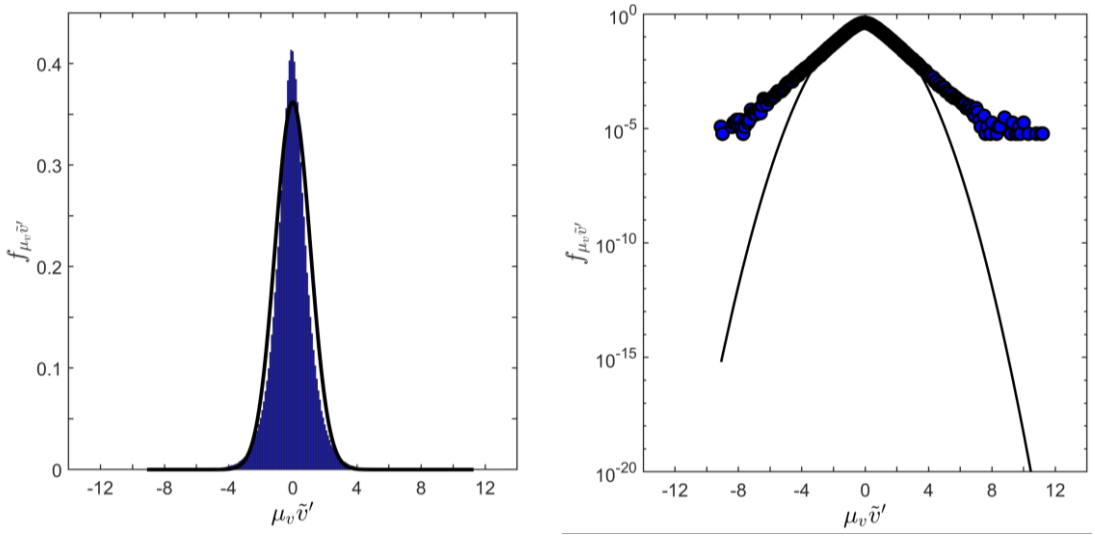

(c) (d)

Figure 7.20 PDF of $\mu_u(t)\tilde{u}'(t)$ and $\mu_v(t)\tilde{v}'(t)$: decimal (a) (c) and logarithmic (b) (d) ordinate.

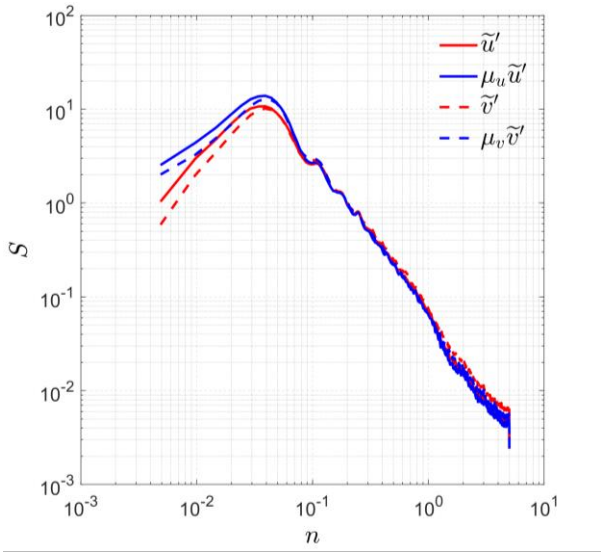

Figure 7.21 Ensemble PSD of $\tilde{u}'$, $\mu_u\tilde{u}'$, $\tilde{v}'$ and $\mu_v\tilde{v}'$.

7.5.7 Gust factor

The gust factor, G_u, based on the directional decomposition approach is expressed by the **Eq. (4.25)**. This quantity plays a key role in the thunderstorm loading and response of structures (Solari et al., 2015, 2016 and 2017).

Table 7.10 summarizes the mean value and the cov of G_u. The mean value of G_u exhibits a clear decrease on increasing the height AGL, while there is no apparent correlation between the cov and the height. It is worth noting that the mean values of G_u detected by the anemometers 1-4 of the Being Tower, those close to the ground, are much larger than those related to the thunderstorm outflows detected at similar heights in the northern Mediterranean (Zhang et al., 2019). Similarly to the turbulence

intensities, as better explained below, this may be due to the fact that in the latter case the thunderstorm outflows mainly come from the sea whereas the Beijing tower is embedded in an urban area.

Table 7.10 Mean values and covs of three wind velocity ratios for thunderstorms

Anem. No.	1	2	3	4	5	6	7	8	9	All
h (m)	8	16	32	47	64	80	140	200	280	-
Mean(G_u)	1.72	1.47	1.42	1.36	1.30	1.28	1.21	1.15	1.17	1.72
Cov(G_u)	0.17	0.09	0.10	0.16	0.09	0.10	0.11	0.07	0.18	0.17

Figure 7.22 (a) and **(b)** show the gust factor as a function of h/z_0 and $\bar{u}_{max}$, respectively. According to **Figure 7.22 (a)**, the gust factor exhibits a slight decrease on increasing h/z_0. **Figure 7.22 (b)** shows that the gust factor G_u clearly decreases on increasing $\bar{u}_{max}$. Both these trends match the results of the previous analyses carried out in the northern Mediterranean. In addition, focusing on the gust factors associated with similar values of h/z_0, between 10^1 and 10^2, the agreement with the Mediterranean outcomes is definitely better.

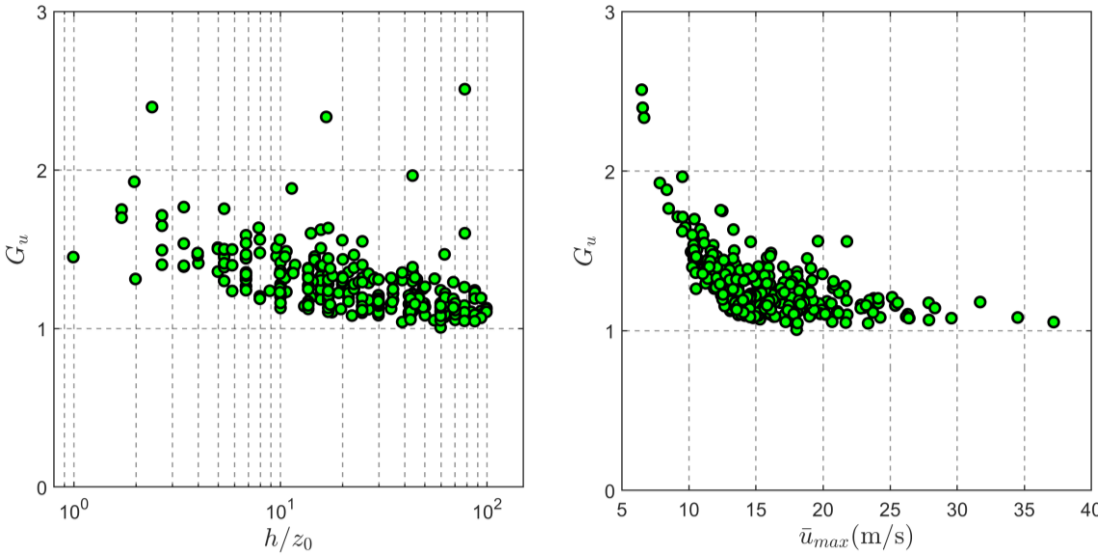

(a) (b)

Figure 7.22 Gust factor for thunderstorm outflows as functions of h/z_0 (a) and $\bar{u}_{max}$ (b).

7.6 Wind speed time-scale structure for a thunderstorm outflow event

Thunderstorm outflows give rise to wind velocity fields that are deeply different from the classical boundary layer wind fields produced by synoptic events. Although many measurements have been carried out of the wind speed in the course of downbursts, most of them are provided by single instruments whereas few simultaneous dense measurements are still available to reconstruct the wind field. The ultrasonic anemometers mounted at nine different heights along the meteorological Beijing

tower from 8 m to 280 m AGL provide a unique opportunity to inspect the time-space (vertical) structure of the wind fields generated by thunderstorm outflows. Herein, a preliminary description of a typical thunderstorm outflow event detected on June 10, 2016 is provided. Systematic analyses of the whole dataset described in section 4 are currently in progress and will be illustrated in future papers.

Figure 7.23 and **Figure 7.24** show the 1-h time history records registered by the anemometers placed at 64 and 140 m heights. Pictures **(a)**, **(b)** and **(c)** show the time-series of the wind speed, direction and temperature raw data, respectively; they also provide their mean values over 1-h (solid lines), and 10-min (dotted lines) periods. In addition, picture **(a)** shows the 1-s peak wind speed (red circle), the 30 s slowly-varying mean wind velocity (cyan line) and its maximum value (pink square).

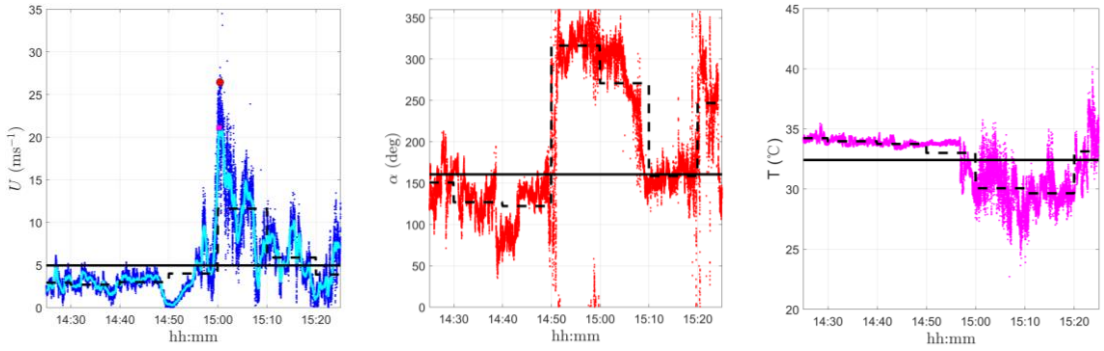

(a) (b) (c)

Figure 7.23 Thunderstorm outflow recorded on 10 June 2016 by the 64 m anemometer: (a) 1-h wind speed time-series; (b) 1-h wind direction time-series; (c) 1-h temperature time-series.

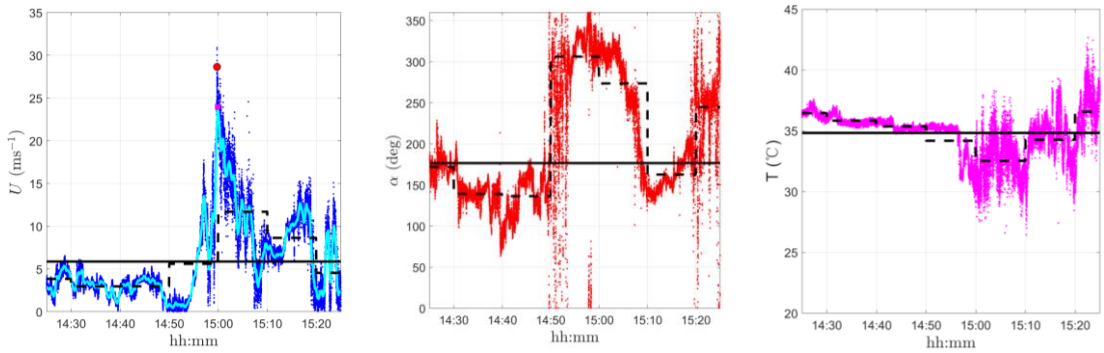

(a) (b) (c)

Figure 7.24 Thunderstorm outflow recorded on 10 June 2016 by the 140 m anemometer: (a) 1-h wind speed time-series; (b) 1-h wind direction time-series; (c) 1-h temperature time-series.

The records depicted by **Figure 7.23** and **Figure 7.24** show a rapid and intense jump of the wind velocity coupled with a direction shift of about 180 deg and a temperature drop of about 5 ℃. These typical features of a thunderstorm outflow are strengthened by a careful weather survey that confirmed the simultaneous presence of thunderstorms on the Beijing area.

The next three sub-sections deal with the wind speed profile (**section 7.61**), the turbulence intensity (**section 7.62**), and the integral length scale (**section 7.63**). Spectral analyses are postponed to future papers.

7.6.1 Wind speed profiles

Figure 7.25 shows the 30-min time histories of the slowly-varying mean wind speed **(a)** and direction **(b)** at 9 different heights for the thunderstorm outflow event examined here; these records are centered around the most intense wind speed. It is worth noting that the sudden and intense jump of the wind speed occurs for all the records, and all of them exhibit evident direction shifts. In particular, a rapid wind rotation clockwise about 200 degrees occurs at around 14:50, when the wind speed begins to increase, followed by a second rapid rotation anti-clockwise about 100 degrees at around 15:09, when the wind speed decreases.

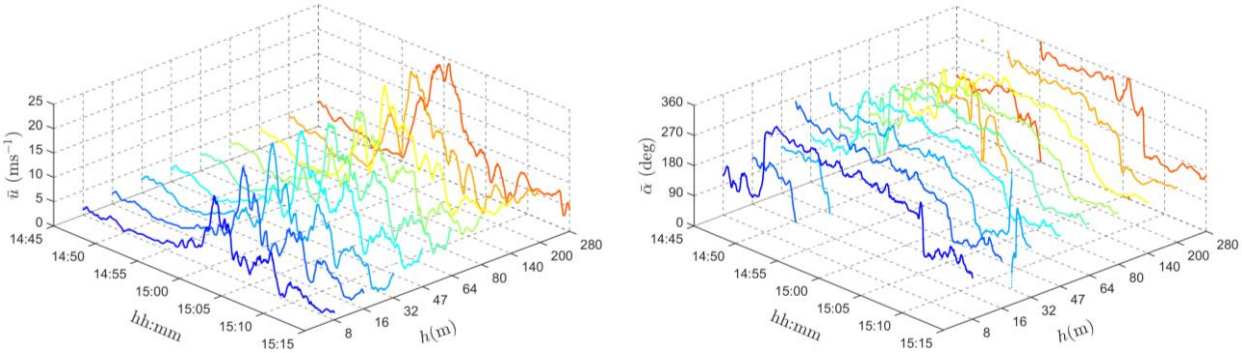

(a) (b)

Figure 7.25 30-min slowly-varying wind speed (a) and direction (b) detected by 9 anemometers for a thunderstorm outflow event at June 10, 2016.

Table 7.11 shows, for each anemometer, the maximum values of the slowly-varying mean wind speed $\bar{u}_{max}$ and of the peak wind speed $\hat{u}$, together with their occurrence times, for each anemometer in the 30 minutes corresponding to **Figure 7.25**. Neither $\bar{u}_{max}$ nor $\hat{u}$ exhibit a regular trend although $\bar{u}_{max}$ seems to increase with the height more regularly than $\hat{u}$. The time elapsed between the earliest and latest occurrence of $\bar{u}_{max}$ for the 9 records detected is 64 s (between 200 m and 8 m); similarly, the time elapsed between the earliest and latest occurrence of $\hat{u}$ is 65 s (between 280 m and 32 m). The time elapsed between $\bar{u}_{max}$ and $\hat{u}$ for the same record falls in the range between 6 and 14 s for the anemometers up to 140 m height whereas it increases between 41 and 57 s for the two highest anemometers.

Table 7.11 Maximum values of the moving average wind speed and gust factors in 1 hour for the event.

No.	1	2	3	4	5	6	7	8	9
h (m)	8	16	32	47	64	80	140	200	280
$\bar{u}_{max}$	15.21	18.82	21.50	21.66	20.81	21.19	23.77	24.12	24.11

$t(\bar{u}_{max})$	15:00:40	15:00:38	15:00:37	15:00:35	15:00:18	15:00:51	14:59:56	14:59:36	15:00:38
$\hat{u}$	21.29	27.35	27.10	28.25	26.39	26.24	28.60	28.31	28.99
$t(\hat{u})$	15:00:26	15:00:25	15:00:46	15:00:29	15:00:26	15:00:02	14:59:45	15:00:17	14:59:41

Figure 7.26 shows the slowly-varying mean wind speed $\bar{u}$ **(a)** and direction $\bar{\alpha}$ **(b)** profiles in the same 30 minutes depicted in **Figure 7.25**. The sudden changes of the mean wind speed and direction can be observed very clearly. In particular, at about 15:00, when the spike of the wind speed occurs, the scheme **(a)** points out a colour change that does not correspond to the monotonic increase of the mean wind speed with the height, which is a typical property of a boundary layer wind profile. **Figure 7.27** clarifies the evolution of the mean wind speed **(a)** and direction **(b)** profiles, showing them at selected instants.

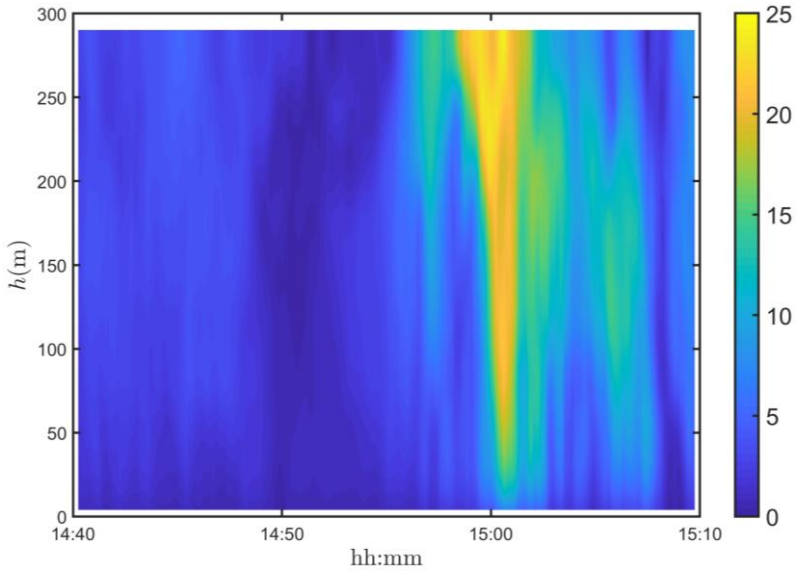

Figure 7.26 30-min time varying wind speed profiles for the thunderstorm outflow event.

The slowly-varying mean wind speed $\bar{u}$ and direction $\bar{\alpha}$ change slightly with height between 14:45 and 14:49, before the thunderstorm event; in this period the magnitude of $\bar{u}$ is relatively small and $\bar{\alpha}$ keeps values lower than 180 deg. At the beginning of the ramp-up phase, namely between 14:51 and 14:55, $\bar{u}$ shows a zigzag trend as a function of height, while $\bar{\alpha}$ changes with the time and the height; more precisely, it is larger than 270 deg for the lower heights and smaller than 180 deg for the higher levels. From 14:55 to 14:59, the $\bar{u}$ value related to the higher heights increases quickly while it keeps smaller values for the lower heights; in the meanwhile, $\bar{\alpha}$ assumes values in the range between 270 and 350 deg.

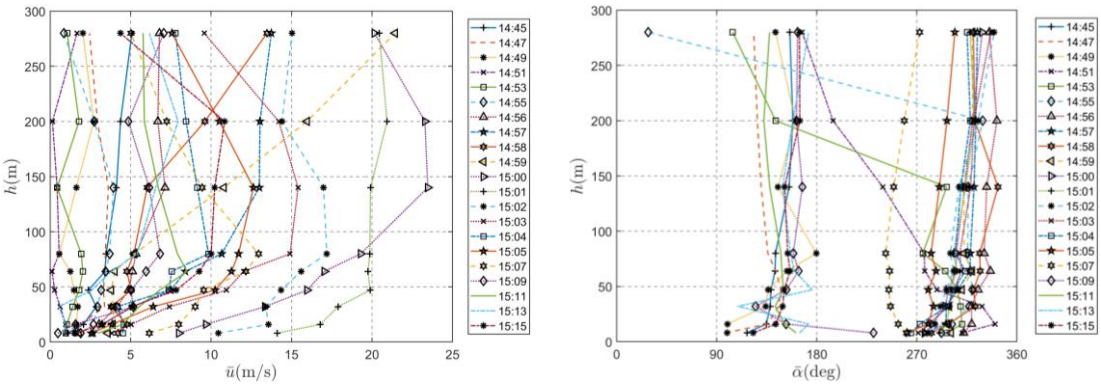

(a) (b)

Figure 7.27 Mean wind speed profile for the thunderstorm outflow at selected instants.

The "nose shape" profile of the slowly-varying mean wind speed (Hjelmfelt, 1988) appears very clearly at 15:00, in proximity of the peak wind speed. At this time, $\bar{u}_{max}$ exhibits its maximum value at 140 m height. Later on the wind speed decreases, the nose shape profile becomes less clear and the height at which $\bar{u}_{max}$ is maximum decreases. After 15:04, the passage of the gust front is mostly concluded. In this period no significant change of direction occurs at different heights. After 15:09, when the mean wind speed becomes very small, the mean wind direction returns to be lower than 180 deg; in particular, it varies a lot with the height near the ground and keeps almost constant values as the height increases.

The sudden appearance and the rapid dissolution of the nose-shape profile of the slowly-varying mean wind velocity is consistent with some LiDAR measurements of the thunderstorm outflows detected in the northern Mediterranean (Burlando et al., 2017b).

7.6.2 Turbulence intensity

Figure 7.28 (a) and **(b)** show the vertical profile of the slowly-varying turbulence intensities at selected instants densely distributed around the occurrence of the peak wind speed. **Figure 7.28 (c)** and **(d)** show the vertical profiles of the mean values of the turbulence intensities over 10-min periods centred on the selected instants. Of course, the latter exhibit a more regular trend and a reduced scatter of values. As described in section 6.3, their abnormal large values and even sharp peaks are disregarded; therefore, in **(a)** and **(b)**, some values are not present.

In the examined case, the longitudinal and lateral turbulence intensities grow during the passage of the gust front. During this period they exhibit a zigzag trend with the height, especially close to the ground. As far as concerns the mean values of the turbulence intensities, both the longitudinal (c) and lateral components (d) show variable trends close to the ground, while they decrease on increasing the height. It seems reasonable to assume that the above described behaviour depends on the urban environment and on the average height of the buildings surrounding the Beijing tower.

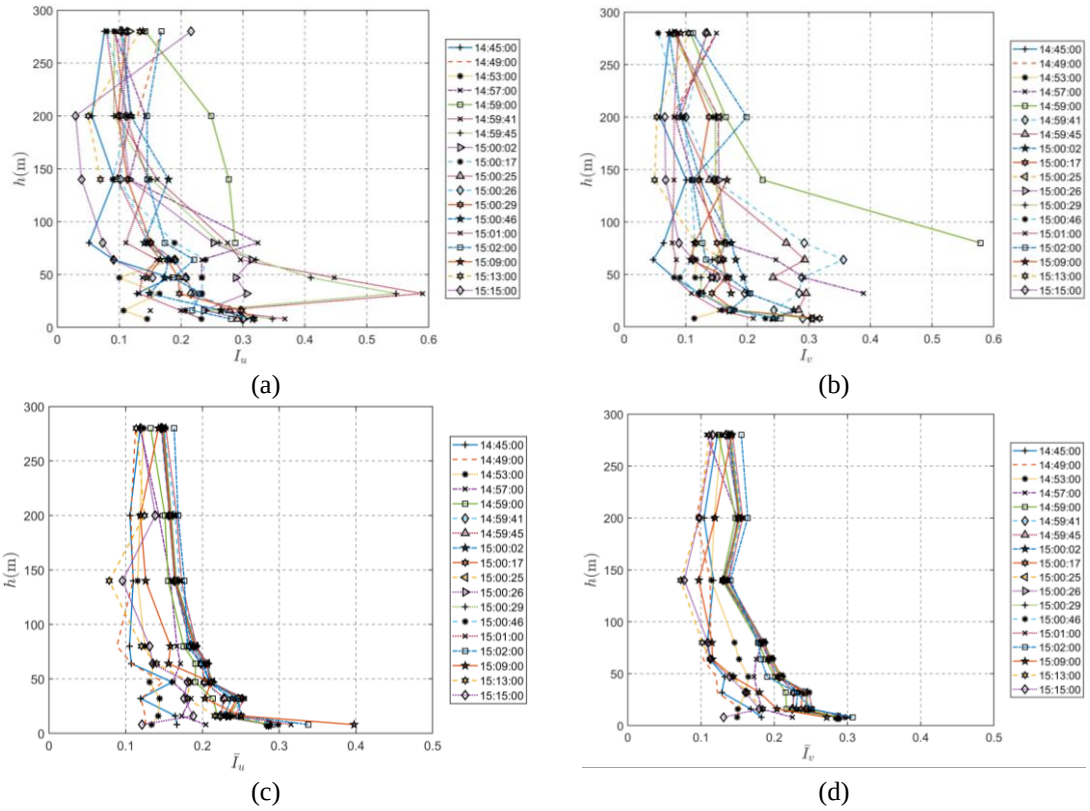

Figure 7.28 30-s slowly-varying turbulence intensity (a) (b) and the 10-min mean turbulence intensity (c) (d) at selected instants for the longitudinal and lateral components.

7.6.3 Turbulence integral length scale

Figure 7.29 shows the vertical profile of the longitudinal and lateral turbulence integral length scales of $\tilde{u}'$ and $\tilde{v}'$, L_u and L_v, at the same selected instants used for **Figure 7.28**.

In the examined case, the longitudinal and lateral turbulence integral length scales grow during the passage of the gust front; this behaviour confirms the trend exhibited by **Figure 7.17 (b)** according to which L_u and L_v increase on increasing the mean wind speed. In this period zigzag vertical profiles occur along the whole range of the height. On increasing the height, L_v becomes a little bit larger than L_u, while L_u is larger than L_v close to the ground. Probably, this trend depends by the peculiarities of the examined event and by the typical scatter of values exhibited by the integral length scale.

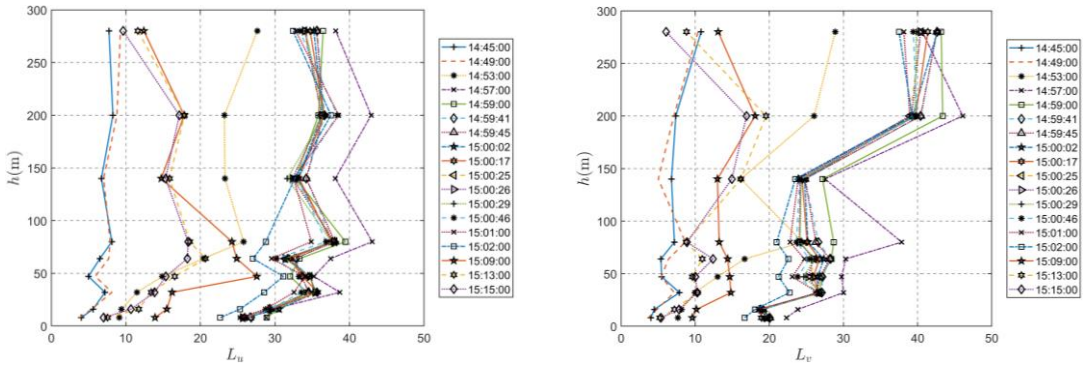

(a) (b)

Figure 7.29 Longitudinal and lateral integral length scales L_u (a) and L_v (b) as a function of h at selected instants.

7.7 Conclusions

This chapter firstly introduces the characteristics of the 325m high meteorological tower in Beijing and the properties of the anemometers installed over the tower. Then it describes the Beijing climate and the database generated by nine ultrasonic anemometers placed at different heights from 8 m to 280 m along the tower. It then illustrates the procedure used to separate the records associated with different wind phenomena. Thanks to this procedure, 314 records corresponding to 70 events labelled as thunderstorm outflows are selected. They represent a good opportunity to study the properties of the thunderstorm outflows in the Beijing urban area and their main characteristics relevant to wind engineering, with special concern for wind actions on structures. They also provide a unique chance to compare such properties with those of the thunderstorm outflows detected in the northern Mediterranean, and to give a preliminary answer to the crucial question whether thunderstorms have similar properties in different areas. The study is carried out through a novel directional signal decomposition strategy, dealing with the records detected by different anemometers as disjoint from each other.

First of all, it is worth noting that the Beijing meteorological tower and the Northern Mediterranean monitoring network have very different properties. First of all they are placed in totally different parts of the planet. The former is embedded in an urban environment and all the instruments are put along a vertical line between 8 and 280 m above the ground level. The latter includes isolated anemometers, mainly placed between 10 and 30 m height, that are distributed along the coast, with the sea on one side and an urban context on the other, frequently involving complex topographic features. On the other hand, in both the sites the anemometers are ultrasonic sensors with a sampling rate of 10 Hz, a comparable period of measurements, around 5 years, is examined, the gathered records are analysed by means of the same procedure and by the same persons. In their whole, the analyses show some differences, several analogies and many identical trends.

The slowly varying mean wind velocity at the Beijing tower shows the essential

features of a ramp-up stage followed by ramp-down stage corresponding to the passage of a gust front. The duration of this passage is similar to that observed in the northern Mediterranean close to the ground whereas on increasing the height above the ground the duration of the most intense part of the thunderstorm outflows increases. This aspect deserves further investigations.

The turbulence intensities at the Beijing tower show, close to the ground, much greater values than those observed in the northern Mediterranean; probably, this is due to the fact that in the latter case the thunderstorm outflows mainly come from the sea whereas the Beijing tower is embedded in an urban area. In addition, the Mediterranean thunderstorms exhibit a quicker variation that probably do not favour the development of a boundary layer flow in equilibrium with the local roughness. Despite this remark, comparing measurements involving similar ratios between the height of the anemometer and the roughness length, the results seem to be much closer between each other. The gust factor exhibit very similar properties.

As far as concerns the reduced turbulent fluctuations and their integral length scales and spectral density functions, the similarity between the data detected in the Beijing urban area and in the northern Mediterranean is so strong as to seem almost surprising. In both these cases the reduced longitudinal and lateral turbulent fluctuations are stationary Gaussian and uncorrelated, the integral length scales are weakly influenced by the roughness length but sensitive to the wind speed, the parameterization of the power spectral densities as a function of a reduced frequency involving the integral length scale is exceptionally robust. It seems reasonable to assume that these results are favoured by the directional decomposition strategy adopted here.

Pending the systematic processing of the entire data base to study the space-time structure of the thunderstorm outflows recorded at the Beijing meteorological tower, some preliminary analyses have been carried out with respect to a sample event. They show the occurrence of the nose profile of the slowly-varying mean wind velocity for a short time interval in proximity of the peak wind speed. They also show, perhaps for the first time, evolutionary profiles of the turbulence intensities and integral scales that highlight the intensification of these quantities near the peak and confirm the complexity of the phenomenon under examination.

It clearly emerges that the disjoint analysis of single wind speed records provides essential elements for the statistical description of the phenomenon as a function of the height above the ground and of other fundamental parameters such as the intensity of the wind speed and the terrain roughness. On the other hand, this analysis cannot clarify the evolutionary properties of the spatial structure of the thunderstorm outflows, a subject that calls for the simultaneous analysis of the records detected by a densely distributed set of anemometers with high sample frequency, namely the instrumentation installed on the Beijing meteorological tower. The development perspectives of the present research are just oriented to this study, an essential issue for understanding this physical phenomenon and for evaluating wind actions and effects on structures due to thunderstorm outflows.

8 Summary and prospect

The wind monitoring network realized for the European Projects “WP” and “WPS” is an inexhaustible source of measurements that highlight the speed and frequency of transient events, likely of convective thunderstorm outflows, often disregarded, especially in the past, from classical wind engineering. And the exact understanding of thunderstorm and their effects on structures already becomes key topic in wind engineering. This PhD thesis mainly focuses on the separation of different phenomena, the extraction and cataloguing of thunderstorm outflows, the novel analytical models of the thunderstorm wind velocity, the characteristics of thunderstorm related to wind loading on structures in two different areas of the world, the comprehensive analysis of field measurements and weather scenarios related to thunderstorms and the extreme wind speed distribution in a mixed wind climate.

In **Chapter 1** of this thesis, the background, motivation and the expected contribution of the current work are presented. Moreover a brief introduction of thunderstorm and their relevant literature review and the state of the art. It can be found that in spite of these previous research, there are still no uniform model for thunderstorm due to their complex properties and the limited data. All of these information lead to research aims and objectives of the thesis.

Chapter 2 is dedicated to the description of the monitoring networks in northern Mediterranean Sea supported by European projects “WP” and “WPS” and the wind dataset with the high resolution contributing to the research of the thesis. In which, the data available with the sample frequency of 10 Hz provided by 14 sensors from 2010 to 2016 are applied and fundamental for extracting a number of thunderstorm outflow records and carrying out the correct and reliable analyses.

Chapter 3 illustrates the procedure used to separate the records associated with different wind phenomena based on information - stationary and Gaussian features - typical of signal analysis but lacking of meteorological contents. Thanks to this method, 277 records (198 events) labelled as thunderstorm outflows are selected and classified into three families according to the time-scale - 10-min, 1-h, 10-h - over which the transient part of the wind speed develops. Besides, according to the peak wind speed, thunderstorm are separated into 4 groups, which presents no clear correlation between the duration of the most intense part of the record and the peak wind speed. It is worth noting, however, that the four events whose peak wind speed exceeds 30 m/s have a short duration, both of which are dominant for the wind loading and response of structures. Overall, the creation of an extended and controlled dataset of thunderstorm outflow records provides robust and reliable estimates of the statistical properties of their signals and components parts.

In **Chapter 4**, a novel decomposition rule of the horizontal component of the wind speed is proposed, which takes explicitly into account the wind direction and decouples the turbulent fluctuations into longitudinal and lateral components. And it applies to both synoptic winds and thunderstorm outflows, contains the classical decomposition rule for synoptic winds as a particular case, and provides a substantial

generalisation of the decomposition rule classically applied to thunderstorm outflows. The spectral content of the signals and a systematic investigation of their statistical properties with regard to 141 thunderstorm outflow records belong to 10-min family is carried out by both of the classical and novel approaches to evaluating them detailedly. Overall, a dominant property of the new decomposition rule is that it neither cancels nor distorts the knowledge acquired so far with regard to thunderstorms outflows, but extends the information relating thereto. The directional decomposition provides robust and reliable estimates of the statistical properties of their signals and components parts. This represents a fundamental step forward towards the implementation of statistical models of thunderstorm downbursts adhering to the reality of these complex phenomena. Besides, the extraction of the longitudinal and lateral turbulence components as functions of the slowly-varying mean wind direction is strategic for the directional analysis of the dynamic behaviour of structures and for its expression in terms of alongwind and crosswind response.

Chapter 5 is devoted to an interdisciplinary effort involving atmospheric science and wind engineering, with the objective of conducting a comprehensive analysis of field measurements and weather scenarios related to nonsynoptic wind systems in the Mediterranean. First of all, one typical event struck the port of Livorno is investigated as a test case and a first step toward inspecting the potential of this combination coupling the synoptic analysis and the near-surface statistical analysis of the anemometric records, and reconfirming the storm as a wet thunderstorm downburst. Then to decrease the burden making this procedure usable for systematic analyses of historical series of such events, an faster approach that integrates the data provided by an anemometric network, with few essential meteorological information that may qualify, albeit preliminarily, the transient intense wind events detected by the network are carried out according to three intense event belonging to the three families. This is the first step to fill the gap and formulate a novel model of the thunderstorm outflows.

Chapter 6 provides a preliminary but representative contribution to the analyses of extreme wind speed distribution in a mixed climate. The analyses carried out are based on the continual measured data detected by 4 anemometers in two ports in order to establish a preliminary but robust procedure and discuss its outcomes concisely. Based on the independent extreme wind speeds selected, the extreme distribution of the peak wind speed is completed by the Type I extreme value model and mixed statistics. It can be found that the wind events with a high return period, the most important for structural safety, are always related to thunderstorm phenomena at least in the seaport areas examined here. Even though they do not seem to be so relevant for assessing extreme wind speeds according to this study, the mixed extreme distribution asymptotically tends to coincide with thunderstorm distribution for high return periods and always provides the highest extreme wind speed values, while the ensemble of all the extremes into a single set underestimates the extreme peak wind speed especially for high return periods, which confirms the necessity of this research. In general the obtained characteristic, weather scenarios and statistics of thunderstorm outflow can provide a reliable description of this complex phenomenon.

Chapter 7 is the application and extension of the above analysis procedure to a dataset detected by the anemometers on Beijing 325m meteorological tower. The favorable feasibility can be found and a new catalogue of thunderstorm outflows is created. It also provides robust and reliable estimates of the statistical properties of their signals and components parts according to the novel directional decomposition approach. In the whole, the analyses show some differences, several analogies and many identical trends. This extends and modifies doubtlessly the existing cognition about these complex phenomena. And the understanding of their key characteristics of major interest for evaluating the wind load on structures in the Beijing urban area and comparison with that in the northern Mediterranean are the fundamental step to carry out a unitary model and analyze systematically the response of structures to thunderstorm outflows in different areas along the longitudinal and lateral direction. In addition, the space-time structure of a sample event are analyzed preliminarily herein, which confirms confirm the complexity of the phenomenon under examination and is the base of the systematic processing of the entire data of the thunderstorm outflows recorded at the Beijing meteorological tower. This contributes to an essential issue for understanding this physical phenomenon and for evaluating wind actions and effects on structures due to thunderstorm outflows.

In general, this thesis creates an unprecedented catalogue of thunderstorm outflow. And a novel directional decomposition approach is proposed, based on which the outflow signals are decomposed into component functions and statistical averages are evaluated. Besides, a wide collection of information is gathered to classify the weather scenarios in which several typical thunderstorms occur and the relevant research is carried to link weather scenarios and wind speed data. Furthermore the probability distributions of extreme wind speed considering thunderstorm outflows in mixed climate are carried out emphasizing the dominance of this intense storm on the design wind velocity. At the end of the research, this analysis procedure is preliminarily applied and extended to the measurement in Beijing tower, which is the first step to understand if this phenomena are similar in different areas of the world. All of these provide a preliminary but comprehensive learning about this phenomena veritably, which can be used to support the creation of a systematic and reliable model of thunderstorm.

There are more investigations worth to do in the future in order to refine the current research, learn the phenomenon in detail, make building safer and more sustainable, and bring about a profound impact on society and its economy:

(1) Thunderstorm detecting

The unprecedented wind monitoring network created by two previous EU projects will be enhanced by a novel LiDAR aiming to detect the position, diameter, direction, and translational speed of downbursts. A semiautomatic expert system can be realised and calibrated through the study of weather scenarios to separate different wind events. Novel catalogues will be created as the more and more data detected that list

the refined parameters of each event and the series of the extended and more controlled independent extreme wind speed values.

(2) Application of the novel signal decomposition

The novel directional decomposition rule of the wind speed discloses several research prospects in many different fields. First, it creates a common background to model and to analyse the wind speed of both synoptic events and thunderstorm outflows. It represents a fundamental step forward towards implementing thunderstorm models adhering to the reality of these complex phenomena. A clear evaluation of the direction shift of thunderstorm outflows is fundamental to recognize the travelling nature of downbursts and to reconstruct their evolution. The decoupling of the longitudinal and lateral turbulence components also for thunderstorm outflows is crucial to inspect the dynamic behaviour of structures in terms of alongwind and crosswind response. The explicit extraction of the slowly-varying mean wind direction opens the doors to take into account the evolution of the angle of attack of the wind speed in the course of transient wind events; this may be crucial for problems dominated by aerodynamic and aeroelastic features.

(3) Characteristic

The author of the thesis wishes to point out five key issues that go beyond this specific topic: 1) the interaction between the downburst and the background flow, and the possibility of separating their effects; 2) the role of the terrain roughness, especially close to the ground; 3) the shape of the slowly-varying mean wind velocity profile, with special regard to its evolution on time; 4) the time-varying coherence function between different heights during a thunderstorm outflow; 5) the extension to more thunderstorm outflows recorded in different areas of the world and repeating these analyses in many areas to understand if thunderstorms are similar or not in different parts of the world, which is crucial to define a uniform model of thunderstorms and study their effects on structures.

(4) Weather scenario

The high-sampling-rate wind speed records detected within a typical wind engineering framework have proven to be beneficial in analyzing thunderstorms. Several outcomes from the atmospheric science framework were later refined using the information provided by the local anemometric network and signal analysis. The present study may therefore form the basis for an extended analysis of nonstationary events in the Mediterranean region using this mixed approach in correlation with the extensive database gathered during the “WP” and “WPS” campaigns. The first implication of this kind of analysis will be its systematic extension to a selection of the most severe wind events recorded by the “WP” and “WPS” anemometric network, aiming to distinguish on a statistical basis the events related to convection. The identification of a statistically relevant set of convectively forced severe wind events will represent the starting point for a novel research effort aimed at establishing a

robust link between the aforementioned local records and the weather scenarios in which they occur. In turn, this procedure will show to what extent the anemometric records and the meteorological surveys may jointly be used to determine the location of origin, size, and motion pattern of thunderstorms. The second implication of this research program is strengthening the link between field measurements and analytical, physical, and numerical simulations through the systematic statistical analysis of a broad range of transient events for which high quality measurements are made available. It is fundamental that such evaluations are carried out within the framework of wind tunnel tests and CFD simulations that may establish a closed loop inside which the simulations are used to refine our knowledge of the structure of thunderstorm events detected through local measurements, whereas local measurements are used to calibrate experiments and numerical techniques.

(5) Extreme wind speed distribution

The prospects for improving these analyses on extreme wind speed distribution relate to three different issues. The first focuses on gathering and analysing new data to strengthen and refine the results above. However, in this way, only the passage of a lot of time may really produce relevant improvements deriving from assembling richer datasets and using refined statistical models, which are unjustified at this stage due to the scarcity of available data. The second consists of pursuing a different strategy based on collecting and analysing the set of the data detected by different anemometers in the same seaport area together, in order to create statistical models of the extreme wind speed that take into account the frequency of occurrence and the plan distribution of thunderstorm outflows with different intensity. The third deals with comprehension of intermediate events with reference to the meteorological viewpoint even before their statistical assessment. In any case further research is necessary.

In conclusion, further research is necessary. As more and more scholars pay attention to the importance of thunderstorm research and the increase of thunderstorm data around the world, the author of this thesis hopes that a unified thunderstorm model will be established in the near future to avoid the disaster caused to human survival. Finally, due to the limited level of the author, there may be shortcomings and mistakes in the thesis. I sincerely request your esteemed review experts and colleagues to criticize and correct.

Appendix A Supplementary data

Table 1 Extreme wind speeds detected in extra-tropical cyclones by LI_01.

No.	Date	Time	$\widehat{U}$	$\overline{U}_{max}$
1	20101031	21:00	20.34	16.12
2	20101108	12:40	23.45	21.34
3	20101110	13:40	22.07	20.02
4	20101126	9:40	20.20	17.69
5	20101201	18:00	20.93	19.16
6	20101203	21:40	21.05	19.30
7	20110121	15:10	21.42	15.42
8	20110301	12:00	22.41	18.60
9	20110307	9:20	21.40	15.55
10	20110919	13:50	21.35	19.12
11	20111007	8:50	20.88	18.94
12	20111015	0:10	22.20	15.93
13	20111025	14:50	20.16	14.40
14	20111205	11:10	22.05	19.76
15	20111216	22:10	33.01	28.20
16	20120106	6:10	24.97	23.02
17	20120210	7:40	22.20	16.40
18	20120424	6:30	20.89	18.39
19	20120912	17:20	22.49	19.65
20	20121105	10:30	22.47	19.85
21	20121204	9:50	23.93	20.35
22	20121227	16:30	21.00	18.56
23	20130122	5:40	22.48	17.97
24	20130318	18:00	27.78	24.32
25	20130524	5:00	22.40	20.55
26	20130530	5:50	20.79	19.05
27	20130916	22:20	20.48	18.13
28	20131010	22:00	22.21	19.48
29	20131110	12:30	22.84	19.81
30	20131121	2:30	22.24	19.19
31	20131202	14:10	24.15	18.65
32	20131225	23:40	22.82	18.75
33	20140206	0:30	23.54	22.18
34	20140209	16:20	20.21	18.23
35	20140214	0:40	21.97	19.80
36	20140323	14:10	22.94	20.72

37	20140708	18:00	21.55	19.10
38	20160207	14:20	20.30	16.59
39	20160209	19:10	22.82	17.82
40	20160302	23:30	23.31	20.86
41	20160305	12:10	24.56	17.18
42	20161106	19:40	25.15	22.75
43	20161129	2:40	21.64	17.16
44	20170113	9:30	25.05	22.44
45	20170118	21:00	23.61	18.07
46	20170204	15:40	20.98	18.36
47	20170228	23:00	21.74	18.98

Table 2 Extreme wind speeds detected in extra-tropical cyclones by LI_02.

No.	Date	Time	$\hat{U}$	$\bar{U}_{max}$
1	20101108	10:30	23.47	19.70
2	20101110	13:40	22.80	20.46
3	20110301	11:00	21.35	17.91
4	20110527	19:30	20.51	14.44
5	20110605	14:30	20.36	18.14
6	20110919	13:40	22.13	18.83
7	20111007	7:30	21.45	18.00
8	20111205	15:40	24.51	18.63
9	20111216	22:20	31.49	24.27
10	20120106	9:00	21.17	16.34
11	20120131	21:50	27.43	19.21
12	20120210	8:30	22.66	18.75
13	20120309	10:30	20.36	16.16
14	20120418	10:50	20.13	17.31
15	20120424	6:20	20.36	15.88
16	20120912	17:10	23.07	18.07
17	20121105	10:20	23.67	19.23
18	20121202	18:20	22.93	19.69
19	20121204	10:40	24.74	18.54
20	20121227	17:10	21.54	16.48
21	20130122	4:10	22.44	19.27
22	20131110	12:20	22.37	19.84
23	20131121	2:20	25.26	20.24
24	20131202	14:20	23.99	19.49
25	20131225	19:10	24.11	19.21
26	20140206	0:30	22.74	19.96
27	20140209	16:10	20.77	17.86

28	20140214	0:30	23.10	17.91
29	20140708	17:50	23.08	17.36
30	20150305	0:40	24.95	19.44
31	20150923	8:10	20.26	16.28
32	20151016	2:50	22.56	18.56
33	20160210	4:00	28.47	23.43
34	20160302	23:10	22.79	19.46
35	20160305	12:50	23.08	18.37
36	20160427	3:40	20.05	17.51
37	20160523	15:00	22.81	16.16
38	20160713	18:10	21.99	15.78
39	20161106	19:50	26.08	19.52
40	20161129	2:50	20.09	17.22
41	20170113	12:50	25.23	21.31
42	20170118	21:40	23.18	19.28
43	20170204	16:20	21.84	17.99
44	20170228	23:50	22.57	17.17

Table 3 Extreme wind speeds detected in extra-tropical cyclones by SP_02.

No.	Date	Time	$\widehat{U}$	$\overline{U}_{max}$
1	20101129	5:00	20.66	16.00
2	20111007	4:30	21.85	18.55
3	20111020	0:30	22.29	14.19
4	20111205	3:50	23.74	19.65
5	20111216	10:40	25.97	20.87
6	20120424	6:00	23.08	16.20
7	20131103	11:00	23.76	18.82
8	20131225	21:00	21.13	17.08
9	20160209	20:20	22.58	14.97
10	20160302	20:00	21.17	17.57

Table 4 Extreme wind speeds detected in extra-tropical cyclones by SP_03.

No.	Date	Time	$\widehat{U}$	$\overline{U}_{max}$
1	20111007	5:20	20.44	16.15
2	20111205	3:00	20.69	17.01
3	20120210	6:10	20.83	16.17
4	20120424	5:40	23.38	20.81
5	20130205	22:30	22.35	17.13
6	20131010	20:50	22.97	18.82
7	20131111	22:00	26.54	20.27

8	20131201	11:40	21.57	16.99
9	20131225	20:40	24.25	20.80
10	20140209	2:20	20.98	17.39
11	20141104	22:10	20.82	14.49
12	20150305	0:30	24.86	18.88
13	20160209	20:10	25.14	19.76
14	20160302	20:00	20.08	17.40
15	20160305	12:40	21.06	18.02

Table 5 Extreme wind speeds detected in thunderstorm outflows by LI_01.

No.	Date	Time	$\widehat{U}$ (m/s)	$\overline{U}_{max}$ (m/s)
1	20101108	19:00	22.70	20.08
2	20110904	15:50	22.83	20.98
3	20111216	22:50	33.65	27.58
4	20121111	5:00	22.87	16.07
5	20121202	18:20	27.30	25.72
6	20130525	13:00	20.57	18.33
7	20131121	23:30	20.49	18.76
8	20140323	21:40	24.01	21.51
9	20140721	3:40	21.05	18.22
10	20141013	14:30	22.78	20.69
11	20141116	0:30	23.44	21.38
12	20141117	20:10	21.48	18.32
13	20141227	15:50	28.50	25.37
14	20151004	5:10	22.03	19.15
15	20151015	22:20	23.74	21.96
16	20151016	1:40	25.75	23.34
17	20151016	2:00	23.30	20.25
18	20160906	17:40	22.14	19.07
19	20170113	13:20	21.92	19.87

Table 6 Extreme wind speeds detected in thunderstorm outflows by LI_02.

No.	Date	Time	$\widehat{U}$ (m/s)	$\overline{U}_{max}$ (m/s)
1	20110904	15:50	22.73	20.13
2	20120120	10:50	19.14	13.81
3	20121111	5:00	19.84	15.31
4	20121207	13:40	18.29	14.60
5	20131121	10:10	18.51	15.57
6	20151004	5:30	21.75	19.23
7	20151028	19:30	23.29	16.30

8	20160906	17:40	24.96	20.78
9	20160916	23:20	29.44	20.67
10	20170113	13:40	20.49	16.52

Table 7 Extreme wind speeds detected in thunderstorm outflows by SP_02.

No.	Date	Time	$\widehat{U}$ (m/s)	$\overline{U}_{max}$ (m/s)
1	20110605	14:50	23.10	18.11
2	20120411	7:20	30.03	23.39
3	20120419	12:50	23.61	16.62
4	20121027	12:30	21.56	15.24
5	20131103	11:10	27.78	18.94
6	20141013	15:50	20.00	16.49
7	20141227	13:30	26.21	20.04
8	20150130	1:20	20.62	16.20
9	20111203	13:00	21.86	15.25

Table 8 Extreme wind speeds detected in thunderstorm outflows by SP_03.

No.	Date	Time	$\widehat{U}$	$\overline{U}_{max}$
1	20110605	14:50	20.70	17.68
2	20110724	0:00	21.18	17.33
3	20111019	21:10	23.63	18.82
4	20111025	15:40	33.98	26.86
5	20120411	7:10	23.40	18.46
6	20120924	13:50	23.69	19.94
7	20121015	0:20	22.53	20.31
8	20131110	10:10	20.33	14.97
9	20131226	7:20	26.31	18.75
10	20140209	2:30	26.39	20.62
11	20140209	3:00	21.55	16.48
12	20141013	15:50	25.18	20.33
13	20141201	0:10	21.37	18.03
14	20141227	13:40	22.24	15.29
15	20150117	2:40	22.80	17.55
16	20160305	13:00	22.89	16.74

Table 9 Extreme wind speeds detected in intermediate events by LI_01.

No.	Date	Time	$\widehat{U}$	$\overline{U}_{max}$
1	20101126	8:10	23.34	21.21
2	20101129	0:40	19.09	17.54

3	20121128	17:50	18.56	14.30
4	20121207	13:40	18.97	17.05
5	20130224	3:30	18.50	16.51
6	20130330	11:00	19.18	14.35
7	20131121	4:30	21.23	19.17
8	20131226	0:30	24.23	18.05
9	20140105	4:40	18.12	15.62
10	20140707	20:10	19.02	17.27
11	20141115	16:20	20.94	17.89
12	20141227	11:30	19.15	16.51
13	20160323	0:20	19.72	15.78
14	20161014	18:50	18.58	13.38
15	20170117	22:30	22.02	17.88
16	20170209	2:40	18.89	14.48
17	20170225	4:40	22.04	18.16

Table 10 Extreme wind speeds detected in intermediate events by LI_02.

No.	Date	Time	$\hat{U}$	$\bar{U}_{max}$
1	20111205	11:00	23.10	16.47
2	20120411	19:20	18.87	11.82
3	20120912	20:00	20.29	15.26
4	20121015	8:20	18.97	15.23
5	20121105	13:50	21.62	15.52
6	20121204	6:20	20.55	16.97
7	20130122	5:30	21.41	16.10
8	20131121	4:30	22.43	19.18
9	20131225	23:20	20.09	14.88
10	20150305	12:00	20.29	16.63
11	20151016	1:50	26.47	21.89
12	20160207	14:00	18.38	13.24

Table 11 Extreme wind speeds detected in intermediate events by SP_02.

No.	Date	Time	$\hat{U}$	$\bar{U}_{max}$
1	20101108	14:50	23.38	16.46
2	20101203	18:30	21.91	15.55
3	20110121	9:40	21.21	15.39
4	20111203	13:00	21.86	15.25
5	20111216	15:00	26.94	21.84
6	20120723	9:30	21.12	14.45
7	20120927	0:50	20.37	16.09

8	20121105	1:40	23.94	17.85
9	20130318	19:10	23.04	18.24
10	20131010	20:20	24.89	21.15
11	20131111	21:10	21.40	15.17
12	20131202	8:20	20.41	13.51
13	20140208	21:40	22.77	18.48
14	20141022	4:20	20.69	14.02
15	20141116	0:30	20.01	13.84
16	20141227	12:50	20.44	11.73
17	20150129	20:50	21.30	16.80
18	20150206	10:50	20.73	12.87
19	20150305	4:30	24.39	17.97
20	20160111	11:30	27.54	17.92

Table 12 Extreme wind speeds detected in intermediate events by SP_03.

No.	Date	Time	$\hat{U}$	$\bar{U}_{max}$
1	20111025	9:30	20.04	12.75
2	20111205	4:30	24.29	19.43
3	20111216	10:20	25.11	18.72
4	20120106	5:40	22.29	14.02
5	20120207	10:10	24.93	15.47
6	20120408	2:10	20.04	13.77
7	20120723	10:10	20.80	15.91
8	20130205	22:10	20.91	16.74
9	20131010	19:00	23.78	17.41
10	20131103	8:20	23.76	18.65
11	20131226	6:40	20.42	14.33
12	20140104	21:40	21.72	17.17
13	20141022	4:30	24.35	15.40
14	20141115	16:20	20.70	16.43
15	20141227	13:20	22.37	16.83
16	20150130	1:20	22.92	17.71
17	20150305	4:10	22.47	14.37
18	20151016	0:00	23.46	15.14
19	20160209	19:50	25.60	19.10

Reference

[1] Abd-Elaal, E. S., Mills, J. E., & Ma, X. (2013). A coupled parametric-CFD study for determining ages of downbursts through investigation of different field parameters. Journal of Wind Engineering and Industrial Aerodynamics, 123, 30-42.

[2] Abd-Elaal, E. S., Mills, J. E., & Ma, X. (2014). Empirical models for predicting unsteady-state downburst wind speeds. Journal of Wind Engineering and Industrial Aerodynamics, 129, 49-63.

[3] Aboshosha, H., Bitsuamlak, G., & El Damatty, A. (2015). Turbulence characterization of downbursts using LES. Journal of Wind Engineering and Industrial Aerodynamics, 136, 44-61.

[4] Aboshosha, H., & El Damatty, A. (2015). Engineering method for estimating the reactions of transmission line conductors under downburst winds. Engineering Structures, 99, 272-284.

[5] Aguilar, E., Auer, I., Brunet, M., Peterson, T. C., & Wieringa, J. (2003). Guidance on metadata and homogenization. Wmo Td, 1186, January, 2003, 1-53.

[6] Ahrens, C. D. (2009). Meteorology today: an introduction to weather, climate, and the environment. Brooks/Cole, Pacific Grove, CA.

[7] Alahyari, A., & Longmire, E. K. (1995). Dynamics of experimentally simulated microbursts. AIAA journal, 33(11), 2128-2136.

[8] AS/NZS 7000, (2010). Overhead Line Design-detailed Procedures. Standards Australia Limited/Standards New Zealand, Sydney, Australian.

[9] Atkins, N. T., & Wakimoto, R. M. (1991). Wet microburst activity over the southeastern United States: Implications for forecasting. Weather and Forecasting, 6(4), 470-482.

[10] Anderson, J. R., Orf, L. G., & Straka, J. M. (1992). A 3-D modelsyystem for simulating thunderstorm microburst outflows. Meteorology and Atmospheric Physics, 49(1-4), 125-131.

[11] Australian Wind Alliance, (2016): https://www.windalliance.org.au/.

[12] Bakke, P. (1957). An experimental investigation of a wall jet. Journal of Fluid Mechanics, 2(5), 467-472.

[13] Ballio, G., Lagomarsino, S., Piccardo, G., Solari, G., 1999. Probabilistic analysis of Italian extreme winds: reference velocity and return criterion. Wind and Structures. 2, 51–68.

[14] Battan, L.J., (1961). The Nature of Severe Storms, Anchor Books, Garden City, New York, 158.

[15] Beck, A.T. and Correa, M.R.S., (2012). Proposal of updated basic wind speeds for Brazil, Revista TECHNE, 64-67 (in Portuguese).

[16] Bjerknes, J. & Solberg, H. (1922). Life cycle of cyclones and the polar front theory of atmospheric circulation. Geophys. Publik., 3(1), 1-18.

[17] Bluestein, H. B., (1995). Observations and Theory of Weather Systems. Vol. II. Synoptic–Dynamic Meteorology in Midlatitudes, Oxford University Press, 608.

[18] Braza, M., Perrin, R., & Hoarau, Y. (2006). Turbulence properties in the cylinder wake at high Reynolds numbers. Journal of fluids and Structures, 22(6-7), 757-771.

[19] Bryan, G. H., & Fritsch, J. M. (2002). A benchmark simulation for moist nonhydrostatic numerical models. Monthly Weather Review, 130(12), 2917-2928.

[20] Burlando, M., Carassale, L., Georgieva, E., Ratto, C. F., & Solari, G. (2007). A simple and efficient procedure for the numerical simulation of wind fields in complex terrain. Boundary-layer meteorology, 125(3), 417-439.

[21] Burlando, M., De Gaetano, P., Pizzo, M., Repetto, M. P., Solari, G., & Tizzi, M. (2013). Wind

climate analysis in complex terrains. Journal of Wind Engineering and Industrial Aerodynamics, 123, 349-362.

[22] Burlando, M., Romanić, D., Solari, G., Hangan, H., & Zhang, S. (2017a). Field data analysis and weather scenario of a downburst event in Livorno, Italy, on 1 October 2012. Monthly Weather Review, 145(9), 3507-3527.

[23] Burlando, M., De Cio, A., Pizzo, M., and Solari, G. (2017b) Analysis of wind vertical profiles of thunderstorm events in the Mediterranean, in: Proceedings of the 9th Asia-Pacific Conference on Wind Engineering, Auckland, New Zealand, 3-7 December 2017, 1-4.

[24] Burlando, M., Tizzi, M., & Solari, G. (2017c). Characteristics of downslope winds in the Liguria Region. WIND AND STRUCTURES, 24(6), 613-635.

[25] Burlando, M., Zhang, S., & Solari, G. (2018). Monitoring, cataloguing, and weather scenarios of thunderstorm outflows in the northern Mediterranean. Natural Hazards & Earth System Sciences, 18(9).

[26] Butler, K., & Kareem, A. (2007). Physical and numerical modeling of downburst generated gust fronts. In Proceedings of the 12th International Conference on Wind Engineering, Cairns, Australia (pp. 791-798).

[27] Buzzi, A., & Tibaldi, S. (1978). Cyclogenesis in the lee of the Alps: A case study. Quarterly Journal of the Royal Meteorological Society, 104(440), 271-287.

[28] Byers, H. R. and Braham, R. R. (1949). The thunderstorm. Report of the Thunderstorm Project, U.S. Government Printing Office, Washington, DC, 287.

[29] Cao, S., Nishi, A., Kikugawa, H., & Matsuda, Y. (2002). Reproduction of wind velocity history in a multiple fan wind tunnel. Journal of wind engineering and industrial aerodynamics, 90(12-15), 1719-1729.

[30] Castino, F., Rusca, L., & Solari, G. (2003). Wind climate micro-zoning: a pilot application to Liguria Region (North Western Italy). Journal of wind engineering and industrial aerodynamics, 91(11), 1353-1375.

[31] Charba, J. (1974). Application of gravity current model to analysis of squall-line gust front. Monthly Weather Review, 102(2), 140-156.

[32] Chay, M., & Albermani, F. (2005). Dynamic Response of a SDOF System Subjected to Simulated Downburst Wind.

[33] Chay, M. T., Albermani, F., & Wilson, R. (2006). Numerical and analytical simulation of downburst wind loads. Engineering Structures, 28(2), 240-254.

[34] Chay, M. T., & Letchford, C. W. (2002). Pressure distributions on a cube in a simulated thunderstorm downburst—Part A: stationary downburst observations. Journal of wind engineering and industrial Aerodynamics, 90(7), 711-732.

[35] Chay, M. T., Wilson, R., & Albermani, F. (2008). Gust occurrence in simulated non-stationary winds. Journal of Wind Engineering and Industrial Aerodynamics, 96(10-11), 2161-2172.

[36] Chen, X. (2008). Analysis of alongwind tall building response to transient nonstationary winds. Journal of structural engineering, 134(5), 782-791.

[37] Chen, L., & Letchford, C. W. (2004a). A deterministic–stochastic hybrid model of downbursts and its impact on a cantilevered structure. Engineering structures, 26(5), 619-629.

[38] Chen, L., & Letchford, C. W. (2004b). Parametric study on the along-wind response of the CAARC building to downbursts in the time domain. Journal of wind engineering and industrial

aerodynamics, 92(9), 703-724.

[39] Chen, L., & Letchford, C. W. (2005a). Proper orthogonal decomposition of two vertical profiles of full-scale nonstationary downburst wind speeds. Journal of Wind Engineering and Industrial Aerodynamics, 93(3), 187-216.

[40] Chen, L., & Letchford, C. W. (2005b). Simulation of multivariate stationary Gaussian stochastic processes: Hybrid spectral representation and proper orthogonal decomposition approach. Journal of Engineering Mechanics, 131(8), 801-808.

[41] Chen, L., & Letchford, C. W. (2006). Multi-scale correlation analyses of two lateral profiles of full-scale downburst wind speeds. Journal of wind engineering and industrial aerodynamics, 94(9), 675-696.

[42] Chen, L., & Letchford, C. W. (2007). Numerical simulation of extreme winds from thunderstorm downbursts. Journal of Wind Engineering and Industrial Aerodynamics, 95(9-11), 977-990.

[43] Choi, E. C. (1999). Extreme wind characteristics over Singapore–an area in the equatorial belt. Journal of Wind Engineering and Industrial Aerodynamics, 83(1-3), 61-69.

[44] Choi, E. C. (2000). Wind characteristics of tropical thunderstorms. Journal of Wind Engineering and Industrial Aerodynamics, 84(2), 215-226.

[45] Choi, E. C. (2004). Field measurement and experimental study of wind speed profile during thunderstorms. Journal of wind engineering and industrial Aerodynamics, 92(3-4), 275-290.

[46] Choi, E. C., & Hidayat, F. A. (2002a). Dynamic response of structures to thunderstorm winds. Progress in Structural Engineering and Materials, 4(4), 408-416.

[47] Choi, E. C., & Hidayat, F. A. (2002b). Gust factors for thunderstorm and non-thunderstorm winds. Journal of wind engineering and industrial aerodynamics, 90(12-15), 1683-1696.

[48] Choi, E. C. C., & Tanurdjaja, A. (2002). Extreme wind studies in Singapore. An area with mixed weather system. Journal of Wind Engineering and Industrial Aerodynamics, 90(12-15), 1611-1630.

[49] CNR-DT 207/2008, 2008. (2010) Guide for the assessment of wind actions and effects on structures. National Research Council, Rome, Italy.

[50] CIGRÉ (Conseil International des Grands Réseaux Électriques /Internatioanal Council on Large Electrical Systems), 2012. Overhead Line Design Guidelines for Mitigation of Severe Wind Storm Damage. Technical Brochure 485, Working Group B2-39.

[51] Cook, N. J. (1982). Towards better estimation of extreme winds. Journal of Wind Engineering and Industrial Aerodynamics, 9(3), 295-323.

[52] Cook, N. J. (1985). The designer's guide to wind loading of building structures part 1: background. Damage survey, wind data and structural classification building research establishment, Garston and Butterworths London.

[53] Cook, N. J. (2014a). Review of errors in archived wind data. Weather, 69(3), 72-78.

[54] Cook, N. J. (2014b). Detecting artefacts in analyses of extreme wind speeds. Wind and Structures, 19(3), 271-294. https://doi.org/10.12989/was.2014.19.3.271

[55] Cook, N. J., & Harris, R. I. (2004). Exact and general FT1 penultimate distributions of extreme wind speeds drawn from tail-equivalent Weibull parents. Structural Safety, 26(4), 391-420.

[56] Cook, N. J., & Harris, R. I. (2008). Postscript to "Exact and general FT1 penultimate distributions of extreme wind speeds drawn from tail-equivalent Weibull parents". Structural Safety, 30(1), 1-10.

[57] Cook, N. J., Harris, R. I., & Whiting, R. (2003). Extreme wind speeds in mixed climates revisited. Journal of Wind Engineering and Industrial Aerodynamics, 91(3), 403-422.

[58] Cramér, H. (2016). Mathematical methods of statistics (PMS-9) (Vol. 9). Princeton university press.

[59] Darwish, M. M., El Damatty, A. A., & Hangan, H. (2010). Dynamic characteristics of transmission line conductors and behaviour under turbulent downburst loading. Wind and Structures, 13(4), 327.

[60] Davenport, A. G. (1961). The application of statistical concepts to the wind loading of structures. Proceedings of the Institution of Civil Engineers, 19(4), 449-472.

[61] Davenport, A. G. (1968). The Dependence of Wind Loads on Meteorological Parameter. Wind effects on Building and Structures, 19-82.

[62] Davies-Jones, R., D. W. Burgess, & M. Foster, (1990). Test of helicity as a forecast parameter. Preprints, 16th Conf. on Severe Local Storms, Kananaskis Park, AB, Canada, Amer. Meteor. Soc., 588–592.

[63] Dawkins, L. C., Stephenson, D. B., Lockwood, J. F., & Maisey, P. E. (2016). The 21st century decline in damaging European windstorms.

[64] De Gaetano, P., Repetto, M. P., Repetto, T., & Solari, G. (2014). Separation and classification of extreme wind events from anemometric records. Journal of Wind Engineering and Industrial Aerodynamics, 126, 132-143.

[65] Deroche, M. S., Choux, M., Codron, F., & Yiou, P. (2014). Three variables are better than one: detection of european winter windstorms causing important damages. Natural Hazards and Earth System Sciences, 14(4), 981-993.

[66] Derrien, M., Le Gléau, H., and Fernandez, P. (2013). Algorithm theoretical basis document for "Cloud Products", Météo France, Toulouse, France, SAF/NWC/CDOP2/MFL/SCI/ATBD/01, 87.

[67] Didden, N., & Ho, C. M. (1985). Unsteady separation in a boundary layer produced by an impinging jet. Journal of Fluid Mechanics, 160, 235-256.

[68] Dotzek, N., Groenemeijer, P., Feuerstein, B., & Holzer, A. M. (2009). Overview of ESSL's severe convective storms research using the European Severe Weather Database ESWD. Atmospheric research, 93(1-3), 575-586.

[69] Droegemeier, K. K., & Wilhelmson, R. B. (1987). Numerical simulation of thunderstorm outflow dynamics. Part I: Outflow sensitivity experiments and turbulence dynamics. Journal of the Atmospheric Sciences, 44(8), 1180-1210.

[70] Duan, Y., Wang, D., Liu, Y. (2017). Radar analysis and numerical simulation of strong convective weather for 'Oriental Star' Depression. Journal of Applied Meteorological Science, 28 (6), 666-677. (in Chinese)

[71] Durañona, V., Sterling, M., & Baker, C. J. (2007). An analysis of extreme non-synoptic winds. Journal of wind engineering and industrial aerodynamics, 95(9-11), 1007-1027.

[72] Durañona, V. (2011). Wind impact on Uruguay: vulnerability to extreme winds and estimation of their risk. In Proc. 13th International Conference on Wind Engineering, Amsterdam.

[73] Durañona, V. (2015). The significance of nonsynoptic winds in the extreme wind climate of Uruguay. June 21-26. In 14th International Conference on Wind Engineering–Porto Alegre, Brazil, 1-18.

[74] Durst, C. S. (1960). Wind speeds over short periods of time. Meteor. Mag, 89(1960), 181-186.

[75] Elawady, A., Aboshosha, H., El Damatty, A., Bitsuamlak, G., Hangan, H., & Elatar, A. (2017). Aero-elastic testing of multi-spanned transmission line subjected to downbursts. Journal of Wind Engineering and Industrial Aerodynamics, 169, 194-216.

[76] Engineering Sciences Data Unit, (1993). Computer program for wind speeds and turbulence properties: flat or hill sites in terrain with roughness changes, ESDU Item 92032, London, UK.

[77] EUMETSAT, (2013). MTG-FCI: ATBD for cloud mask and cloud analysis product, European Organization for the Exploitation of Meteorological Satellites (EUMETSAT), Darmstadt, Germany.

[78] Fisher, R. A., & Tippett, L. H. C. (1928). Limiting forms of the frequency distribution of the largest or smallest member of a sample. In Mathematical Proceedings of the Cambridge Philosophical Society (Vol. 24, No. 2, pp. 180-190). Cambridge University Press, April.

[79] Flay, R. G. J., & Stevenson, D. C. (1988). Integral length scales in strong winds below 20 m. Journal of Wind Engineering and Industrial Aerodynamics, 28(1-3), 21-30.

[80] Fovell, R. G., & Ogura, Y. (1989). Effect of vertical wind shear on numerically simulated multicell storm structure. Journal of the Atmospheric Sciences, 46(20), 3144-3176.

[81] Fujita, T. T. (1981). Tornadoes and downbursts in the context of generalized planetary scales. Journal of the Atmospheric Sciences, 38(8), 1511-1534.

[82] Fujita, T. T., & Wakimoto, R.M.. (1981). Five scales of airflow associated with a series of downbursts on 16 july 1980. Monthly Weather Review, 109(7).

[83] Fujita, T. T. (1985). Downburst: microburst and macroburst. University of Chicago Press, Chicago, IL.

[84] Fujita, T. T. (1986). DFW microburst on August 2, 1985. 1st ed. Satellite and Mesometeorology Research Project, Dept. of the Geophysical Sciences, University of Chicago, Chicago, IL, 154.

[85] Fujita, T. T. (1990). Downbursts: meteorological features and wind field characteristics. Journal of wind engineering and industrial aerodynamics, 36, 75-86.

[86] Gast, K. D., & Schroeder, J. L. (2003). Supercell rear-flank downdraft as sampled in the 2002 thunderstorm outflow experiment. In Proc., 11th Int. Conf. on Wind Engineering (11ICWE), , June, 2233-2240.

[87] Gast, K. D., & Schroeder, S. (2004). Extreme wind events observed in the 2002 thunderstorm outflow experiment, October. In 22nd Conf. on Severe Local Storms. [Available online at https://ams.confex.com/ams/11aram22sls/ webprogram/Paper81653.html.]

[88] GB50009-2012, (2012). Load code for the design of buiding structures.

[89] Geerts, B. (2001). Estimating downburst-related maximum surface wind speeds by means of proximity soundings in New South Wales, Australia. Weather and forecasting, 16(2), 261-269.

[90] Glauert, M. B. (1956). The wall jet. Journal of Fluid Mechanics, 1(6), 625-643.

[91] Craig Goff, R. (1976). Vertical structure of thunderstorm outflows. Monthly Weather Review, 104(11), 1429-1440.

[92] Goldman, J. L., & Sloss, P. W. (1969). Structure of the leading edge of thunderstorm cold-air outflow.

[93] Gomes, L., & Vickery, B.J. (1976). On thunderstorm wind gusts in Australia. Civ. Eng. Trans. Ind. Eng. Aust. 18: 33-39.

[94] Gomes, L., & Vickery, B. J. (1977). On the prediction of extreme wind speeds from the parent distribution. Journal of Wind Engineering and Industrial Aerodynamics, 2(1), 21-36.

[95] Gomes, L., & Vickery, B. J. (1977/1978). Extreme wind speeds in mixed wind climates. Journal of Wind Engineering and Industrial Aerodynamics, 2(4), 331-344.

[96] Greenway, M. E. (1979). An analytical approach to wind velocity gust factors. Journal of Wind Engineering and Industrial Aerodynamics, 5(1-2), 61-91.

[97] Gumbel, E.J., 1958. Statistics of Extreme. Columbia University, New York.

[98] Gunter, W. S., & Schroeder, J. L. (2015). High-resolution full-scale measurements of thunderstorm outflow winds. Journal of Wind Engineering and Industrial Aerodynamics, 138, 13-26.

[99] Guo, S. L. (1990). A discussion on unbiased plotting positions for the general extreme value distribution. Journal of Hydrology, 121(1-4), 33-44.

[100] Hangan, H., Roberts, D., Xu, Z., & Kim, J. (2003). Downburst simulation. Experimental and numerical challenges. In Proceedings of the 11th International Conference on Wind Engineering, Lubbock, Texas, Electronic Version. 2241-2248.

[101] Harris, R. I. (2009). XIMIS, a penultimate extreme value method suitable for all types of wind climate. Journal of Wind Engineering and Industrial Aerodynamics, 97(5-6), 271-286.

[102] Harris, R. I. (2014). A simulation method for the macro-meteorological wind speed and the implications for extreme value analysis. Journal of Wind Engineering and Industrial Aerodynamics, 125, 146-155.

[103] Harris, R. I. (2017). The Level Crossing Method applied to mean wind speeds from "mixed" climates. Structural Safety, 67, 54-61.

[104] Hawes H., Dempsey D. (1993), Review of recent Australian transmission line failures due to high intensity winds. Proceedings of the Task Force of High Intensity Winds on Transmission Lines, Buenos Aires.

[105] Hjelmfelt, M. R. (1988). Structure and life cycle of microburst outflows observed in Colorado. Journal of Applied Meteorology, 27(8), 900-927.

[106] Hjelmfelt, M. R., Roberts, R. D., Orville, H. D., Chen, J. P., & Kopp, F. J. (1989). Observational and numerical study of a microburst line-producing storm. Journal of the Atmospheric Sciences, 46(17), 2731-2744.

[107] Rosenberger, J. L., & Gasko, M. (1983). Understanding robust and exploratory data analysis.

[108] Hoaglin, D.C., Mosteller, F., Tukey, J.W. (Eds.), 1983. Understanding robust and exploratory data analysis. John Wiley & Sons, N.Y.

[109] Holmes, J. (2003). Discussion on Generalized extreme gust wind speeds distributions by E. Cheng, C. Yeung. Journal of Wind Engineering & Industrial Aerodynamics, 7(91), 965-967.

[110] Holmes, J. D. (2015). Wind loading of structures. CRC press.

[111] Holmes, J. D., & Moriarty, W. W. (1999). Application of the generalized Pareto distribution to extreme value analysis in wind engineering. Journal of Wind Engineering and Industrial Aerodynamics, 83(1-3), 1-10.

[112] Holmes, J. D., & Oliver, S. E. (2000). An empirical model of a downburst. Engineering structures, 22(9), 1167-1172.

[113] Holmes, J. D., Baker, C. J., English, E. C., & Choi, E. C. C. (2005). Wind structure and codification. Wind and Structures, 8(4), 235-250.

[114] Holmes, J. D., Hangan, H. M., Schroeder, J. L., Letchford, C. W., & Orwig, K. D. (2008). A forensic study of the Lubbock-Reese downdraft of 2002. Wind and Structures, 11(2), 137-152.

https://doi.org/10.12989/was.2008.11.2.137

[115] Holmes, J. D., & Ginger, J. D. (2012). The gust wind speed duration in AS/NZS 1170.2. Australian Journal of Structural Engineering, 13(3), 207-217.

[116] Holmes, J. D., Allsop, A. C., & Ginger, J. D. (2014). Gust durations, gust factors and gust response factors in wind codes and standards. Wind and Structures, 19(3), 339-352.

[117] Huang, G., & Chen, X. (2009). Wavelets-based estimation of multivariate evolutionary spectra and its application to nonstationary downburst winds. Engineering Structures, 31(4), 976-989.

[118] Huang, G., Chen, X., Liao, H., & Li, M. (2013). Predicting tall building response to nonstationary winds using multiple wind speed samples. Wind and Structures, 17(2), 227-244.

[119] Huang, G., Zheng, H., Xu, Y. L., & Li, Y. (2015). Spectrum models for nonstationary extreme winds. Journal of Structural Engineering, 141(10), 04015010.

[120] Hui, Y., Li, B., Kawai, H., Yang, Q.S. (2017). Non-stationary and non-Gaussian characteristics of wind speeds. Wind and Structures, 24(1), 59-78.

[121] Huang, G.Q., Jiang, Y., Peng, L.L., Solari G., Liao, H.L., Li, M.S. (2019). Characteristics of Intense Wind in Mountain Area Based on Field Measurement, Journal of Wind Engineering and Industrial Aerodynamics, 190, 166-182.

[122] Ivan, M. (1986). A ring-vortex downburst model for flight simulations. Journal of Aircraft, 23(3), 232-236.

[123] Järvi, L., Punkka, A. J., Schultz, D. M., Petäjä, T., Hohti, H., Rinne, J., ... & Vesala, T. (2007). Micrometeorological observations of a microburst in southern Finland. In Atmospheric Boundary Layers . Springer, New York, NY, 187-203.

[124] Jenkinson, A. F. (1955). The frequency distribution of the annual maximum (or minimum) values of meteorological elements. Quarterly Journal of the Royal Meteorological Society, 81(348), 158-171.

[125] Karmakar, S., Quadir, D. A., & Das, M. K. (2017). Numerical simulation of physical and dynamical characteristics associated with the severe thunderstorm on April 5, 2015 at Kushtia and Jhenaidah. Natural Hazards, 86(3), 1127-1146.

[126] Kasperski, M. (2002). A new wind zone map of Germany. Journal of Wind Engineering and Industrial Aerodynamics, 90(11), 1271-1287.

[127] Kasperski, M. (2009). Wind fields in gust fronts. Proceedings of the 11th Americas Conference on Wind Engineering, Puerto Rico.

[128] Kim, J., & Hangan, H. (2007). Numerical simulations of impinging jets with application to downbursts. Journal of Wind Engineering and Industrial Aerodynamics, 95(4), 279-298.

[129] Knupp, K. R. (1989). Numerical simulation of low-level downdraft initiation within precipitating cumulonimbi: Some preliminary results. Monthly weather review, 117(7), 1517-1529.

[130] Kruger, A. C., Goliger, A. M., Retief, J. V., & Sekele, S. (2010). Strong wind climatic zones in South Africa.

[131] Kwon, D. K., & Kareem, A. (2009). Gust-front factor: New framework for wind load effects on structures. Journal of structural engineering, 135(6), 717-732.

[132] Kwon, D. K., & Kareem, A. (2013). Generalized gust-front factor: a computational framework for wind load effects. Engineering Structures, 48, 635-644.

[133] Kwon, D. K., & Kareem, A. (2014). Revisiting gust averaging time and gust effect factor in

ASCE 7. Journal of Structural Engineering, 140(11), 06014004.

[134] Lagomarsino, S., Piccardo, G., & Solari, G. (1992). Statistical analysis of high return period wind speeds. Journal of Wind Engineering and Industrial Aerodynamics, 41(1-3), 485-496.

[135] Landreth, C. C., & Adrian, R. J. (1990). Impingement of a low Reynolds number turbulent circular jet onto a flat plate at normal incidence. Experiments in Fluids, 9(1-2), 74-84.

[136] Launder, B.E. and Rodi, W. (1981). The turbulent wall jet. Progress in aerospace sciences, 19, 81-128.

[137] Le, T. H., & Caracoglia, L. (2015). Reduced-order wavelet-Galerkin solution for the coupled, nonlinear stochastic response of slender buildings in transient winds. Journal of Sound and Vibration, 344, 179-208.

[138] Letchford, C. (1999). Turbulence and topographic effects in simulated thunderstorm downdrafts by wind tunnel jet. Proc,. 10th ICWE, Copenhagen, 1999.

[139] Letchford, C. W., Mans, C., & Chay, M. T. (2002). Thunderstorms—their importance in wind engineering (a case for the next generation wind tunnel). Journal of Wind Engineering and Industrial Aerodynamics, 90(12-15), 1415-1433.

[140] Letchford, C. W., & Ghosalkar, M. (2004). Extreme wind speed climatology in the United States Mid-West. In 6th UK Conference on Wind Engineering , Vol. 1, 5.

[141] Li, C. Q. (2000). A stochastic model of severe thunderstorms for transmission line design. Probabilistic engineering mechanics, 15(4), 359-364.

[142] Li, Q.S., Zhi, L.H., & Hu, F., (2009). Field monitoring of boundary layer wind characteristics in urban area. Wind and Structures, 12(6), 553-574.

[143] Li, C., Li, Q. S., Xiao, Y. Q., & Ou, J. P. (2012). A revised empirical model and CFD simulations for 3D axisymmetric steady-state flows of downbursts and impinging jets. Journal of Wind Engineering and Industrial Aerodynamics, 102, 48-60.

[144] Li, H. H. (2015). Spatio-temporal distribution statistical analysis and experimenrs of wind field characteristics and wind loads on structures of downbust. (Doctoral dissertation).

[145] Liao, X., Yu, B., & Lu, L. (2009). Climatology and Nowcasting Methods for Thunderstorm Gale in Beijing. Meteorolodical Monthly, 35(9), 18-29.

[146] Lieblein, J., (1974). Efficient methods of extreme-value methodology. Report NBSIR 74-602, National Bureau of Standards, Washington, D.C.

[147] Lin, W. E., & Savory, E. (2006). Large-scale quasi-steady modelling of a downburst outflow using a slot jet. Wind and structures, 9(6), 419-440.

[148] Liu, H. G. (2001). Characterisyics and numerical simulation of microburst. Acta Meteorologica Sinica, 259(2),183-195.

[149] Liu, J. Y., & Orville, H. D. (1969). Numerical modeling of precipitation and cloud shadow effects on mountain-induced cumuli. Journal of the Atmospheric Sciences, 26(6), 1283-1298.

[150] Lombardo, F. T., Main, J. A., & Simiu, E. (2009). Automated extraction and classification of thunderstorm and non-thunderstorm wind data for extreme-value analysis. Journal of Wind Engineering and Industrial Aerodynamics, 97(3-4), 120-131.

[151] Lombardo, F. T., Smith, D. A., Schroeder, J. L., & Mehta, K. C. (2014). Thunderstorm characteristics of importance to wind engineering. Journal of Wind Engineering and Industrial Aerodynamics, 125, 121-132.

[152] Lompar, M., Ćurić, M., & Romanic, D. (2017). Simulation of a severe convective storm using a

numerical model with explicitly incorporated aerosols. Atmospheric Research, 194, 164-177.

[153] Lundgren, T. S., Yao, J., & Mansour, N. N. (1992). Microburst modelling and scaling. Journal of fluid mechanics, 239, 461-488.

[154] Mahoney III, W. P. (1988). Gust front characteristics and the kinematics associated with interacting thunderstorm outflows. Monthly weather review, 116(7), 1474-1492.

[155] Mason, M. S., Letchford, C. W., & James, D. L. (2005). Pulsed wall jet simulation of a stationary thunderstorm downburst, Part A: Physical structure and flow field characterization. Journal of wind engineering and industrial aerodynamics, 93(7), 557-580.

[156] Mason, M. S., Wood, G. S., & Fletcher, D. F. (2009). Numerical simulation of downburst winds. Journal of Wind Engineering and Industrial Aerodynamics, 97(11-12), 523-539.

[157] Mason, M. S., Fletcher, D. F., & Wood, G. S. (2010). Numerical simulation of idealised three-dimensional downburst wind fields. Engineering Structures, 32(11), 3558-3570.

[158] Matsumoto, M. (2007). Drag forces on 2-D cylinders due to sudden increase of wind velocity. In Proceedings of 12th International Conference on Wind Engineering, 1727-1734.

[159] Mattocks, C., & Bleck, R. (1986). Jet streak dynamics and geostrophic adjustment processes during the initial stages of lee cyclogenesis. Monthly weather review, 114(11), 2033-2056.

[160] McCann, D. W. (1994). WINDEX—A new index for forecasting microburst potential. Weather and forecasting, 9(4), 532-541.

[161] McCarthy, P., & Melsness, M. (1996). Severe weather elements associated with hydro tower failures near Grosse.

[162] McConville, A. C., Sterling, M., & Baker, C. J. (2009). The physical simulation of thunderstorm downbursts using an impinging jet. Wind and structures, 12(2), 133-149.

[163] McCullough, M., Kwon, D. K., Kareem, A., & Wang, L. (2014). Efficacy of averaging interval for nonstationary winds. Journal of Engineering Mechanics, 140(1), 1-19.

[164] McGinley, J. (1982). A diagnosis of Alpine lee cyclogenesis. Monthly Weather Review, 110(9), 1271-1287.

[165] McTaggart-Cowan, R., Galarneau Jr, T. J., Bosart, L. F., & Milbrandt, J. A. (2010a). Development and tropical transition of an Alpine lee cyclone. Part I: case analysis and evaluation of numerical guidance. Monthly Weather Review, 138(6), 2281-2307.

[166] McTaggart-Cowan, R., Galarneau Jr, T. J., Bosart, L. F., & Milbrandt, J. A. (2010b). Development and tropical transition of an Alpine lee cyclone. Part II: Orographic influence on the development pathway. Monthly Weather Review, 138(6), 2308-2326.

[167] Miguel, L. F. F., Riera, J. D., & Miguel, L. F. F. (2018). Assessment of downburst wind loading on tall structures. Journal of Wind Engineering and Industrial Aerodynamics, 174, 252-259.

[168] Miller, M. J., & Pearce, R. P. (1974). A three-dimensional primitive equation model of cumulonimbus convection. Quarterly Journal of the royal meteorological society, 100(424), 133-154.

[169] Mitchell, K. E., & Hovermale, J. B. (1977). A numerical investigation of the severe thunderstorm gust front. Monthly weather review, 105(5), 657-675.

[170] Mogil, H. M. (2007). Extreme weather: Understanding the science of hurricanes, tornadoes, floods, heat waves, snow storms, global warming and other atmospheric disturbances. Black Dog & Leventhal, 210-221.

[171] Mueller, C. K., & Carbone, R. E. (1987). Dynamics of a thunderstorm outflow. Journal of the

Atmospheric sciences, 44(15), 1879-1898.

[172] Natalini, B., Lassig, J. L., Natalini, M. B., & Palese, C. (2012). Wind-induced damage in two regions of Argentina. Journal of Civil Engineering and Architecture, 6(2), 167.

[173] Nicholls, M., Pielke, R., & Meroney, R. (1993). Large eddy simulation of microburst winds flowing around a building. Journal of Wind Engineering and Industrial Aerodynamics, 46, 229-237.

[174] NOAA: Federal Meteorological Handbook No. 1 – Surface weather observations and reports (FCM-H1-2005). National Oceanic and Atmospheric Administration, US Department of Commerce, Washington, D. C., 2005.

[175] Oliver, S. E., Moriarty, W. W., & Holmes, J. D. (2000). A risk model for design of transmission line systems against thunderstorm downburst winds. Engineering structures, 22(9), 1173-1179.

[176] Orf, L. G., & Anderson, J. R. (1999). A numerical study of traveling microbursts. Monthly Weather Review, 127(6), 1244-1258.

[177] Orf, L. G., Anderson, J. R., & Straka, J. M. (1996). A three-dimensional numerical analysis of colliding microburst outflow dynamics. Journal of the atmospheric sciences, 53(17), 2490-2511.

[178] Orf, L., Kantor, E., & Savory, E. (2012). Simulation of a downburst-producing thunderstorm using a very high-resolution three-dimensional cloud model. Journal of wind engineering and industrial aerodynamics, 104, 547-557.

[179] Ortego, M. I., Egozcue, J. J., & Tolosana-Delgado, R. (2014). Bayesian trend analysis of extreme wind using observed and hindcast series off the Catalan coast, NW Mediterranean Sea. Natural Hazards and Earth System Sciences, 14(9), 2387-2397.

[180] Orville, H. D. (1965). A numerical study of the initiation of cumulus clouds over mountainous terrain. Journal of the Atmospheric Sciences, 22(6), 684-699.

[181] Orwig, K. D., & Schroeder, J. L. (2007). Near-surface wind characteristics of extreme thunderstorm outflows. Journal of Wind Engineering and Industrial Aerodynamics, 95(7), 565-584.

[182] Oseguera, R. M., & Bowles, R. L. (1988). A simple, analytic 3-dimensional downburst model based on boundary layer stagnation flow.

[183] Palutikof, J. P., Brabson, B. B., Lister, D. H., & Adcock, S. T. (1999). A review of methods to calculate extreme wind speeds. Meteorological applications, 6(2), 119-132.

[184] Pastushkov, R. S. (1975). The effects of vertical wind shear on the evolution of convective clouds. Quarterly Journal of the Royal Meteorological Society, 101(428), 281-291.

[185] Peng, L., Huang, G., Chen, X., & Yang, Q. (2018). Evolutionary Spectra-Based Time-Varying Coherence Function and Application in Structural Response Analysis to Downburst Winds. Journal of Structural Engineering, 144(7), 04018078.

[186] Pistotnik, G., Holzer, A. M., Kaltenböck, R., & Tschannett, S. (2011). An F3 downburst in Austria—A case study with special focus on the importance of real-time site surveys. Atmospheric research, 100(4), 565-579.

[187] Ponte Jr, J., & Riera, J. D. (2007). Wind velocity field during thunderstorms. Wind and structures, 10(3), 287-300.

[188] Ponte Jr, J., & Riera, J. D. (2010). Simulation of extreme wind series caused by thunderstorms in temperate latitudes. Structural Safety, 32(4), 231-237.

[189] Poreh, M., Tsuei, Y. G., & Cermak, J. E. (1967). Investigation of a turbulent radial wall jet.

Journal of Applied Mechanics, 34(2), 457-463.

[190] Proctor, F. H. (1987a). The terminal area simulation system. Volume 1: Theoretical formulation.

[191] Proctor, F. H. (1987b). The terminal area simulation system. Volume 2: Verification cases.

[192] Proctor, F. H. (1988). Numerical simulations of an isolated microburst. Part I: Dynamics and structure. Journal of the atmospheric sciences, 45(21), 3137-3160.

[193] Proctor, F. H. (1989). Numerical simulations of an isolated microburst. Part II: Sensitivity experiments. Journal of the atmospheric sciences, 46(14), 2143-2165.

[194] Qin, L., Li, Y. D., & Gao, S. T. (2006). The synoptic and climatic characteristic studies of thunderstorm winds in Beijing. Climatic and Environmental Research, 11(6), 754-762.

[195] Rasmussen, E. N., & Blanchard, D. O. (1998). A baseline climatology of sounding-derived supercell andtornado forecast parameters. Weather and forecasting, 13(4), 1148-1164.

[196] Repetto, M. P., Burlando, M., Solari, G., De Gaetano, P., & Pizzo, M. (2017). Integrated tools for improving the resilience of seaports under extreme wind events. Sustainable cities and society, 32, 277-294.

[197] Repetto, M. P., Burlando, M., Solari, G., De Gaetano, P., Pizzo, M., & Tizzi, M. (2018). A web-based GIS platform for the safe management and risk assessment of complex structural and infrastructural systems exposed to wind. Advances in Engineering Software, 117, 29-45.

[198] Rex, D. F. (1950). Blocking action in the middle troposphere and its effect upon regional climate. Tellus, 2(4), 275-301.

[199] Riera, J.D., 2013. Personal communication on the Brazilian wind code and extreme wind value analyses carried out in Brazil.

[200] Riera, J. D., & Nanni, L. F. (1989). Pilot study of extreme wind velocities in a mixed climate considering wind orientation. Journal of Wind Engineering and Industrial Aerodynamics, 32(1-2), 11-20.

[201] Riera, J. D., & Ponte Jr, J. (2012). Recent Brazilian research on thunderstorm winds and their effects on structural design. Wind and Structures, 15(2), 111-129.

[202] Riera, J. D., Viollaz, A. J., & Reimundin, J. C. (1977). Some recent results on probabilistic models of extreme wind speeds. Journal of Wind Engineering and Industrial Aerodynamics, 2(3), 271-287.

[203] Roberts, J. F., Champion, A. J., Dawkins, L. C., Hodges, K. I., Shaffrey, L. C., Stephenson, D. B., ... & Youngman, B. D. (2014). The XWS open access catalogue of extreme European windstorms from 1979 to 2012. Natural Hazards and Earth System Sciences, 14, 2487-2501.

[204] Romanić, D., Ćurić, M., Zarić, M., Lompar, M., & Jovičić, I. (2016). Investigation of an extreme Koshava wind episode of 30 January–4 February 2014. Atmospheric Science Letters, 17(2), 199-206.

[205] Romanic, D., LoTufo, J., & Hangan, H. (2019). Transient behavior in impinging jets in crossflow with application to downburst flows. Journal of Wind Engineering and Industrial Aerodynamics, 184, 209-227.

[206] Rowcroft, J. (2011). Vertical wind shear profiles in downburst events and the insufficiency of wind turbine design codes. In 14th Australasian Wind Engineering Society Workshop, 50-53.

[207] Selvam, R. P., & Holmes, J. D. (1992). Numerical simulation of thunderstorm downdrafts. Journal of wind engineering and industrial aerodynamics, 44(1-3), 2817-2825.

[208] Sengupta, A., & Sarkar, P. P. (2008). Experimental measurement and numerical simulation of an

impinging jet with application to thunderstorm microburst winds. Journal of Wind Engineering and Industrial Aerodynamics, 96(3), 345-365.

[209] Sherman, D. J. (1987). The passage of a weak thunderstorn downburst over an instrumented tower. Monthly weather review, 115(6), 1193-1205.

[210] Snedeker, R. S. (1971). A study of free jet impingement. Part 1. Mean properties of free and impinging jets. Journal of fluid Mechanics, 45(2), 281-319.

[211] Simiu, E., Filliben, J. J., & Shaver, J. R. (1982). Short-term records and extreme wind speeds. Journal of the Structural Division, 108(11), 2571-2577.

[212] Simiu, E., & Scanlan, R. H. (1996). Wind effects on structures: fundamentals and applications to design.

[213] Simiu, E., & Heckert, N. A. (1996). Extreme wind distribution tails: a “peaks over threshold” approach. Journal of Structural Engineering, 122(5), 539-547.

[214] Solari, G. (1993). Gust buffeting. I: Peak wind velocity and equivalent pressure. Journal of Structural Engineering, 119(2), 365-382.

[215] Solari, G., & Piccardo, G. (2001). Probabilistic 3-D turbulence modeling for gust buffeting of structures. Probabilistic Engineering Mechanics, 16(1), 73-86.

[216] Solari, G., & Tubino, F. (2002). A turbulence model based on principal components. Probabilistic engineering mechanics, 17(4), 327-335.

[217] Solari, G., Repetto, M. P., Burlando, M., De Gaetano, P., Pizzo, M., Tizzi, M., & Parodi, M. (2012). The wind forecast for safety management of port areas. Journal of Wind Engineering and Industrial Aerodynamics, 104, 266-277.

[218] Solari, G. (2014). Emerging issues and new frameworks for wind loading on structures in mixed climates. Wind and Structures, 19(3), 295-320.

[219] Solari, G., Burlando, M., De Gaetano, P., & Repetto, M. P. (2015a). Characteristics of thunderstorms relevant to the wind loading of structures. Wind and Structures, 20(6), 763-791.

[220] Solari, G., De Gaetano, P., & Repetto, M. P. (2015b). Thunderstorm response spectrum: fundamentals and case study. Journal of Wind Engineering and Industrial Aerodynamics, 143, 62-77.

[221] Solari, G. (2016). Thunderstorm response spectrum technique: Theory and applications. Engineering Structures, 108, 28-46.

[222] Solari, G., Rainisio, D., & De Gaetano, P. (2017). Hybrid simulation of thunderstorm outflows and wind-excited response of structures. Meccanica, 52(13), 3197-3220.

[223] Solari, G., & De Gaetano, P. (2018). Dynamic response of structures to thunderstorm outflows: Response spectrum technique vs time-domain analysis. Engineering Structures, 176, 188-207.

[224] Song, Y., Achberger, C., & Linderholm, H. W. (2011). Rain-season trends in precipitation and their effect in different climate regions of China during 1961–2008. Environmental Research Letters, 6(3), 034025.

[225] Srivastava, R. C. (1985). A simple model of evaporatively driven dowadraft: Application to microburst downdraft. Journal of the Atmospheric Sciences, 42(10), 1004-1023.

[226] Srivastava, R. C. (1987). A model of intense downdrafts driven by the melting and evaporation of precipitation. Journal of the atmospheric sciences, 44(13), 1752-1774.

[227] Steiner, J. T. (1973). A three-dimensional model of cumulus cloud development. Journal of the Atmospheric Sciences, 30(3), 414-435.

[228] Straka, J. M., & Anderson, J. R. (1993). Numerical simulations of microburst-producing storms: Some results from storms observed during COHMEX. Journal of the atmospheric sciences, 50(10), 1329-1348.

[229] Stucki, P., Brönnimann, S., Romppainen-Martius, O., Welker, C. S., Imhof, M., von Wattenwyl, N., & Philipp, N. (2014). A catalog of high-impact windstorms in Switzerland since 1859. Natural Hazards and Earth System Sciences, 14(11), 2867-2882.

[230] Su, Y., Huang, G., & Xu, Y. L. (2015). Derivation of time-varying mean for non-stationary downburst winds. Journal of Wind Engineering and Industrial Aerodynamics, 141, 39-48.

[231] Takayama, H., Niino, H., Watanabe, S., & Sugaya, J. (1997). Downbursts in the northwestern part of Saitama Prefecture on 8 September 1994. Journal of the Meteorological Society of Japan. Ser. II, 75(4), 885-905.

[232] Tamura, Y., & Cao, S. (2012). International group for Wind-related disaster risk reduction (IG-WRDRR). Journal of Wind Engineering and Industrial Aerodynamics, 104, 3-11.

[233] Tang, C., & Hong, G. X. (2011). 3D engineering model of downburst evolution in thunderstorm. Procedia Engineering, 17, 141-150.

[234] Thom, H. C. S. (1967). Toward a universal climatological extreme wind distribution. Wind Effects on Buildings and Structures, 1.

[235] Thom, H. C. S. (1968a). New distributions of extreme wind speeds in the United States. J. Struct. Div., ASCE 94: 1787-1801.

[236] Thom, H. C. S., (1968b). Toward a universal climatological extreme wind distribution, in: Schriever, W.R. (Ed.), Proceedings of the International Research Seminar on Wind effects on buildings and structures, Ottawa, Canada, University of Toronto Press, I, 669-683.

[237] Thom, H. C. S., (1968c). New distributions of extreme wind speeds in the United States. J. Struct. Div. ASCE 94, 1787-1801.

[238] Tian, Y., Yang, Q., Yang, N., Li, B., & Chen, B. (2011). Statistical spectrum model of wind velocity at Beijing Meteorological Tower. Science China Technological Sciences, 54(11), 2869.

[239] Torrielli, A., Repetto, M. P., & Solari, G. (2013). Extreme wind speeds from long-term synthetic records. Journal of Wind Engineering and Industrial Aerodynamics, 115, 22-38.

[240] Torrielli, A., Repetto, M. P., & Solari, G. (2014). A refined analysis and simulation of the wind speed macro-meteorological components. Journal of Wind Engineering and Industrial Aerodynamics, 132, 54-65.

[241] Trautner, C., Ojdrovic, R., Schafer, B. W., & Jones, N. P. (2013). An Investigation of the Collapse of the Dallas Cowboys Practice Facility. In Forensic Engineering 2012: Gateway to a Safer Tomorrow, 1268-1277.

[242] Trigo, I. F., Bigg, G. R., & Davies, T. D. (2002). Climatology of cyclogenesis mechanisms in the Mediterranean. Monthly Weather Review, 130(3), 549-569.

[243] Twisdale, L. A., & Vickery, P. J. (1992). Research on thunderstorm wind design parameters. Journal of Wind Engineering and Industrial Aerodynamics, 41(1-3), 545-556.

[244] Ulbrich, U., Leckebusch, G. C., & Donat, M. G. (2013). Windstorms, the most costly natural hazard in Europe. Natural disasters and adaptation to climate change, 109-120.

[245] Vega, R., & Letchford, C. W. (2009). Extreme wind climatorlogy in mixed climates. In 11th America's Conference on Wind Engineering, 1.

[246] Vermeire, B. C., Orf, L. G., & Savory, E. (2011a). Improved modelling of downburst outflows

for wind engineering applications using a cooling source approach. Journal of Wind Engineering and Industrial Aerodynamics, 99(8), 801-814.

[247] Vermeire, B. C., Orf, L. G., & Savory, E. (2011b). A parametric study of downburst line near-surface outflows. Journal of Wind Engineering and Industrial Aerodynamics, 99(4), 226-238.

[248] Vicroy, D. D. (1991). A simple, analytical, axisymmetric microburst model for downdraft estimation. NASA Technical Memorandum 104053.

[249] Vicroy, D. D. (1992). Assessment of microburst models for downdraft estimation. Journal of Aircraft, 29(6), 1043-1048.

[250] Von Mises, R. (1936). La distribution de la plus grande de n valeurs. Rev. Math. Union Interbalcanique, 1, 141-160.

[251] Wakimoto, R. M. (1982). The life cycle of thunderstorm gust fronts as viewed with Doppler radar and rawinsonde data. Monthly Weather Review, 110(8), 1060-1082.

[252] Wakimoto, R. M. (1985). Forecasting dry microburst activity over the high plains. Monthly Weather Review, 113(7), 1131-1143.

[253] Weisman, M. L., & Klemp, J. B. (1982). The dependence of numerically simulated convective storms on vertical wind shear and buoyancy. Monthly Weather Review, 110(6), 504-520.

[254] Weisman, M., (2003). Convective storms: overview, in: J.R. Holton J.A. Curry and J.A. Pyle, eds.: J.R. Holton J.A. Curry and J.A. Pyle, Encyclopedia of Atmospheric Sciences, Academic Press, 2002, pp. 548-559.

[255] Weissman, I. (1978). Estimation of parameters and large quantiles based on the k largest observations. Journal of the American Statistical Association, 73(364), 812-815.

[256] Weiss, L. (1971). Asymptotic inference about a density function at an end of its range. Naval Research Logistics Quarterly, 18(1), 111-114.

[257] Whittingham, H. E. (1964). Extreme wind gusts in Australia, in: Bulletin No. 46, Commonwealth Bureau of Meteorology, Melbourne, Australia.

[258] Wieringa, J. (1996). Representativity of extreme wind data. In Hydrology of Disasters, Springer, Dordrecht, 19-40.

[259] Wilson, J. W., Roberts, R. D., Kessinger, C., & McCarthy, J. (1984). Microburst wind structure and evaluation of Doppler radar for airport wind shear detection. Journal of Climate and Applied Meteorology, 23(6), 898-915.

[260] Wisner, C., Orville, H. D., & Myers, C. (1972). A numerical model of a hail-bearing cloud. Journal of the Atmospheric Sciences, 29(6), 1160-1181.

[261] Wolfson, M. M. (1990). Understanding and predicting microbursts (Doctoral dissertation, Massachusetts Institute of Technology).

[262] Wood, G. S., Kwok, K. C., Motteram, N. A., & Fletcher, D. F. (2001). Physical and numerical modelling of thunderstorm downbursts. Journal of Wind Engineering and Industrial Aerodynamics, 89(6), 535-552.

[263] Xu, X., & Zhang, S. (2019). Property of a Typical Urban Thunderstorm Outflow Relevant to Wind Load on Structures. IOP Conference Series: Earth and Environmental Science, 218(1), 012086.

[264] Xu, Z., & Hangan, H. (2008). Scale, boundary and inlet condition effects on impinging jets. Journal of Wind Engineering and Industrial Aerodynamics, 96(12), 2383-2402.

[265] Yao, J., & Lundgren, T. S. (1996). Experimental investigation of microbursts. Experiments in

Fluids, 21(1), 17-25.

[266] Yeo, D. (2011) Database-assisted design for high-rise structures in mixed extreme wind climates. In 13th Int. Conf. on Wind Engineering, July.

[267] Yu, Y., Li, J. L., Xie, J., & Liu, C. (2016). Climatic characteristics of thunderstorm days and the influence of atmospheric environment in Northwestern China. Natural Hazards, 80(2), 823-838.

[268] Zhang, Y. (2006). Status quo of wind hazard prevention for transmission lines and countermeasures. East China Electric Power, 34(3), 28-31.

[269] Zhang, Y., Hu, H., & Sarkar, P. P. (2013). Modeling of microburst outflows using impinging jet and cooling source approaches and their comparison. Engineering Structures, 56, 779-793.

[270] Zhang, S., Solari, G., De Gaetano, P., Burlando, M., & Repetto, M. P. (2018a). A refined analysis of thunderstorm outflow characteristics relevant to the wind loading of structures. Probabilistic Engineering Mechanics, 54, 9-24.

[271] Zhang, S., Solari, G., Yang, Q., & Repetto, M. P. (2018b). Extreme wind speed distribution in a mixed wind climate. Journal of Wind Engineering and Industrial Aerodynamics, 176, 239-253.

[272] Zhang, S., Solari, G., Burlando, M., & Yang, Q. (2019). Directional decomposition and properties of thunderstorm outflows. Journal of Wind Engineering and Industrial Aerodynamics, 189, 71-90.

[273] Zhu, S., & Etkin, B. (1985). Model of the wind field in a downburst. Journal of Aircraft, 22(7), 595-601.

[274] Zipser, E. J. (1977). Mesoscale and convective–scale downdrafts as distinct components of squall-line structure. Monthly Weather Review, 105(12), 1568-1589.

Publications

Journal paper

- ***Zhang, S.***, Solari, G.*, De Gaetano, P., Burlando, M., Repetto, M. P. (2018). A refined analysis of thunderstorm outflow characteristics relevant to the wind loading of structures. Probabilistic Engineering Mechanics, 54, 9-24. DOI: 10.1016/j.probengmech.2017.06.003.
- ***Zhang, S.***, Solari, G., Yang, Q.S., Repetto, M. P.* (2018). Extreme wind speed distribution in a mixed wind climate. Journal of Wind Engineering and Industrial Aerodynamics, 176, 239-253. DOI: 10.1016/j.jweia.2018.03.019.
- ***Zhang, S.****, Solari, G., Burlando, M., Yang, Q.S. (2019). Directional decomposition and properties of thunderstorm outflows. Journal of Wind Engineering and Industrial Aerodynamics, 189, 71-90. DOI: 10.1016/j.jweia.2019.03.014.
- ***Zhang, S.****, Yang, Q.S., Solari, G., Huang, G.Q., Li, B. (2019). Characteristics of thunderstorm outflows in Beijing urban area. Journal of Wind Engineering and Industrial Aerodynamics, 195, 104011.
- Burlando, M.*, ***Zhang, S.***, Solari, G. (2018). Monitoring, cataloguing and weather scenarios of thunderstorm outflows in the Northern Mediterranean. Natural Hazards and Earth System Sciences, 18(9), 2309-2330. DOI: 10.5194/nhess-2018-45.
- Burlando, M.*, Romanić, D., Solari, G., Hangan, H., ***Zhang, S.*** (2017). Field data analysis and weather scenario of a downburst event in Livorno, Italy, on 1 October 2012. Monthly Weather Review, 145(9), 3507-3527. DOI: 10.1175/MWR-D-17-0018.1.

Conference paper

- ***Zhang, S.***, Solari, G., Burlando, M., Repetto, M.P. (2016). Advances in properties of thunderstorm outflows relevant to the wind loading of structures. The 14th International Symposium on Structural Engineering, October 12-15, 2016, Beijing, China.
- ***Zhang, S.***, Solari, G., Yang, Q.S. and Repetto, M.P. (2017). Statistical analysis of extreme wind speed in a mixed wind climate. The 7th European and African Conference on Wind Engineering, July 4-7, 2017, Liège, Belgium.
- ***Zhang, S.*** (2017). Analysis of weather scenario, characteristics and statistics of thunderstorm outflows based on measured data. China Young Researchers Conference 2017, December 23, 2017, Chongqing, China.
- Solari, G., ***Zhang, S.***, Burlando, M., Yang, Q.S. (2018). Directional decomposition and properties of thunderstorm outflows relevant to wind engineering. The 7th International Symposium on Computational Wind Engineering, June 18-22, 2018, Seoul, Republic of Korea.
- ***Zhang, S.***, Yang, Q.S., Solari, G. (2019). Comparison of thunderstorm outflow characteristics in the northern Mediterranean and Beijing urban area. The 15th International Conference on Wind Engineering (ICWE15), September 1-6, 2019, Beijing, China.